ESD TDR 63-425

* 19.75

THE MITRE CORPORATION

(2) # 19.75

SR-19

THE MITRE CORPORATION

Rte. 62 Bedford, Massachusetts

(6) THEORETICAL STUDIES
ON GROUND
SHOCK PHENOMENA

(18) ESD
(19) TDR 63-195

7 NA
NA
9 NA (10)

by

(11) + 60.

(12) 93p.

(13) NA

Melvin L. Baron,
Hans H. Bleich and
Paul Weidlinger

DDC
AUG 15 1963
TISIA B

of

Paul Weidlinger, Consulting Engineer
400 Madison Avenue, New York 17, N. Y.

October 1960.

14 Mitre SR-1

16-17 NA

20 1

21 NA

~~1. This document has been prepared for corporation use only. It has not been reviewed by Office of Security Review, Department of Defense, and therefore, is not intended for public release. Further dissemination or reproduction in whole or in part of the material within this document shall not be made without the express written approval of The MITRE Corporation (Technical Information Services)~~

2. The research reported in this document was supported by the Department of the Air Force under Air Force Contract AF-33 (600) 39852

(15)

FORWARD

The MITRE Corporation is concerned with the survivability of the Air Force Command and Control Systems. It conducts studies in this general area in order to determine the levels at which various systems components fail and investigates various alleviating measures which may be employed to raise the levels of survivability.

One phase of this work is concerned with the behavior of deep underground hard command posts excavated in soil and rock when subjected to nuclear attack.

This document reports on some of the work being done by Paul Weidlinger, Consulting Engineer, New York City.

John J. O'Sullivan
The MITRE Corporation

ACKNOWLEDGEMENTS

This report contains contributions by the following individuals, consisting of the staff and consultants of the office of Paul Weidlinger, Consulting Engineer, New York, New York:

Miss Alva T. Matthews, Engineer
Mr. Raymond Parnes, Engineer
Mr. Ronald Check, Engineer
Dr. C.C. Chao, Consultant - (Stanford University)
Dr. Jerome L. Sackman, Consultant - (University of California)
Dr. Mario G. Salvadori, Associate - (Columbia University)
Dr. Richard Skalak, Consultant - (Columbia University)
Dr. Frank DiMaggio, Consultant - (Columbia University).

A special note of thanks is due to Mr. Charles Lecht and Mr. Charles McCarthy of the MITRE Corporation for their help in the preparation of the programs for the various numerical computations which were required, and for the supervision of the computations which were executed on the I.B.M. 704 of the MITRE Corporation. The cooperation of Mr. William Lone of the MITRE Corporation in expediting the numerical programming and computational work was greatly appreciated by all concerned.

THEORETICAL STUDIES ON GROUND SHOCK PHENOMENA

Table of Contents

Part I - Free Field Effects

Page

Part II - Diffraction Effects

Appendices

GENERAL INTRODUCTION

This report contains a series of technical discussions and papers concerned with the theory of wave propagation in solids with special application to ground shock phenomena. It is a summary which provides the theoretical background to some of our investigations on these topics, initiated in the early part of 1957, and which are still actively pursued at the present.

The report deals with the two major subjects of interest namely, free field effects and diffraction phenomena both, in regions where neither thermodynamic effects nor very large displacements have significant influence on the overall physical picture. This restriction eliminates the crater and its immediate vicinity from the province of our investigations. This means that effects outside of the crater region, but caused by phenomena within this region are only crudely represented by our analytical work. Numerical evaluations of these effects should preferably be started with input data obtained from these close-in calculations. These researches (conducted by Brode at The RAND Corporation) were not concluded during the present project, and for this reason the validity of some of our conclusions must be bracketed within suitable space and time intervals.

Attention must be paid to the relation of the mathematical model to the expected physical behavior of the material. Our researches show that many of the significant quantities due to fundamental consideration are not very sensitive to variations of physical models. For example, the P wave, generated by a surface burst in an elastic solid, appears in an only slightly changed form and intensity in an elastic fluid, and it is found again with small modifications in a viscoelastic medium. Similarly in granular solids, the essential attenuation of particle velocities and stresses is not too sensitive to quite large variations of physical parameters.

In the case of Rayleigh waves we were able to establish the region beyond which they do not contribute significantly to the free field stresses, even though the amplitude of these waves obtained by elastic theory within this region itself is larger than what the physical properties of the material can justify. While these computations furnish only upper bounds of the quantities required, their implications are physically meaningful and of practical significance.

The diffraction problem has so far only been considered in the elastic medium, and it has led to important conclusions regarding the amplification of free field stresses around underground openings. These same effects brought out some new results regarding the applicability of frequency-amplitude (or shock) spectra: it is found that at high frequencies the diffracted spectrum is significantly different from that of the free field spectrum.

The implications and the applicability of theoretical findings are discussed in this report and more detail is contained in some earlier studies ([17], [18], and [19]). We come to the conclusion that within the limitations outlined, the results of our theoretical work can be applied with confidence to practical problems dealing with ground shock effects.

The above work was undertaken to provide urgently needed answers on problems related to the vulnerability of underground structures: Some of the earlier classified feasibility studies ([18] and [19]), prepared under pressure of deadlines, were issued containing only numerical results, or educated guesses, based, however, on rather extensive theoretical researches.

The purpose of the present report therefore is to supply in some detail the background and data on which our previous recommendations were based. It attempts to gather some of the loose ends and to summarize our current knowledge gleaned from our own investigations and from the work of others. The theoretical results are discussed in the report itself, while some of the detailed derivations are in the Appendices.

A considerable part of the information which is summarized here is based on our earlier researches which have been published or are to be published in the near future in technical journals(*), but recent theoretical results which, at the present are not available in other form are contained in Appendices C, D and E.

Some of our current investigations which could not be included at the present time, but which will be reported in the near future are as follows:

Static and quasi-dynamic high pressure experimental work on granular media;

Wave propagation in visco-elastic media.

In spite of the rather extensive coverage of the various topics which have been considered by us and many other researchers, there are a great number of gaps in our knowledge, which have important implications on the general problem of vulnerability of underground structures. The most significant which are in need of urgent solution, are as follows:

Failure mechanism and failure criteria of cavities in elastic media.

Diffraction of stress waves in non-circular openings.

(*) These are denoted by (*) in the list of References.

Evaluation of the effects of tunnel linings.

Three-dimensional wave propagation in granular media.

Diffraction of stress waves in granular media.

Rayleigh wave attenuation due to non-linear and/or plastic effects.

Experimental verifications and research.

While the above list is far from exhaustive, it is uncomfortably long; past experience with similar topics leads us to suspect that studies on these subjects may bring about surprising and possibly aggravating discoveries. While we are working at the present on some of these topics, we are not as yet in a position to report significant progress in these areas.

PART I

FREE FIELD EFFECTS

FREE-FIELD EFFECTS

1. INTRODUCTION

The following contains a summary of available theoretical results on free-field effects due to (hypothetical) Megaton explosions on the surface of semi-infinite media of various idealized properties.

The ultimate purposes of the presentation are conclusions for actual media like rock or soil with complex properties difficult to analyze or even to describe. The problem of rock-like media is approached by considering a succession of materials having gradually more complex properties. In this manner certain conclusions drawn for cases of simple properties can be extrapolated for more complex ones by qualitative reasoning. The writers believe that estimates applicable in judging realistic situations in rock have been obtained in this manner by considering the succession: acoustic inviscid fluid, linear elastic solid, non-linear elastic solid.

As contribution to the problem of soils additional studies of wave propagation in locking media have been made. Most of the work concerns one-dimensional wave propagation, but the case of spherical waves has now also been treated.

To have an understanding of the meaning of the analytical results it is necessary to use a realistic pressure time history in computing examples. Such a history is indicated in Fig.(1-1), which represents computed values of surface pressures for a 20MT surface burst [1]. It is pertinent that the pressure at any time acts over a circular area of radius r_o with constant intensity except at the periphery, where a pressure spike appears. It will be found very important that the velocity of increase of the radius of the circle, i.e. the velocity of the shock in air, at early times is very large, much larger than the seismic velocities in the ground. The shock velocity in air at 19 ms, e.g. is still V = 34,000 feet per second, and therefore larger than the seismic velocities of any likely medium; however, at 290 ms the velocity has decreased to V = 7,200 feet per second which is less than the seismic velocity of some rocks.

For qualitative considerations it is of interest to have information on the impulse $I = \int p \, dt$ of the surface pressure. Fig.(1-2) shows I at the center of the explosion as a function of the time t_o.

The following recurring symbols are adhered to in the body of the report[*]

r, R and z	coordinates as in Fig.(2-1).
c	velocity of sound in <u>fluid</u>, velocity of <u>shear</u> waves in linear elastic solid.
c_p, c_R	velocity of dilatational and Rayleigh waves, respectively, in linear elastic solid.
G, λ, μ	modulus of rigidity, Lamé's constants, respectively

---

[*] Different symbols may be used in the Appendices, as they are taken from various sources.

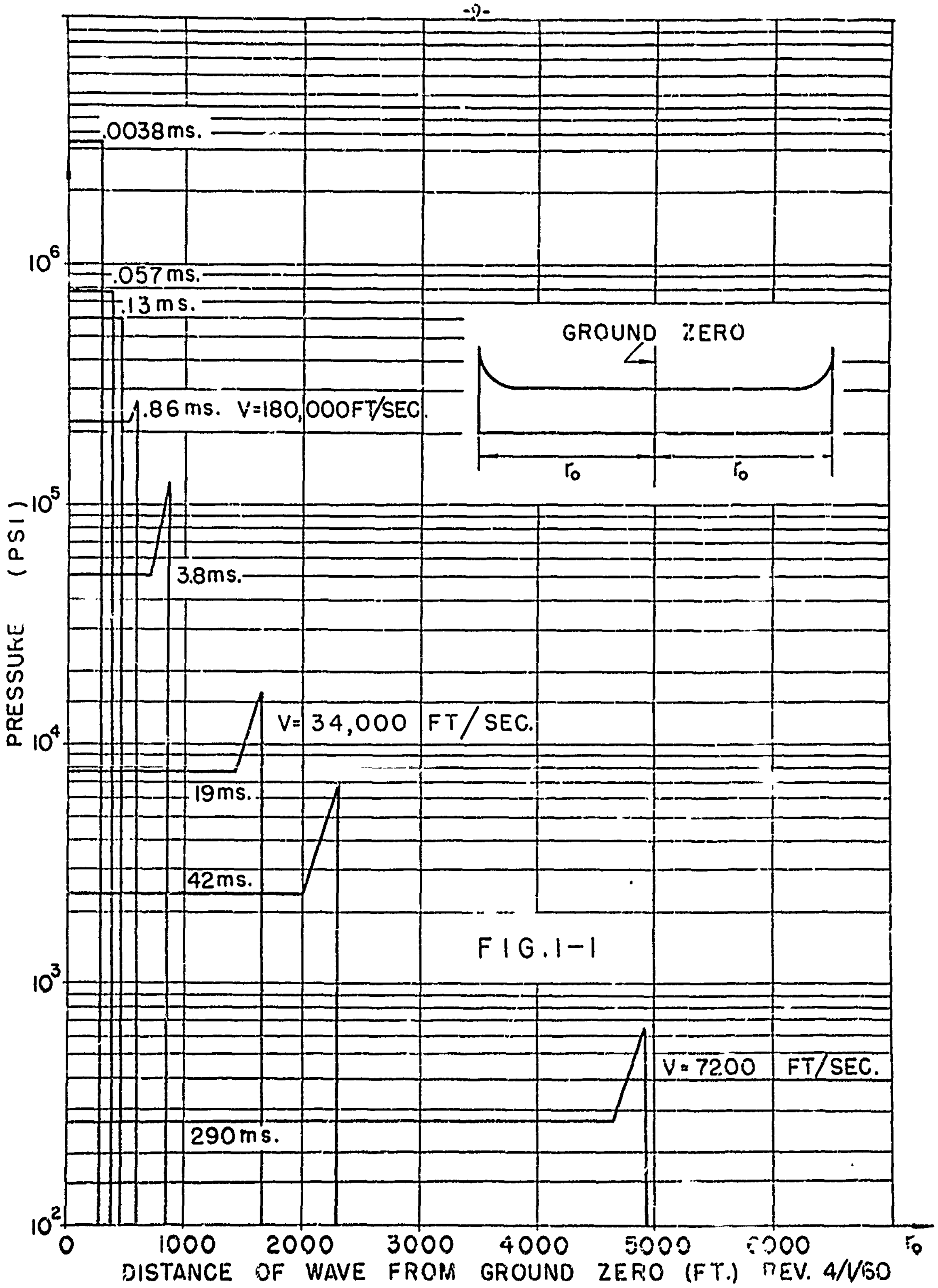

FIG.1-1

REV. 4/1/60

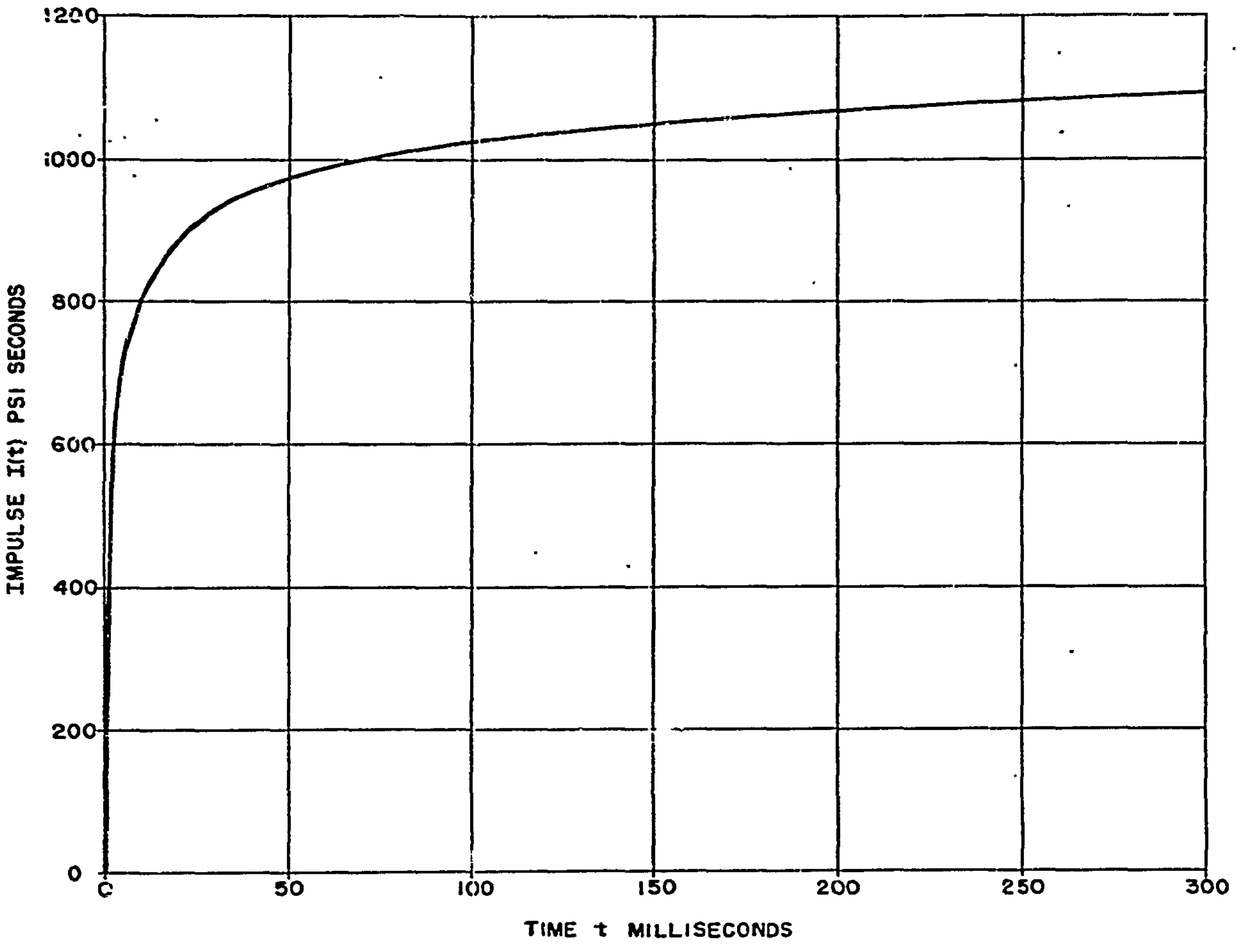
IMPULSE I(t) PSI SECONDS
1200
1000
800
600
400
200
0
0
50
100
150
200
250
300
TIME t MILLISECONDS

FIG.1-2

2. HALF SPACE OF ACOUSTIC INVISCID FLUID

The effect of a pressure p(r, t) on the surface of a half space can be obtained for the case of an acoustic$^{(*)}$ fluid from the solution for a concentrated point load. The load is a unit step load in time, of intensity H(t). The solutions for the pressure can be written in closed form [2]

$$p = \frac{\cos\theta}{2\pi Rc} \quad \delta\left(t - \frac{R}{c}\right) + \frac{\cos\theta}{2\pi R^2} \; H\left(t - \frac{R}{c}\right) \qquad (2\text{-}1)$$

where r, R, z and θ are defined in Fig.(2-1).

p is the pressure in the fluid

$$H(x) = \begin{cases} 0 & \text{if } x < 0 \\ 1 & \text{if } x \geq 0 \end{cases}$$ is a symbol defining a unit step function.

$$\delta(x) = \frac{dH(x)}{dx}$$ is Dirac's Delta Function

Using the applied pressure p(r, t) defined in Fig.(1) and c = 5000 feet per second, Figs.(2-2) to (2-4) give computed pressures for points r = 0, and r = 2000 feet at various depths.

a) Effects under Ground Zero, $r \simeq 0$.

Figs.(2-2), (2-3) consider points at $r \simeq 0$, directly under the center of the explosion. For the first 2.2 ms (Fig. 2) the given pressure at z = 0 and the computed ones at 500 feet and 2000 feet depth are undistinguishable. For later times, Fig.(3) differences occur, the deviations occurring earlier at greater depth. It is significant that for a few milliseconds (except for time delay) the pressure signal just under ground zero is independent of the depth. This is due to the fact that the pressure p(r, t) spreads on the surface with such a large velocity that one could assume simultaneous application of a uniform pressure over some radius r_0 (Fig. 1-1)

---

* Note that in acoustic theory only first order terms are retained, such that the equations become linear. This linearity permits the use of superposition.

shows that this pressure is at early times nearly uniform, the spikes containing only a small portion of the total load).

If a uniform pressure p(t) is applied on the surface of a semi-infinite fluid, the problem becomes one of one-dimensional wave propagation, and in the acoustic case considered here, the pressure signal propagates then without change. If a uniform pressure is applied only over a circular area, a point directly under the load receives a signal equal to the applied pressure for a limited time, later the pressure drops as illustrated in Fig.(2-4) for $r = 0$, $z = 500$. The point where the pressure drops is defined by the arrival time of a signal from the periphery of the loaded circle. The situation in Figs.(2) and (3) is similar, but due to the expansion of the loaded area one cannot find an exact time t up to which one-dimensional wave propagation applies; instead one can estimate a time t up to which one-dimensional wave propagation should be a good approximation. The time in which the approximation is valid will of course be a function of the depth, z, (and of the seismic velocity and weapon size).

This rather elementary explanation was presented in such detail because the above qualitative reasoning is valid not only for the case of a linear elastic solid, but also for complicated non-linear and/or non-elastic media. Even in such cases pressure waves due to the blast pressures on the surface must be, for a certain time, one-dimensional in nature, permitting manageable numerical solutions. These solutions should be good approximations for a definable range of time.

b) Effects in the high-pressure (superseismic) range when $z << r$

As a typical example Equations (2-1) were used to obtain the pressure at a typical point $r = 2000$ feet, $z = 500$ feet in the range of high pressures. The result is shown in Fig.(2-5) where the computed points are compared with the surface pressure at the same radius, $r = 2000$ feet. It is seen that the pressures at a depth of 500 feet differ only little from those on the surface.

The small differences between the pressures on the surface and at a depth $z \ll r$ are due to the fact that the velocity V of the pressure wave in air passing over the point is very much larger than the seismic velocity c in the medium. The first portion of the pressure signal, say up to 50 ms after arrival, is due to the airpressure passing over the point, the very first signal originating from a point F, see Fig.(5a). As a first approximation, the actual pressure on the surface might be replaced by a plane pressure wave progressing with constant velocity $V > c$ and without change in shape of the pressure wave. This problem has an elementary solution; a wave on the surface $p = f(t - x/V)$ produces an inclined plane wave in the fluid, $p(t - \xi/c)$, Fig.(2-6). The angle α depends on the ratio V/c, and the pressure signal p_z at any point has the same shape as the surface pressure, $p_z = f(t - t_a)$, where t_a is a time delay.

In the high pressure range where the velocity of the shock front in air $V \gg c$, the pressure below the surface in the fluid can therefore be approximated by the surface pressure. By purely qualitative reasoning one can conclude that this must be so for a very short time after arrival, and if the depth z is very small. It is therefore important to note that Fig.(2-5) shows that a reasonably good approximation is obtained even at a depth $z = r/4$ and for the entire time range where the pressures are substantial. It appears that $z = r/4$ is sufficiently small to satisfy the original assumption $z \ll r$.

It is interesting to discuss the difference between this approximation and the computed points. At first arrival the actual pressure must be equal to the peak air pressure at the point F (Fig. 5a) on the surface, which pressure is a little larger than the peak for r = 2000 feet. (One could therefore improve the approximation for the peak pressure by using the pressure history at F.) Subsequently, for a limited time, the computed pressures due to the loads according to Fig. (1-1) are lower than the surface pressure, similar to the situation for r = 0 in Fig. (2-3). However, at later times, t > 150 ms, the computed pressures exceed the approximate ones somewhat. This is caused by the high applied pressures within the central circle r ~ 1000 feet, shortly after the explosion. Waves generated from this high pressure area arrive at this time; the effect at the point considered is however only small, because these pressures are remote and act only over a relatively small area. A computation confirming that the effect of the early high pressure in a typical case is not significant was however required, because the relative magnitude of the effects compared depends on the rapidity of the decay of the applied air pressure. For a very much larger, or very much smaller weapon, the situation might be different.

The simplifying approximation of assuming that the shape of the surface pressure does not change, and that this pressure progresses with constant velocity, V, has been tested above at a point where the shock velocity V is several times larger than the seismic velocity c. The same assumption, we will call it the "steady state solution", can be made with good results if the velocity V is appreciably smaller than c, but the pressure in the fluid will not have the character of Fig. (2-6). A theoretical solution for this case can be derived from [3]. Without pursuing the matter further, it should be stressed that the approximation must necessarily become poor if V and c differ little, regardless whether V > c or V < c. In the superseismic case caution is therefore indicated unless $V \geq 1.5c$. Further numerical work to find how close to V = c the approximation may be used is planned.

Returning to the superseismic range, it is important that the analysis for the fluid, based on the approximation, indicates no attenuation of the pressure with depth. (This conclusion can of course only apply for the range $z \ll r$ for which the approximation can be valid.) If the approximation were not used small differences with depth would be found, but there would be no appreciable attenuation, until the depth z becomes comparable to the radial distance r. (In the subseismic range, on the other hand, an analysis using the same approximation indicates substantial attenuation.)

The situation for the fluid, which in itself is not pertinent, has been discussed at length because equivalent approximations can be made for the elastic solid or other media. Mathematically speaking the steady state solution in the superseismic range is an asymptotic approximation, for short time after arrival; because the air pressure signal used is the one for a point on the surface at the distance r from ground zero (not for point F, Fig. 5a, where the first signal originates) the approximation as proposed here is also restricted to sufficiently small depth z, such that the pressures at the two points do not differ noticeably.(*)

(*) It would be an unwarranted refinement to use the pressure at point F as basis, because the location of this point would require a cumbersome computation for each depth z. Yet, if the actual air pressure varies so rapidly that the pressure at F differs appreciably from the pressure exactly above the point considered, the signal would be affected by these variations within a short time after first arrival. In such a case the steady state approximation would be poor and useless anyway.

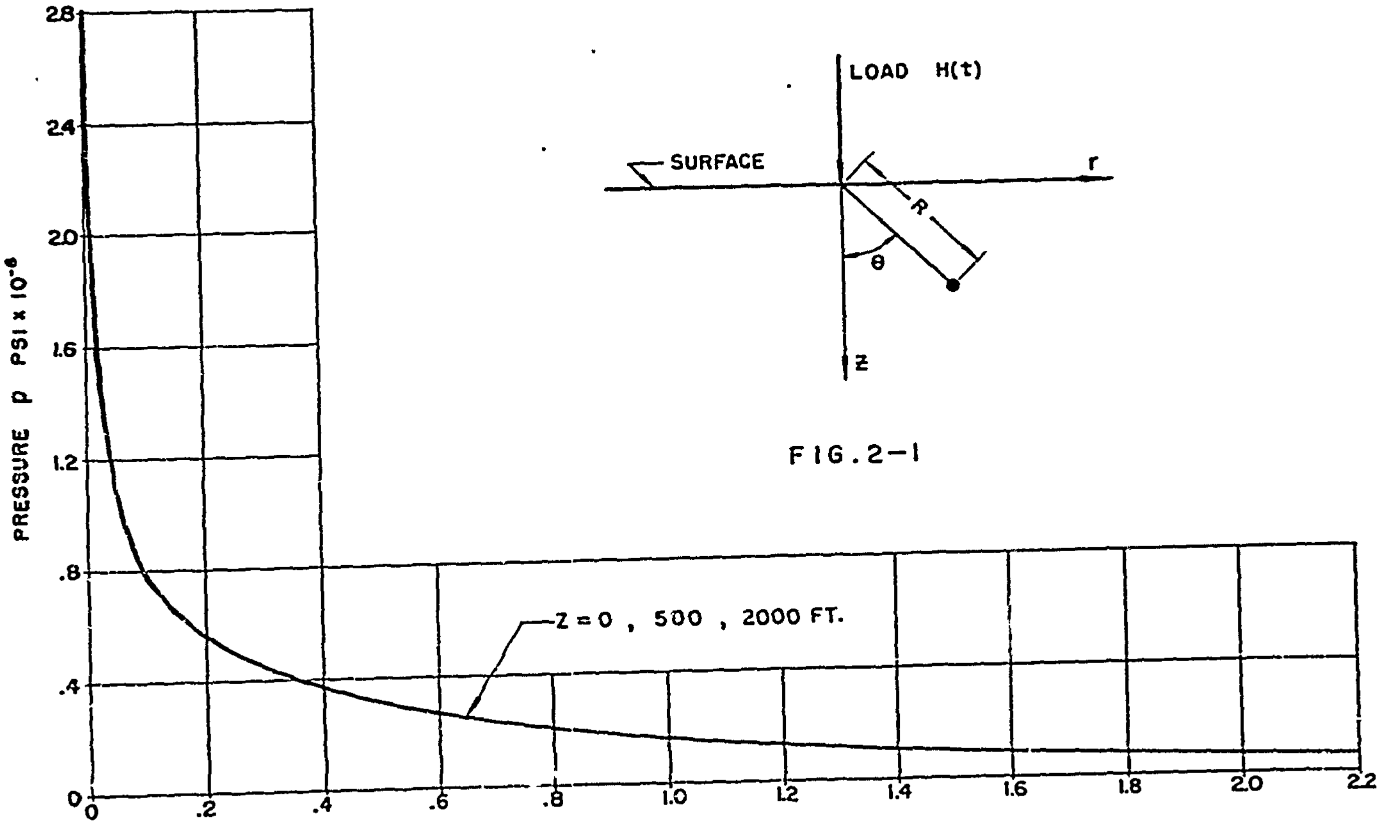

FIG.2-1

FIG.2-2 PRESSURE AT r = 0

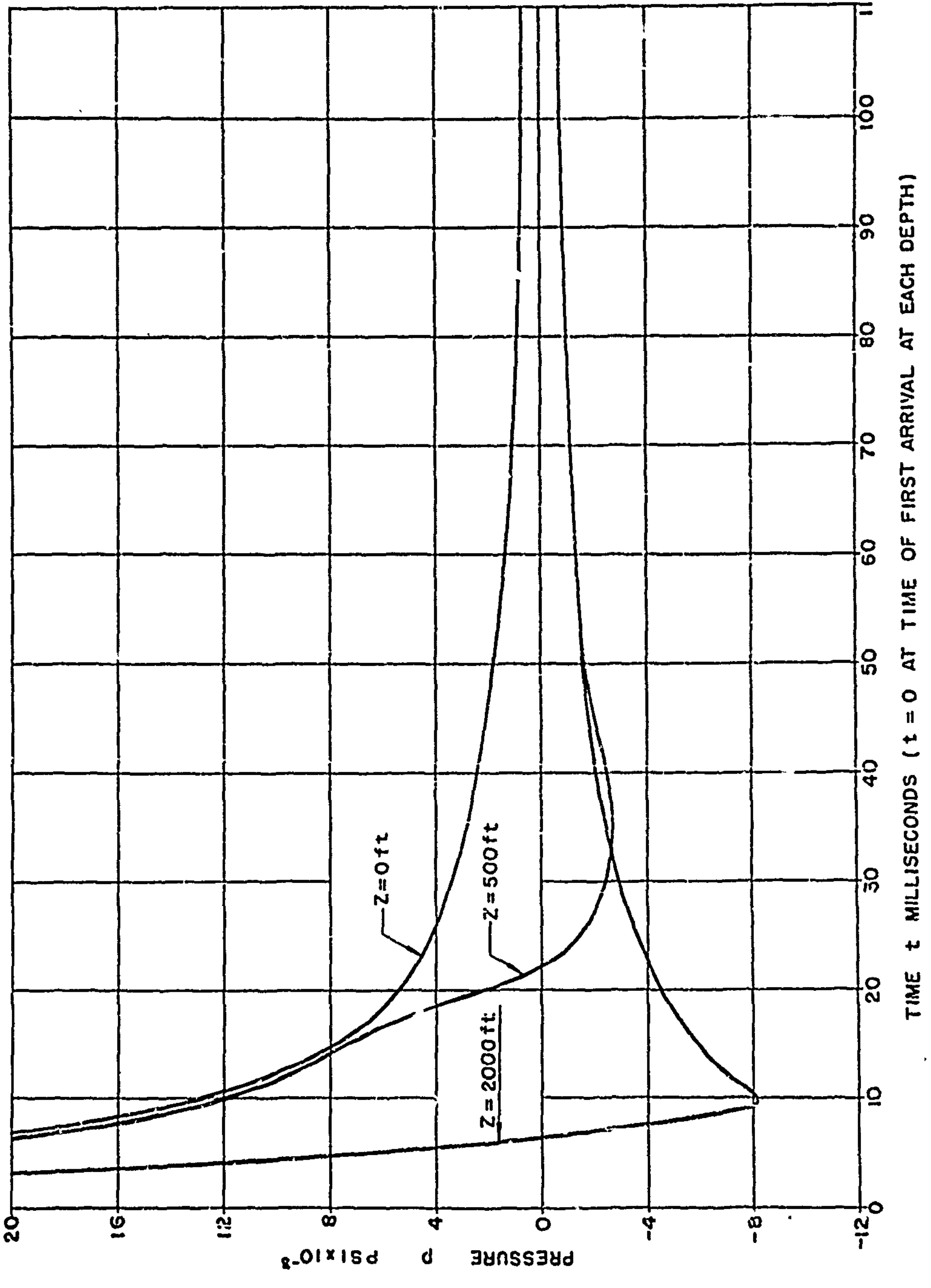
PRESSURE p PSI×10^-8
20
16
12
8
4
0
-4
-8
-12
TIME t MILLISECONDS (t = 0 AT TIME OF FIRST ARRIVAL AT EACH DEPTH)
0
10
20
30
40
50
60
70
80
90
100
110
Z=0ft
Z=500ft
Z=2000ft

FIG. 2—3

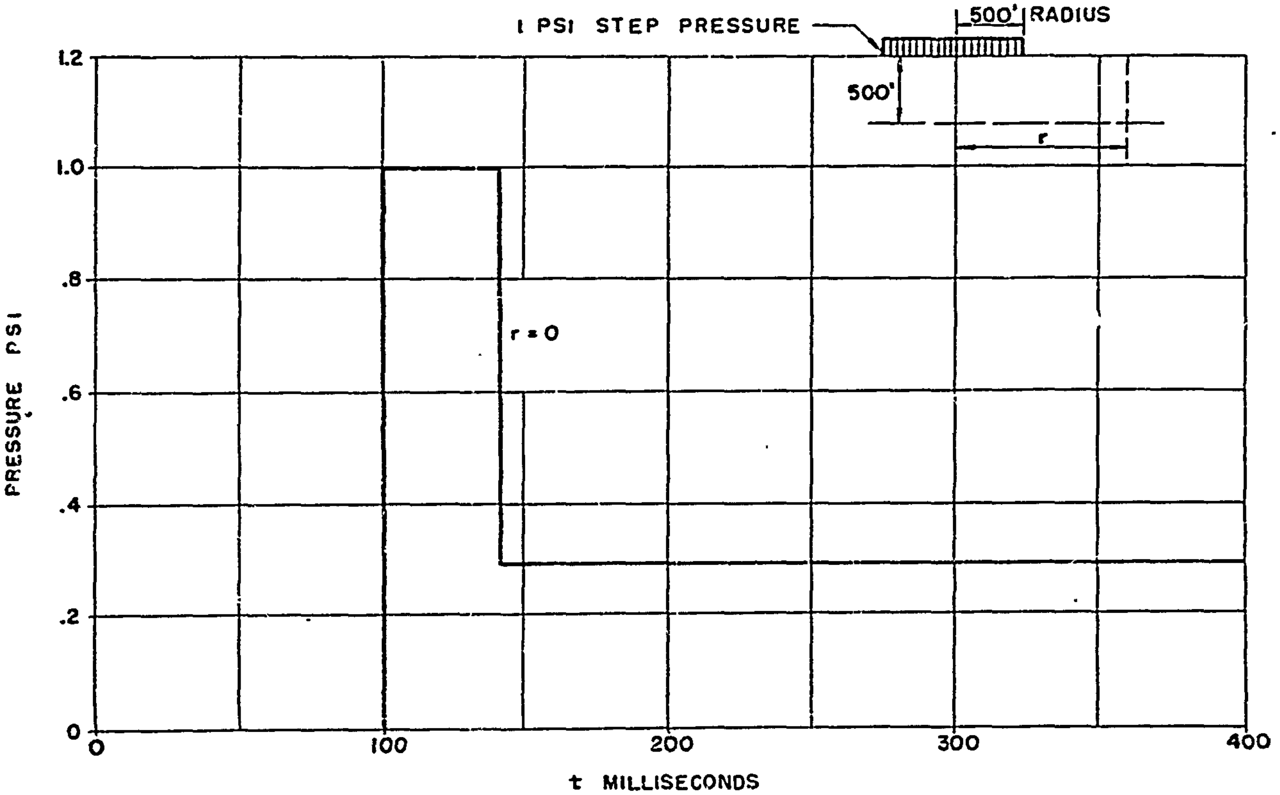
I PSI STEP PRESSURE
500' RADIUS
500'
r
r = 0
PRESSURE PSI
1.2
1.0
.8
.6
.4
.2
0
0
100
200
300
400
t MILLISECONDS

FIG. 2 – 4

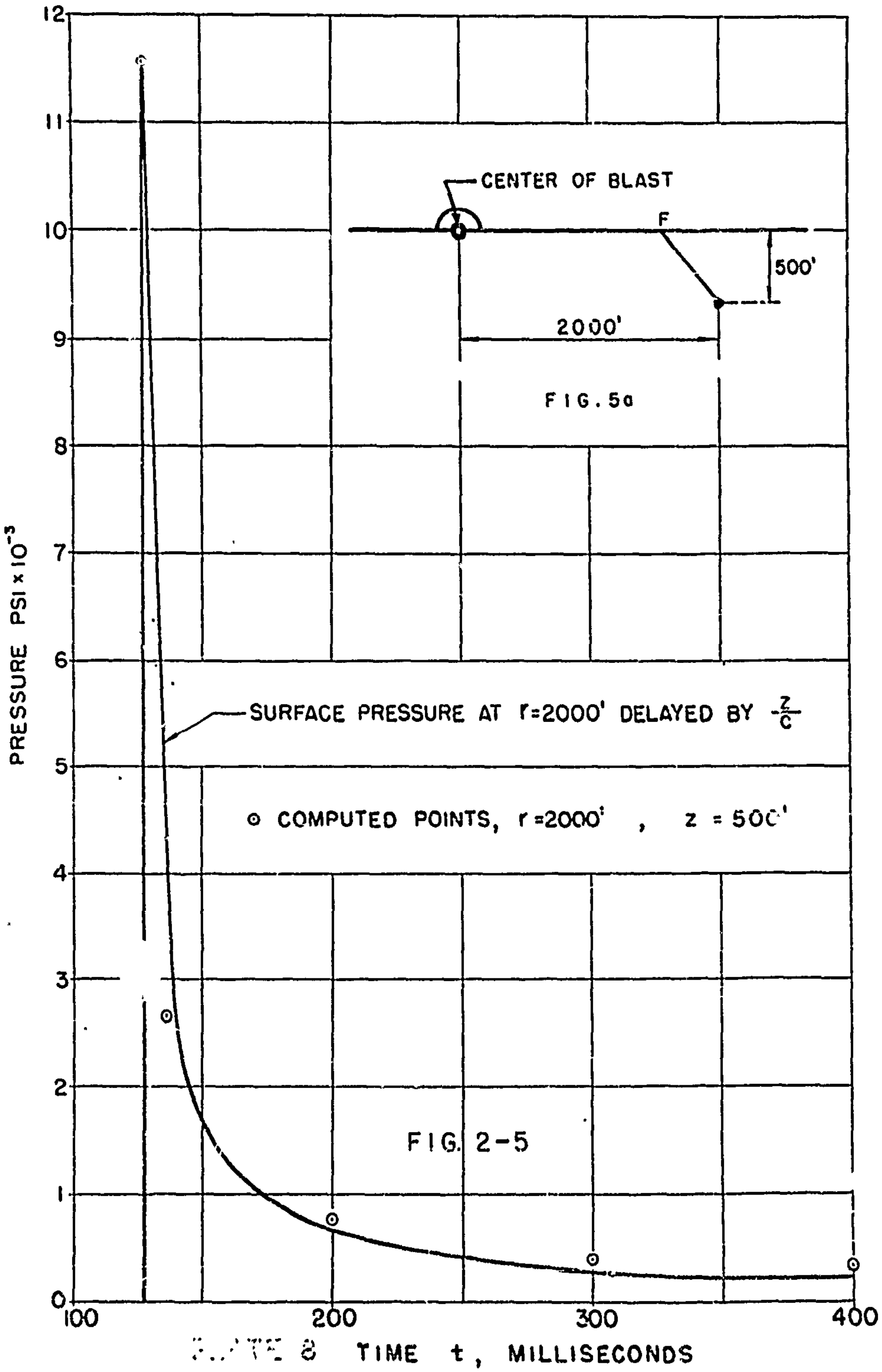

FIG. 2-5

PLATE 8

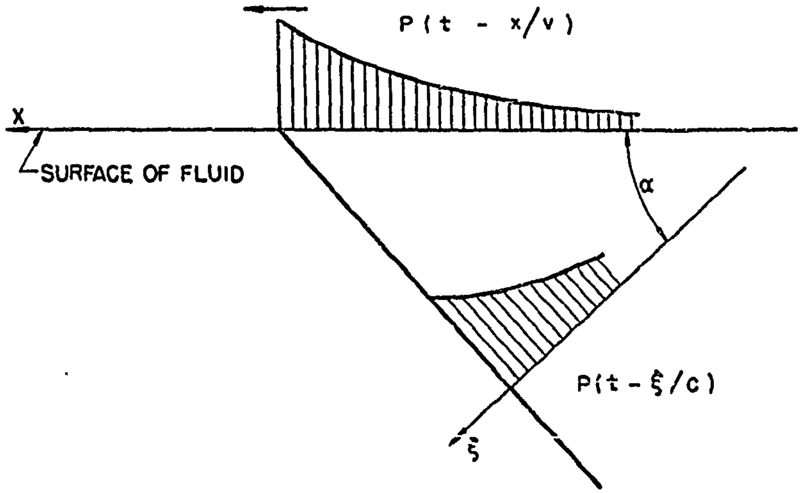

FIG. 2-6

9

3. HALF SPACE OF LINEAR-ELASTIC SOLID.

The effect of an applied surface pressure according to Fig.(1-1) can be obtained again by superposition from the effect of a concentrated step load. However, the effect of the latter is much more complicated than in the case of an accustic fluid.

a) Effect of a concentrated step load.

The literature [4], [5] contains formal solutions for the displacements of the surface due to buried horizontal and vertical step loads. By virtue of a dynamic reciprocal theorem [6], [7] it is concluded that the vertical and horizontal components of the displacements due to a step load on the surface, are, respectively, equal to the vertical displacements of the surface due to vertical and horizontal step loads acting below the surface, see Fig. (3-1). The above-named papers furnish formal expressions for the displacements for the present problem; expressions for the strains and stresses can be obtained by routine manipulations. However, the expressions are not in closed form, they require the very cumbersome numerical evaluation of definite integrals. A series of displacement histories was computed and graphically presented in [4]. While extremely helpful for purposes of the general discussion which follows, these graphs could not be utilized for the numerical determination of stresses or displacements due to the surface pressure, Fig.(1-1). Numerical results reported below had to be developed from the available theoretical expressions.

General information on wave propagation phenomena in elastic solids can be found in standard texts, defining P-waves of dilatation (velocity c_P) and S-waves of distortion (velocity $c < c_P$). In addition the existence of surface waves, called Rayleigh waves (velocity $c_R < c$), is established. Knowledge of these wave types permits a purely qualitative description of the state of stress in a half space due to a concentrated step load, Fig.(3-2).

At a given time t after application of the load, the discontinuities associated with the fronts of the P and S waves will have reached the surface of spheres of diameters tc_P and tc, respectively. Further, the region between the S and P fronts is divided by a conical surface SP, locating the Van Schmidt front. The Rayleigh waves will be of importance on the surface at or near R, somewhat behind the S-front.

Considering a point r, z, Fig.(3-2), the wave fronts will progress with time; the P and S fronts will pass through any point, while the SP front will only pass through points for which the ratio z/r is less than a critical value which is a function of the ratio c_S/c_P. Rayleigh waves will be only noticeable near the surface, i.e. if z/r is very small. This qualitative description is borne out by Fig.(3-3), giving the vertical deflection $v = w_P$ according to Reference (4) for three ratios z/r. For r/z = 0.5 only the P and S waves pass the point; for r/z = 5 the SP front appears, and there is a faint trace of the Rayleigh wave; for r/z = 40 the Rayleigh wave is fully developed and is a major effect.

It will be noticed that the response curves in Fig.(3-3) at the P and S fronts show peculiarities, i.e. discontinuities or infinite values. These are due to the singularity in the mathematical fiction of the assumed "concentrated point load." If the effect of a physically possible distributed load is computed by integration over the response from the concentrated point load, it is found that undue peculiarities disappear.

Response curves for other displacements or stresses will obviously be of a similar complicated nature, having various ranges as functions of r/z and of the nondimensional time $\tau = ct/R$. To find the response due to the pressure defined in Fig.(1-1) by a purely numerical integration process, covering the entire response range in r/z and τ, would become extremely involved and time consuming even using modern computer equipment. For this reason an attempt will be made to recognize the important effects in each location of interest and to find suitable approximations, similar to, or more general than those developed in Section (2) for the liquid half space.

b) Effects under ground zero, $r \simeq 0$

Consider a point A at $r \simeq 0$ at some depth $z >> r$, Fig. (3-4), at a time t quite soon after arrival of the first signal from a surface pressure $p(r, t)$ of the type shown in Fig. (1-1). At this time only the surface pressure acting within a circle of radius ρ, (see Fig. 3-4) can contribute to the response of point A. The integration over the effects of a concentrated load on the surface will then involve only curves which have the nature of the curve for $r/z = 0.5$ in Fig. (3-3). To define the response in this range ($r/z < 1/\sqrt{2}$) the jumps at the P and S fronts were obtained (in closed form) from the theory. The result for the vertical displacement w is shown in Fig. (3-5). The portion of the curves between the P and S fronts, and the portion following the S front are graphically given in [4]. They are so close to straight lines that they were approximated by straight lines to obtain a single idealized response. (The level of the horizontal line for $\tau > 1$ is defined by the static deflection, known from Boussinesq's solution.)

Using this approach the vertical velocity $\dot{w}$ of a point at $z = 1000$ feet was computed for several values of t. The results are shown in Fig. (3-6) and compared with the vertical velocity $\dot{w}_0$ on the surface. It is seen that in the time range plotted the velocity histories on the surface and at the depth of 1000 feet cannot be distinguished. The situation corresponds to the one shown in Fig. (2-2) for the fluid; and we draw again the conclusion that in this location, $r \simeq 0$, the assumption of one-dimensional wave propagation will give a good approximation for the important, early, high-pressure part of the signal.

For a linear-elastic material one-dimensional wave propagation implies no attenuation of pressure with depth; this conclusion, however, must not be applied to actual materials which will behave non-linear at high pressure levels near ground zero. The non-linear case is discussed later, Section(5).

c) Effects in the high-pressure (superseismic) range at moderate depth, $z \ll r$

In the corresponding case of the fluid, treated in 2 (b), it was found that the response for a considerable length of time (several hundred ms) could be approximately determined from a steady state solution. This solution was the response due to an applied plane pressure $p = f(t - x/V)$, where $f(t)$ is the pressure history on the surface above the point considered, and V is the velocity of the shock in air at this point.

Using the same general reasoning as in the case of the fluid, one comes again to the conclusion that at moderate depth, $z \ll r$, the early portion of the response in the elastic solid can be obtained with good approximation by computing the response to the simplified steady pressure pulse $p = f(t - x/V)$. The solution for this problem is available [8] and enclosed as Appendix A(*). However, it must not be concluded without further investigation that this approximation will be sufficient for a considerable time, as in the previous example for the fluid. When discussing the latter case, Fig.(2-5), it was pointed out that the computed pressures for $t > 200$ ms were larger than the approximate values, which was ascribed to effects originating in the region of very high pressures near $r = 0$ shortly after the explosion.

(*) There is a printing error in [8] for the superseismic case, which is corrected in the Appendix.

To have a basis for judging the accuracy of the response of the elastic solid at later times, it is necessary to consider effects originating in the region of high pressure. This could be done by a complete numerical determination of the response to a step load from [4] and [5] and subsequent integration for the prescribed load p(r, t). The very extensive numerical work required is however not required. By qualitative consideration of the energy available, one can reason that the effects of the P and S waves from the region of high pressures will be of the same order of magnitude as the pressure wave effects in case of the fluid, and as far as the effects of P and S waves go the steady state approximation in the solid should be as good, or as poor, as in the fluid. This reasoning does not include, however, the energy transmitted by surface waves. It is obvious that the energy of surface waves passing through a point at some distance r will be a function of $1/r$, while the energy in P and S waves decreases as $1/r^2$. Rayleigh wave effects decay therefore slower than the other effects and cannot be judged on the basis of an example for the fluid. Stresses or displacements caused by Rayleigh waves originating in the high pressure region must therefore be computed, and if substantial they must be added to the "steady state solutions." As Rayleigh wave effects decrease rapidly with depth, their relative importance compared with the effects described by the steady state solution will depend on the depths of the point considered. For sufficiently deep points the Rayleigh effects will become negligible, but the depths where this occurs are not known beforehand. It was therefore necessary to develop an analytical procedure for the determination of Rayleigh (surface wave) effects.

This suggests that the response in this range may be obtained approximately by using the "steady state solution" and adding, if necessary, the Rayleigh wave effects. It is now appropriate to consider the steady state solution and its limitations.

Discussion of Steady-State Solution

If a pressure wave $p(t - x/V)$ travels with constant superseismic velocity $V \geq c_p > c$ on the surface of a (linear) elastic solid, it produces an inclined plane P-wave and an inclined plane S-wave in the solid, as shown in Fig. (3-7). The intensity of these pressure and shear waves is proportional to $p(t)$, the factors and angles of inclination depend on the ratio V/c_p and on Poisson's ratio, see Appendix A. Fig. (3-7) shows two cases $V/c_p = 1.5$ and 3, both indicating that the P wave has nearly the same intensity as the applied surface pressure while the S wave is less important. The theoretical solution has the character of Fig. (3-7) as long as $V \geq c_p$. However, as the velocity V approaches c_p the strengths of the waves vary rapidly as function of V/c_p, as seen from the following table (*) (for Poisson's ratio 1/4).

	P-Wave	S-Wave
$\frac{V}{c_p}$	σ/p	τ/p
3.0	0.99	0.22
1.5	0.96	0.45
1.4	0.96	0.49
1.3	0.97	0.52
1.2	0.99	0.56
1.1	1.05	0.59
1.05	1.19	0.58
1.01	1.71	0.46
1.001	2.40	0.21
1	3	0

(*) The situation is also presented graphically in the Appendix, Fig. A-2.

The sensitivity of the solution for ratios $V/c_p \leq 1.1$ indicates clearly that the steady-state solution for such ratios cannot be used as approximation. One can easily give an alternative reason why the steady-state solution becomes poor and invalid as $V/c_p \to 1$. When this ratio approaches unity the inclination of the P front goes toward $\alpha \to 90^\circ$; if one considers the target point A in Fig. (3-8), the first signal will originate from a point F whose horizontal distance (because of $\alpha \simeq 90^\circ$) is quite large compared to the depth. Signals from other intermediate points, say F', will arrive a very short time later. Obviously, if the horizontal distance AF is large, the pressures at F and at intermediate points F' will differ radically, and a steady-state approximation becomes invalid except for very small values of z, and for a very short time after arrival of the first signal.

One can use the above consideration to judge the applicability in cases of small ratios, $V/c_p < 1.5$, by comparing pressure and velocity above the point considered with these at point F. In the case $V/c_p = 1.5$ shown in Fig. (3-7), the angle of the P-wave is $\alpha = 41^\circ 50'$; considering a target A at a depth $z = 500$ feet, the horizontal component of the distance is $AF = z \sin \alpha = 333$ feet. Variations of pressure and velocity V in such a distance are such that the result for this particular depth may still be considered a crude approximation.

Whenever the steady-state solution becomes unsatisfactory the early part of the signal could be determined by using idealized curves for the response due to a concentrated load, similar to the one shown in Fig. (3-5). Further work in this direction appears desirable because the range where the steady state approximation is unsuitable is still of practical interest. However, even by using idealized response curves the numerical integrations required are likely to be cumbersome.

Determination of Rayleigh Wave Effects.

The analysis contained in [4] and [5] was carried further, [9], and expressions for stresses and displacements due to the surface waves generated by a concentrated load are given in Appendix B. The expressions are in closed form, and represent the major portion of the total response for large ratios r/z and in the vicinity of $\tau = \frac{ct}{R} = c_R/c$. E.g., the expressions found will give a very good approximation of the portion near $\tau \sim 0.9$ of the curve for $r/z = 40$ in Fig. (3-3).

As example the stress σ_{zz} due to surface waves is given in Fig. (3-9). It is seen that effects occur only during a short period of time, of the order two to three times z/c, where z is the depth of the point considered.

To obtain the Rayleigh effects from the surface forces due to the pressure history in Fig. (1-1), a formal double integral is derived in Appendix B. Its evaluation for typical locations required the use of an IBM 704. The analysis indicates that the stresses σ_{rr} are larger than the other stresses, $\sigma_{\theta\theta}$, σ_{zz} , σ_{rz} such that the importance of Rayleigh effects generally may be judged by considering σ_{rr}. Figs. (3-10) and (3-11) show the computed time history of the stresses σ_{rr} at a number of depths in two locations. Fig. (3-10) presents the stresses at r = 2000 ft. for a medium having $\nu = 1/4$, c = 10,000 ft/sec ($c_p \simeq$ 17,000 ft/sec). Fig. (3-11) gives similar results for r = 3200 ft. for a medium with $\nu = 1/4$, but having c = 6000 ft/sec. ($c_p \simeq$ 10,000 ft/sec). The decrease of Rayleigh stresses with depth is quite evident.

Comparisons of stresses due to Rayleigh effects and due to the effects of P- and S-waves are shown in Figs. (3-12) and (3-13). The former shows σ_{zz} and σ_{rr} for r = 2000 ft. at a depth of 100 ft. for the same medium for which Fig. (3-10) applies. In this location the velocity V of the shock in air is larger than $c_p \simeq$ 17,000 ft/sec., and the "steady state solution," Appendix A, could be used to compute the pressure waves arriving ahead of the surface waves. The time t used in the graphs is counted with respect to the instant of the explosion at $r = 0$. The two spikes in σ_{zz} represent the arrival of the P- and S-waves, respectively. Similar spikes occur in σ_{rr}, except that the one due to the S-wave is not in the same direction as the one due to the P-wave, such that the stresses σ_{rr} remain high only for a short time. Fig. (3-12) shows that in this location the peak values of the signal from P- and S-waves are larger than Rayleigh stresses, but the duration of high Rayleigh stresses in σ_{rr} is longer. Depending on the response time of the target Rayleigh stresses may or may not be ignorable. At greater depth of course the effects of the P- and S-waves do not change materially, while Rayleigh effects decrease rapidly, such that the latter will become immaterial.

Fig. (3-13) shows a similar comparison for $r = 3200$ ft. at 100-ft. depth for the medium used in connection with Fig. (3-11).

Additional numerical results are presented in Appendix B. Attention is drawn to the fact that the formulae developed in Appendix B canno be applied for points on the surface, $z = 0$, because negative powe of z occur. As a consequence computational difficulties would arise for very small depth, and only results for points at a depth of 25 feet or more were obtained.

The trend of these results as a function of the depth is such that rather large stresses σ_{rr} and $\sigma_{\theta\theta}$ can be expected near the surface.(*) The existence of such high stresses in the elastic analysis make it inapplicable to actual situations near the surface $z \rightarrow 0$ such that the additional effort required to derive an appropriate analysis for shallow depth was not expended.

(*) The vertical stress σ_{zz} and the shear stress σ_{rz} or the free surface must vanish.

The occurrence of high Rayleigh stresses near the surface in itself is a limitation to the applicability of the linear elastic theory to actual solutions. Referring as example to the situation in Fig. (3-12), at a distance of $r = 2000$ ft., the air pressures acting at the surface are such that the use of linear elastic theory is reasonable because the stresses obtained from the steady-state solutions are sufficiently low. The stresses due to Rayleigh waves (which occur at a later time) at this horizontal distance at the depth $z \sim 100$ ft. will also be small enough to be in the elastic range, but, as the same can not be said near the surface, the Rayleigh stresses everywhere can not be considered reliable; the values computed by the theory are presumably much too large. Combining this consideration with the effect of the crater, discussed in Section 6b., the Rayleigh stresses in Figs. (3-10) to (3-13) should be considered as upper bounds only.

d) Effects outside the superseismic range, at depth $z \ll r$.

It is noted that even outside the superseismic range the effects at shallow depth $z \ll r$ can be divided into a signal due to the air pressure passing over the target point, and a Rayleigh signal. The latter can be determined by the method previously outlined, which does not depend on a particular location of the target point. Appendix B contains also results for subseismic locations.

To obtain the effect of the air pressure passing over the target point one can try to use the steady state approximation. The solution to the steady state problem is available [8] but it is somewhat more complex than in the superseismic range.(*) There are actually two ranges, depending on whether $V > c$ or $V < c$. Further, a steady state solution will again be useless if the velocity is close to c_p. Another trouble spot has been

---

(*) Potentially useful expressions for the steady-state solutions due to exponentially decaying pressures are contained in [16]. They might be utilized to tabulate the solutions.

pointed out by Miles [10]. The steady-state solution indicates infinite stresses, and becomes inapplicable if $V = c_R$, where c_R is the Rayleigh wave speed. A formulation for a surface pressure with varying speed was obtained in Reference [10] to overcome this difficulty. No numerical results are available at present. The combination of the steady state solution and of the Rayleigh wave contributions gives therefore only a partial answer in this range.(*) It should be stressed that the steady-state solutions outside the superseismic range indicate attenuation of the response with depth; this would indicate--at least in the theoretical elastic medium--that the surface wave effects outside the superseismic range may remain significant at larger depth than the superseismic range.

(*) No computations to check the accuracy of the steady-state approximations (similar to Fig. 2-5) appear to have been made by anyone. Such a check may be desirable because qualitative considerations lead to the suspicion that this approximation outside the superseismic range might be poor.

APPLICATION OF DYNAMIC RECIPROCAL THEOREM

w_p VERTICAL SURFACE DISPLACEMENT DUE TO VERTICAL FORCE H(t) (PEKERIS)

w_c VERTICAL SURFACE DISPLACEMENT DUE TO HORIZONTAL FORCE (CHAO)

w VERTICAL DISPLACEMENT } DUE TO VERTICAL FORCE ON SURFACE
v HORIZONTAL DISPLACEMENT }

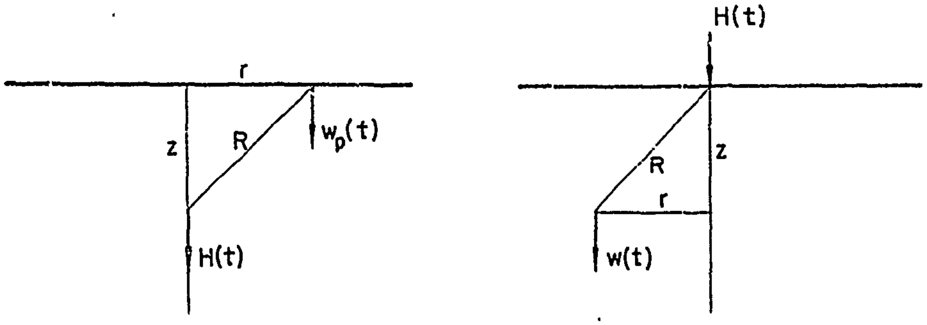

$w(t) = w_p(t)$

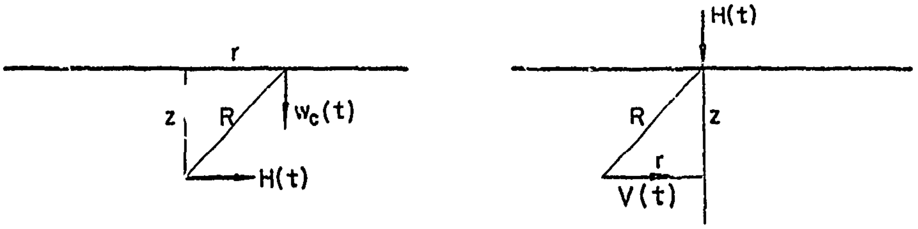

$V(t) = w_c(t)$

FIG. 3-1

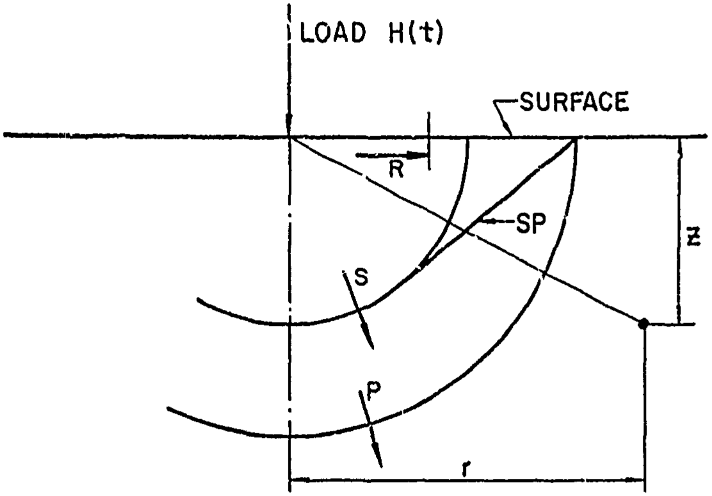

FIG. 3-2

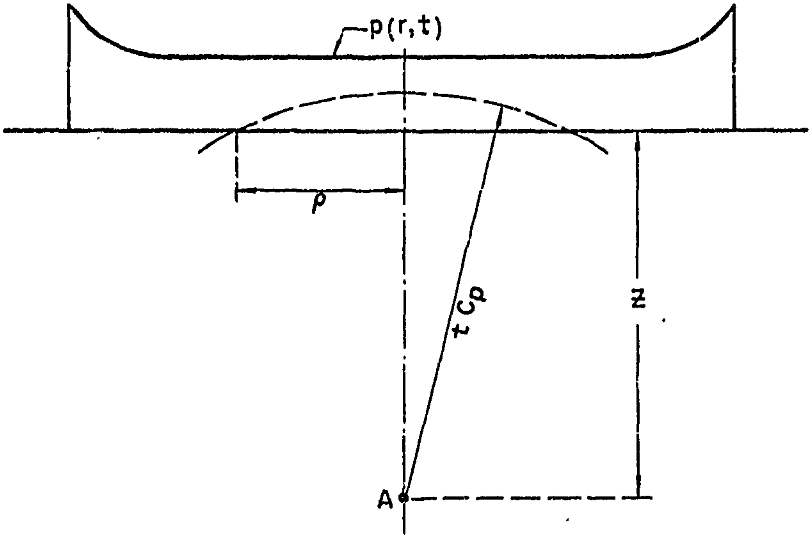

FIG. 3-4

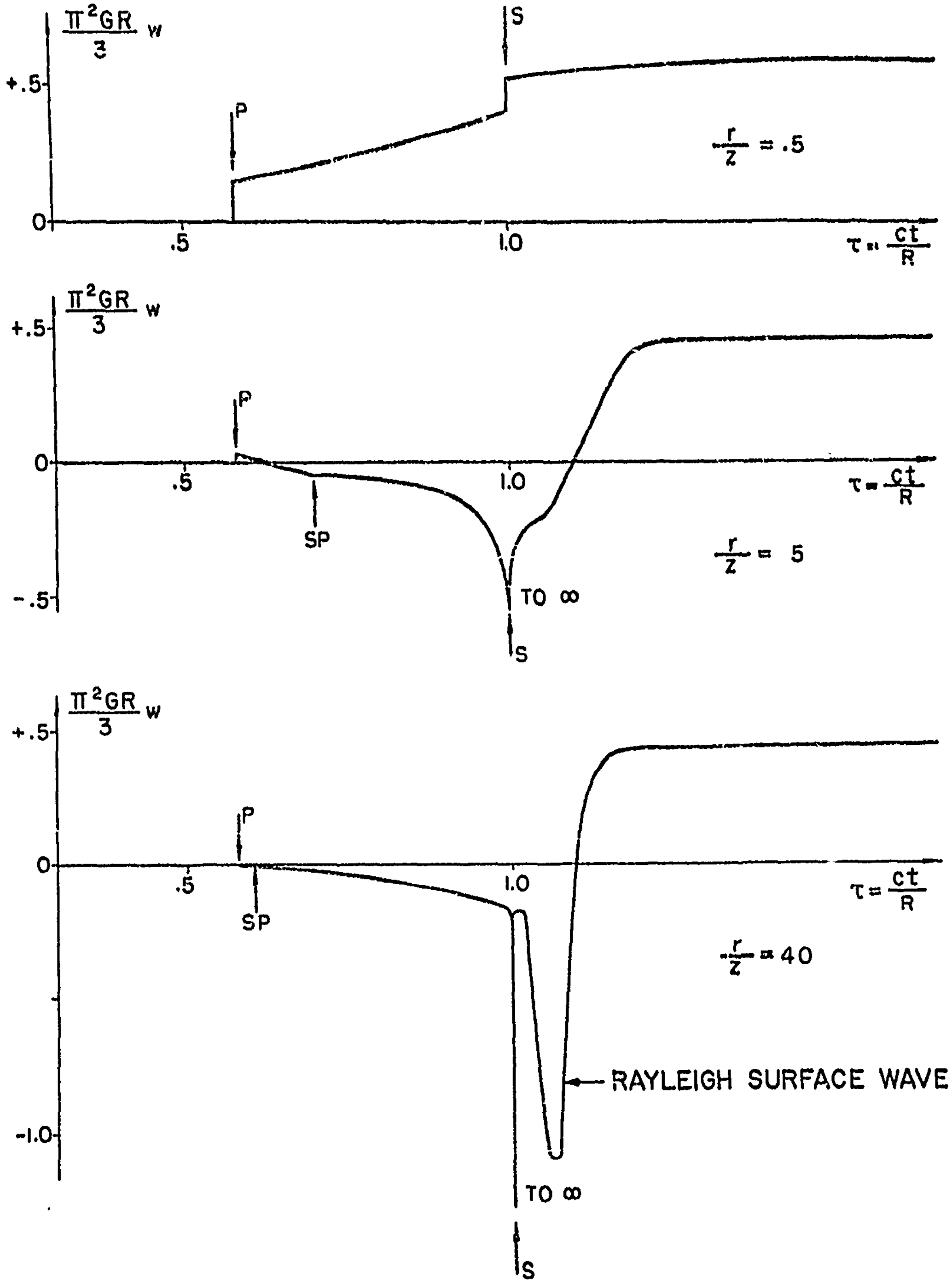

FIG. 3-3

DISPLACEMENTS OBTAINED BY PEKERIS AND LIFSON

IDEALIZED $w(h,\tau)$ FOR $\frac{r}{z} \leq \frac{1}{\sqrt{2}}$

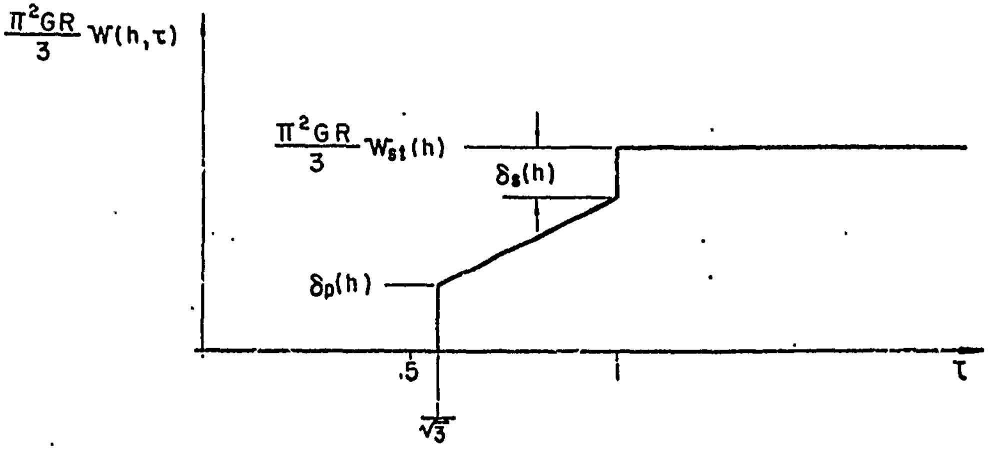

$$h = \frac{z}{R}$$

$$\delta_p(h) = \frac{\pi h \, (1 + 2h^2)}{6\left[(1 + 2h^2)^2 + 4h(1 - h^2)(2 + h^2)^{1/2}\right]}$$

$$\delta_s(h) = \frac{\pi(1 - h^2)(h^2 - 2/3)^{1/2}}{3\left[(2h^2 - 1)^2 + 4h(1 - h^2)(h^2 - 2/3)^{1/2}\right]}$$

$$\frac{\pi^2 GR}{3} W_{st}(h) = \frac{\pi}{24}(3 + h^2)$$

FIG. 3-5

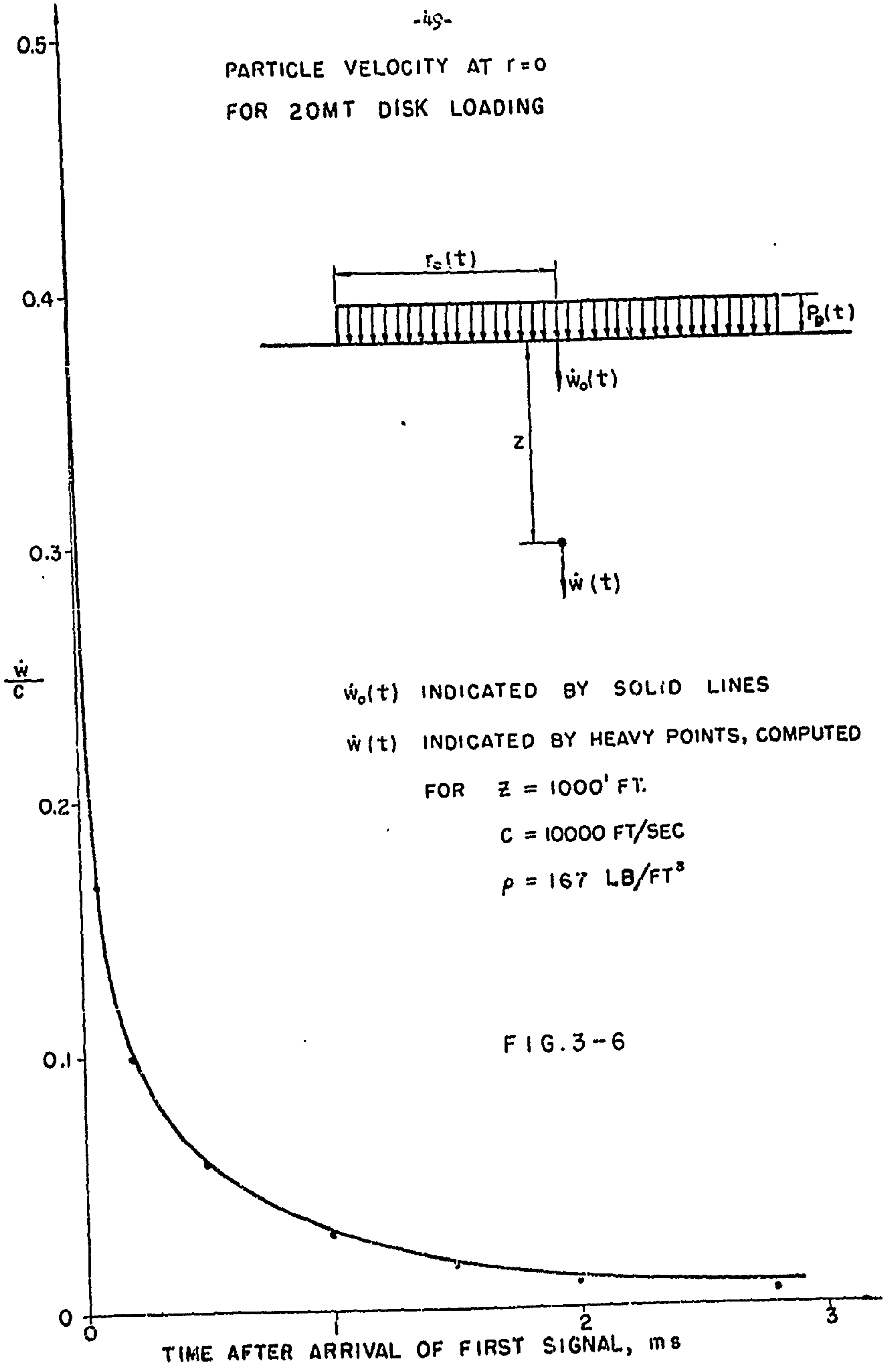

PARTICLE VELOCITY AT $r=0$
FOR 20MT DISK LOADING

$\dot{w}_0(t)$ INDICATED BY SOLID LINES

$\dot{w}(t)$ INDICATED BY HEAVY POINTS, COMPUTED
FOR $z = 1000'$ FT.
$C = 10000$ FT/SEC
$\rho = 167$ LB/FT^3

FIG. 3-6

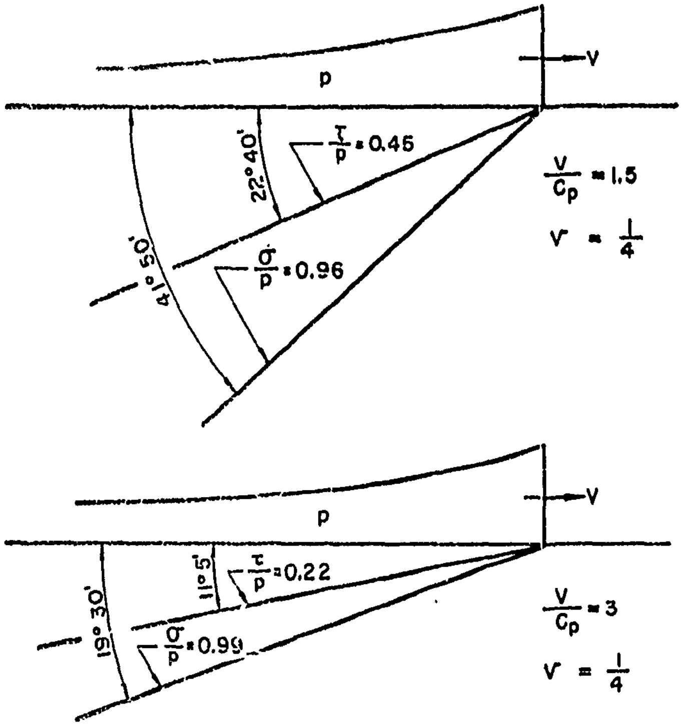
p
V
τ/p = 0.46
22°40'
41°50'
σ/p = 0.96
V/C_p = 1.5
ν = 1/4
p
V
11°5'
τ/p = 0.22
19°30'
σ/p = 0.99
V/C_p = 3
ν = 1/4

FIG. 3-7

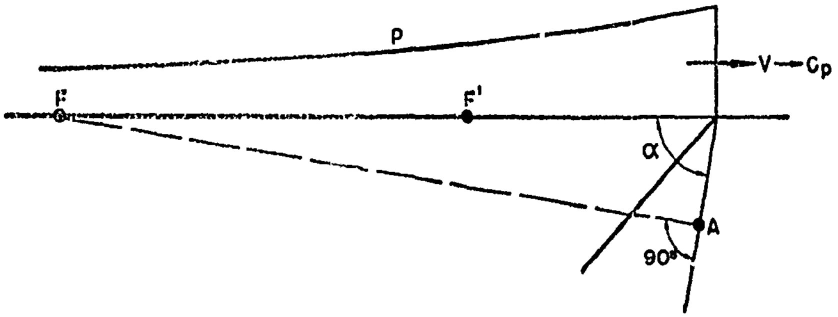
p
V
C_p
F
F'
α
A
90°

FIG. 3-8

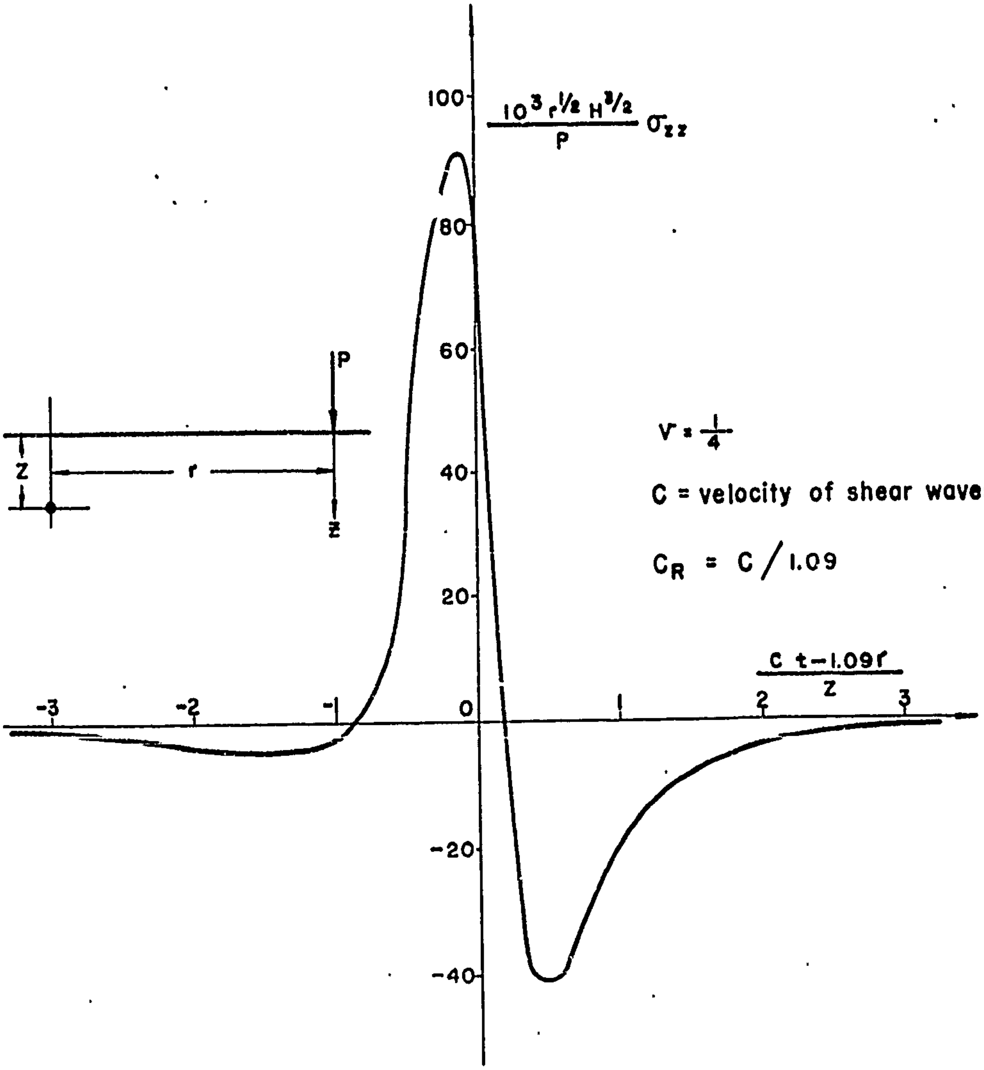
100
80
60
40
20
0
-20
-40
$\frac{10^3 r^{1/2} H^{3/2}}{P} \sigma_{zz}$
-3
-2
-1
1
2
3
$\frac{Ct-1.09r}{Z}$
P
Z
r
z
$\nu = \frac{1}{4}$
C = velocity of shear waves
$C_R = C/1.09$

FIG.3-9

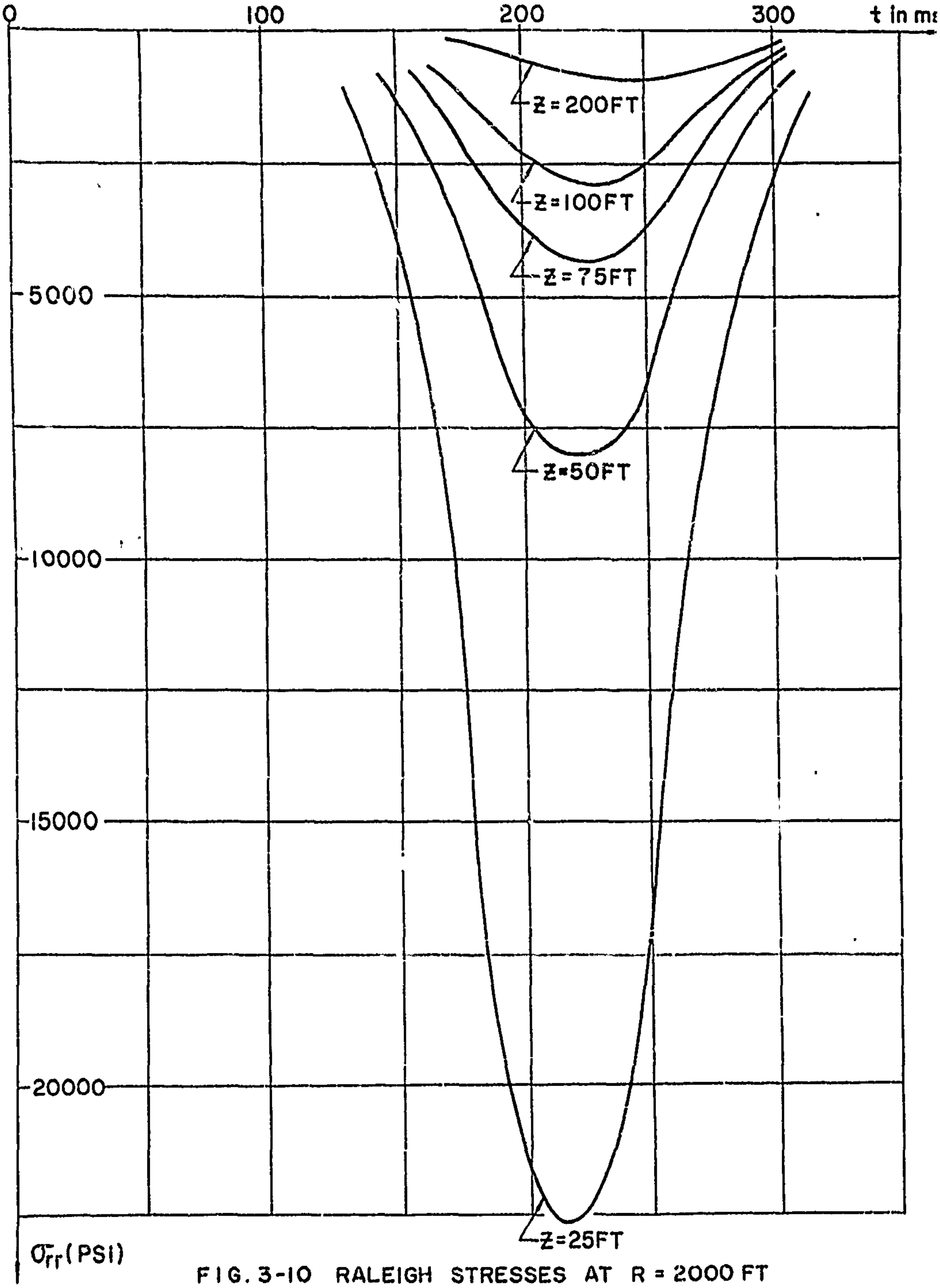

FIG. 3-10 RALEIGH STRESSES AT R = 2000 FT
(C = 10000 FT/SEC)

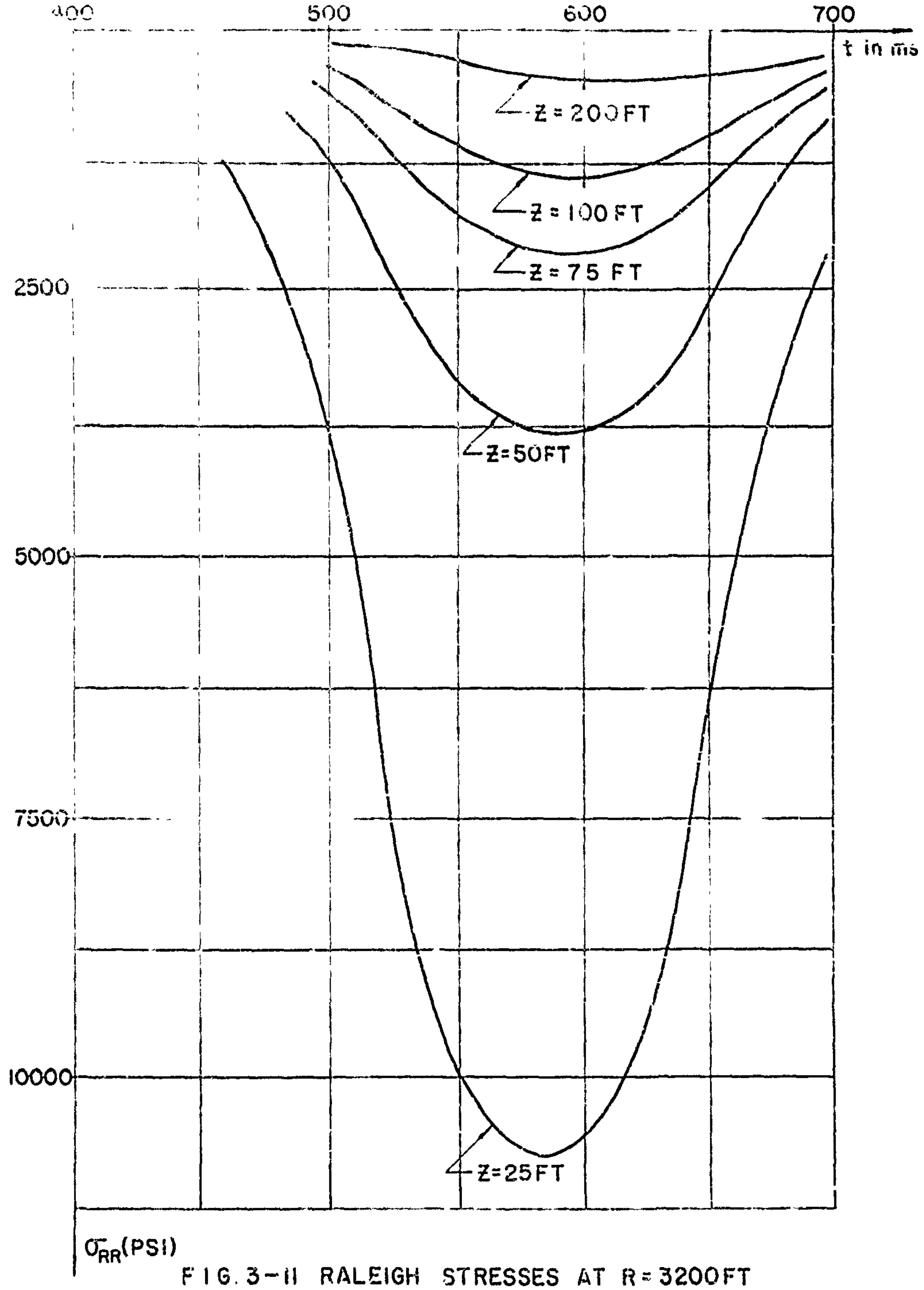

FIG. 3-11 RALEIGH STRESSES AT R = 3200 FT
(C = 6000 FT/SEC)

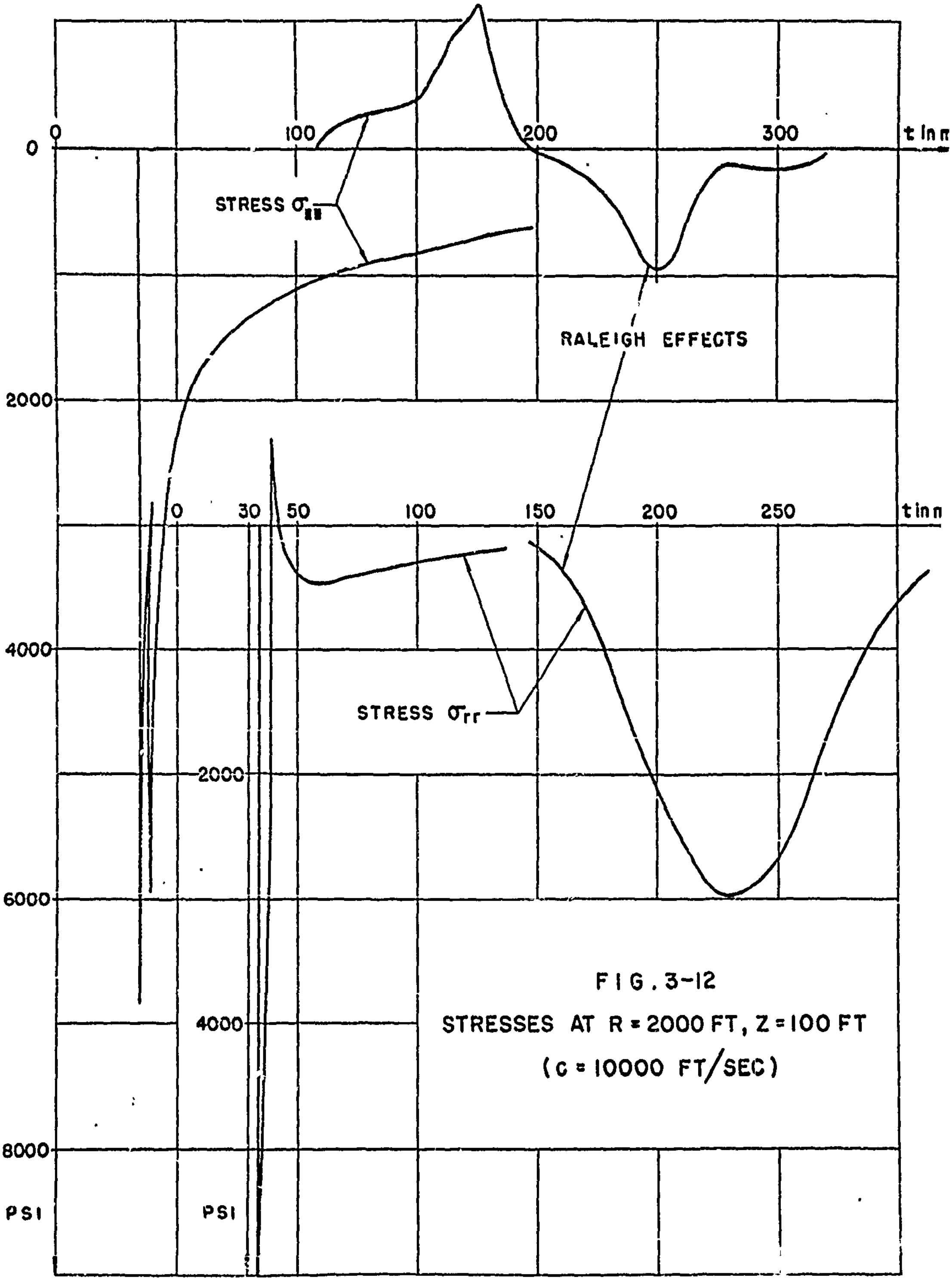

FIG. 3-12
STRESSES AT R = 2000 FT, Z = 100 FT
(c = 10000 FT/SEC)

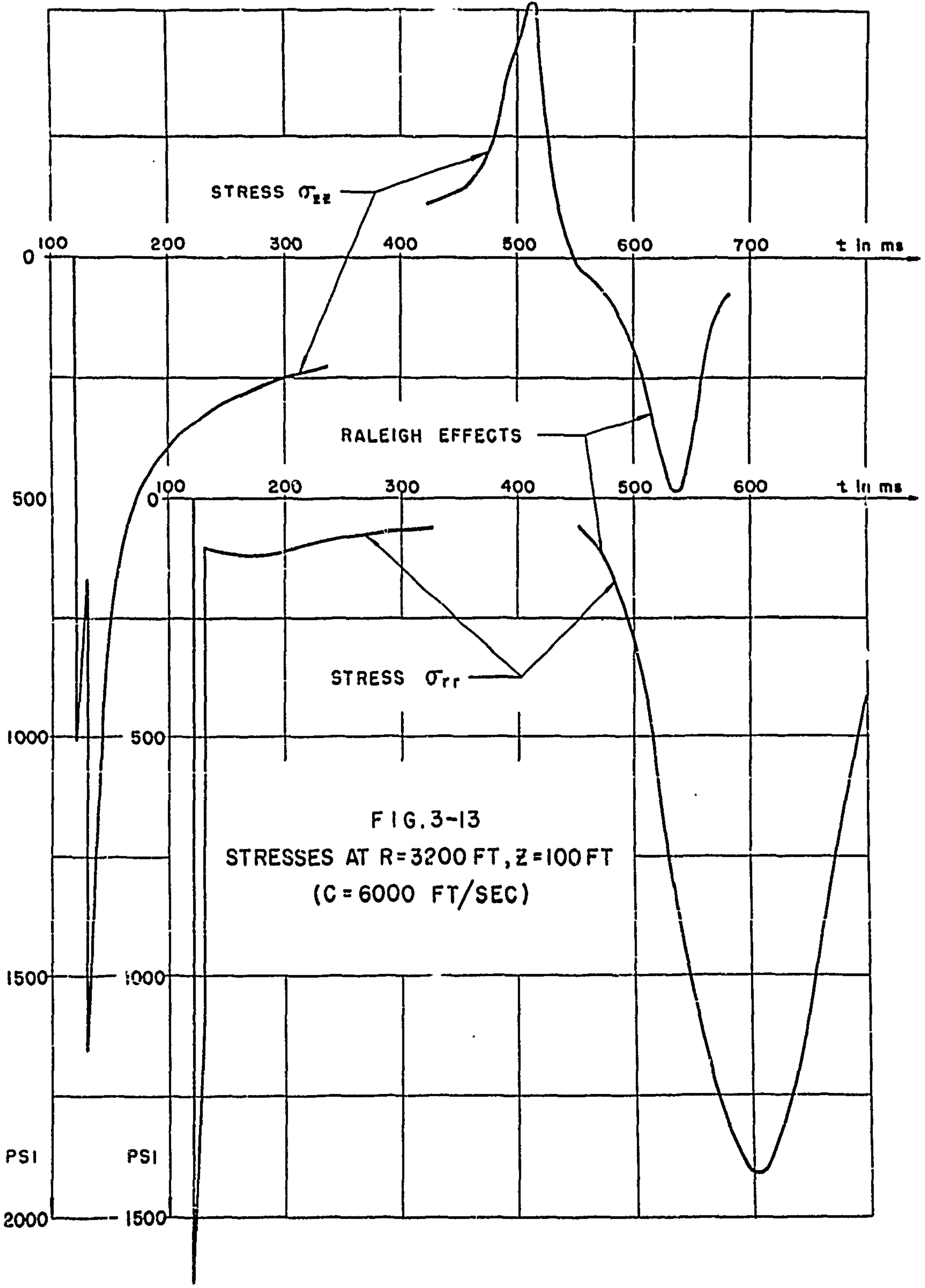

FIG. 3-13
STRESSES AT R = 3200 FT, Z = 100 FT
(C = 6000 FT/SEC)

4. LAYERED MEDIA

In spite of the fact that layering, or gradual changes of the medium with depth will have pronounced effects, only a few applicable solutions are available. This is due to the complexity of the problems of layered media. The steady state case of a pressure pulse progressing with constant speed V on the surface of a fluid layer above a fluid half space, Fig. (4-1) has been considered [3] without restriction as to the value of the velocity V.

The equivalent problem for a layered elastic solid has been solved [11] in an elementary manner, but only in the superseismic range, i.e. when V is larger than the sound velocities in either medium. Fig. (4-2) shows stresses σ_{zz} due to a step wave of constant pressure, when the velocities of $c_p(2)$ and $c^{(2)}$ in the lower medium are twice those in the upper one. It is seen that the vertical stresses σ_{zz} both at points in the upper and at points in the lower medium are increased by the reflections from the interface. If the applied pressure on the surface has a decaying history, a case which is treated in [11], the reflections may be less important, because they are added to a reduced stress from the direct signal. However, it must be emphasized that layering always increases the vertical stresses if the velocity of sound increases with depth. Reduction of pressure, indicating a protection, occurs only in the unusual case when the sound velocity decreases with depth. The reverse applies for vertical displacements and accelerations; they decrease due to layering if the sound velocity increases with depth. The approach used in Reference [11] can be extended to any number of layers, as long as the velocity V is larger than the sound velocities in any layer.

A problem involving a layer of fluid over an elastic half-space has been treated theoretically and experimentally in Reference [12], where the response from a point explosion in the layer has been obtained, Fig. (4-3). The emphasis in this paper was on waves propogated on the interface. It is experimentally possible to measure pressures in a fluid reliably, and good agreement between theory and experiment was obtained.

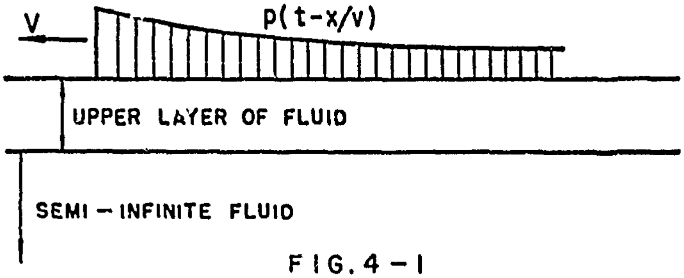
V
p(t-x/v)
UPPER LAYER OF FLUID
SEMI – INFINITE FLUID

FIG. 4-1

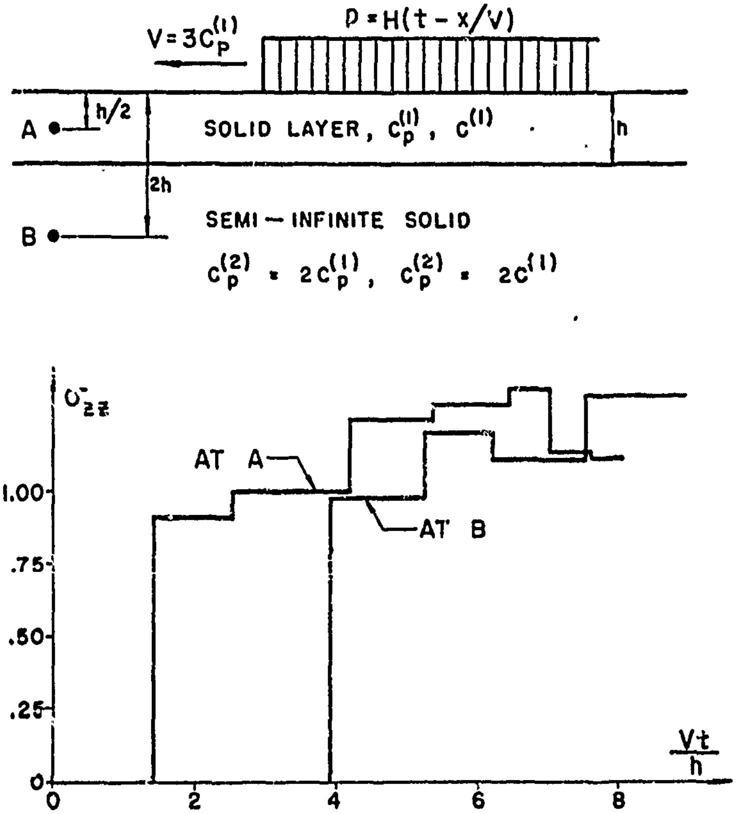
$V=3C_p^{(1)}$
$p = H(t-x/V)$
A
h/2
SOLID LAYER, $C_p^{(1)}$, $C^{(1)}$
h
2h
B
SEMI – INFINITE SOLID
$C_p^{(2)} = 2C_p^{(1)}$, $C_p^{(2)} = 2C^{(1)}$
σ_{zz}
AT A
AT B
1.00
.75
.50
.25
0
0
2
4
6
8
$\frac{Vt}{h}$

FIG. 4-2

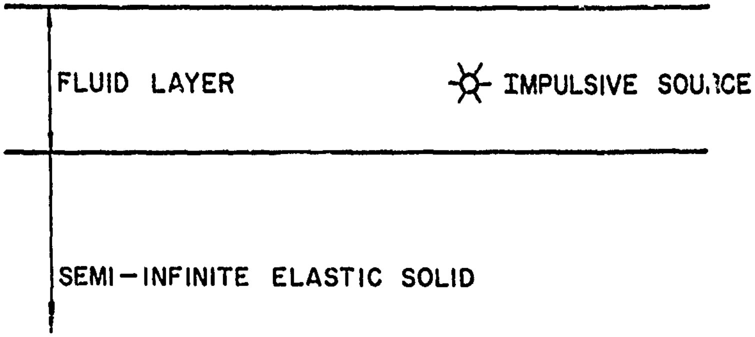

FIG. 4-3

5. ONE-DIMENSIONAL WAVE PROPAGATION IN A NON-LINEAR ELASTIC MEDIUM.

In Sections (2) and (3) it could be demonstrated that for the cases of linear behavior of fluids and elastic solids the assumption of one-dimensional wave propagation gives good results for the early part of the response of points below ground zero, $r \simeq 0$. This conclusion can be drawn qualitatively for any other medium if the velocity of wave propagation is much smaller than the velocity of the blast wave on the surface.

The early pressures near $r \simeq 0$ in actual situations are so high that non-linear effects must occur in any conceivable medium. It is therefore very important that the effect of pressure distributions of the type given in Fig. (1-1) can be determined as a problem in one-dimensional wave propagation, because such a problem--even if non-linear--can be handled by numerical methods. As a matter of fact some useful general conclusions can be drawn for a general class of non-linear elastic cases.

Consider a rod-like element of the half-space, Fig. (5-1). The "rod" has unit cross-sectional area and extends from the surface $z = 0$ to $z = \infty$. In the present situation the horizontal strains must vanish such that the area of the rod does not change. Let Fig. (5-2) be the appropriate stress-strain diagram of vertical stress σ versus vertical strain ϵ. For sufficiently small stress, say $\sigma < \sigma_L$, the law may be assumed to be linear. Let a decaying pressure pulse $p(t) = \sigma\ (0, t)$ be applied to the rod, such that the peak of $p(t)$ is larger than σ_L.

The response for the case described above could be computed numerically for any given stress-strain diagram. However, an equivalent problem has been considered in [34], Sec. II for a bi-linear (plastic-elastic) medium. The medium has the stress-strain diagram, shown in Fig. (5-3), which is a special case of the one indicated in Fig. (5-2). Fig. (5-4) shows the stress response for an example, which can be considered typical. The example was computed for an input pressure at $z = 0$ which had a peak of 184,000 psi, while at points below the surface, $z = 500$ feet and $z = 700$ feet, much smaller peak stresses were found. On the other hand, stresses at $t = 100$ ms or more after arrival at the lower levels were larger than the corresponding input stresses. (The reduction of peak stresses must be compensated by some increase of stresses at later time to satisfy the law of conservation of momentum.)

From the above example one concludes that in the non-linear case a reduction in peak pressure with depth (attenuation) is to be expected. This attenuation will however only continue until the peak pressure has dropped to the value σ_L, defining linear behavior in the stress-strain diagram Fig. (5-2).

As long as the applied load is such that the assumption of one-dimensional wave propagation is reasonable one must expect peak pressures of the magnitude of the stress σ_L defining linear behavior. Some idea of the level of σ_L can be gained from the simple tests on granites described in Appendix F. It is seen that the stress-strain relations are fairly linear, up to fracture on the 15,000 to 20,000 lb. level. In the case of plane wave propagation where transverse strains and therefore fractures similar to the tests are inhibited, it is to be expected that a nearly linear relation will hold up to even higher stresses, $\sigma_L > 20{,}000$ lb/in.^{2}

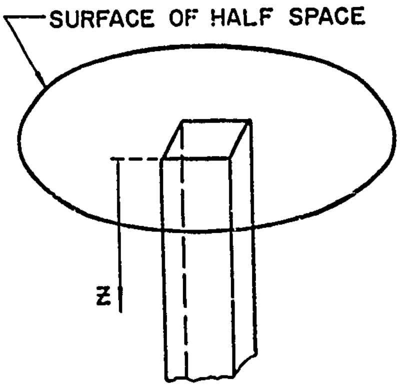

FIG. 5-1

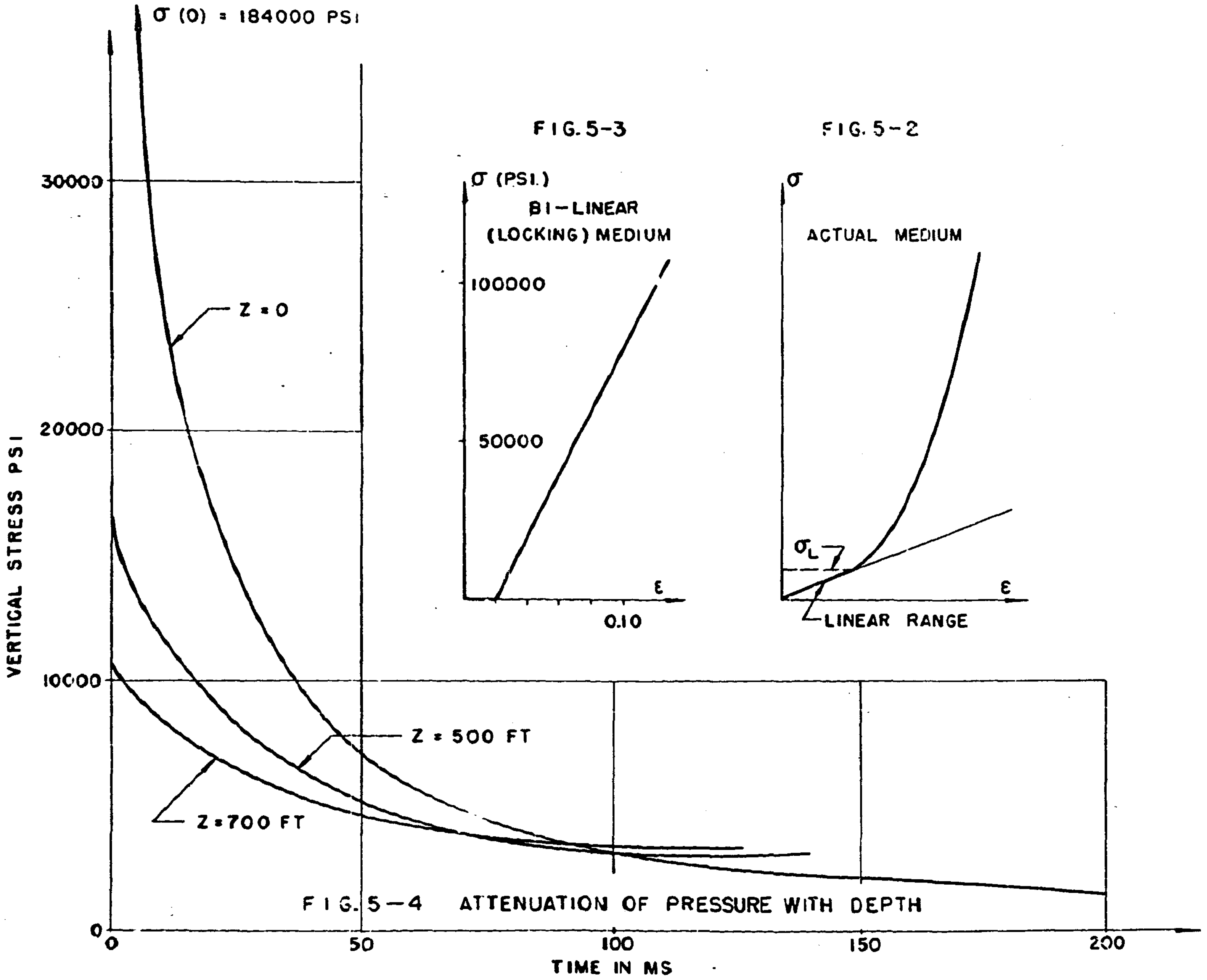

FIG. 5-3

FIG. 5-2

FIG. 5-4 ATTENUATION OF PRESSURE WITH DEPTH

6. USE OF THEORETICAL RESULTS FOR PREDICTIONS IN ROCK.

When comparing the complexity of an actual situation with the relative simplicity of the problems analyzed, it should be clear that theoretical solutions can not give a complete picture of stresses everywhere, but can--at best--permit a rough estimate of the stress field in certain locations at certain times. In view of the scarcity of experimental information, the theoretical solutions must be exploited by searching through qualitative reasoning for situations where they apply.

Before discussing specific locations, it is convenient to list major effects not appearing at present in the theoretical solutions. Concerning the effect of the explosion, only the air pressure on the surface has been considered, ignoring not only heat and radiation effects, but also effects due to the direct impact of the casing at the point of explosion. Concerning behavior of the material, high pressure levels requiring an equation of state are not within the range of this study, which eliminates the crater region from further consideration. On the stress level considered here, materials might not behave elastically but in a viscous or plastic manner, or exhibit other dissipative mechanisms. The fact that only small strains are considered should also be mentioned but is, on this stress level, not likely to be serious, as the strain will not exceed a few per cent.

a) Target locations below the crater.

Consider a target below the crater; it may be at twice the depth of the crater, Fig. (6-1). Without knowing the pressure history exactly, we know that very high pressures are propagated downward over an area exceeding the diameter of the crater.

While the formation of a crater is evidence that the situation is not really a "plane wave" situation, the fact that the crater is a flat bowl dissipative effects are not likely to be very important (which does not mean that solutions including such effects should not be sought). Estimates of the first signal based on steady state solutions, particularly in the superseismic range, should therefore be of real significance. The pronounced difference according to theory between superseismic and subseismic ranges, the former having no or negligible attenuation of peak pressure with depth, while the latter has pronounced attenuation, can be expected to be a real fact.

The situation concerning the second signal is much more uncertain, because it is due to forces acting in the crater region where the elastic theory can not possibly apply. The elastic theory predicts Rayleigh (surface) waves as the major signal to be received; now, the existence of such waves requires an interaction between direct and shear stresses, such that they do not occur in a fluid. At high pressures in the crater region the material is acting like a fluid, and one is led to conclude that the inception of surface waves will be inhibited, and that the elastic theory will grossly exaggerate surface waves. For this reason the Rayleigh stresses computed in Appendix B must be considered too high, presumably very much too high.(*)

There is a second reason why the Rayleigh stresses in actuality must be less than found from the elastic theory. If the stresses found were otherwise correct, those near the surface are larger than rocks are likely to withstand. It would not matter if such high stresses were nearly hydrostatic, but the state of stress in surface waves is inherently deviatory

---

(*) When arguing that the actual stresses due to surface waves are smaller than given by elastic theory, one should not be misled into the conclusion that they can always and everywhere be ignored. It should be remembered that at very large distances seismological experience proves beyond doubt that Rayleigh waves are the dominant effect. There must therefore be a transition range beyond which surface waves can not be ignored.

(i.e. having considerable shear deformation). The region near the surface ought therefore to be analyzed as an elastic-plastic medium which would lead to lower stresses.(*)

Pending further study the Rayleigh stresses obtained in Appendix B can be considered only as an upper bound. Such a bound is useful because whenever comparison of the first part of the response indicates that it exceeds the Rayleigh stresses in importance, the latter can be safely ignored. E.g., in the superseismic range this permits determination of a depth below which Rayleigh stresses are certain to be small compared to the early response.

(*) Any other dissipative effect would also lead to lower stresses due to surface waves. Such waves in a visco-elastic medium have recently been considered [15].

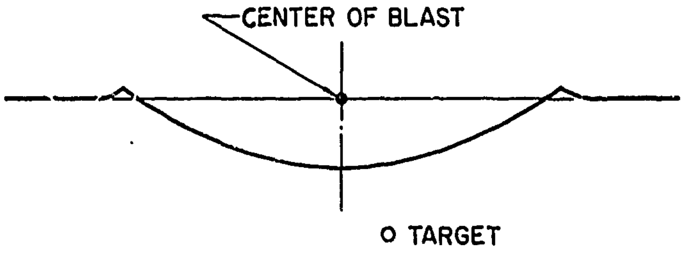

FIG. 6-1

7. WAVE PROPAGATION IN GRANULAR MEDIA.

The behavior of certain solids under very high intensity, confined or hydrostatic pressure is characterized by a non-linear stress-strain relation of positive curvature which, upon unloading, shows large permanent strains. This response is manifested at different pressure levels in various materials: at low pressures in foam-rubber, in the 100 to 16,000 psi range in granular soils and presumably at much higher pressures in porous or solid rocks.

A typical stress-strain diagram of this type is shown on Figure (7 1); this diagram can be idealized by various linear diagrams shown in Figures (7-2), (7 ·3) and (7-4).

Figures (7 2) (a),(b) and (c) show a class of materials known as locking media (a), or materials of limited compressibility, (b) and (c). These materials have the property of becoming essentially incompressible or rigid upon compression when a critical strain ϵ_c is reached. At that instant a sudden locking or compaction of the medium occurs, and upon unloading the permanent strain ϵ_c remains.

If a certain amount of residual elasticity exists after compaction or locking, the material can be represented by the bi-linear diagram shown on Figure (7-3). If the irreversible compaction proceeds gradually, the stress-strain relation is that of Figure (7-4). This material acts elastically on loading and unloads with a permanent set as shown in the figure.

Rather extensive literature is available on the static behavior of locking media, [24] and [25] and plane wave propagation in both locking media, [Figure 7-2 (a), (b) and (c)], and in the type of material shown on Figure (7-4) which has also been investigated ([26] and [27]). More recently, problems of wave propagation in bi-linear materials of the type shown in Figure (7-3) have been solved. Spherical waves in locking media are explored in References [29], [30] and [31].

Most of these investigations find application in researches connected with the prediction of ground shock effects due to thermonuclear blasts, [32] and [33], or are concerned with the detection of underground nuclear tests, [30] and [31]. An application to the design of invulnerable, deep underground shelters is considered in References [18] and [19], and a general discussion of these topics is found in Reference [34].

Some of the relevant results, such as shock-velocity and the attenuation of peak pressure intensities with depth may be summarized as follows:

If the surface of a semi-infinite locking medium of the type shown in Figure (7-2a) is subjected to a decaying pressure p(t) the shock velocity $\dot{z}$ of the front located at a depth z is given in [26] and [27] by:

$$\dot{z} = I[2\rho\epsilon_c \int I(t)dt]^{-1/2} \qquad (7\text{-}1)$$

where ρ is the density of the medium, and I, the impulse of the applied pressure, is

$$I = \int p(t)dt \qquad (7\text{-}2)$$

The amplitude of the peak stress σ_z is related to the depth z by:

$$\sigma_z = \frac{I^2}{\rho\epsilon_c} z^{-2} \qquad (7\text{-}3)$$

For a medium which shows a gradually irreversible compaction (Figure 7-4), the above quoted-reference gives the propagation velocity as:

$$c_o = (E/\rho)^{-1/2} = \text{constant} \qquad (7\text{-}4)$$

where E is the elastic modulus of the medium. The attenuation of the peak stress with depth follows the law:

$$\sigma_z = I c_o z^{-1} \qquad (7\text{-}5)$$

Numerical evaluation of the stresses and particle velocities in a locking medium, (Figure 7-2a), subjected to high intensity blast pressures discloses the following significant results [18].

(a) The intensity of peak stresses (and of the particle velocities) in locking media attenuates very rapidly with depth. (See Figure 7-5).

(b) The attenuation of these quantities is to a surprising degree insensitive to variations of the parameters of the medium. For example, at a high yield surface burst near ground zero, the intensity of stresses beyond a depth of 500 feet differs only slightly for materials which have a wide range of critical strains (ϵ_c = 0.02 to 0.10 as shown on Figure 7-5).

(c) The existence of residual elasticity has an equally slight influence: A locking medium with a critical strain of ϵ_c = 0.02 is compared with a bi-linear medium of identical critical strain but with a residual elastic modulus of $E = 10^6$ psi in Figure (7-6) and we note that the attenuation of peak stresses beyond about 500 feet of depth is not significantly affected. These phenomena have been found to exist for a rather wide range of variations for both parameters (ϵ_c and E) and are the subject of detailed investigations in Reference [28].

These conclusions are of interest because they show that the essential and significant attenuation of blast pressures can be anticipated in a large variety of dry granular soils. Consequently, the free field parameters should be predictable if a limited amount of information is available regarding subsurface conditions.

As mentioned previously the theory of spherical wave phenomena in locking media has been applied to study the effects of underground explosions. In [29] the effect of an exploding point mass is considered with a view towards exploring the effect of the so-called "direct ground-shock", (i.e. the exploding casing of the weapon) in a granular soil.

It is found that the spherical shock at a radius R propagates with the velocity:

$$\dot{R} = \dot{R}_o[1 + (\frac{R}{r_m})^3]^{-\mu} \tag{7-6}$$

where the kinetic energy of the mass M of the casing is:

$$\frac{1}{2} M\dot{R}_o^2$$

and the quantities:

$$r_m^3 = \frac{M}{4\pi\rho(\epsilon_c^{-3} - \epsilon_c^{-2})\epsilon_c^6} \tag{7-7}$$

and

$$\mu = \frac{1}{2} + \frac{1 - \epsilon_c^3}{6(\epsilon_c^{-1} - 1)} \tag{7-8}$$

are constant characteristics of the medium and of the casing.

It is expected that this work will also shed some light on the problem of a surface burst, as an early time approximation of the direct ground shock effect.

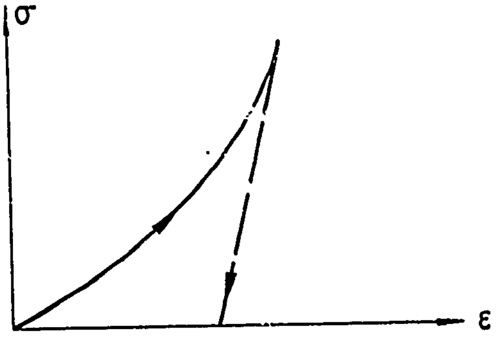

FIG. 7-1

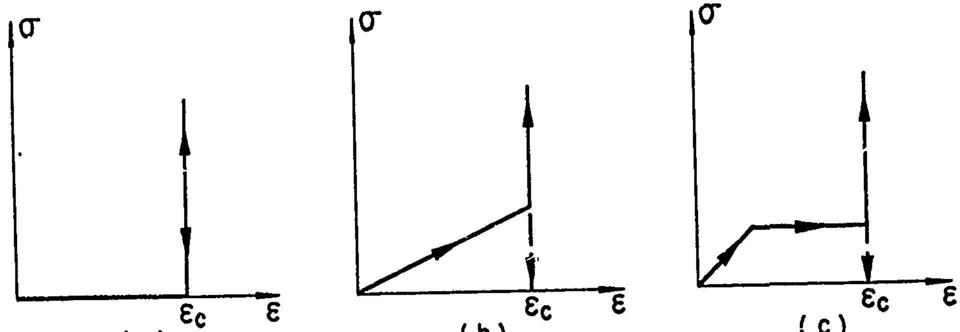

(a) (b) (c)

FIG. 7-2

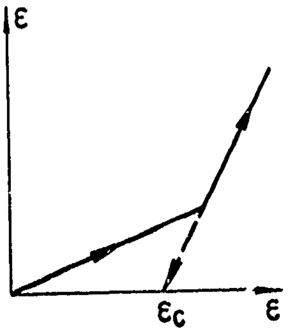

FIG. 7-3

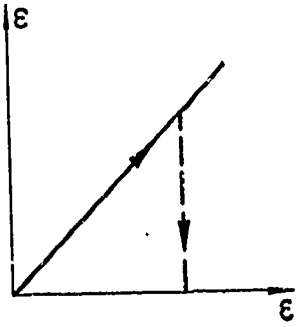

FIG. 7-4

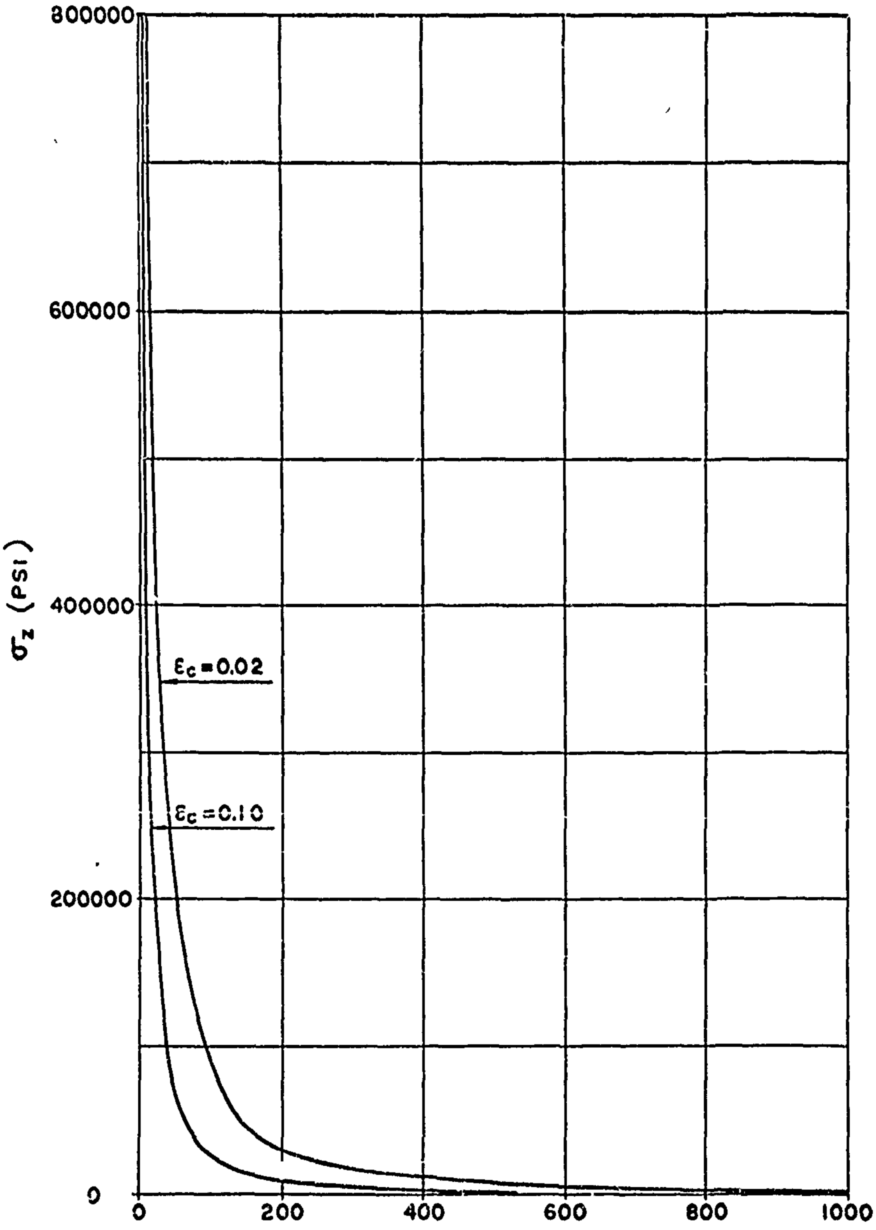
800000
600000
400000
200000
0
σ_z (PSI)
$\varepsilon_c = 0.02$
$\varepsilon_c = 0.10$
0
200
400
600
800
1000
z (FEET)

FIG.7-5

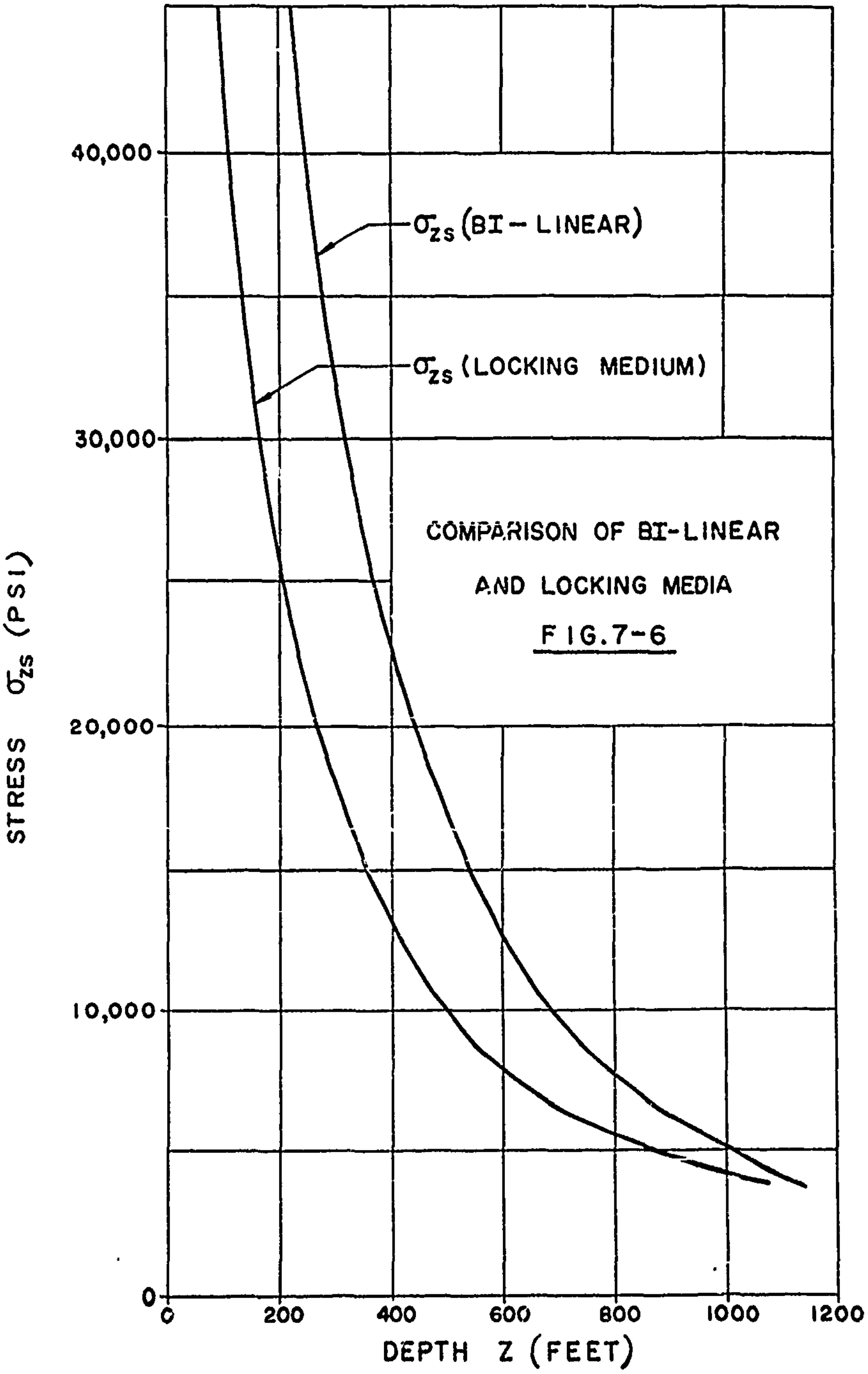

COMPARISON OF BI-LINEAR AND LOCKING MEDIA

FIG. 7-6

PART II

DIFFRACTION EFFECTS

DIFFRACTION EFFECTS

8. INTRODUCTION

Thermonuclear explosions on the surface of an elastic half-space produce a complex stress pattern in the medium. In the most general case, the circularly-symmetric surface pressures from the explosion, which expand radially outward from Ground Zero in space and decay in time, produce a stress pattern at points in the medium in which the two principal stresses change in magnitude and in direction with time. The diffraction of the stress field by a cavity containing a hardened underground installation must be considered with a view towards obtaining the following information:

1) Stresses produced by the dynamic loading of the cavity with a view towards determining the strength of the cavity as a whole. In addition, the velocities, displacements and accelerations of points on and near the cavity boundaries are required for the determination and evaluation of shock effects and for the establishment of failure criteria for the cavity and its contents.

2) Shock spectra for a) the total accelerations imparted to the contents of the cavity, and b) the relative displacements of the contents of the cavity (relative to the cavity boundaries) when the cavity is enveloped by the stress waves produced by the explosion. The contents of the cavity may be shock mounted and the shock spectra are required for an optimalization of the design of the installation.

The solution to the general problem of the diffraction of the rather complicated stress field by the cavity in an elastic medium can be constructed for cases of interest by the superposition of the results obtained from some basic less complicated problems which are considered in Part II. Specifically, the diffraction of the stress field produced by P (dilatational) and S (shear) waves respectively with plane wave fronts are considered. In both cases the general solution is obtained for a step pressure in time which can be used as influence coefficients to give the results for waves with arbitrarily time varying pressures by means of Duhamel integrals.

The solution of these problems (stresses, velocities and displacements) can be used to construct solutions for the general case in which the incoming stress history has a more complicated character.

Moreover, they are of direct use and importance in the superseismic range ($V > c_p$) in which the loading on the cavity has been shown to consist of P and S waves with plane fronts carrying pressure components which decay in time [see Appendix A]. For this range, the solutions represent an approximate answer to the actual physical problem and can be used directly.

The above theory has been determined with the assumption that the cavity containing the installation is not lined. Practically speaking, the problem of the cavity lining--structural or anti-spalling--is quite important in the design of these installations and must be studied. A method of attack in which the results obtained for unlined cavities are used as influence coefficients in integral equations for the corresponding solutions to cavities with linings is also developed in this report [Section 11].

Section (9) gives the results for stresses, velocities and displacements produced at the boundary of the cavity as it is enveloped by plane P and S waves. Curves are presented for the case in which the pressure inputs in the waves are step functions in time, as well as for waves with particular time decaying pressures produced by a hypothetical 20 MT surface burst. In addition, the superposition of the incoming P and S waves is shown for a particular tunnel location.

Section (10) contains the shock spectra curves for the total acceleration and relative displacement of installations which are shock mounted in the cavity. It is assumed that the equipment can be mounted in several different ways and shock spectra are presented for several cases of interest. Heretofore, shock spectra used in this type of design were computed from free field input pressures, and the effects of the diffraction of the waves by the cavity were neglected. The shock spectra of Section (10) include the diffraction effects and are consequently more appropriate; they will now supersede the free field spectra and should be of considerable use in obtaining more accurate design data for the shock mounting of the cavity contents.

Section (11) presents an outline of the theory by which the various results obtained for an unlined cavity can be used to determine the corresponding results for a cavity with a given elastic lining. Numerical solutions of the resulting integral equations are not yet available, but should be completed in the near future for several cases of interest.

Section (12) presents some general conclusions relative to the results obtained in Sections (9)-(11).

Following the format of Part I, the theoretical formulations of the work are presented in Appendices C, D, E, while the results are reported in Sections (9), (10), (11), (12). The results of some tests to determine the elastic properties of granite under static loading are given in Appendix (F). The following recurring symbols are adhered to in Part II of this report.

c_p Velocity of pressure (P) waves in a linear elastic solid.

c_s Velocity of shear (S) waves in a linear elastic solid.

The velocity c appearing in the abscissa of the various curves in Part II refers to the velocity of the incoming wave as shown in the figure or noted.

9. STRESSES, VELOCITIES, AND DISPLACEMENTS PRODUCED IN AN ELASTIC MEDIUM BY THE DIFFRACTION OF PLANE "P" AND "S" WAVES BY A CYLINDRICAL CAVITY

An infinitely long cylindrical cavity in an infinite elastic homogeneous and isotropic medium is acted on by a plane shock wave whose wave front is parallel to the axis of the cavity. The shock wave propagates through the medium with a constant velocity c_p ("P" wave) and envelops the cavity (Fig. 9.1). For generality, it is assumed that the direct stress components carried by the wave are $\sigma U(t)$ and $\epsilon\sigma U(t)$, which are respectively parallel and perpendicular to the direction of wave propagation.

The solution of this problem for the inputs $\sigma U(t)$, $(\epsilon = 0)$ or $\epsilon\sigma U(t)$ only, may be used to construct the solutions to problems in which the free field has a more general nature. For the superseismic range, in which a component of the input is actually a plane wave, the value of ϵ for a plane wave front must be taken as $\epsilon = -1/3$.

Preliminary results for the stress field produced at the boundary of the cavity by the incoming "P" wave have been reported in [17], [18], [19], while the complete plane strain solution to the problem has been given in [20]. The present paper extends these results to include both P and S waves. In addition, results are presented for the velocity and displacement fields produced in the medium at and near the cavity boundary. The theoretical development for the velocities and displacements are presented in Appendix D.

Although the true physical problem under consideration requires a semi-infinite medium with a roughly plane boundary at $z = 0$, it is easily shown [Ref. 18, Pg. 36] that in the range of practical interest, the plane boundary essentially has no effect during times of interest and the results obtained by considering the medium to be infinite will be satisfactory for tunnels where depth "D" is greater than 4 to 5 times the radius "a". For such installations, the major effects such as maximum hoop stresses, occur at the boundary of the cavity at times considerably shorter than the arrival time of the relief wave from the plane surface at $z = 0$.

a) Hoop stress produced at the boundary of a cavity [20].

Figs. (9-2)-(9-8) show the hoop stresses $\sigma_{\theta\theta}$ produced at points on the cavity boundary by various stress waves which envelop the cavity. The stresses at two points are presented: $\theta = 0^{\circ}$, the point at which the shock front first hits the tunnel; and $\theta = 90^{\circ}$, the point at which the maximum stress concentration is expected. In determining $\sigma_{\theta\theta}$ by the analytical procedure given in [20], only the terms $n = 0, 1, 2$ plus the free field stress components were included; the analytical justification for terminating the series after the $n = 2$ term is presented in [18], Pg. 41 and [20].

Fig. (9-2) shows the hoop stress at $r = a$, which is produced by an incoming plane shock wave with a step pressure distribution in time. The pressure component $\epsilon U(t)$ at right angles to the direction of propagation of the wave is taken equal to zero. The results obtained at long times must approach the well known static solution for a cylindrical hole in a uniaxial pressure field, i.e., a stress amplification at $\theta = 90^{\circ}$ of 3 (compression), while the stress at $\theta = 0^{\circ}$ is a tension equal in magnitude to unity. It is seen that the stress concentration is amplified by the dynamic loading in the ratio of 3.28 to 3 at 4 transit times, at $\theta = 90^{\circ}$ and 1.16 to 1.00 at $\theta = 0^{\circ}$. It may be noted that for a step pressure wave, the problem is essentially of a quasi-static nature; since the dynamic amplifications are small percentagewise. It is also of considerable interest to note that maximum stresses are produced at about four to five transit times of the shock wave across the cavity.

Fig. (9-3) shows the hoop stress at $r = a$ which is produced by an incoming plane shock wave which has no pressure in the direction of propagation of the wave and a pressure $\epsilon U(t)$ in the direction perpendicular to the propagation direction of the wave.

The results of Fig. (9-2) and (9-3) may be used to construct, by suitable integrations, solutions for cases in which the free field pressure is of a more general nature.

Fig. (9-4) shows the stress $\sigma_{\theta\theta}$ at $\theta = 0^\circ$ and $\theta = 90^\circ$ for a plane step shock wave with a plane front progressing with a velocity c_p, i.e. the standard P wave of linear elasticity theory. The requirement of a plane front necessitates a transverse pressure component with $\epsilon = -1/3$ i.e., $-1/3\ U(t)$ (Fig. 9-1) as well as a pressure $U(t)$ in the direction of wave propagation. For the dynamic loading, the stress amplifications are from 2.667 to 2.92 at $\theta = 90^\circ$ (compression) and from 0.00 to +0.11 at $\theta = 0^\circ$ (tension). These results may be used directly to obtain meaningful results in the superseismic range in which the waves which envelop the cavity are essentially plane waves.

The hoop stress $\sigma_{\theta\theta_s}$ produced by a step shock wave may be used as an influence function to determine the corresponding stress produced by a wave with a time varying pressure, $P(t)$, by the Duhamel integral(*) (Fig. 9-5).

$$\sigma_{\theta\theta} = P_0 \sigma_{\theta\theta_s} + \int_0^t \frac{dP(\tau)}{d\tau} \sigma_{\theta\theta_s} (t-\tau)\, d\tau \qquad (9\text{-}1)$$

To illustrate the above procedure, Figs. (9-6)-(9-7) present the hoop stresses produced by plane waves with decaying pressure time histories.

The pressure time histories of the P waves which envelop the cavity are taken as those produced on the surface by a 20 MT surface burst at the 6500 psi (2400 ft. from G.Z.) contour and the 2000 psi (3200 ft. from G.Z.)

(*) Because, only a limited number of modes have been used in determining the stress due to the plane shock wave, the Duhamel integral should not be applied when the pressure-time history, $P(t)$, contains significant high frequency components with time constants of less than 1/2 of one transit time.

contour. These pressure time curves have been given by Brode [1]. The cavity is considered to have a radius of 17.5 ft. in an elastic medium in which $c_p = 17,300$ ft/sec and $c_s = 10,000$ ft/sec.

Fig. (9-6) gives the stress $\sigma_{\theta\theta}$ at $\theta = 0^o$ and $\theta = 90^o$ for a plane P wave with a Brode pressure input with $P_o = 2000$ psi. Due to the decay of the pressure with time, the Duhamel integral shows a maximum compressive stress of 4500 psi at $\theta = 90^o$ while the tension at $\theta = 0^o$ is 290 psi. Fig. (9-7) shows the corresponding curves for a pressure input with $P_o = 6500$ psi. The maximum compressive stress at 90^o is 12,300 psi, while the tension at $\theta = 0^o$ is 930 psi. It is of interest to note that the amplification of the compressive stress over P_o at $\theta = 90^o$ was 2.25 for the 2000 psi loading and 1.89 for the 6500 psi loading, as compared to 2.92 for a step pressure loading. Since the pressure-time decay for the 2000 psi wave was considerably slower than that for the 6500 psi wave, the hoop stresses are closer to those for a step wave.

Fig. (9-8) shows the hoop stress at $\bar{\theta} = 0^o$ and $\bar{\theta} = 45^o$ for a plane step shear wave with a plane front and a constant velocity c, i.e. the standard S wave of linear elasticity theory. At long times, the stress approaches the static solution for a cylindrical hole in a bi-axial pressure field which produces the shear stress distribution which is carried by the wave; i.e. a stress amplification at $\bar{\theta} = 45^o$ of 4 (compression). It is seen that the stress is amplified by the dynamic loading in the ratio of 4.37 to 4 at 45^o and t = 4 transit times, and .112 to 0 at $\bar{\theta} = 0^o$. It may be noted that as in the case of the P wave enveloping the cavity, the problem for a step pressure input is essentially quasi-static in nature (since the dynamic amplifications are small percentagewise) and that maximum hoop stresses are produced about two to three transit times of the S wave across the cavity. The theoretical results for the diffraction of the S wave by the cavity can be derived from the theory for the P wave; this development is given in Appendix (C).

In the superseismic range ($V > c_p$), the pressure waves that propagate through the medium are standard P and S waves with plane fronts and propagation velocities c_p and c_s respectively. These waves can be considered to have the same pressure-time history as the surface pressure, and amplitude factors which are given by Fig. (A-2), Appendix A. The P and S waves are inclined to the surface by the angles $\alpha = \sin^{-1} \frac{V}{c_p}$ and $\beta = \sin^{-1} \frac{V}{c_s}$, respectively. If the cavity is located at a sufficient depth [see Sec. 6] so that surface wave effects are negligible, one can obtain a realistic picture of the stress build-up at the cavity boundary by superimposing the incoming P and S waves with their proper amplitude factors and time delays (due to different angles of inclination and different velocities of propagation).

As an example of the superposition procedure described above, consider a cavity of radius a = 17.5 ft. in an elastic medium in which $c_p = 17,300$ ft/sec and $c_s = 10,000$ ft/sec. The cavity is located at a depth of 500 ft. at the 6500 psi surface pressure contour from a 20 MT surface burst, i.e., at a distance of about 2000 ft. from Ground Zero. The air shock velocity at this distance is about 22,000 ft/sec; this corresponds to a Mach number $M = \frac{V}{c_p} = 1.27$. From Appendix A, the P wave has an amplitude factor of 0.97 and is inclined at an angle $\alpha = 51^{\circ}$-54' to the horizontal surface, while the S wave has an amplitude factor of 0.53 and an angle of inclination of $\beta = 26^{\circ}$-48'. [See Fig.(9-9)] Fig. (9-10) shows the hoop stress which is produced at various points on the cavity boundary by the superposition of the P and S waves with their appropriate time factors. Due to the difference in propagation velocities of the two waves, the delay time between the arrival of the P and S waves is considerably in excess of 5 transit times.

Consequently, by the time the shear wave arrives at the cavity, the hoop stresses produced by the P wave have decayed sufficiently so that the peak of the sum of the stresses produced by the two waves ($\theta \simeq 20^{0}$) is still lower than the peak hoop stress at $\theta = 90^{0}$ produced by the P wave at early times, before the arrival of the S wave. It may be noted that the maximum peak stress of 11,930 psi (compression) is in excess of the allowable stress which a granite rock could reasonably be expected to carry; therefore, one must consider lower pressure contours for the case of unlined cavities.

Fig. (9-11) shows the stress $\sigma_{\theta\theta}$ at $\theta = 0^{0}$ and $\theta = 90^{0}$ for a plane P wave with a constant velocity of propagation, $c_p = 10,393$ ft/sec. [c = 6000 ft/sec.] and a pressure time history corresponding to the surface pressure at the 3200 ft [2000 psi] contour. The air blast at this contour has a velocity of 12,100 ft/sec., thus making the case superseismic with a Mach number of 1.17 and consequently an amplitude factor of 1.0 in the P wave.(*) The cavity has a radius, a = 17.5 ft. The maximum hoop stress is produced at $\theta = 90^{0}$ and has a magnitude of 4500 psi. This is a reasonable stress for a good granite to carry and one may conclude that a reasonable pressure limit for feasible underground installations will be in the neighborhood of the 2000 psi contour for the hypothetical 20 MT surface burst under consideration.

<u>Comparison with the results of Ref. [21].</u>

The analysis presented in Sec. (9) is based on the mode approach requiring an expansion of the stresses as a function of θ in a Fourier series. In the response to a step wave, the higher terms of the series could be ignored, and only the terms up to and including n = 2 were used. It is

---

(*) See Appendix A, Fig. (A-2). As pointed out, the steady-state solution for a Mach number so close to unity may not be very accurate and the actual hoop stresses at the points in question will be somewhat lower.

interesting to note that results are available from an alternative analysis, which permit checking of the present results over part of the circumference of the tunnel.

The alternative analysis [21] is also approximate; it applies only for limited values of the angle $|\theta| \leq 60^\circ$. The hoop stress $\sigma_{\theta\theta}$ taken from Fig. (7) of Ref. [21] is plotted in Fig. (9-12). This figure also shows the peak values of this stress $\frac{\sigma_{\theta\theta}}{\sigma}$ found by the present analysis(*) for $\theta = 22.5^\circ$, 45°, 60° and 90°. It is seen that the values for 22.5° and 45° agree quite well; for 60° the present analysis gives nearly 10% more stress than Ref. [21]. As the latter becomes more and more approximate as θ increases, the present theory is believed to be the better value. Finally, for $\theta = 90^\circ$, Ref. [21] gives no result at all, but states an extrapolation that the maximum value of $\frac{\sigma_{\theta\theta}}{\sigma}$ is about 2. The present analysis indicates that this extrapolation was not justified, the actual value being about 3.

It is easily seen that the maximum stress $\frac{\sigma_{\theta\theta}}{\sigma}$ for a step wave can not possibly be 2, but must be larger than 2. This can be concluded from the fact that the dynamic peak stress must be larger, or at least equal to the static peak stress. The latter is $\frac{\sigma_{\theta\theta}}{\sigma} = 2.52$ for $\nu = 0.33$ and 2.67 for $\nu = 0.25$.

To find the maximum amplification of stress for a step wave, or for a decaying wave with a decay constant of more than one half of a transit time, it is therefore appropriate to use the present analysis rather than the extrapolation in [21]. To find the response due to pressure waves which have very fast decays, the present mode approach is not suitable, but the approach of [21] could be used instead. Numerical work for such a purpose, considerably beyond that presented in [21], would be required.(**) Moreover,

---

(*) Note that Ref. [21] and the present analysis use a different value of Poisson's ratio, i.e. $\nu = 0.33$ and $\nu = 0.25$, respectively.

(**) An estimate of the pressure at early times, given in [18], pp. 42-43, is also available and may sometimes suffice.

it should be noted that situations in which the pressure decay is sufficiently fast such that the present analysis becomes unsuitable, will occur only very close to Ground Zero, i.e., in a region of extremely high pressure.

b) Velocities and displacements produced at points in the elastic medium.

The displacement and velocity components w, v, $\dot{w}$ and $\dot{v}$ which are produced at points in the elastic medium by a plane step shock wave are given by Eq. (34)-(37), Appendix D. Numerical results are presented for these quantities at points on the cavity boundary, $r = a$. As in the case of the stresses, the velocities and displacements produced by a step shock wave may be used as influence functions to determine the corresponding quantities produced by a wave with a time varying pressure P(t), by a Duhamel integral similar to Eq. (9-1).(*) In turn, these results can be used as input functions for the determination of shock effects which are imparted to shock mounted installations within the cavity. They will be used in the determination of the acceleration and displacement shock spectra which are presented in Section (10).

Fig. (9-13)-(9-14) show the displacements and velocities produced by a plane step shock wave at the boundary points, $\theta = 0^\circ$ and $\theta = 90^\circ$. At these points, the motion is purely radial, i.e. v and $\dot{v} = 0$. More comprehensive results are given in Fig. (7)-(8), Appendix D, in which the velocities $\dot{w}$ and $\dot{v}$ are given for other points on the cavity boundary.

The rigid body translational motion of the cavity boundary in which the cavity maintains its cylindrical shape and translates in the direction of the incoming step shock wave, is extracted from the total motion in Sec. (6), Appendix D. Fig. (9-15) shows the rigid body displacement, velocity and

---

(*) See Appendix (E), Part III-a, for the formal derivation of expressions for the velocities and displacements produced at points on the cavity boundary by waves with Brode pressure inputs.

acceleration of the cavity boundary, under the step pressure shock wave loading. These results may also be used as influence coefficients in Duhamel integrals to obtain corresponding quantities produced by shock waves with time varying pressure histories. Results of this type for waves with Brode pressure inputs, will be used as input functions for the determination of acceleration and displacement shock spectra in Section (10).

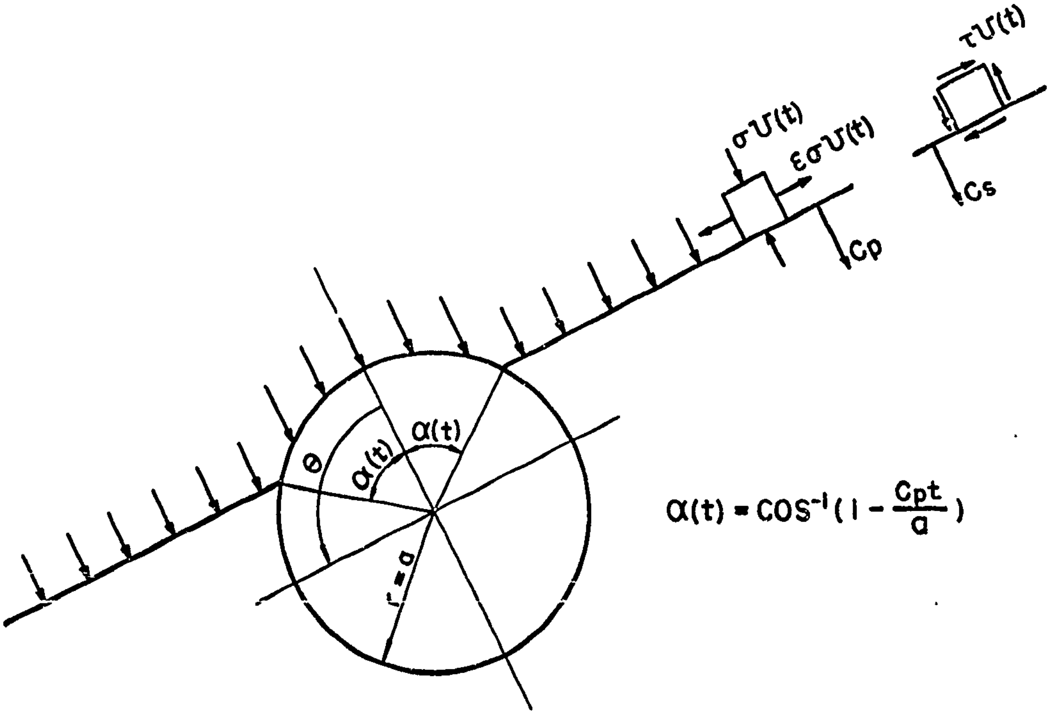

FIG. 9-1

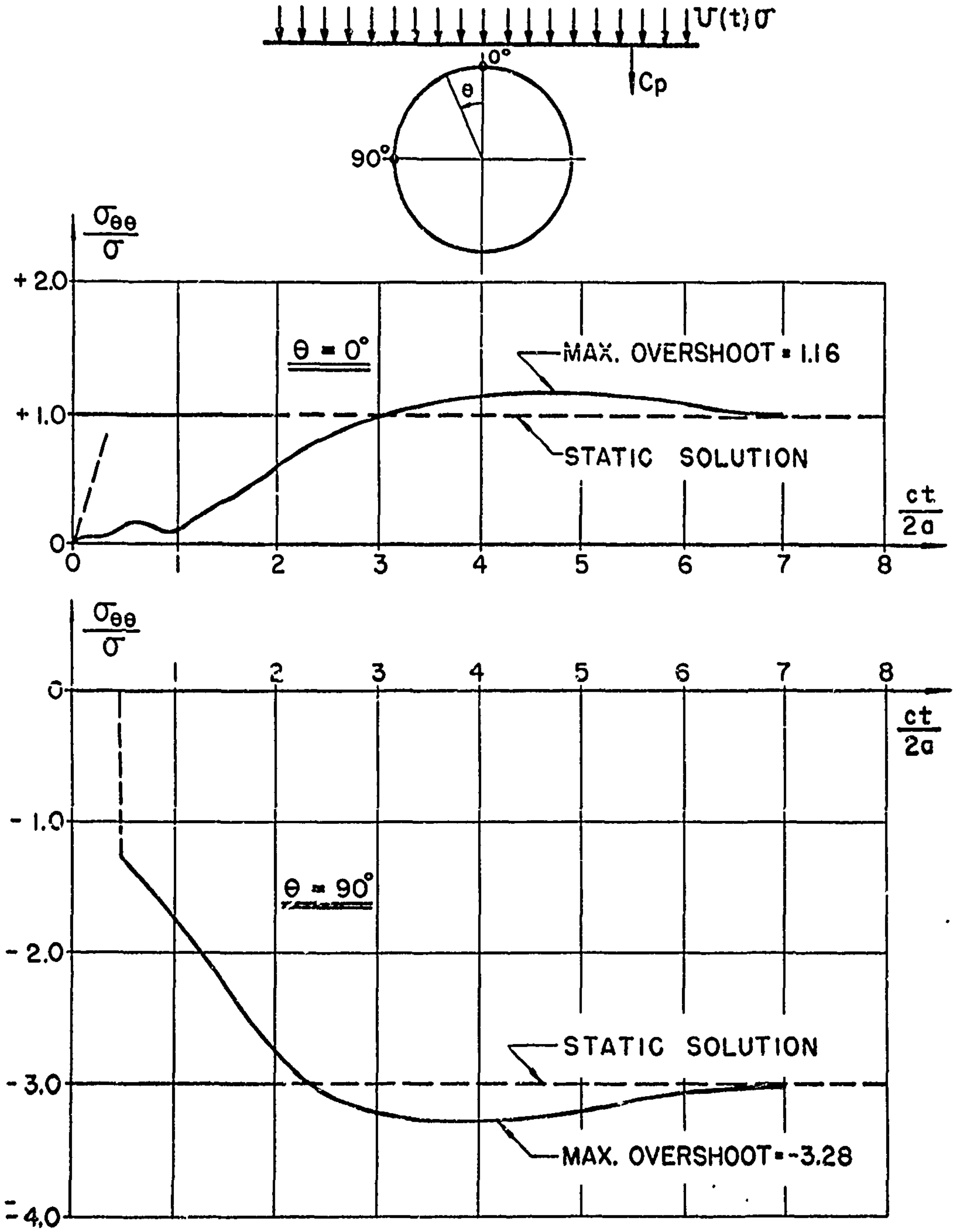

FIG. 9-2 INCOMING STEP PRESSURE $\sigma U(t)$; $\varepsilon = 0$

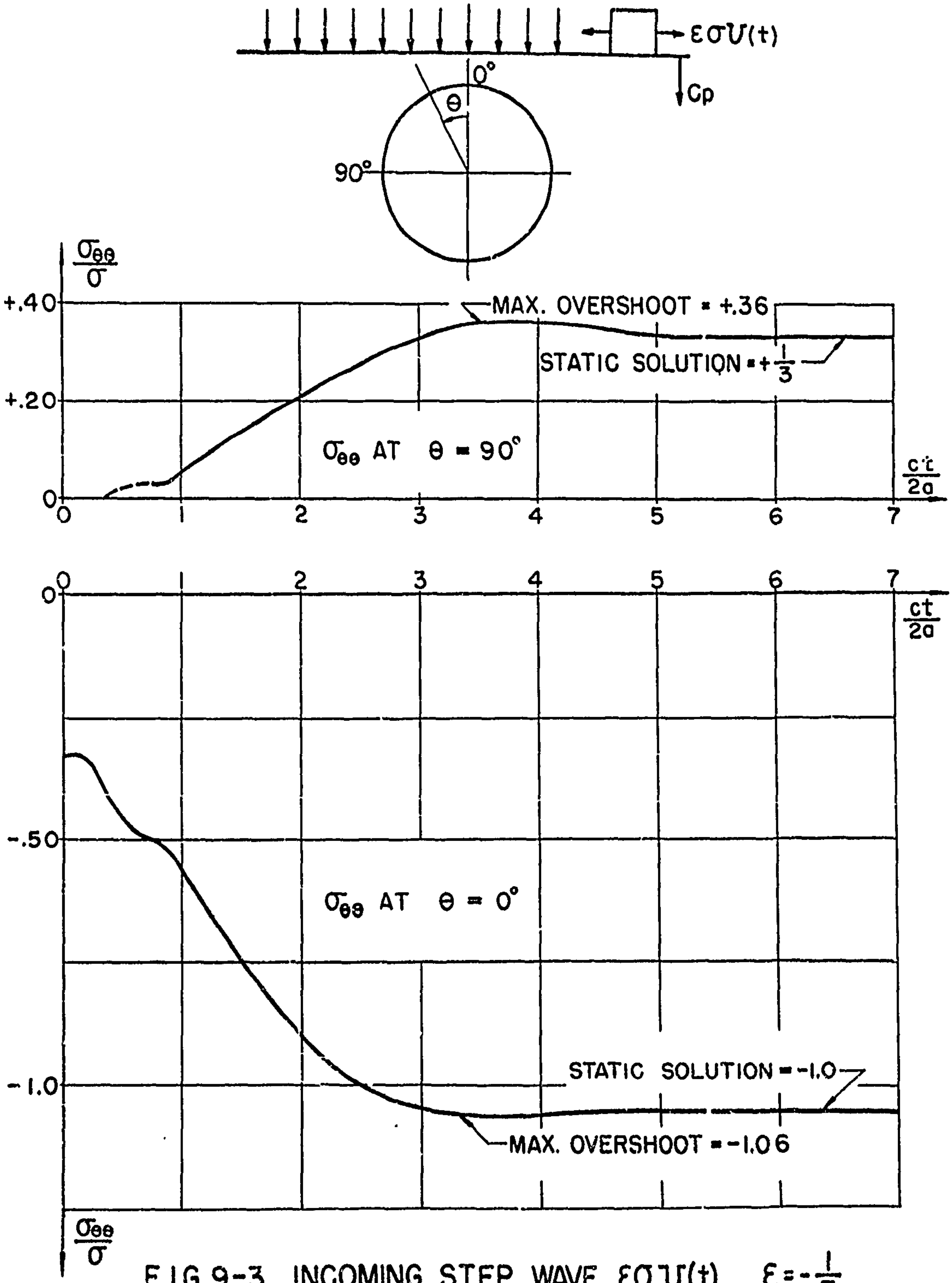

FIG.9-3 INCOMING STEP WAVE $\varepsilon\sigma U(t)$, $\varepsilon = -\frac{1}{3}$

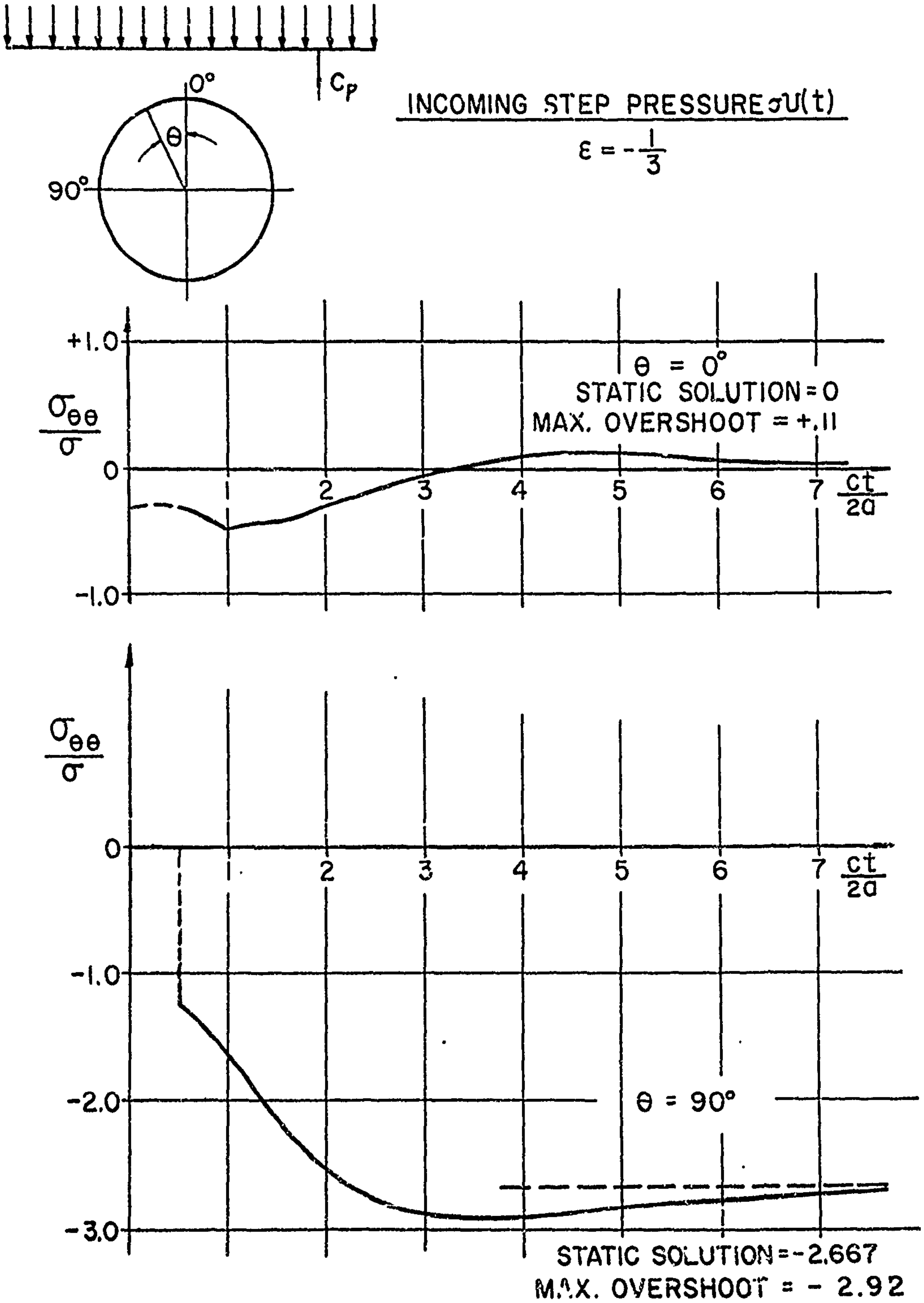
INCOMING STEP PRESSURE σU(t)

$\varepsilon = -\frac{1}{3}$

FIG. 9-4

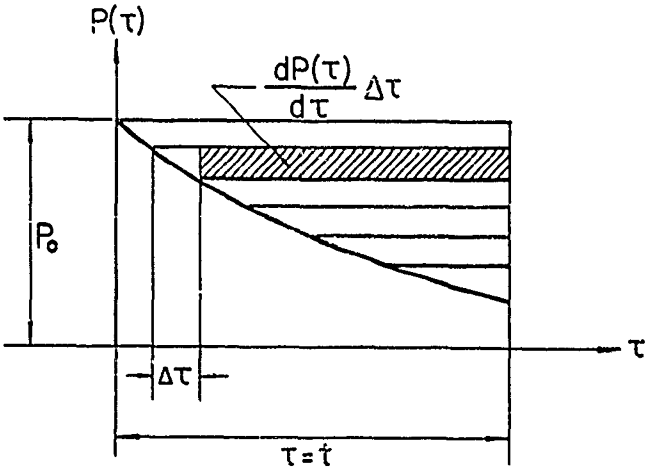

FIG.9-5 DUHAMEL INTEGRAL

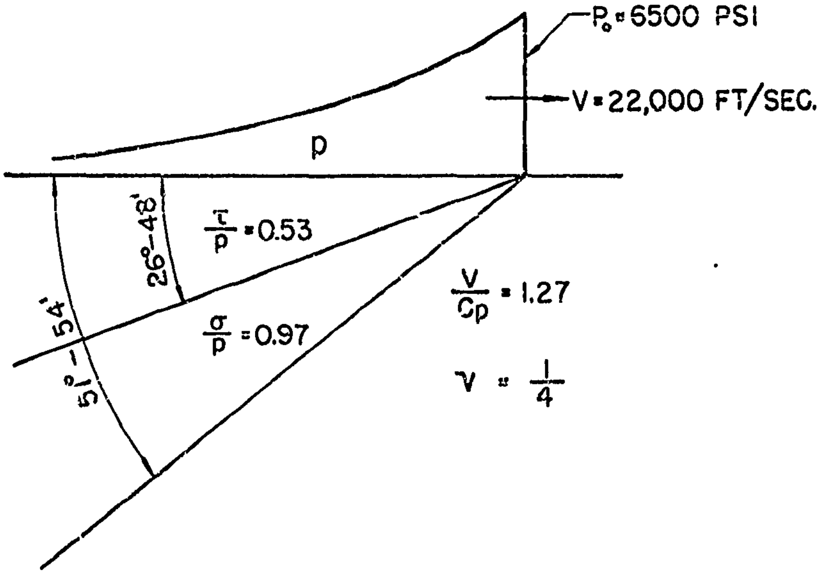

FIG.9-9

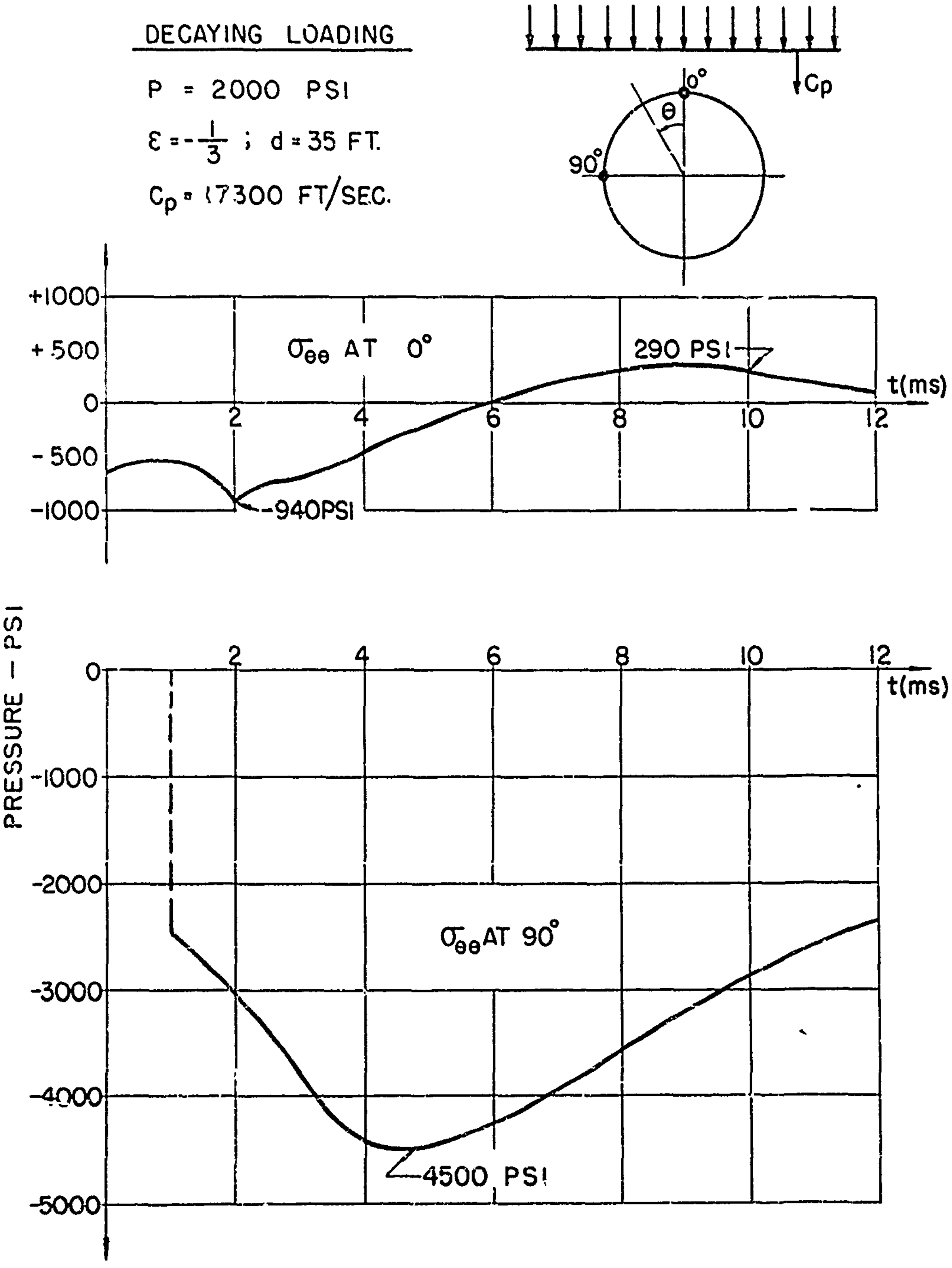
DECAYING LOADING
P = 2000 PSI
ε = -1/3 ; d = 35 FT.
Cp = 17300 FT/SEC.
0°
θ
90°
Cp
+1000
+500
0
-500
-1000
σθθ AT 0°
290 PSI
-940PSI
t(ms)
2
4
6
8
10
12
PRESSURE — PSI
0
-1000
-2000
-3000
-4000
-5000
σθθ AT 90°
-4500 PSI
t(ms)

FIG. 9-6

DECAYING LOADING

P_0 = 6500 psi

$\epsilon = -1/3$, d = 35 ft.

c_p = 17,300 ft./sec.

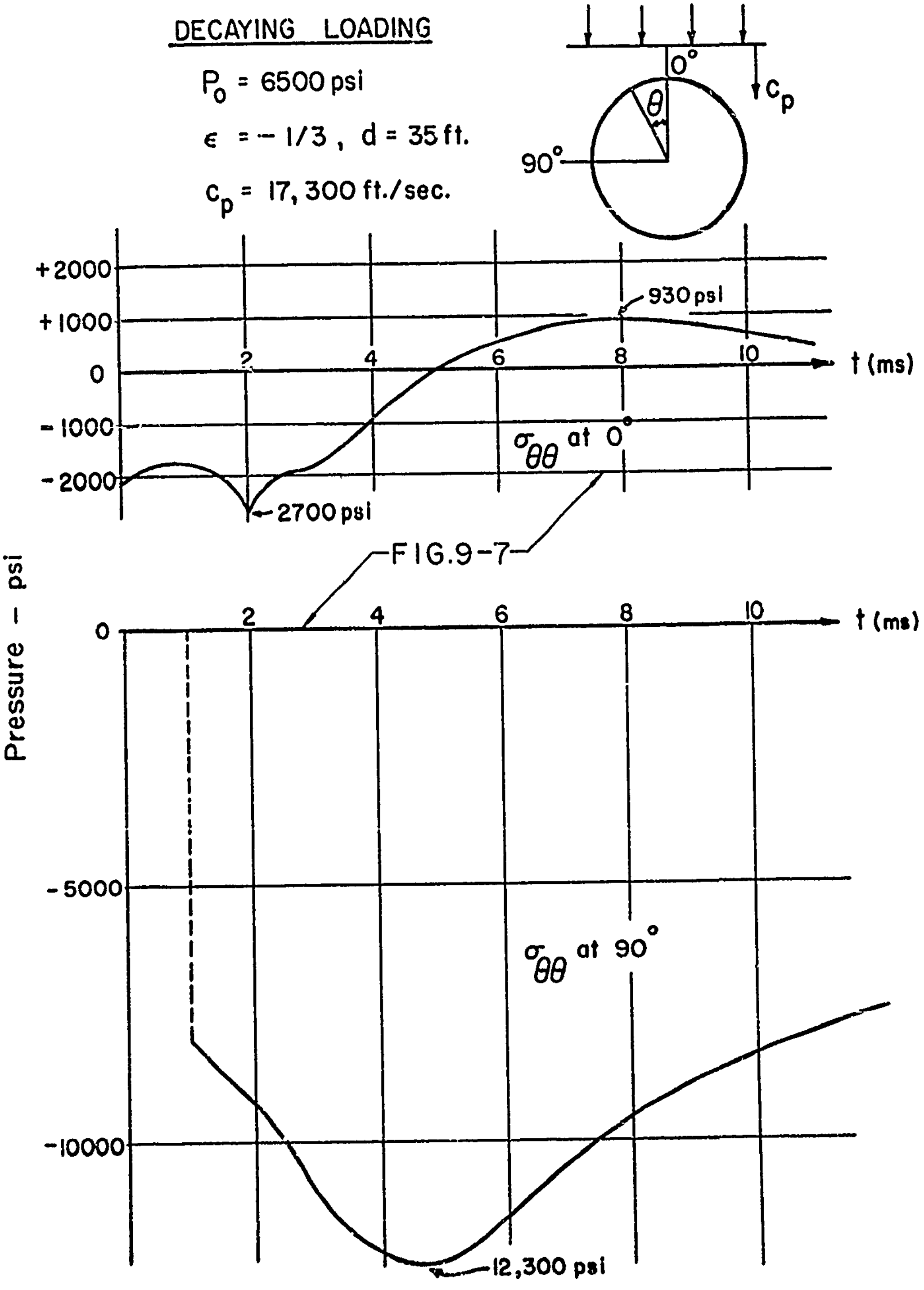

FIG.9-7

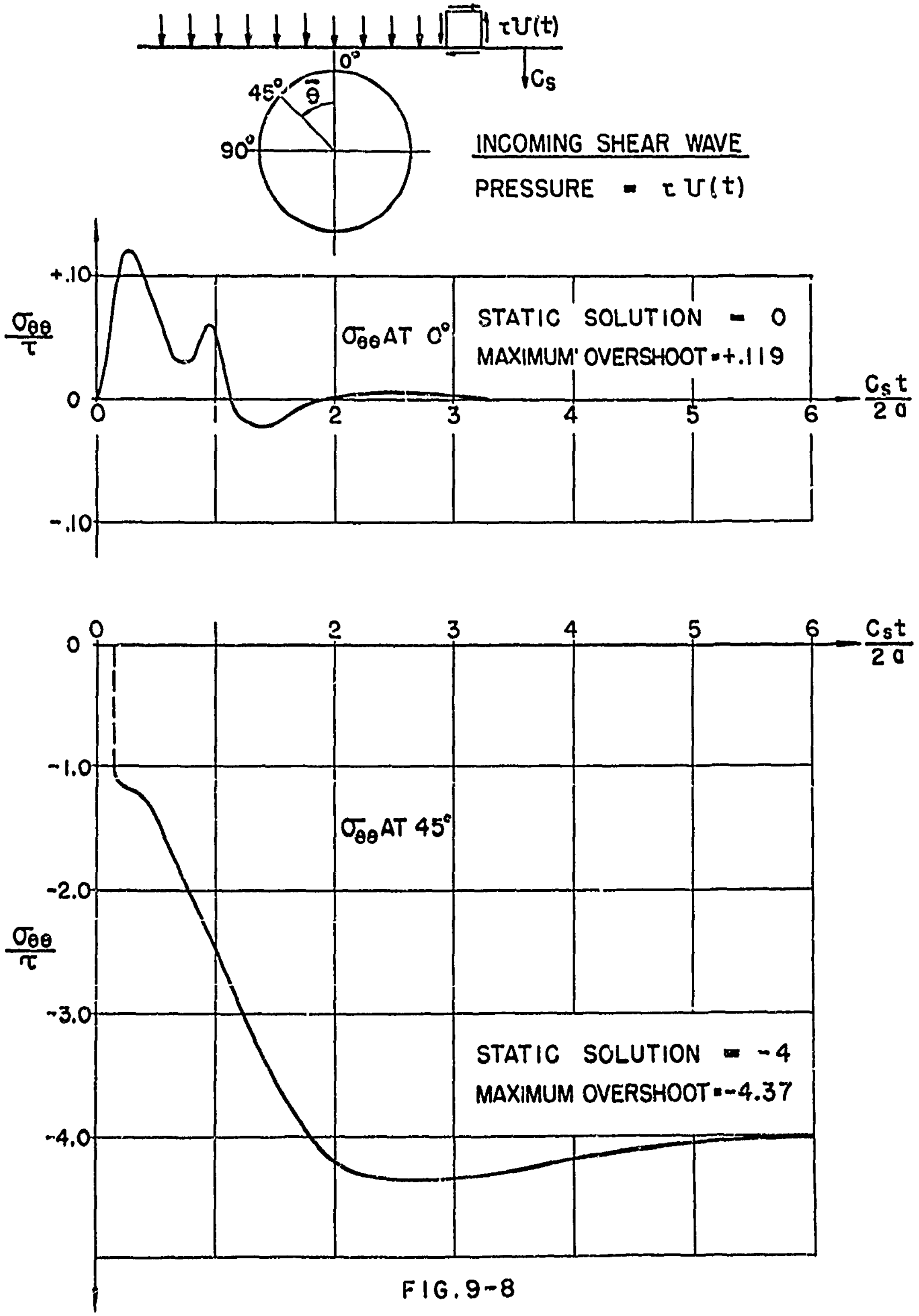
τU(t)
0°
45°
θ̄
90°
Cs
INCOMING SHEAR WAVE
PRESSURE = τ U(t)
+.10
0
-.10
σθθ/τ
σθθ AT 0°
STATIC SOLUTION = 0
MAXIMUM OVERSHOOT = +.119
0
1
2
3
4
5
6
Cst/2a
σθθ AT 45°
0
-1.0
-2.0
-3.0
-4.0
STATIC SOLUTION = -4
MAXIMUM OVERSHOOT = -4.37

FIG. 9-8

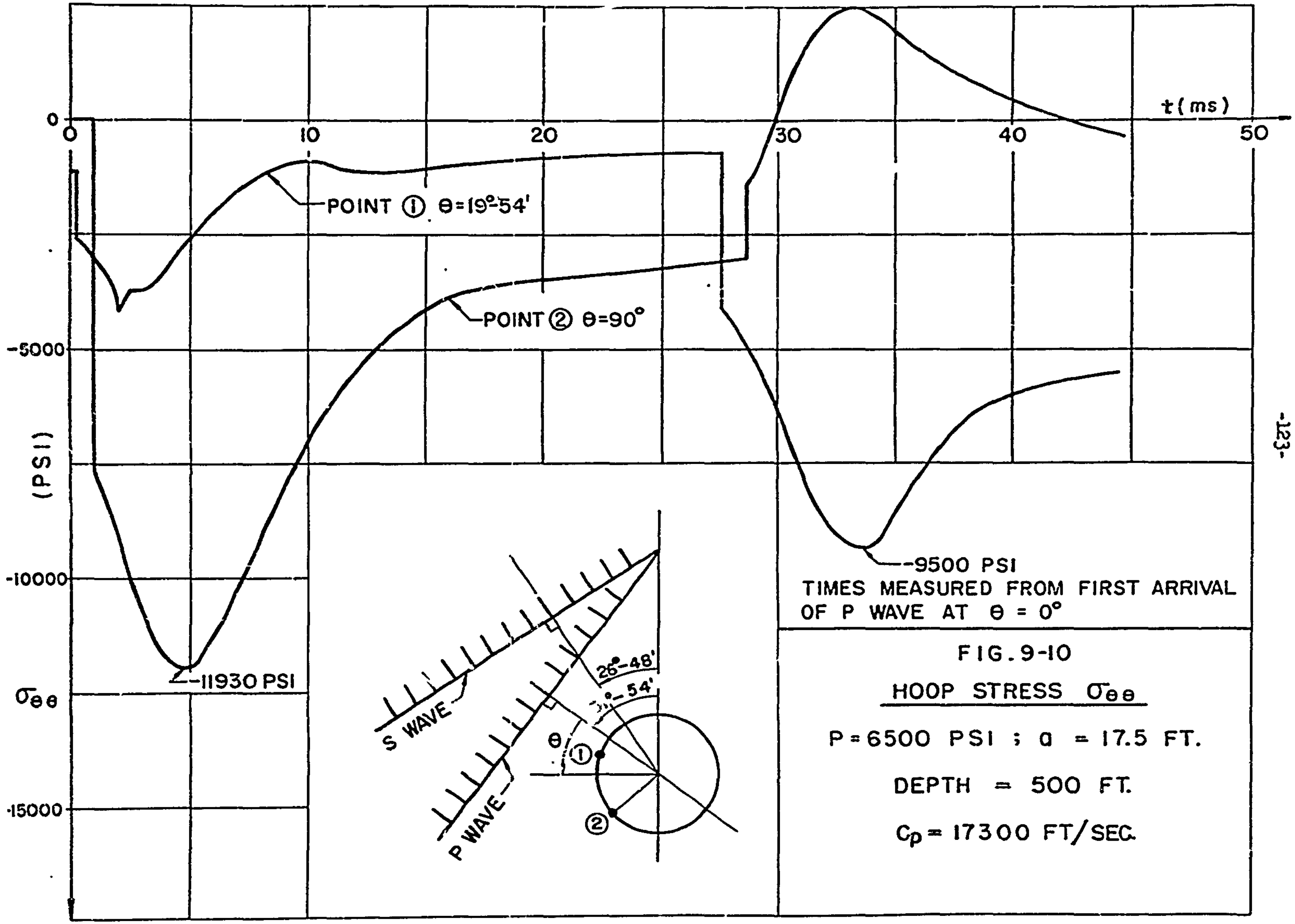

TIMES MEASURED FROM FIRST ARRIVAL OF P WAVE AT θ = 0°

FIG. 9-10

HOOP STRESS $\sigma_{\theta\theta}$

P = 6500 PSI ; a = 17.5 FT.

DEPTH = 500 FT.

C_p = 17300 FT/SEC.

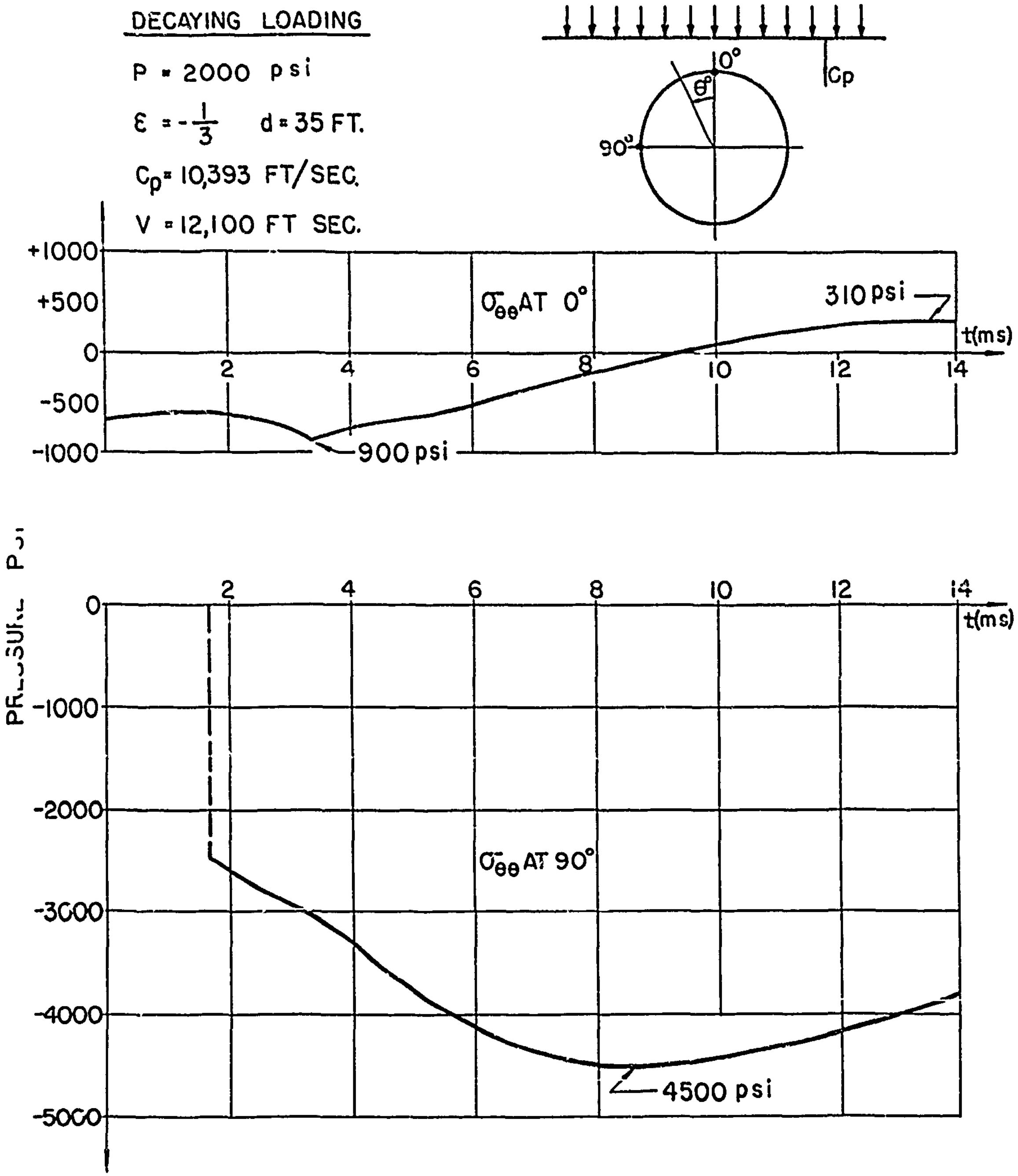
DECAYING LOADING
P = 2000 psi
ε = -1/3 d = 35 FT.
Cp = 10,393 FT/SEC.
V = 12,100 FT SEC.
0°
θ°
90°
Cp
+1000
+500
0
-500
-1000
2
4
6
8
10
12
14
t(ms)
σθθ AT 0°
310 psi
900 psi
PRESSURE P
0
-1000
-2000
-3000
-4000
-5000
2
4
6
8
10
12
14
t(ms)
σθθ AT 90°
4500 psi

FIG.9-11

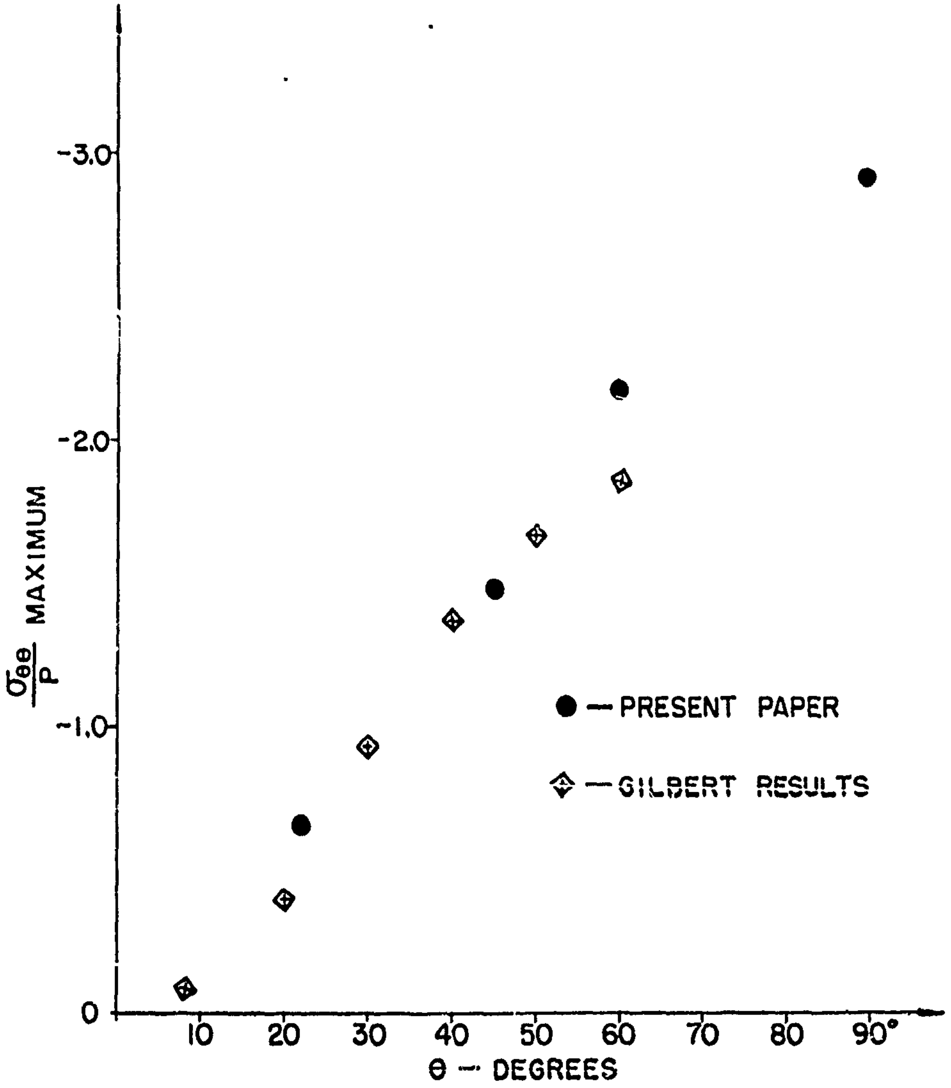
-3.0
-2.0
-1.0
0
$\frac{\sigma_{\theta\theta}}{P}$ MAXIMUM
10
20
30
40
50
60
70
80
90°
θ — DEGREES
● — PRESENT PAPER
◈ — GILBERT RESULTS

FIG. 9—12

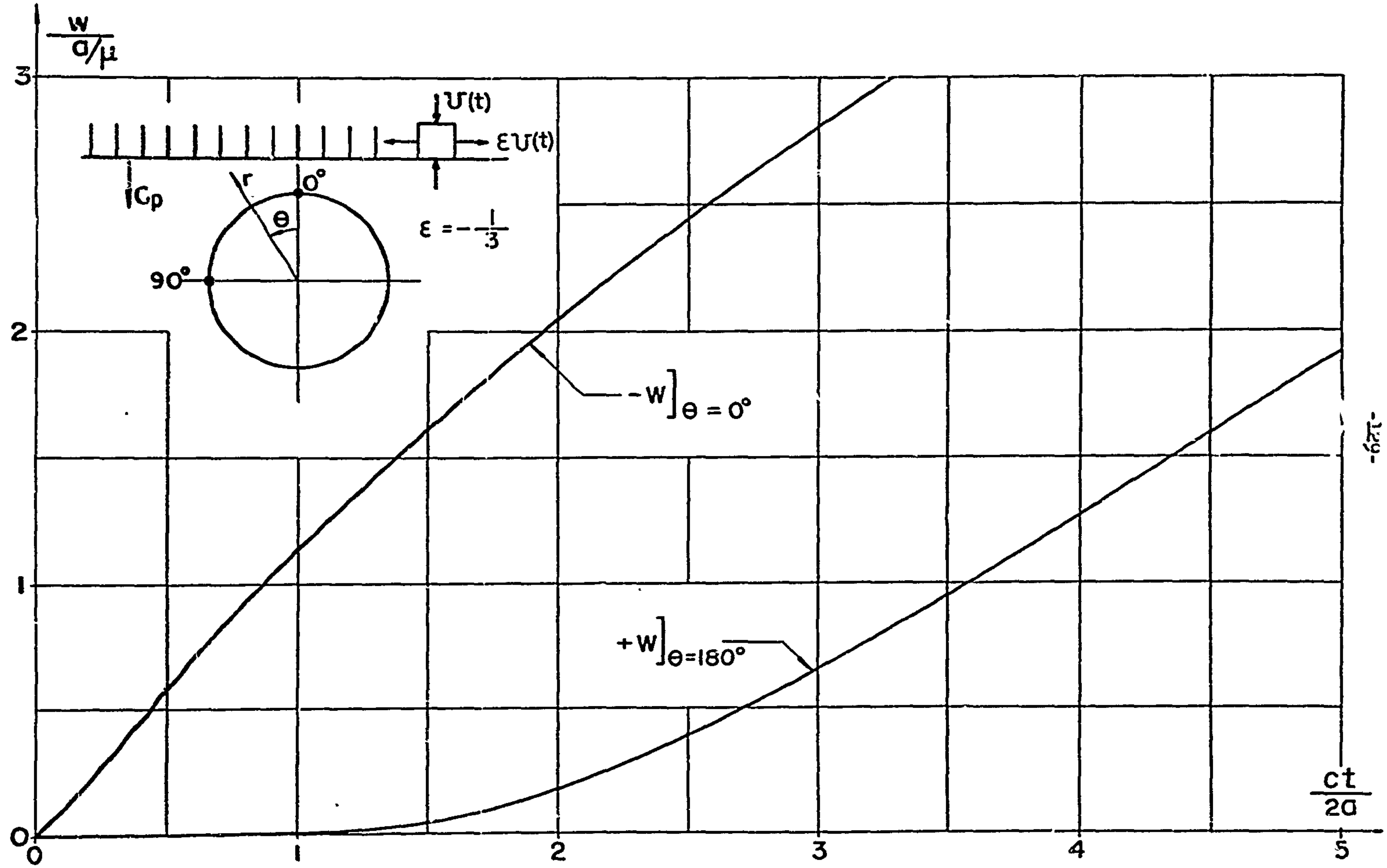

FIG. 9-13 RADIAL DISPLACEMENT W

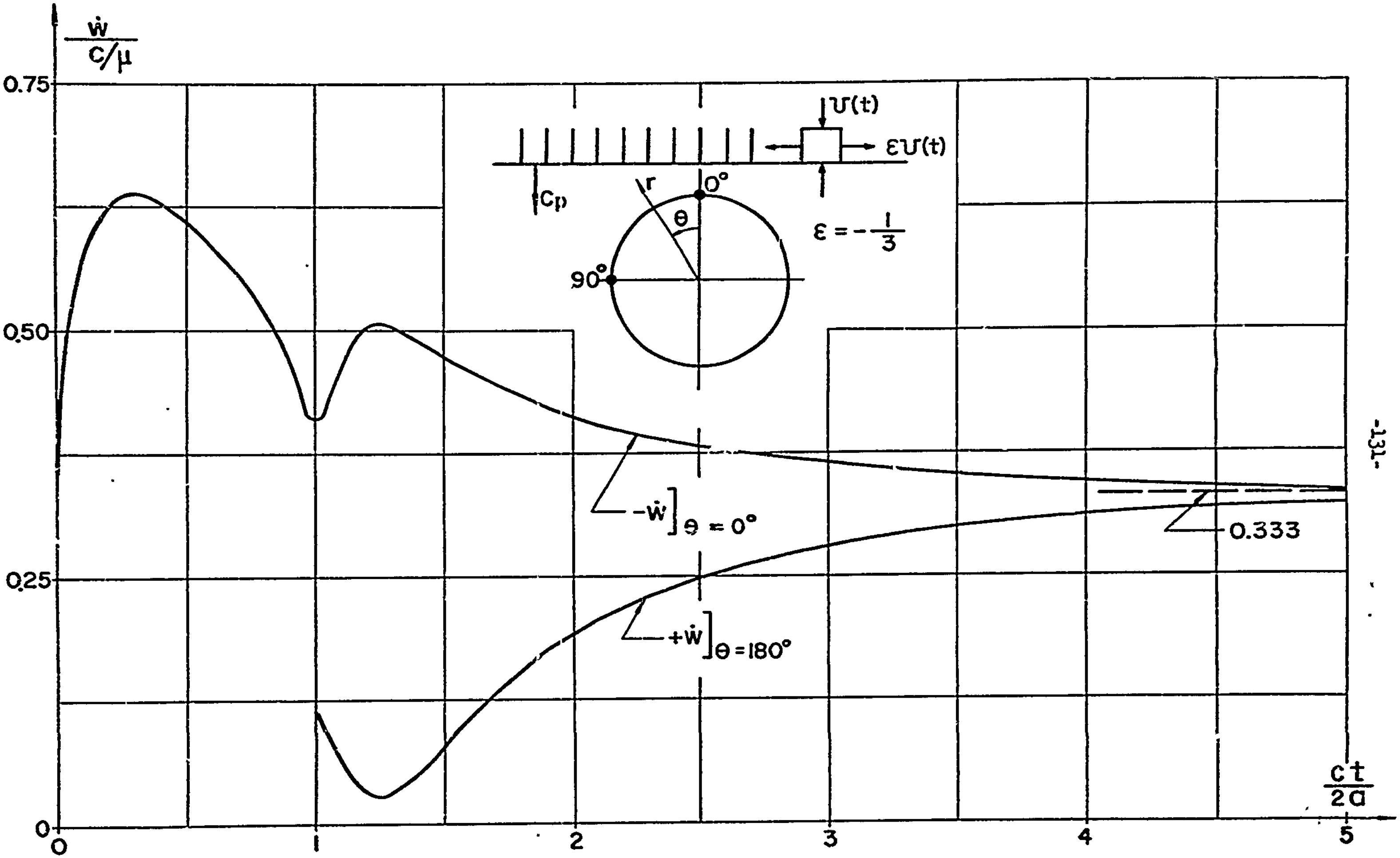

FIG. 9-14 RADIAL VELOCITY $\dot{w}$

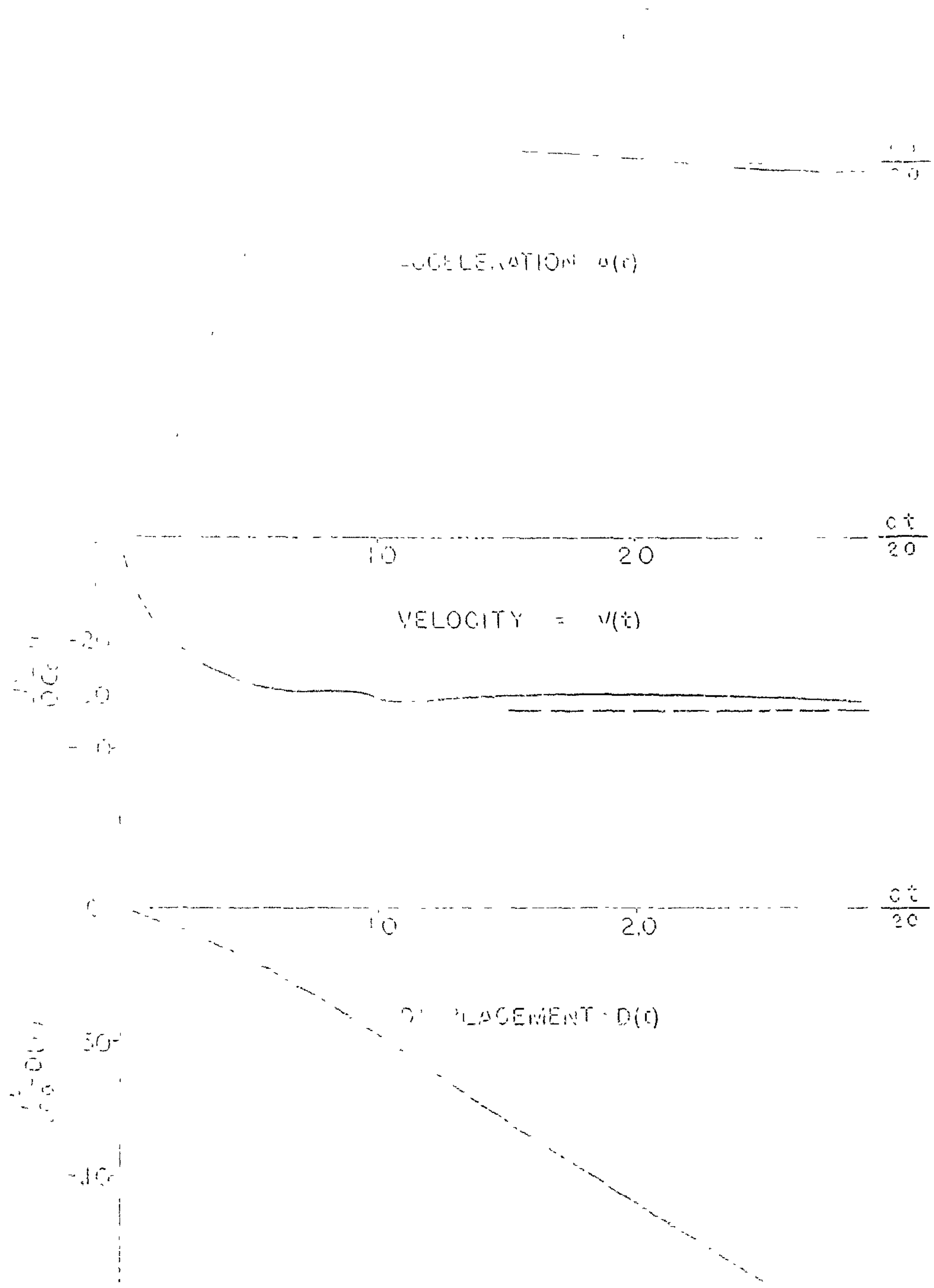

FIG. 4.15 [illegible] RIGID BODY MOTION OF [illegible]

10. SHOCK SPECTRA FOR INSTALLATIONS IN CYLINDRICAL CAVITIES IN ELASTIC MEDIA

In many cases, the various installations which are placed in underground cavities will contain components which are quite shock sensitive. Consequently, they will require special mountings which are capable of absorbing the shock effects produced by the pressure loading on the cavity. Shock spectra for accelerations and displacements are frequently utilized in the design of shock mounted equipment. The present section presents typical shock spectra for a) the motion of various points on the cavity boundary, and b) the rigid body (mean) motion of the cavity as a whole.

The analytical formulation for the development of shock spectra has been presented in detail in Appendix (E). Two particularly useful types of spectra are considered: 1) spectra for the peak absolute acceleration which is imparted to a shock mounted installation in the cavity; 2) spectra for the peak relative displacement of the installation in the cavity, with respect to the motion of points on the cavity boundary to which it is attached. The former spectra give the acceleration design requirements for a given shock mounted installation; the latter give clearance requirements for the mounting of the installation within the cavity.

The shock spectra developed in the present Section and in Appendix (E) *include* the effects due to the diffraction of the shock wave by the cavity. Heretofore, shock spectra which were used in the design of underground installations were computed from free field input pressures only, that is from the readings of a pressure gage at a point in a medium with no tunnel, and the effects of the diffraction of the shock wave by the be determined from the analysis in Appendix (D); the procedure for obtaining the total displacement under the combined P and S wave loading, is identical to that described in Section (9) for the determination of the hoop stress.

(a) Shock Spectra for the Rigid Body Motion of the Cavity.

Consider a mass M which is mounted to the boundary of a cavity by either of the two methods shown in Figure (10-1). In the first case, the mass is connected to the boundary at many points; each mounting is characterized as being a linear spring. For this case, the relative motion of any two points on the cavity boundary will be averaged out by the springs which are connected to the other support points. Consequently, the mass M will react to the average motion of the cavity which is a rigid body translation of the cavity in the direction of the shock wave propagation. In the second case, the mass is connected as rigidly as possible to a stiff structural lining. Again, the mass will react to the rigid body translation of the cavity as a whole.

Figure (10-2) shows acceleration and relative displacement spectra for the rigid body motion of a cavity of radius $r = 17.5$ feet in an elastic medium where $c_p = 17,300$ feet/sec. The cavity is subjected to a P wave carrying a Brode pressure input with $P_o = 6500$ psi for a 20 MT surface burst. For comparison, the corresponding acceleration spectrum from the free field pressures only is shown as a dotted line. It is noted that for higher frequency components, the free field accelerations are much larger than those in the spectrum from the analysis of Appendix (E) which includes the diffraction effects; the difference increases rapidly as the frequency increases. The difference is due to two causes: 1) the be determined from the analysis in Appendix (D); the procedure for obtaining the total displacement under the combined P and S wave loading, is identical to that described in Section (9) for the determination of the hoop stress.

(a) Shock Spectra for the Rigid Body Motion of the Cavity.

Consider a mass M which is mounted to the boundary of a cavity by either of the two methods shown in Figure (10-1). In the first case, the mass is connected to the boundary at many points; each mounting is characterized as being a linear spring. For this case, the relative motion of any two points on the cavity boundary will be averaged out by the springs which are connected to the other support points. Consequently, the mass M will react to the average motion of the cavity which is a rigid body translation of the cavity in the direction of the shock wave propagation. In the second case, the mass is connected as rigidly as possible to a stiff structural lining. Again, the mass will react to the rigid body translation of the cavity as a whole.

Figure (10-2) shows acceleration and relative displacement spectra for the rigid body motion of a cavity of radius r = 17.5 feet in an elastic medium where c_p = 17,300 feet/sec. The cavity is subjected to a P wave carrying a Brode pressure input with P_o = 6500 psi for a 20 MT surface burst. For comparison, the corresponding acceleration spectrum from the free field pressures only is shown as a dotted line. It is noted that for higher frequency components, the free field accelerations are much larger than those in the spectrum from the analysis of Appendix (E) which includes the diffraction effects; the difference increases rapidly as the frequency increases. The difference is due to two causes: 1) the diffraction effect which is maximum at relatively early times, and thus affects the high frequency portion of the shock spectrum, and 2) the fact that the rigid body motion of the cavity produces the shock spectrum for the configurations in Figure (10-1) rather than the motion of a particle subjected to the full free field pressure. The spectrum for the relative displacement of the shock mounted mass M with respect to the motion of the cavity boundary is also shown in the figure.

Figure (10-3) shows similar results for the same cavity in the elastic medium. In this case, the cavity is subjected to a P wave with a Brode pressure input with P_o = 2000 psi. Again, a 20 MT surface burst is considered. This case is felt to be more realistic with respect to an actual installation, since it has been shown in Section (9) that shelters in rock at the 2000 psi contour might be theoretically feasible.

(b) Shock Spectra for the Motion of Individual Points on the Cavity Boundary.

Consider a mass M which is mounted by a linear spring to a point on the boundary of the cavity. Figure (10-4) shows the shock spectra for the motion at the boundary point $\theta = 0^o$. Again, the input wave is produced by a 20 MT surface burst, and the peak pressure P_o is 6500 psi. It is seen that the free field accelerations in this case are considerably lower than the accelerations from the analysis of Appendix (E), particularly at high frequencies. This is to be expected, since the presence of the free cavity boundary gives rise initially to a doubling of the particle velocity at the boundary point $\theta = 0^o$ and consequently, to an increase in the displacement at the boundary points at early times. Hence, the high frequency accelerations at the point $\theta = 0^o$ are considerably higher than those obtained from the free field analysis and the more accurate analysis which includes the diffraction effects must be used. The spectrum for the relative displacement of the shock mounted mass M with respect to the motion of the cavity boundary at $\theta = 0^{\circ}$ is also shown in the figure.

Figure (10-5) shows the shock spectra for the motion of the boundary point $\theta = 180^{\circ}$ under the action of a P wave from a 20 MT surface burst with a peak pressure, $P_o = 6500$ psi. In this case, the free field acceleration spectrum is considerably higher than the spectrum including the diffraction effects; the diffraction actually decreases the displacement input and consequently the high frequency accelerations.

The motion of the cavity boundary at the points $\theta = 0^{\circ}$ and $\theta = 180^{\circ}$ that have been considered thus far is purely radial; the tangential component v is equal to zero at all times(*). Hence, the linear oscillator concept can be applied in determining shock spectra for equipment in the cavity which is connected to these points. However, other points on the cavity boundary will undergo both radial and tangential displacements and shock spectra for both directions are required. Consequently, the shock mounting of equipment to such points must be capable of absorbing accelerations in both the radial and tangential directions, i.e. an essentially "two-way" shock mounting is required.

(c) Conclusions

It is obvious that the most favorable conditions for shock effects will be encountered if the equipment is shock mounted in the cavity such that it will react to the average motion of the cavity (rigid body motion) rather than to the motion of individual points on the boundary of the tunnel. Such mountings may be difficult to obtain practically. However

---

(*) It should be noted that this is only true if the S wave effects can be neglected.

if such a mounting can be achieved, the equipment will be subjected to shock accelerations which are considerably smaller than those given by the free field shock spectra.

In the case of equipment which is attached to a point on the tunnel circumference, the spectra allowing for diffraction differs considerably from the free field spectra. The peak accelerations for a point $\theta = 0^\circ$ are considerably increased by the diffraction. However, the opposite situation prevails at $\theta = 180^\circ$, in which the shock accelerations including diffraction effects are lower than the "free field"values.

In each case, the design accelerations for high frequency components are greatly influenced by the diffraction effects of the wave by the cavity. Consequently, it is felt that the more accurate theory of Appendix (E), which includes these effects, should be used in the development of shock spectra and design criteria.

It should be noted that the shock spectra which have been presented in this Section as examples, are based on an input of a sharp fronted pressure (P) wave with a zero rise time. For the case of a wave with a finite rise time, the intensity of the high frequency portions of the shock spectra would be substantially decreased.

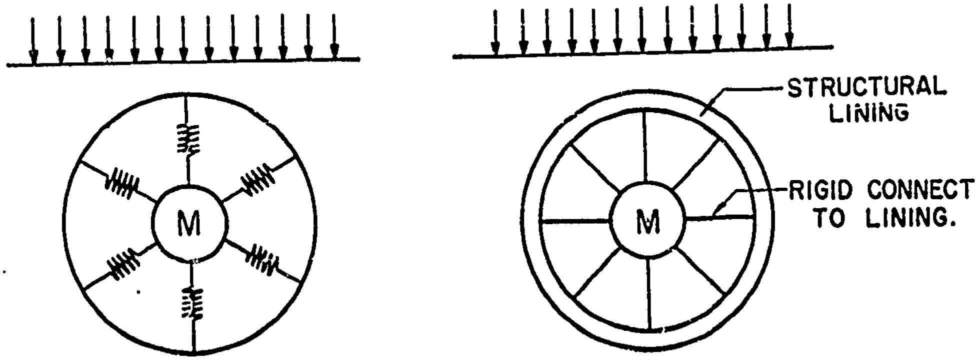

FIG.10-1

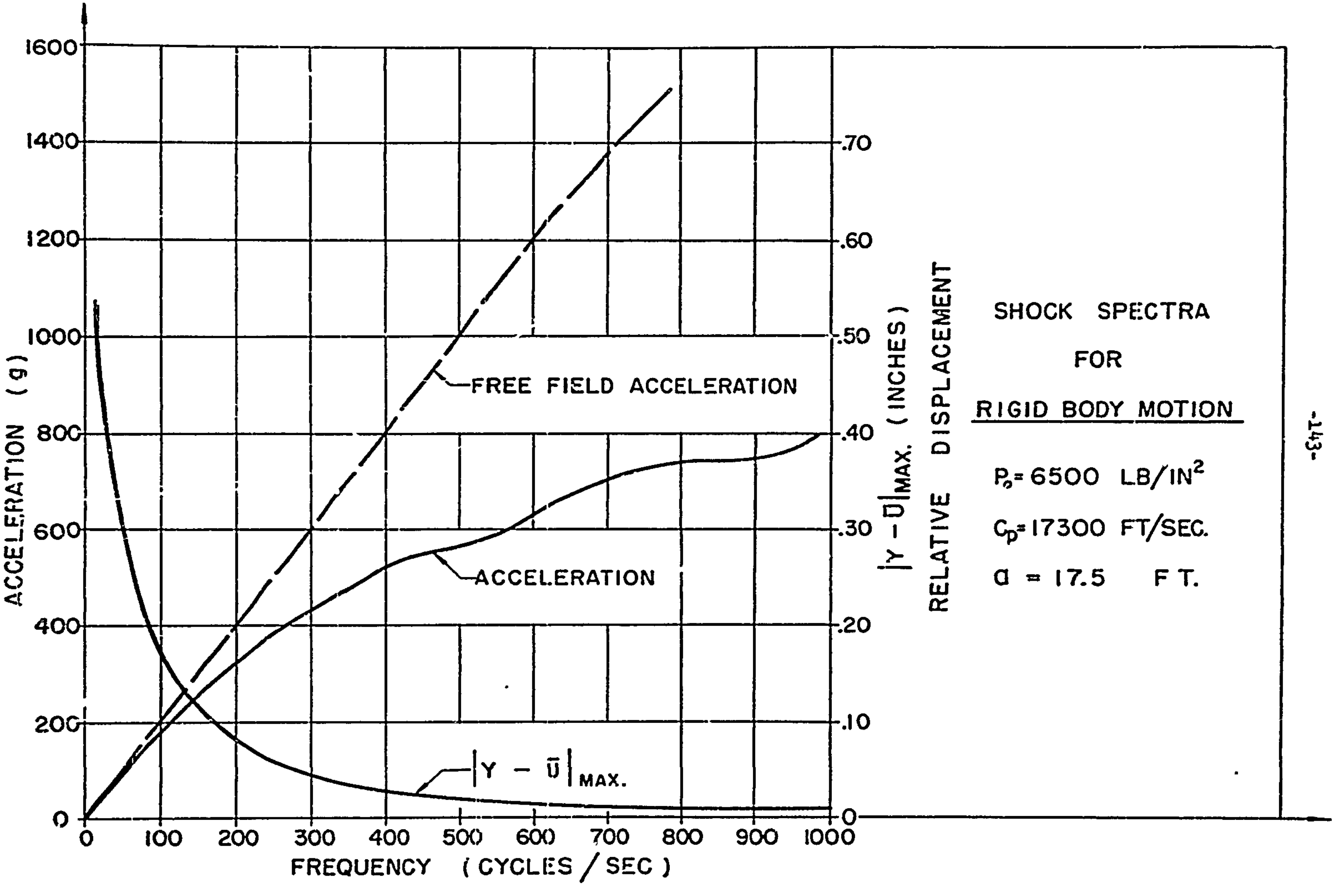
SHOCK SPECTRA
FOR
RIGID BODY MOTION
P_o = 6500 LB/IN^2
C_p = 17300 FT/SEC.
a = 17.5 FT.
ACCELERATION (g)
0
200
400
600
800
1000
1200
1400
1600
$|Y - \bar{U}|_{MAX.}$ (INCHES)
RELATIVE DISPLACEMENT
0
.10
.20
.30
.40
.50
.60
.70
FREE FIELD ACCELERATION
ACCELERATION
$|Y - \bar{U}|_{MAX.}$
0
100
200
300
400
500
600
700
800
900
1000
FREQUENCY (CYCLES / SEC)

FIG. 10-2

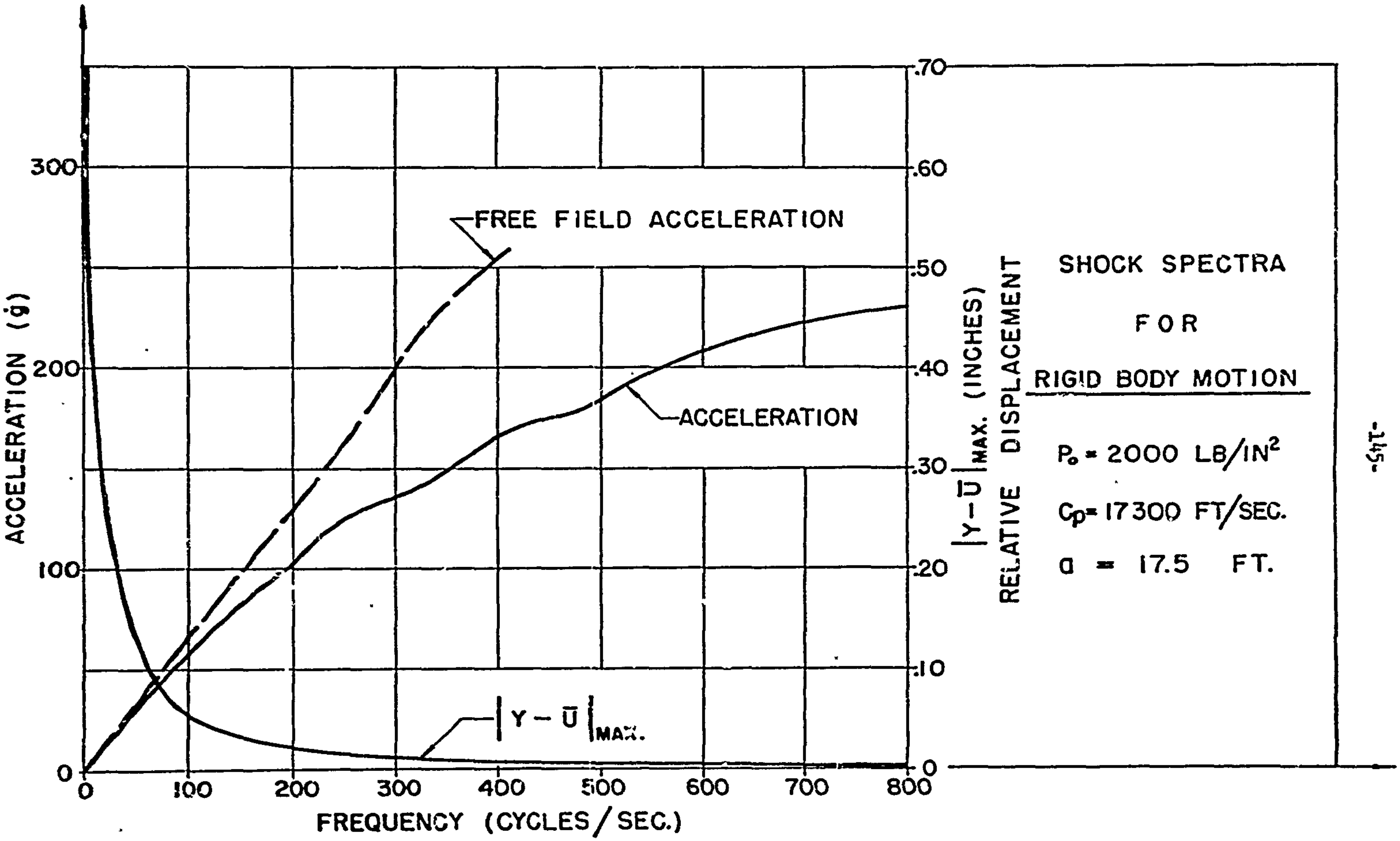
SHOCK SPECTRA
FOR
RIGID BODY MOTION
P_o = 2000 LB/IN^2
C_p = 17300 FT/SEC.
a = 17.5 FT.
FREE FIELD ACCELERATION
ACCELERATION
$|Y-\bar{U}|_{MAX.}$
ACCELERATION (g)
0
100
200
300
$|Y-\bar{U}|_{MAX.}$ (INCHES) RELATIVE DISPLACEMENT
0
.10
.20
.30
.40
.50
.60
.70
FREQUENCY (CYCLES/SEC.)
0
100
200
300
400
500
600
700
800

FIG.10-3

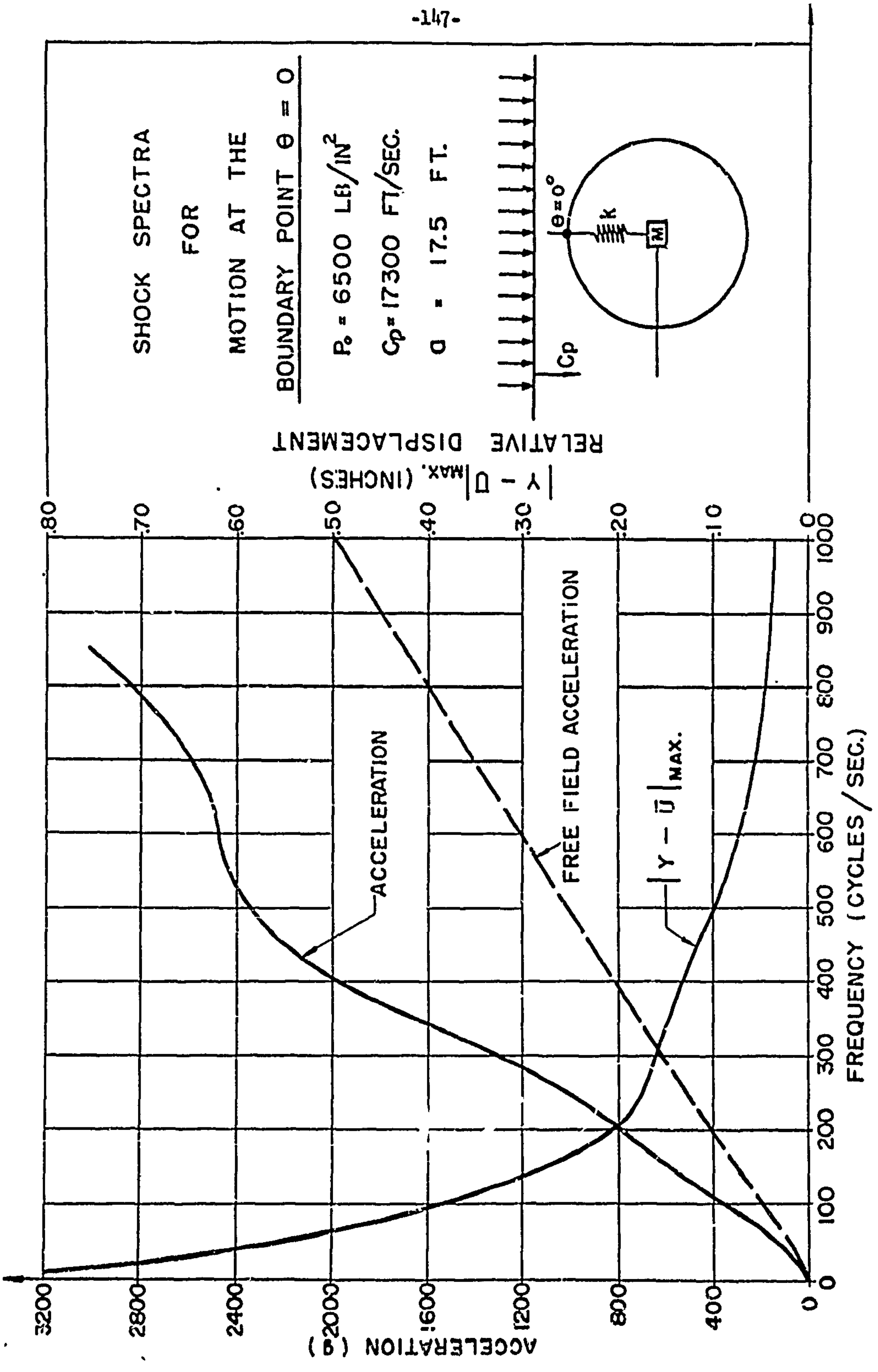
SHOCK SPECTRA
FOR
MOTION AT THE
BOUNDARY POINT θ = 0
P_o = 6500 LB/IN²
C_p = 17300 FT/SEC.
a = 17.5 FT.
C_p
θ=0°
k
M
ACCELERATION (g)
0
400
800
1200
1600
2000
2400
2800
3200
|Y − Ū|MAX. (INCHES)
RELATIVE DISPLACEMENT
0
.10
.20
.30
.40
.50
.60
.70
.80
FREQUENCY (CYCLES/SEC.)
0
100
200
300
400
500
600
700
800
900
1000
ACCELERATION
FREE FIELD ACCELERATION
|Y − Ū|MAX.

FIG. 10-4

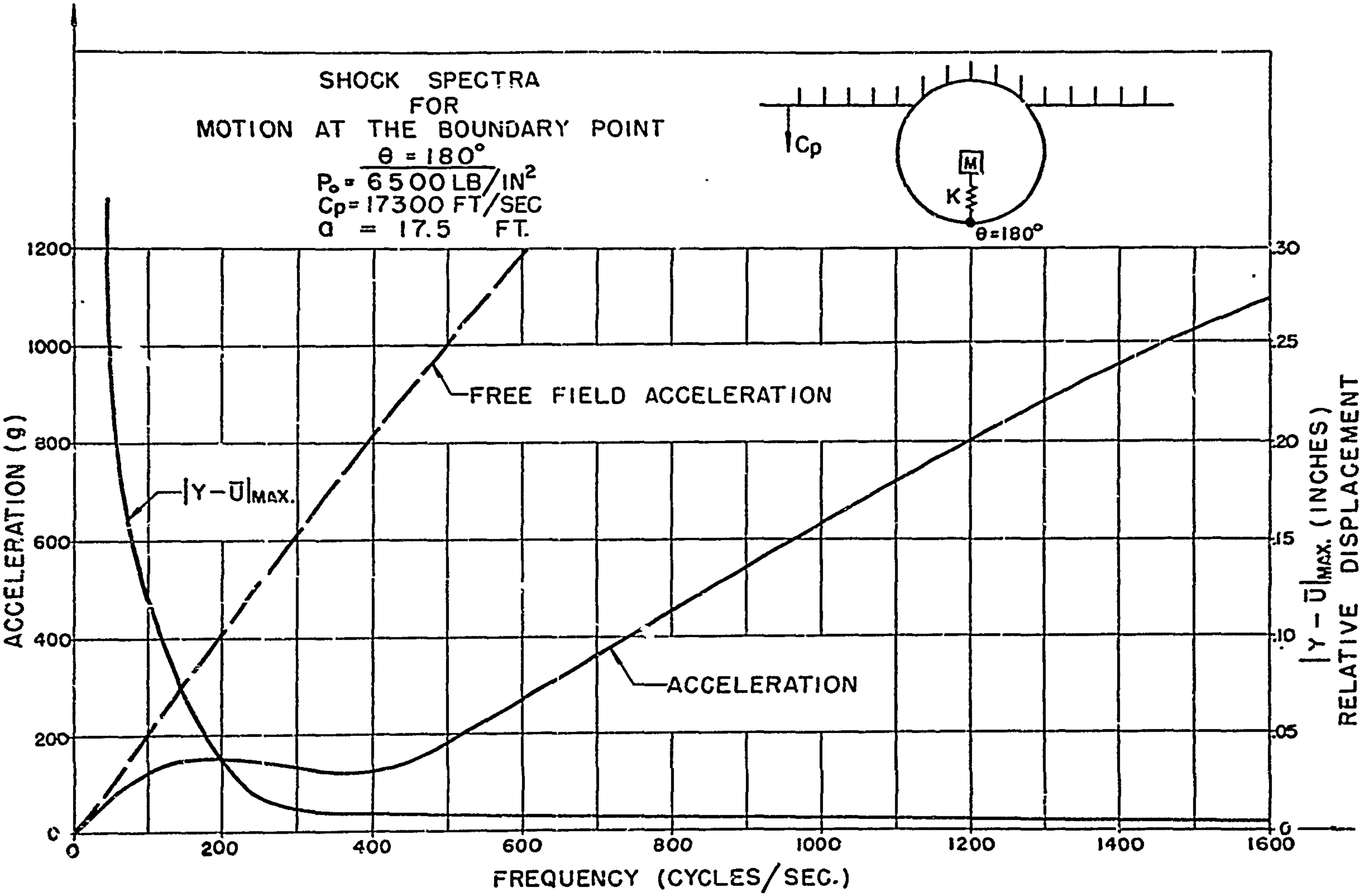
SHOCK SPECTRA
FOR
MOTION AT THE BOUNDARY POINT
θ = 180°
P₀ = 6500 LB/IN²
Cp = 17300 FT/SEC
a = 17.5 FT.
Cp
M
K
θ=180°
FREE FIELD ACCELERATION
|Y−Ū|MAX.
ACCELERATION
ACCELERATION (g)
0
200
400
600
800
1000
1200
FREQUENCY (CYCLES/SEC.)
0
200
400
600
800
1000
1200
1400
1600
|Y − Ū|MAX. (INCHES)
RELATIVE DISPLACEMENT
0
.05
.10
.15
.20
.25
.30

FIG.10-5

11. Diffraction of Pressure Waves by a Cylindrical Elastically Lined Cavity in an Elastic Medium.

The stresses and motions produced by the diffraction of pressure waves by an unlined cylindrical cavity in an elastic medium have been studied in Reference [20] and Appendices (C) and (D). It is of interest to evaluate the effect of the use of a structural elastic lining for the cavity boundary. Particularly, the effect of such a lining on the strength of the cavity as a whole and on the boundary displacements which are the input functions for the determination of shock spectra for installations within the cavity, must be studied.

The problem considered is that of an elastic shell in an infinite elastic medium under the action of a plane step pressure wave which travels through the medium and envelops the cavity. A method of solution which utilizes the solution for the corresponding unlined cavity problem as influence coefficients can be used to obtain the corresponding results for the elastically lined cavity. Such a method has already been applied successfully for a radially symmetric problem in an acoustic medium [22]. The generalization of this method for the present problem is considerably more complex and represents a major computational effort. This effort is currently under way; consequently, only an outline of the method of solution is presented in this Section.

An infinitely long elastically lined cylindrical cavity in an infinite elastic homogeneous and isotropic medium is acted on by a plane pressure wave whose front is parallel to the axis of the cavity. The shock wave propagates through the medium with a constant velocity c_p and envelops the cavity [Fig. (11-1)].

a) Determination of the Equations of Motion for the Shell.

The response of the elastic lining*) to the transverse shock wave is studied by considering the shell in vacuo as a separate structure responding to the dynamic forces exerted by the surrounding elastic medium and by the incoming shock wave. Using the modes of free vibration of the shell in vacuo as generalized coordinates, its response can be expanded in terms of the infinite number of these modes. The mode shapes and the corresponding frequencies that are required have been developed in Reference [23]. Let the displacement of the shell be written in terms of the generalized coordinates $\bar{q}_o$, $\bar{q}_n$ and q_n $(n \neq 0)$:

$$w(\theta,t) = \bar{q}_o(t) + \sum_{n=1}^{\infty}\left[q_n(t) + \bar{q}_n(t)\right] \cos n\theta \qquad (11\text{-}1)$$

$$v(\theta,t) = \sum_{n=1}^{\infty}\left[\frac{q_n(t)}{d_n} - d_n\bar{q}_n(t)\right] \sin n\theta \qquad (11\text{-}2)$$

The quantities q_n are the coordinates for the primarily inextensional motions of the shell; the quantities $\bar{q}_o$ and $\bar{q}_n$ are the coordinates for the primarily extensional motions.

The coefficient d_n is given by the relation

$$d_n = \frac{n^2-1}{2n} - \left[\frac{(1-n^2)^2}{2n}\right]\frac{I}{a^2A} + \frac{1}{2}\left[\left(\frac{n^2+1}{n}\right)^2 + \left(\frac{2(1-n^2)^3}{n^2}\right)\frac{I}{a^2A} + \left(\frac{(1-n^2)^4}{n^2}\right)\frac{I^2}{a^4A^2}\right]^{\frac{1}{2}} \qquad (11\text{-}3)$$

For properties of practical interest and for the lower modes $(n \leq 5)$, there is little coupling between the bending and extensional effects because $a^2A \gg I$.

---

*) The lining is now essentially an elastic shell in an infinite elastic medium.

For such cases, $d_n = n$ and the frequencies*) ω_n^2 and $\bar{\omega}_n^2$ are given by

$$\omega_n^2 = \frac{\bar{E}I(1-n^2)^2 n^2}{ma^4(n^2+1)} \tag{11-4}$$

$$\bar{\omega}_n^2 = \frac{\bar{E}A}{ma^2}(n^2+1) \tag{11-5}$$

where $\bar{E} = \frac{E}{1-\nu^2}$, I and A are the moment of inertia of the cross section of the shell with respect to a principal axis at right angles to the plane of the ring and the cross sectional area of the ring respectively, and m is the mass per unit area of the elastic lining.

The equations of motion for the shell may be written in terms of the generalized coordinates q_n and $\bar{q}_n$:

$$\ddot{q}_n + \omega_n^2 q_n = \frac{Q_n}{m_n} \qquad n = 1, 2, 3, \ldots \tag{11-6}$$

$$\ddot{\bar{q}}_n + \bar{\omega}_n^2 \bar{q}_n = \frac{\bar{Q}_n}{\bar{m}_n} \qquad n = 0, 1, 2, 3, \ldots \tag{11-7}$$

where Q_n and $\bar{Q}_n$ are generalized forces and m_n and $\bar{m}_n$ are the generalized masses:

$$m_n = m\left(1 + \frac{1}{d_n^2}\right) \tag{11-8}$$

$$\bar{m}_n = m(1 + d_n^2). \tag{11-9}$$

The generalized forces $Q_n(t)$ and $\bar{Q}_n(t)$ will be evaluated later in this Section.

---

*) For cases in which the coupling between the bending and the extensional motions is significant, the frequencies must be determined from the expressions given by Eq. (A-8) of Reference [23].

b) The Response of the Boundary of an Unlined Cylindrical Cavity - Determination of Influence Coefficients.

The displacements at the boundary of an unlined cavity to a step pressure wave have been evaluated in Appendix (D) of this paper. Essentially, the results were obtained by the addition of an effect produced by the free field component of the incoming shock wave plus the effects produced by the application of corrective boundary tractions which are required to produce a traction free surface at the cavity boundary. For the present purpose, the free field components must be expanded into a Fourier series in θ, and added to the corresponding components from the corrective tractions. Finally, the total motion of points on the boundary of the unlined cavity is obtained in the form

$$w = \sum_{n=0}^{\infty} F_n(t) \cos n\theta \tag{11-10}$$

$$v = \sum_{n=1}^{\infty} G_n(t) \sin n\theta \tag{11-11}$$

Two additional coefficients are required from the unlined cavity problem. They are respectively: 1) the boundary displacements $w_A(t) \cos n\theta$ and $v_A(t) \sin n\theta$ produced by the applied boundary tractions $\sigma_{rr_n} = U(t) \cos n\theta$; $\sigma_{r\theta_n} = 0$ [Fig. (11-2)]; 2) the boundary displacements $w_B(t) \cos n\theta$ and $v_B(t) \sin n\theta$ produced by the applied boundary tractions $\sigma_{rr_n} = 0$; $\sigma_{r\theta_n} = U(t) \sin n\theta$ [Fig. (11-3)]. These quantities can be evaluated from the results of Appendix (D) and will be used as influence coefficients in Duhamel integrals for the analytical determination of the generalized coordinates $q_n(t)$ and $\overline{q}_n(t)$.

c) Derivation of Integral Equations for the Evaluation of the Generalized Coordinates $q_n(t)$ and $\bar{q}_n(t)$.

Consider an elastically lined cavity in the medium under the action of the step shock wave. The total radial and tangential displacements of the shell boundary can be derived from the superposition of the corresponding displacements of the unlined boundary plus the displacement produced by unknown radial and tangential forces X(t) and Y(t) respectively which are required to force the unlined cavity into a compatible displacement with the elastically lined cavity. The forces X(t) and Y(t) [Fig. (11-4)] are expanded into a Fourier series in θ:

$$X(t) = \sum_{n=0}^{\infty} X_n(t) \cos n\theta \qquad (11\text{-}12)$$

$$Y(t) = \sum_{n=1}^{\infty} Y_n(t) \sin n\theta \qquad (11\text{-}13)$$

The compatibility equation on the radial and tangential displacements of the shell can be written in terms of the generalized coordinates $q_n(t)$ and $\bar{q}_n(t)$, and the forces $X_n(t)$ and $Y_n(t)$. The sum of the displacements due to 1) the shock wave on the unlined cavity; 2) the applied boundary tractions $\sigma_{rr} = X_n(t) \cos n\theta$, $\sigma_{r\theta} = 0$; 3) the applied boundary tractions $\sigma_{rr} = 0$, $\sigma_{r\theta} = Y_n(t) \sin n\theta$, must be set equal to the actual displacements of the shell itself [Eq. (11-1)-(2)].

The radial and tangential displacements produced by the traction $\sigma_{rr} = X_n(t) \cos n\theta$, $\sigma_{r\theta} = 0$, applied to the cavity boundary, can be evaluated in terms of the known displacement coefficients $w_A(t)$ and $v_A(t)$ from the Duhamel integrals*):

---

*) The derivation of formulas of the type given by Eq. (11-14)-(11-15) is shown in detail in Reference [22].

$$w = \int_0^t \frac{dX_n(\tau)}{d\tau} w_A(t-\tau)d\tau \qquad (11\text{-}14)$$

$$v = \int_0^t \frac{dX_n(\tau)}{d\tau} v_A(t-\tau)d\tau \qquad (11\text{-}15)$$

In a similar manner, the radial and tangential displacements due to the boundary tractions $\sigma_{rr} = 0$, $\sigma_{r\theta} = Y_n(t) \sin n\theta$, are evaluated in terms of the known displacement coefficients $w_B(t)$ and $v_B(t)$ from the Duhamel integrals:

$$w = \int_0^t \frac{dY_n(\tau)}{d\tau} w_B(t-\tau)d\tau \qquad (11\text{-}16)$$

$$v = \int_0^t \frac{dY_n(\tau)}{d\tau} v_B(t-\tau)d\tau \qquad (11\text{-}17)$$

The compatibility equations for the shell displacements thus become:

$$F(t) + \int_0^t \frac{dX_n(\tau)}{d\tau} w_A(t-\tau)d\tau + \int_0^t \frac{dY_n(\tau)}{d\tau} w_B(t-\tau)d\tau = q_n(t) + \overline{q}_n(t) \qquad (11\text{-}18)$$

$$G(t) + \int_0^t \frac{dX_n(\tau)}{d\tau} v_A(t-\tau)d\tau + \int_0^t \frac{dY_n(\tau)}{d\tau} v_B(t-\tau)d\tau = \frac{q_n(t)}{d_n} + d_n\overline{q}_n(t) \qquad (11\text{-}19)$$

Eq. (11-18)-(11-19) are a pair of coupled integral equations on the unknown elastic forces $X_n(t)$ and $Y_n(t)$.

The generalized forces $Q_n(t)$ and $\overline{Q}_n(t)$ which appear in Eq. (11-6)-(11-7) are now determined as functions of the unknown forces $X_n(t) \cos n\theta$ and $Y_n(t) \sin n\theta$. A set of two simultaneous linear equations in $X_n(t)$ and $Y_n(t)$ are obtained. These equations are then solved simultaneously for $X_n(t)$ and $Y_n(t)$ as functions of the generalized coordinates q_n and $\overline{q}_n$:

$$X_n(t) = f\,(q_n, \bar{q}_n, \omega_n, \bar{\omega}_n) \tag{11-20}$$

$$Y_n(t) = g\,(q_n, \bar{q}_n, \omega_n, \bar{\omega}_n) \tag{11-21}$$

Substituting Eq. (11-20)-(11-21) into Eq. (11-18)-(11-19), a set of coupled integral equations on the generalized coordinates q_n and $\bar{q}_n$ are obtained.

These equations can be solved by numerical methods, using finite difference theory. Essentially, the integrals in Eq. (11-18)-(11-19) are replaced by finite difference summations from which recurrence formulas for the coordinates $q_n(t+k)$ and $\bar{q}_n(t+k)$ are obtained in terms of their known values at previous time steps.

Once the generalized coordinates q_n and $\bar{q}_n$ are evaluated, the displacements of the shell are computed from Eq. (11-1)-(11-2). Similarly, the shell velocities and accelerations are also computed.

The direct stress (hoop stress) in the shell is evaluated from the relations

$$\sigma = \frac{E}{(1-\nu^2)}\,\epsilon \tag{11-22}$$

$$\epsilon = \frac{1}{a}\,(v + v_\theta). \tag{11-23}$$

Substituting Eq. (11-1)-(11-2) into the above equations, the n^{th} component of the direct hoop stress becomes

$$\sigma_{\theta\theta_n} = \frac{E}{(1-\nu^2)a}\,(n^2+1)\bar{q}_n \cos n\theta \tag{11-24}$$

The n^{th} component of the flexural stress σ_B in the shell is given by

$$\sigma_{B_n} = \frac{(n^2-1)Ed}{a} (q_n + \bar{q}_n) \cos n\theta \qquad (11-25)$$

where d is the distance from the neutral axis of the shell to its extreme fiber. The total hoop and bending stresses are evaluated by summation of the components $\sigma_{\theta\theta_n}$ and σ_{B_n} respectively.

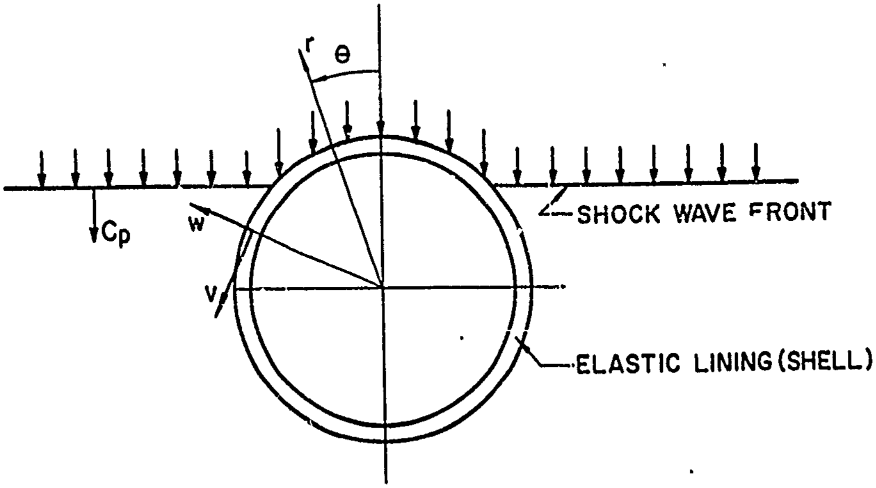

FIG. II-1

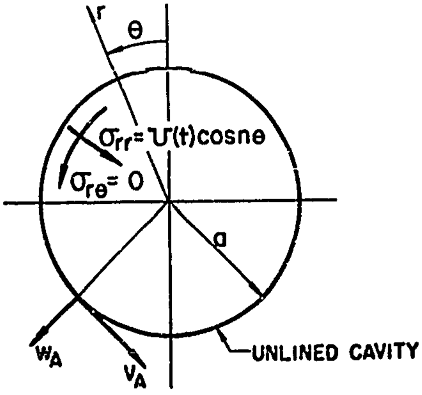

FIG. II-2

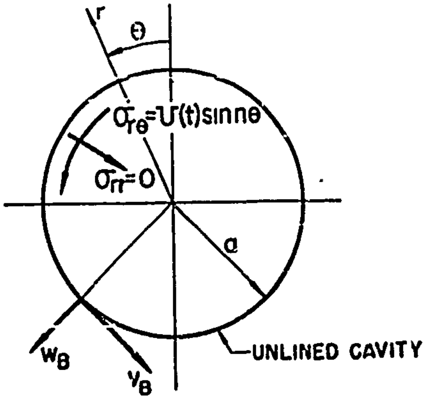

FIG. II-3

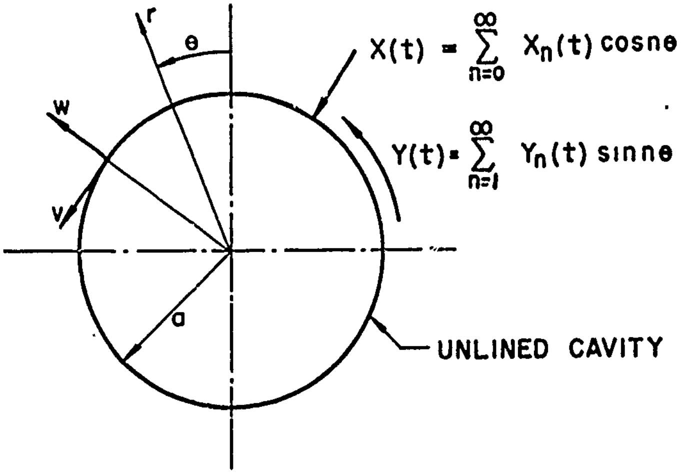
r
θ
w
v
a
$X(t) = \sum_{n=0}^{\infty} X_n(t) \cos n\theta$
$Y(t) = \sum_{n=1}^{\infty} Y_n(t) \sin n\theta$
UNLINED CAVITY

FIG. II-4

12. CONCLUSION AND SUMMARY -- DIFFRACTION EFFECTS

Sections (9)-(11) have considered three basic theoretical problems which may be of use in the analysis and design of underground structures and their contents. These problems are respectively: 1) the stress, velocity and displacement fields produced in an elastic medium by the diffraction of plane P and S waves by an unlined cylindrical cavity; 2) the determination of shock spectra for installations that are mounted in cylindrical cavities in elastic media; and 3) the stresses, velocities and displacements for the case of the diffraction of plane P and S waves by a cylindrical elastically lined cavity, i.e. a structural shell which would house an installation.

The shock waves have been assumed to have plane fronts which are parallel to the axis of the cavity. The plane wave solutions can be applied directly to the superseismic range ($V > c_p$). Moreover, they can be used to construct by superposition, the solution to more general diffraction problems in which the stress field produced by the surface explosion does not consist of plane waves but is considerably more complicated. The problem of the envelopment of the cavity by a shock wave with a wave front perpendicular to the axis of the cavity, has not as yet been treated, and remains to be analyzed.

It should be noted that the limitations on the use of an elastic theory which are noted in Part (I) also hold for the present cases. The application of the theoretical results obtained in Sections (9)-(11) is valid only in those portions of the medium in which the assumption of linear elasticity is tenable. It may be inferred from Appendix (F) that this is not an unreasonable assumption outside of the crater region in a good granite rock.

Specific conclusions on the use and applicability of the various theoretical results are given in each Section and will not be repeated here. It may be noted however that for a pressure wave with a step pressure input, the hoop stresses produced on the boundary of an unlined cavity are essentially quasi-static and reach their maximum values after 3-4 envelopment times, i.e. the dynamic amplifications are small percentage wise. Results for waves with decaying pressure-time histories are easily derived from the corresponding step pressure results by means of Duhamel integrals.

The velocities and displacements of the cavity boundary are used as input functions for determining acceleration and relative displacement frequency spectra for shock mounted installations in the cavity. The shock spectra which include the diffraction effects and are consequently more appropriate, differ considerably from the free field spectra, particularly in the high frequency ranges. In addition, it appears that the most favorable conditions for shock effects will be encountered if the equipment is shock mounted so that it will react to the average (rigid body) motion of the cavity.

Results for an elastically lined cavity in an elastic medium can be obtained from the corresponding solutions for the unlined cavity. The theoretical method leads to a set of simultaneous linear integral equations which may be solved numerically. This large effort is currently under way, and it is hoped that the results will be available in the near future.

It is felt that the theoretical problems considered here represent a basic first theoretical development leading to a rational design procedure for underground structures. A great deal of further theoretical study involving diffraction effects in dissipative and granular (compressible) media will also be required for locations of practical importance and interest in which the elastic theory will not be applicable.

REFERENCES AND APPENDICES

REFERENCES.

(1) Brode, H.: "Space Plots of Pressure, Density and Particle Velocity for the Blast Wave from a Point Source in Air", RAND Report, RM-1913-AEC, June 1957.

(2) Cole, J.D. and Huth, J.H.: "Impulsive Loading on an Elastic Half Plane", RAND Report, P-467, December 1953.

(3) Miles, J.W.: "On the Response of a Layered Half-Space to a Moving Load", Space Technology Laboratories, T.N.-59-0000-00227, Report E.M.9-2, January 1959.

(4) Pekeris, C.L. and Lifson, H.: "Motion of the Surface of a Uniform Elastic Half-Space Produced by a Buried Pulse", J. Acoust. Soc. America, Vol. 29, No. 11, pp. 1233-1238.

(5) Chao, C.C.: "Dynamical Response of an Elastic Half-Space to Tangential Surface Loadings", J. Appl. Mech., September 1960, p. 559.

(6)* DiMaggio, F.L. and Bleich, H.H.: "An Application of a Dynamic Reciprocal Theorem", J. Appl. Mech., December 1959, p. 678.

(7) Graffi, D.: "Sui Teoremi di Reciprocita nei Fenomini Dipendendi dal Tempo", Annali di Matematica, Ser. 4, Vol. 18, 1939, pps. 178-200.

(8) Cole, J.D. and Huth, J.H.: "Elastic Stresses Produced in a Half-Plane by Steadily Moving Loads", RAND Report P-884, January 1956. Also J. Appl. Mech., Vol. 25, December 1958.

(9)* Chao, C.C., Bleich, H.H. and Sackman, J.L.: "Surface Waves in an Elastic Half-Space", RAND Report P-2066, August 1960.

(10) Miles, J.W.: "On the Response of an Elastic Half-Space to a Moving Blast Wave", Space Technology Laboratories GM-TR-0165-00524, November 1958.

(11)* Sackman, J.L.: "Load Moving with Superseismic Speed Over a Layered Elastic Solid". To be published as a RAND Report.

(12) Reever, W.L., Vining, T.F. and Strick, E.: "Propagation of Elastic Wave Motion from an Impulsive Source Along a Fluid/Solid Interface", Royal Soc. (London) Phil. Trans. Ser. A., No. 1000, September 1959.

(13) Pekeris, C.L.: "The Seismic Surface Pulse", Proc. National Academy of Science, Vol. 41.7, pp 469-480, 1955.

(14) Sommerfeld, A.: "Uber die Ausbreitung der Wellen in der drahtlosen Telegraphie", Annalen der Physik, Folge, H, Vol. 28, pp 665-736, 1909.

(15) Lubliner, J.: "Surface Waves in a Viscoelastic Half-Space", ONR Project Nr 064-417, Report No. 9, Columbia University, April 1960.

(16) Cinelli, G. and Fugelso, L.F.: "Theoretical Study of Ground Motion Produced by Nuclear Blasts", Report AFSWC-TR.-60-8, American Machine and Foundry Co., October 1959.

(17)* Baron, M.L., Bleich, H.H. and Weidlinger, P.: "Progress Report on Some Theoretical Investigations on the Vulnerability of Deep Underground Openings in Rock", Proceedings of the Second RAND Protective Construction Symposium, March 1959, pp. 925-961.

(18)* "Survivability of Air Defense Systems for the MITRE Corporation, October 1959 - Ground Shock Report", Paul Weidlinger, Consulting Engineer - Guy B. Panero, Engineers, (Secret), October 1959.

(19)* "Survivability of Air Defense Systems for the MITRE Corporation, March 1960 - Second Ground Shock Report", Paul Weidlinger, Consulting Engineer - Guy B. Panero, Engineers, (Secret), March 1960.

(20)* Baron, M.L. and Matthews, A.T.: "Diffraction of a Pressure Wave by a Cylindrical Cavity in an Elastic Medium", to be published as a RAND Report.

(21) Gilbert, J.F.: "Elastic Wave Interaction with a Cylindrical Cavity", E.H. Plesset Associates, Inc., December 1, 1959, Air Force Ballistic Missile Division, Contract AF04(647)-342.

(22) Baron, M.L.: "Response of Nonlinearly Supported Boundaries to Shock Waves", J. Appl. Mech., Vol. 24, No. 4, December 1957, pp. 501-506.

(23) Baron, M.L.: "The Response of a Cylindrical Shell to a Transverse Shock Wave", Proceedings of the Second U.S. National Congress of Applied Mechanics, 1955, p. 201.

(24) Prager, W.: "On Ideal Locking Materials", Transactions, Society of Rheology, Vol. 1, 1957, pp. 169-175.

(25) Phillips, A.: "A Theory of Ideal Locking Materials", Yale University, Contract NR-064-415, February 1958.

(26)* Salvadori, M.G., Skalak, R. and Weidlinger, P.: "Stress Waves in Dissipative Media", Transactions, New York Academy of Sciences, Ser. II, Vol. 21, No. 5, 1959, pp. 427-434.

(27)* Salvadori, M.G., Skalak, R. and Weidlinger, P.: "Waves and Shocks in Locking and Dissipative Media", Proceedings A.S.C.E., Vol. 68, No. E.M.2, April 1960.

(28)* Skalak, R. and Weidlinger, P.: "The Attenuation of Stress Waves in Bi-Linear Media", (To be published).

(29)* Salvadori, M.G., Skalak, R. and Weidlinger, P.: "Spherical Waves in an Ideal Locking Medium", (To be published).

(30) Kompaneets, A.S.: "Shock Waves in Plastic Compacting Media", Proc. Academy of Science, U.S.S.R., Vol. 106, No. 1, pp. 49-52.

(31) Zvolinskii, N.V.: "On the Emission of an Elastic Wave from a Spherical Explosion in the Ground", P.M.M. (Journal of Applied Mathematics and Mechanics), Vol. 24, No. 1, 1960, pp. 126-135.

(32)* Salvadori, M.G. and Weidlinger, P.: "Induced Ground Shock in Granular Media", Space Technology Laboratories, Report No. 1, March 1958.

(33)* Salvadori, M.G. and Weidlinger, P.: "Induced Ground Shock in Granular Media", Space Technology Laboratories, Report No. 2, July 1958.

(34)* Weidlinger, P.: "On the Application of the Theory of Locking Media to Ground Shock Phenomena", The MITRE Corporation, June 1960.

(35) Brode, H.L.: "The Effect of a Nuclear Bomb Blast Due to the Loss of Energy by Thermal Radiation", RAND Report RM-2076, December 1957.

Appendix A

STEADY STATE RESPONSE OF AN ELASTIC HALF-SPACE DUE TO A SURFACE PRESSURE MOVING WITH SUPERSEISMIC SPEED.

This Appendix considers the plane strain problem of finding displacements and stresses produced by the uniform motion of a distributed normal load $p(t - x/V)$ on the surface of an elastic half-space (Figure A-1). The speed V of the loading is greater than the propagation velocities c and c_p in the medium. It is assumed that the load has been acting for a sufficiently long time such that a steady state situation is established.

Figure (A-1) depicts the geometry. The coordinate system x, z is fixed in space, while $\bar{x}$, $\bar{z}$ is the coordinate system with origin at the front of the load and moving with the load with constant velocity V. (If the two coordinate systems coincide at $t = 0$, then $x = Vt - \bar{x}$, $z = \bar{z}$.) The displacements and stresses are obtained by superposition from the solution for the uniformly moving concentrated line load, Reference [8]. The results listed hereafter apply for the case where the two Lame constants are equal, $\lambda = \mu$. The horizontal and vertical displacements, u and v, respectively are

$$\left.\begin{aligned} u &= \frac{1}{\mu}\left[K_1 P\left(t - \frac{x + z\cot\alpha}{V}\right) + K_2 \cot\beta\, P\left(t - \frac{x + z\cot\beta}{V}\right)\right] \\ v &= \frac{1}{\mu}\left[-K_1 \cot\alpha\, P\left(t - \frac{x + z\cot\alpha}{V}\right) + K_2\, P\left(t - \frac{x + z\cot\beta}{V}\right)\right] \end{aligned}\right\} \qquad (1)$$

The stresses are:

$$\sigma_{zz} = (\cot^2\beta - 1)\, K_1 p' t - \frac{x + z\cot\alpha}{V}) - 2\cot\beta K_2 p\left(t - \frac{x + z\cot\beta}{V}\right) \qquad (2)$$

$$\left.\begin{aligned} \sigma_{xz} &= (\cot^2\beta - 1)\, K_2 \left[p\left(t - \frac{x + z\cot\alpha}{V}\right) - p\left(t - \frac{x + z\cot\beta}{V}\right)\right] \\ \sigma_{xx} &= (3 + \cot^2\alpha)\, K_1\; p\left(t - \frac{x + z\cot\alpha}{V}\right) + 2\cot\beta K_2 p\left(t - \frac{x + z\cot\beta}{V}\right) \end{aligned}\right\}, \quad (2)$$

where

$$\left.\begin{aligned} &\alpha = \sin^{-1}\frac{V}{c_p} \qquad \beta = \sin^{-1}\frac{V}{c} \qquad \frac{c_p}{c} = \sqrt{3} \\ &K_1 = -\frac{1}{2}\left[\frac{\cot 2\beta}{\cot\alpha + \cot\beta\cot^2 2\beta}\right] \\ &K_2 = \frac{1}{2\cot\beta}\left[\frac{\cot\alpha}{\cot\alpha + \cot\beta\cot^2 2\beta}\right] \end{aligned}\right\} \quad (3)$$

the function P is the integral of the function p defining the applied load,

$$P(\eta) = V\int_0^{\eta} p(\xi)\,d\xi \qquad (4)$$

The shear wave velocity and pressure wave velocity are respectively c and c_p. The pressure p is positive when acting in the positive z direction, and σ_{zz} and σ_{xx} are positive if tensile.

It is also convenient to have expressions for the strengths of the plane P-and S-waves generated by the moving load. The strength of the P-wave is best defined by the normal stress σ at right angles to the plane of its wave front. (See Figure 1) Similarly, the strength of the S-wave is defined by the shear stress τ in the plane of its wave front.

For $\lambda = \mu$, the values of σ and τ are:

$$\left.\begin{aligned} &\sigma\left(t - \frac{x + z\cot\alpha}{V}\right) = -\frac{3}{K_3}\, p\left(t - \frac{x + z\cot\alpha}{V}\right) \\ &\tau\left(t - \frac{x + z\cot\beta}{V}\right) = -\frac{\sin 2\alpha}{K_3\cos 2\beta}\, p\left(t - \frac{x + z\cot\beta}{V}\right) \\ &K_3 = 1 + 2\cos^2\alpha + \sin 2\alpha\tan 2\beta \end{aligned}\right\} \quad (5)$$

A plot of the quantities σ/p and τ/p is shown in Figure (2). It is seen that, except near $V/c_p = 1$, the ratio $|\sigma/p|$ is nearly equal to unity; $|\tau/p|$ varies appreciably, its maximum being about 0.60. The consequences of the sensitivity of the solution near $V/c_p = 1$ are discussed in the body of the report.

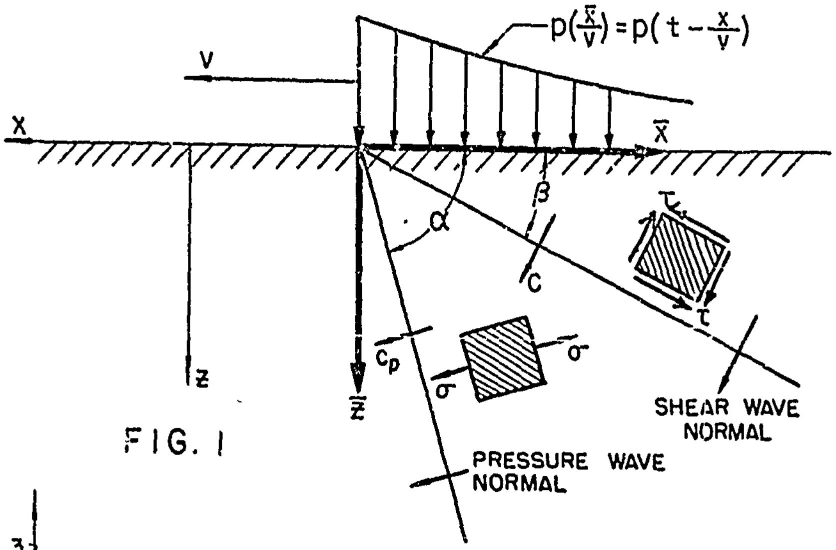
$p(\frac{\bar{x}}{V}) = p(t - \frac{x}{V})$
V
X
$\bar{X}$
β
α
C
τ
τ
C_p
σ
σ
z
$\bar{z}$
SHEAR WAVE NORMAL
PRESSURE WAVE NORMAL

FIG. 1

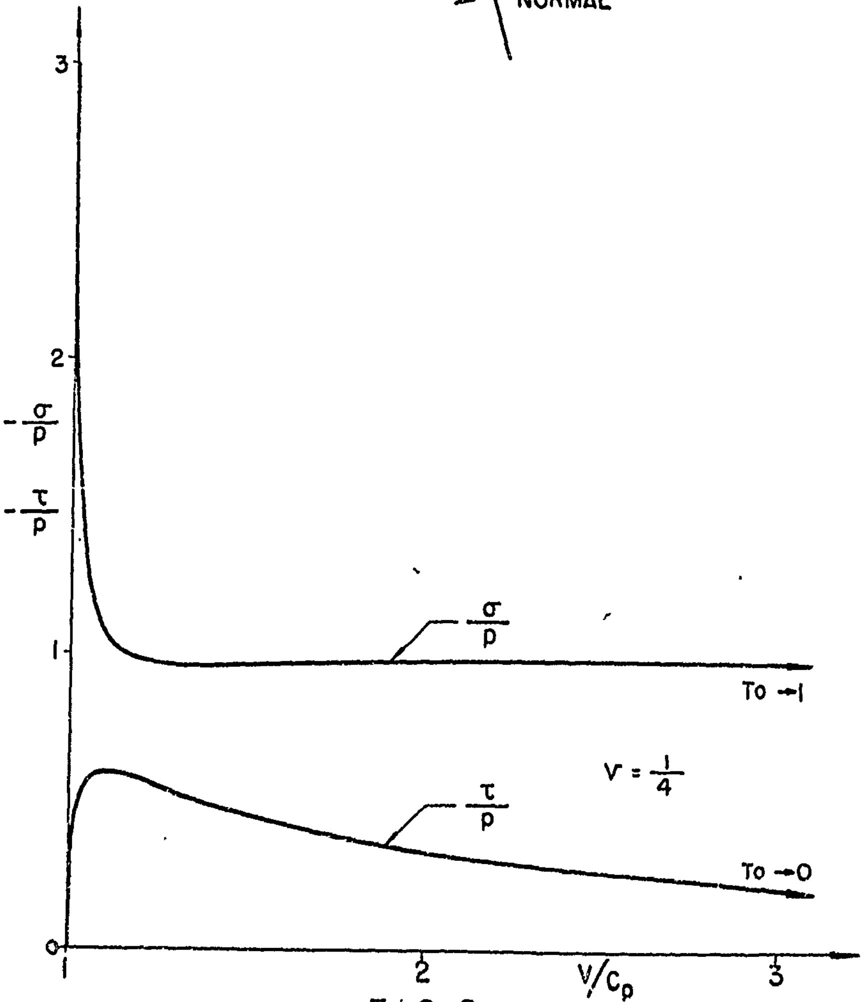
3
2
1
0
$-\frac{\sigma}{p}$
$-\frac{\tau}{p}$
$\frac{\sigma}{p}$
To → 1
$\nu = \frac{1}{4}$
$\frac{\tau}{p}$
To → 0
1
2
3
V/C_p

FIG. 2

Appendix B

SURFACE WAVES IN AN ELASTIC HALF SPACE

At large distances from a disturbance, the major effects near the surface are due to Rayleigh Waves. This has been discovered theoretically by Rayleigh and is well confirmed by seismological experience. It is the purpose of the present paper to give suitable expressions for the determination of Rayleigh effects due to transient normal pressures on the surface. Specifically, closed form solutions are presented for the effect of a concentrated load, suddenly applied and maintained thereafter. Any general pressure distribution may then be treated by integration in space and time.

The complete effect of a suddenly applied concentrated load has been treated by Pekeris [1, 2]*, who also obtained response curves for certain displacements requiring lengthy numerical integrations. As noted by Pekeris [2], and long ago found by Sommerfeld [3], the surface effects can be obtained by the transform approach as contributions of certain poles, ignoring branch integrals which occur in a complete solution. This approach is used hereafter. Introducing the clearly appropriate simplification of considering the depth small versus the radial distance from the force, relatively simple closed form expressions will be obtained for stresses and displacements.

By superposition this concentrated force solution can be used to obtain approximate solutions for various types of distributed pressure loadings on the surface of the half-space. As an example, expressions are given for the displacement and stress components caused by a surface pressure (with an intensity varying in time) uniformly distributed over a circular disk of increasing radius.

---

*) References are listed at the end of this Appendix.

Analysis

The geometry of the problem is depicted in Figure (1) where a concentrated force P (positive downward, and varying with time as the step function) acts on the surface of an elastic half-space. Reference [1] (Equations (3), (9), (16)-(19)) gives the Hankel-Laplace transforms of the potentials from which the transforms of the vertical and radial displacements, u_z and u_r, respectively may be derived:

$$u_z(r, t) = \frac{P}{4\pi^2 \mu i} \int_0^\infty d\xi \int_{a-i\infty}^{a+i\infty} J_0(\xi r)\xi \left[(2\xi^2 + k^2)e^{-k\alpha z+pt} - 2\xi^2 e^{-k\beta z+pt}\right]\left[\frac{\alpha k}{M(\xi)}\right]\frac{dp}{p}$$

$$u_r(r, t) = \frac{P}{4\pi^2 \mu i} \int_0^\infty d\xi \int_{a-i\infty}^{a+i\infty} J_1(\xi r) \left[(2\xi^2 + k^2)e^{-k\alpha z+pt} - (2\xi^2 + h^2)^{1/2}(\xi^2 + k^2)^{1/2}e^{-k\beta z+pt}\right]\left[\frac{\xi^2}{M(\xi)}\right]\frac{dp}{p} \qquad (1)$$

where

$$h^2 = (\frac{p}{c_p})^2 \qquad k^2 = (\frac{p}{c})^2 \qquad c^2 = \frac{\mu}{\rho} \quad , \quad c_p^2 = \frac{\lambda + 2\mu}{\rho} = 3c^2$$

$$k\alpha = (\xi^2 + h^2)^{1/2} \qquad k\beta = (\xi^2 + k^2)^{1/2} \qquad i = \sqrt{-1} \qquad (1a)$$

$$M(\xi) = (2\xi^2 + k^2)^2 - 4k^2\xi^2\alpha\beta$$

For simplicity, similar to [1], the two Lamé constants have been set equal, $\lambda = \mu$. In order to insure decay of the displacements at infinity, the branch of the square root must be chosen to yield a positive real part.

The approximate solution for the Rayleigh phase is obtained from Equations (1) by utilizing only the residues of the integrals at the

(Rayleigh) poles, $p = \pm \frac{ib\xi}{\gamma}$, with $\gamma = (\frac{1}{2})(3 + \sqrt{3})^{1/2}$ (reference [2]).

The contribution from the poles is:

$$u_z = -\frac{P}{\pi\mu r}\left[\frac{(\gamma^2 - \frac{1}{3})^{1/2}}{\dot{F}(\gamma)}\right] \operatorname{Im}\left\{\frac{1 - 2\gamma^2}{(\nu^2 - 1)^{1/2}} + \frac{2\gamma^2}{(\omega^2 - 1)^{1/2}}\right\} \tag{2}$$

$$u_r = \frac{P}{\pi\mu r}\left[\frac{\gamma}{\dot{F}(\gamma)}\right] \operatorname{Re}\left\{(1 - 2\gamma^2)\left[1 - \frac{\nu}{(\nu^2 - 1)^{1/2}}\right] + 2(\gamma^2 - 1)^{1/2}(\gamma^2 - \tfrac{1}{3})^{1/2}\left[1 - \frac{\omega}{(\omega^2 - 1)^{1/2}}\right]\right\}$$

where, again, that branch of the square root must be taken which yields a positive real part, and where

$$\omega = \left[\tau + i\ell\,(\gamma^2 - 1)^{1/2}\right]\Big/\gamma$$

$$\nu = \left[\tau + i\ell\,(\gamma^2 - \tfrac{1}{3})^{1/2}\right]\Big/\gamma \tag{2a}$$

$$\tau = \frac{ct}{r}, \quad \ell = \frac{z}{r}, \quad \dot{F}(\gamma) = -\frac{8\sqrt{3}}{3}\,\gamma$$

Since only the Rayleigh phase is being considered, these expressions are only applied to shallow depths ($\ell \ll 1$) and to values of the time near the arrival time of the Rayleigh wave ($\tau \doteq \gamma$). Using these restrictions, Equations (2) may be approximately simplified to the final form:

$$u_z = K_1(\gamma^2 - \tfrac{1}{3})^{1/2} \operatorname{Im}\left[(1 - 2\gamma^2)\, z_1^{-1/2} + 2\gamma^2\, z_2^{-1/2}\right]$$

$$u_r = K_1\, \gamma \operatorname{Re}\left[(1 - 2\gamma^2)\, z_1^{-1/2} + 2(\gamma^2 - 1)^{1/2}(\gamma^2 - \tfrac{1}{3})^{1/2}\, z_2^{-1/2}\right] \tag{3}$$

where

$$K_1 = \frac{3P}{8\sqrt{6\gamma}\,\pi\mu r^{1/2} z^{1/2}} \tag{3a}$$

$$z_1 = \frac{\tau - \gamma}{\ell} + i(\gamma^2 - \tfrac{1}{3})^{1/2}$$

$$z_2 = \frac{\tau - \gamma}{\ell} + i(\gamma^2 - 1)^{1/2}$$

From these expressions for the displacements, expressions for the stress components may be derived by routine differentiation where $\ell \ll 1$, $\tau \doteq \gamma$ is used again:

$$\sigma_{zz} = K_2\,(2\gamma^2 - 1)^2\ \mathrm{Re}\left[z_1^{-3/2} - z_2^{-3/2}\right]$$

$$\sigma_{rz} = K_2\,(-2\gamma)(\gamma^2 - \tfrac{1}{3})^{1/2}\ \mathrm{Im}\left[z_1^{-3/2} - z_2^{-3/2}\right] \qquad (4)$$

$$\sigma_{\theta\theta} = K_2\,\left(\frac{1 - 2\gamma^2}{3}\right)\ \mathrm{Re}\left[z_1^{-3/2}\right]$$

$$\sigma_{rr} = K_2\,(1 - 2\gamma^2)\ \mathrm{Re}\left[(2\gamma^2 + \tfrac{1}{3})\, z_1^{-3/2} + (1 - 2\gamma^2)\, z_2^{-3/2}\right]$$

where

$$K_2 = \frac{3P}{16\sqrt{6\gamma}\,\pi r^{1/2} z^{3/2}} \qquad (4a)$$

The numerical evaluation of Equations (3), (4) is simple. Not only are the expressions in closed form, but each of the responses, for a given medium, is solely a function of a single parameter, the non-dimensional time τ. Figure(2) shows as example the vertical stress σ_{zz} (note $\frac{\tau - \gamma}{\ell} = \frac{ct - \gamma r}{z}$).

Equations (3) and (4) may be utilized to obtain approximate solutions for various types of pressure loadings on the surface of the elastic half-space. Consider as an example the loading depicted in Figure(3). A normal load of intensity p (varying in time) is distributed uniformly over a circular disk of increasing radius R. Assuming further that $R \ll r$, the solution may be written

$$u_m = K_3 \int_0^t p(\tau)\,d\tau \int_{-R(\tau)}^{R(\tau)} \left[R^2(\tau) - x^2\right]^{1/2} \bar{u}_m\,dx \quad (m = r,\ z\ ) \qquad (5)$$

where

$$K_3 = -\frac{3P}{8\sqrt{6\gamma}\,\pi\mu r^{1/2} z^{3/2}}$$

$$\bar{u}_z = (\gamma^2 - \tfrac{1}{3})^{1/2} \,\mathrm{Im}\left[(1 - 2\gamma^2)\,\bar{Z}_1^{-3/2} + 2\gamma^2\,\bar{Z}_2^{-3/2}\right]$$

$$\bar{u}_r = \gamma\,\mathrm{Re}\left[(1 - 2\gamma^2)\bar{Z}_1^{-3/2} + 2(\gamma^2 - \tfrac{1}{3})^{1/2}(\gamma^2 - 1)^{1/2}\,\bar{Z}_2^{-3/2}\right] \qquad (5a)$$

$$\bar{Z}_1 = \frac{1}{z}(ct - \gamma r - c\tau - \gamma x) + i(\gamma^2 - \tfrac{1}{3})^{1/2}$$

$$\bar{Z}_2 = \frac{1}{z}(ct - \gamma r - c\tau - \gamma x) + i(\gamma^2 - 1)^{1/2}$$

and

$$\sigma_{mn} = K_4 \int_0^t p(\tau)\,d\tau \int_{-R(\tau)}^{R(\tau)} \left[R^2(\tau) - x^2\right]^{1/2} \bar{\sigma}_{mn}\,dx \quad (m, n = r, \theta, z) \qquad (6)$$

where

$$K_4 = -\frac{9\,c}{16\sqrt{6\gamma}\,\pi r^{1/2} z^{5/2}}$$

$$\bar{\sigma}_{zz} = (2\gamma^2 - 1)^2\,\mathrm{Re}\left[\bar{Z}_1^{-5/2} - \bar{Z}_2^{-5/2}\right] \qquad (6a)$$

$$\bar{\sigma}_{rz} = -2\gamma(\gamma^2 - \tfrac{1}{3})^{1/2}\,\mathrm{Im}\left[\bar{Z}_1^{-5/2} - \bar{Z}_2^{-5/2}\right]$$

$$\bar{\sigma}_{\theta\theta} = \left(\frac{1 - 2\gamma^2}{3}\right)\mathrm{Re}\left[\bar{Z}_1^{-5/2}\right]$$

$$\bar{\sigma}_{rr} = (1 - 2\gamma^2)\,\mathrm{Re}\left[(2\gamma^2 + \tfrac{1}{3})\,\bar{Z}_1^{-5/2} + (1 - 2\gamma^2)\,\bar{Z}_2^{-5/2}\right]$$

Equations (3) and (4) break down for $z = 0$, and the integration procedure (5), (6) can therefore not be used for the surface $z = 0$ either. The determination of responses from transient distributed loads for $z = 0$ requires a separate approach starting from the transform expressions for these loads, or equivalent procedures of going to the limit $z \to 0$.

[illegible] $\sigma_{\theta\theta}$, σ_{rz} and σ_{zz} [illegible] the surface pressures in the neighborhood of [illegible] been obtained. The evaluation of the double integral [illegible] ( ), represents a major computational effort for [illegible] interest. The integration was done numerically, [illegible] finite difference integration formulas (Simpson's Rule) for both [illegible] and time integrations. The variable upper and lower limits [illegible] space integration added materially to the numerical complexity of the problem.

The integral over space (in the variable [illegible]) which utilized the influence coefficients $\bar{\sigma}_{mn}$ was replaced by a finite difference mesh for application to Simpson's rule for integration. The rapidly oscillating characteristic of the influence coefficients $\bar{\sigma}_{mn}$ necessitated the use of an extremely fine mesh in these calculations; in many cases several hundred points were required for <u>each</u> integration corresponding to an upper and lower limit of $R(\tau)$. Curves for these coefficients $\bar{\sigma}_{mn}$ are given in Figs. (4)-(7) and illustrate the necessity for the fine mesh required in the space integration.

The pressure-time curve, $p(\tau)$, and the range-time curve, $R(\tau)$, corresponding to a hypothetical 20 M.T. surface explosion are shown in Figs. (8)-(9). As we are primarily interested in the Rayleigh effects generated by the high intensity surface pressures in the neighborhood of Ground Zero, the pressure and range curves were cut off after a certain time t_c in the computational program. The integration in time, using these functions as inputs was also made using Simpson's rule for the integration procedure.

The computations were made, by necessity using an IBM 704 computer. The complete numerical analysis as well as the detailed computer program will be presented in detail in a forthcoming paper [4].

Results were obtained at various depths below three surface pressure contours for the 20 M.T. surface burst. First, an elastic medium in which $c = 10,000$ ft/sec., $\nu = 1/4$ was considered. The pressure contours chosen were at $R = 2000$ ft. [10,000 psi contour], $R = 3200$ ft. [2,000 psi contour] and $R = 500$ ft. [700 psi contour].

Figs. (10)-(12) show the attenuation of the peak stresses σ_{rr}, $\sigma_{\theta\theta}$ and σ_{zz} with depth at the 2000 ft., 3200 ft. and 5000 ft. distances from Ground Zero for the elastic medium with $c = 10,000$ ft/sec. and a weight of 167 lb/ft^3. These curves are useful in determining the depth at each location below which Rayleigh wave effects are small and may be neglected. The reader is referred to the discussion of the determination of Rayleigh wave effects in Sec. (3) of the report and to the results presented in Fig. (3-10)-(3-13).

The stresses produced by a 20 M.T. surface explosion on a slower elastic medium in which $c = 6000$ ft/sec. but whose weight was the same, i.e. 167 lb/ft^3, were also obtained for $R = 3200$ ft. [2000 psi contour] at various depths. Fig.(13) show the attenuation of the peak stresses σ_{rr}, $\sigma_{\theta\theta}$ and σ_{zz} with depth at this location.

Some typical stress versus time histories for Rayleigh effects are shown for σ_{rr}, $\sigma_{\theta\theta}$ and σ_{zz} at the indicated range and depth in Figs.[(14)-(16)].

References

1. Pekeris, C. L. "The Seismic Surface Pulse", Proc. National Academy of Science, Vol. 41.7, pp 469-480, 1955

2. Pekeris, C. L. and Lifson, Hanna, "Motion of the Surface of a Uniform Elastic Half-Space Produced by a Buried Pulse", Journal of Acoustical Society of America, Vol. 29, No. 11, pp 1233-1238, Nov. 1957

3. Sommerfeld, A. "Uber die Ausbreitung der Wellen in der drahtlosen Telegraphie", Annalen der Physik 4. Folge, Vol. 28, pp 667-736, 1909

4. Baron, M. L. and Lecht, C. "Surface Wave Effects from Surface Explosions in an Elastic Half-Space", Forthcoming paper.

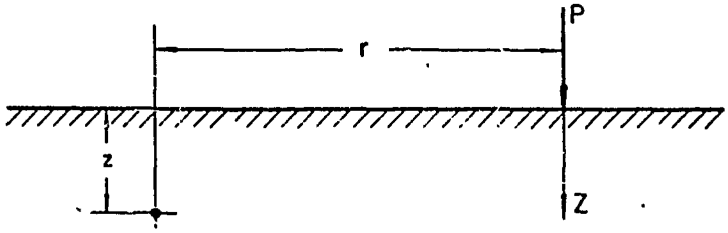

FIG. 1

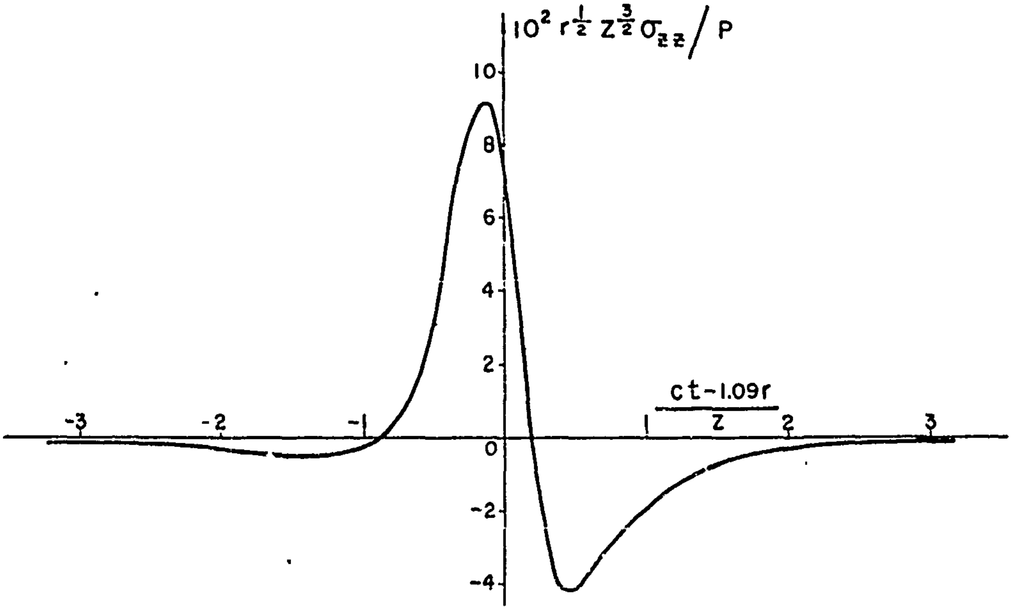

FIG. 2

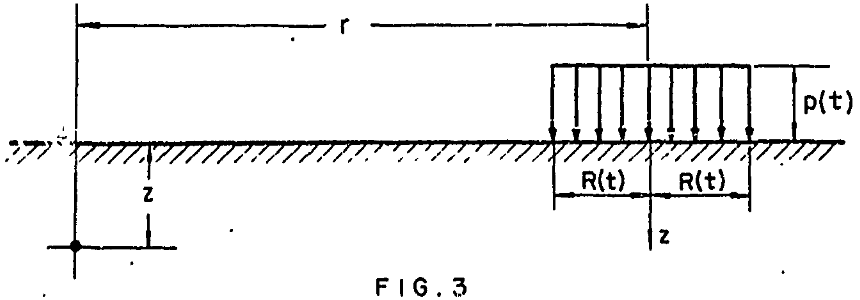

FIG. 3

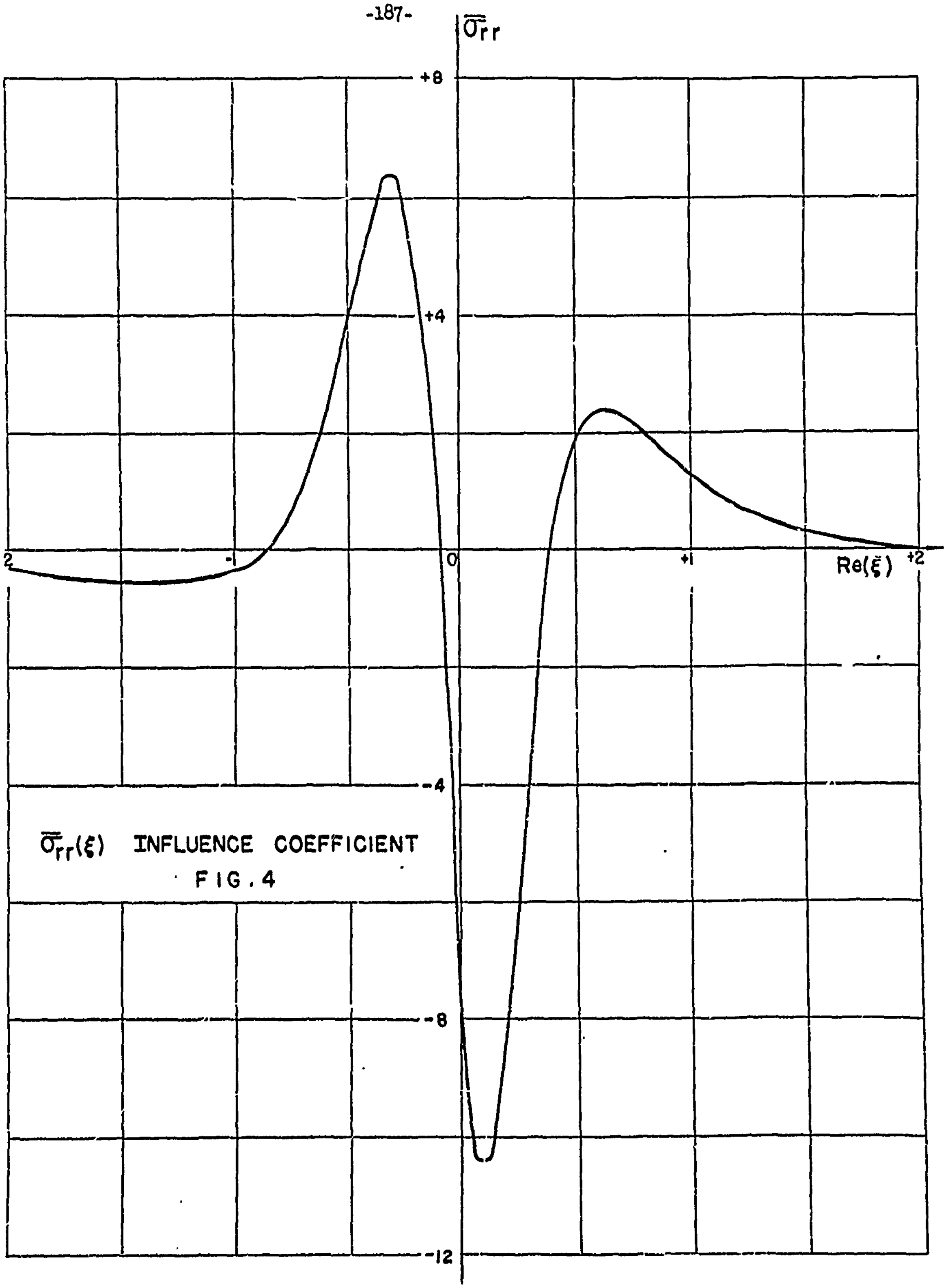

$\overline{\sigma}_{rr}(\xi)$ INFLUENCE COEFFICIENT

FIG. 4

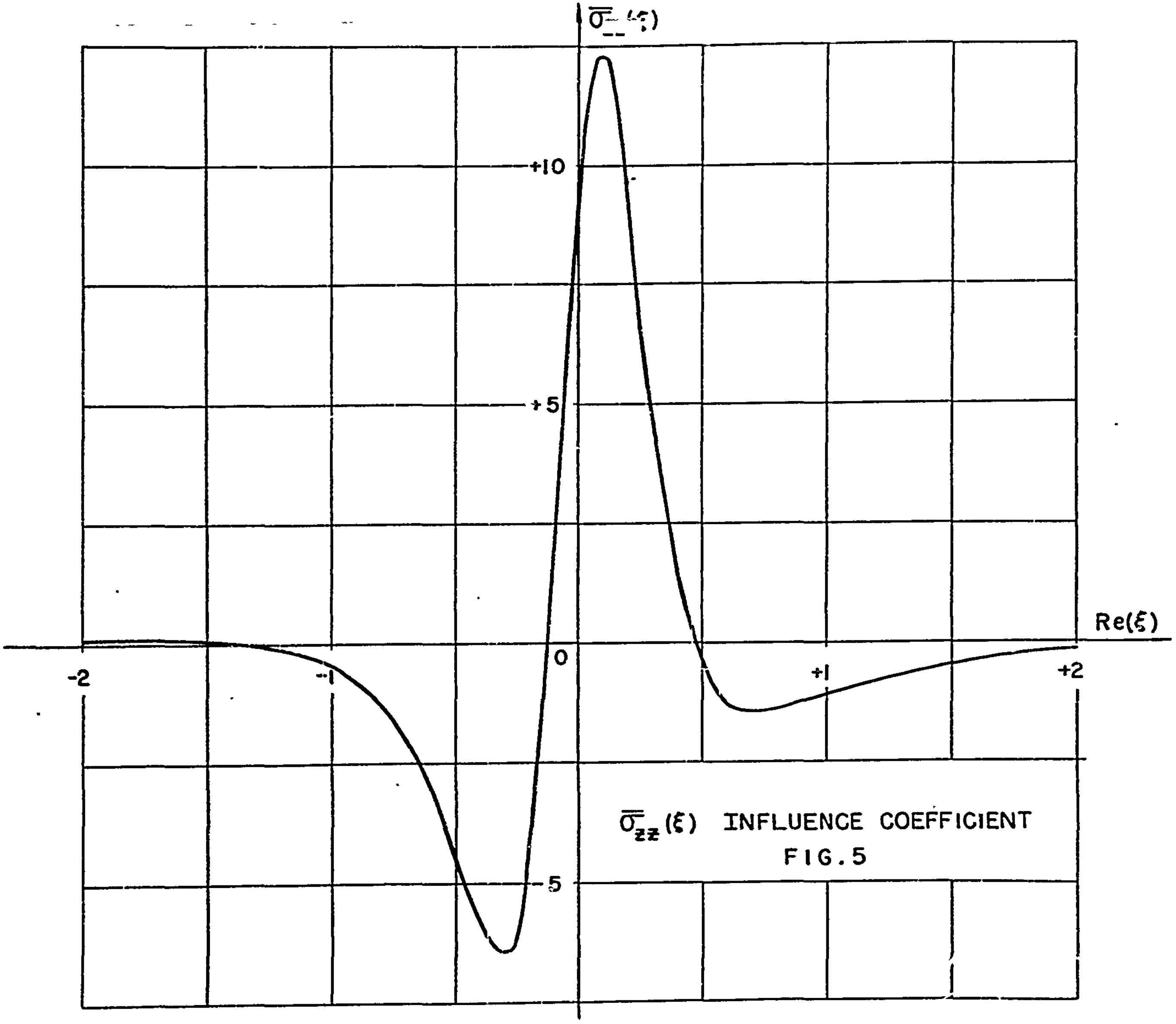

$\overline{\sigma}_{zz}(\xi)$ INFLUENCE COEFFICIENT

FIG. 5

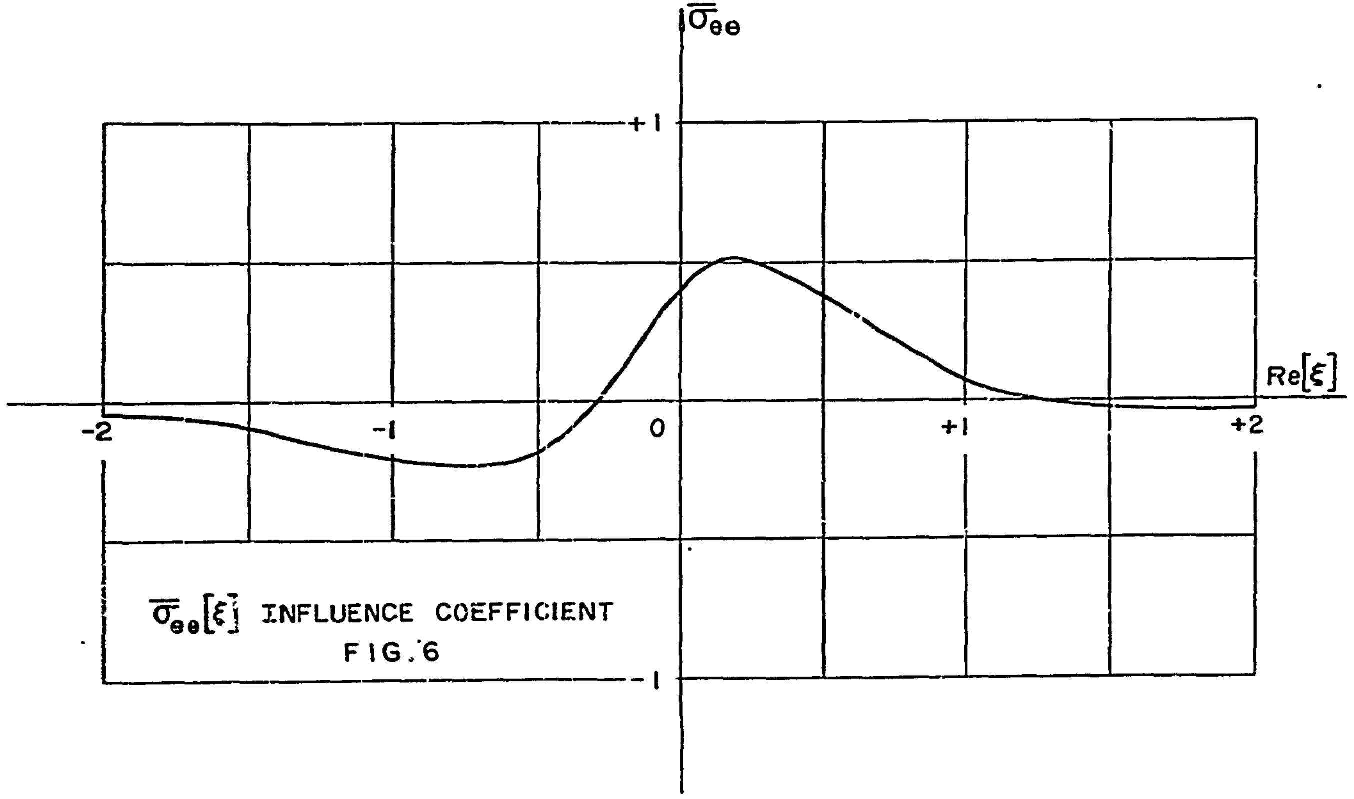

$\overline{\sigma}_{\theta\theta}[\xi]$ INFLUENCE COEFFICIENT

FIG. 6

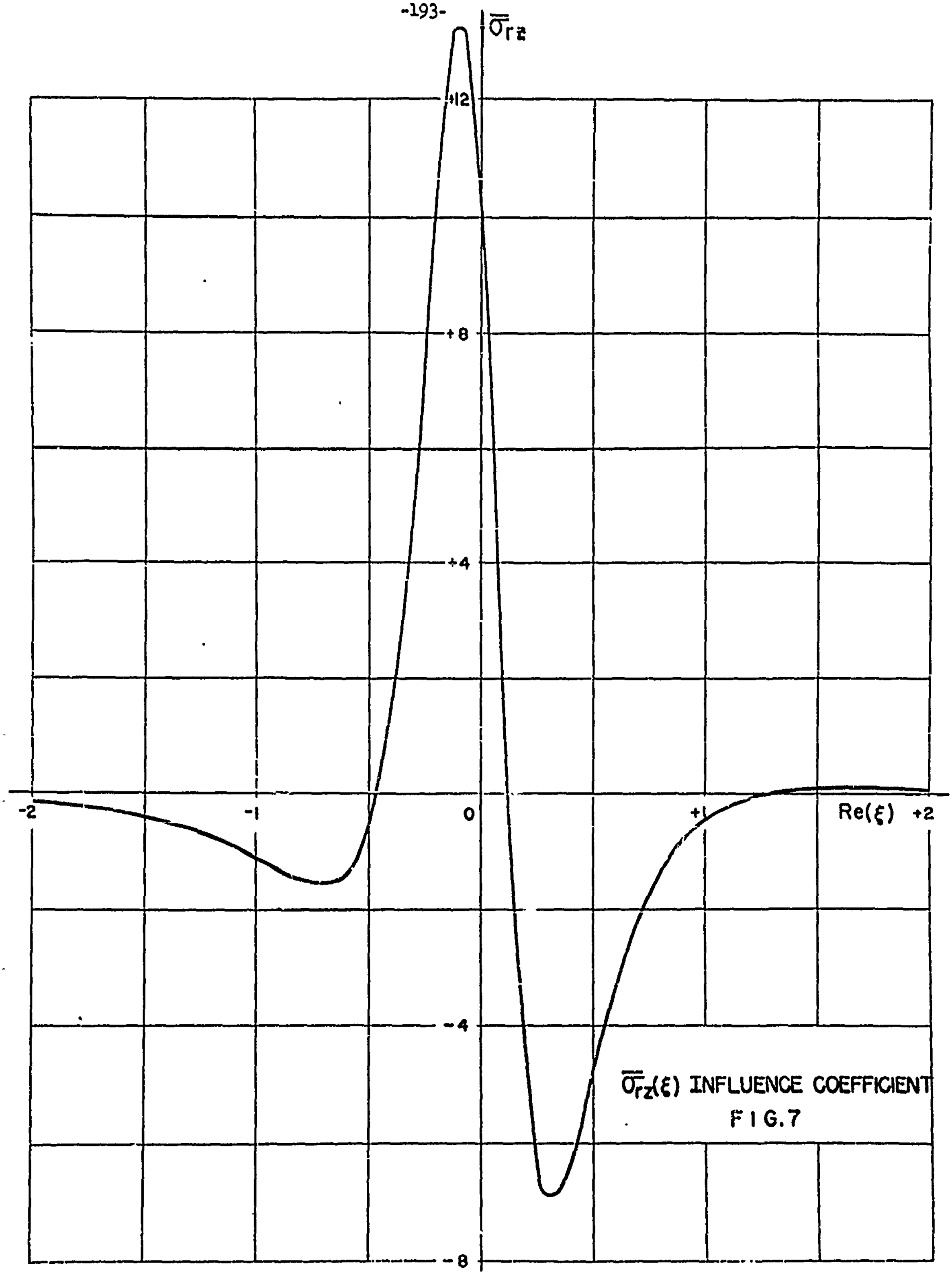

$\overline{\sigma}_{rz}(\xi)$ INFLUENCE COEFFICIENT

FIG.7

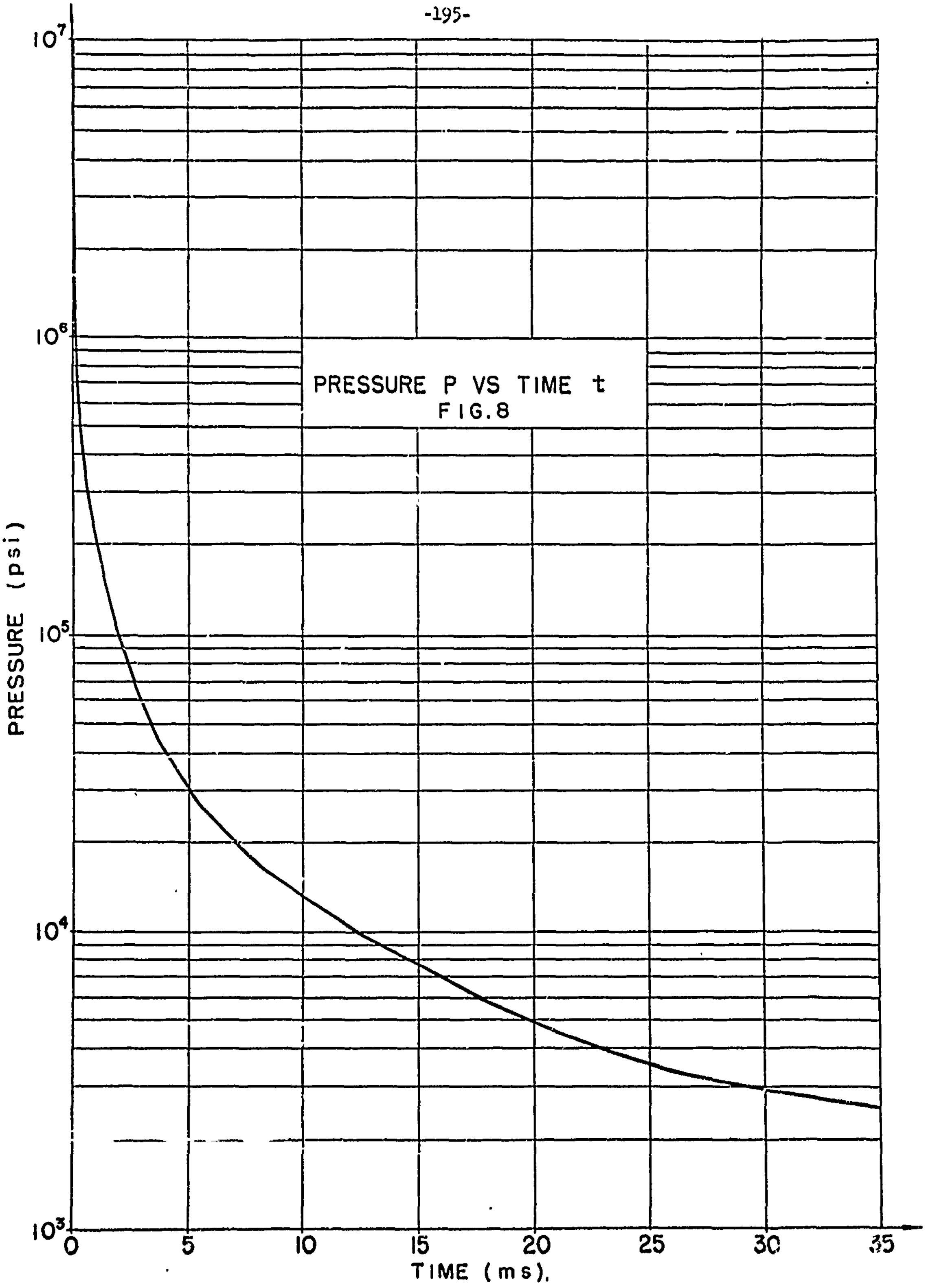
PRESSURE P VS TIME t
FIG.8
PRESSURE (psi)
10^7
10^6
10^5
10^4
10^3
0
5
10
15
20
25
30
35
TIME (ms).

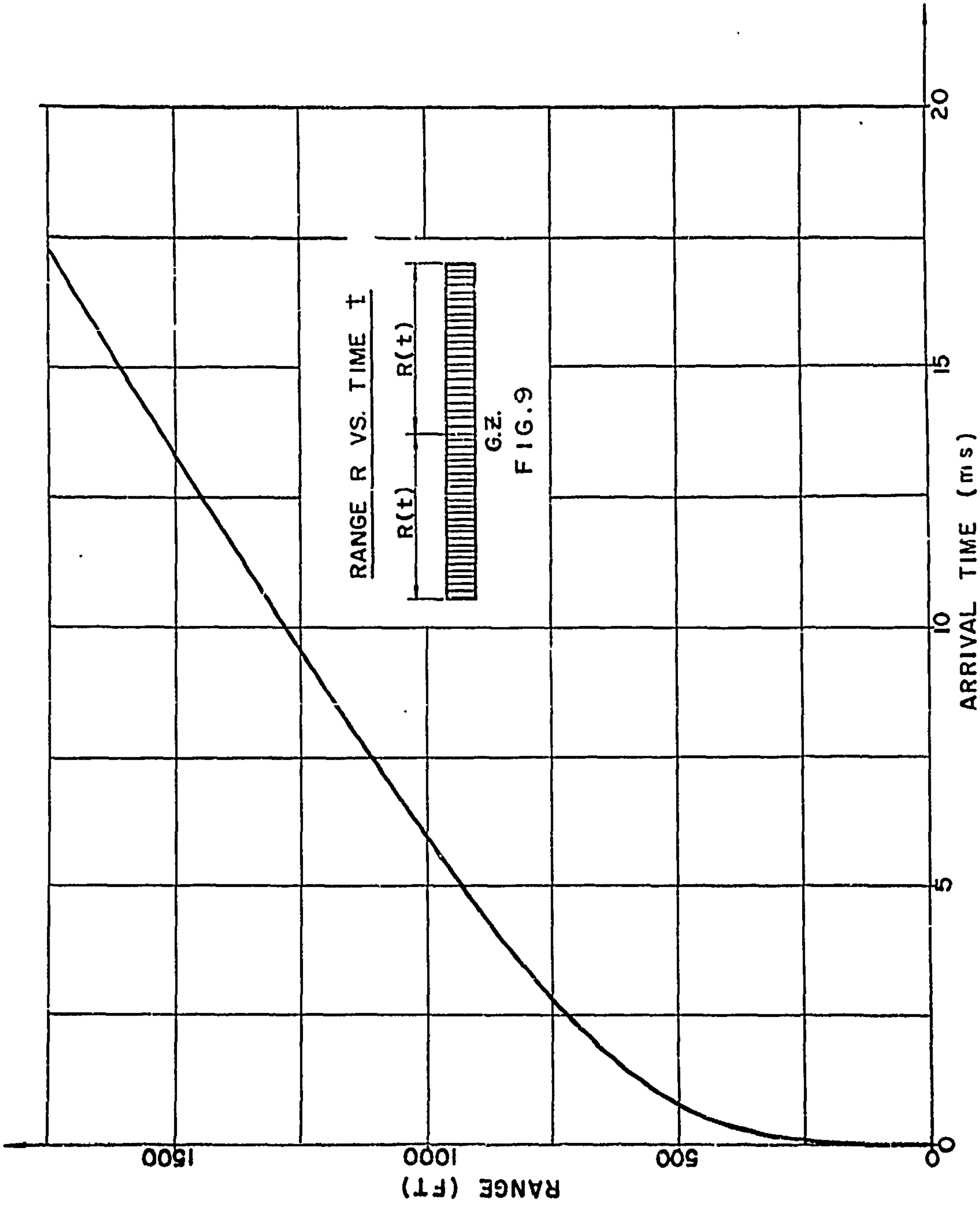
RANGE R VS. TIME t
R(t)
R(t)
G.Z.
ARRIVAL TIME (ms)
0
5
10
15
20
RANGE (FT)
0
500
1000
1500

FIG. 9

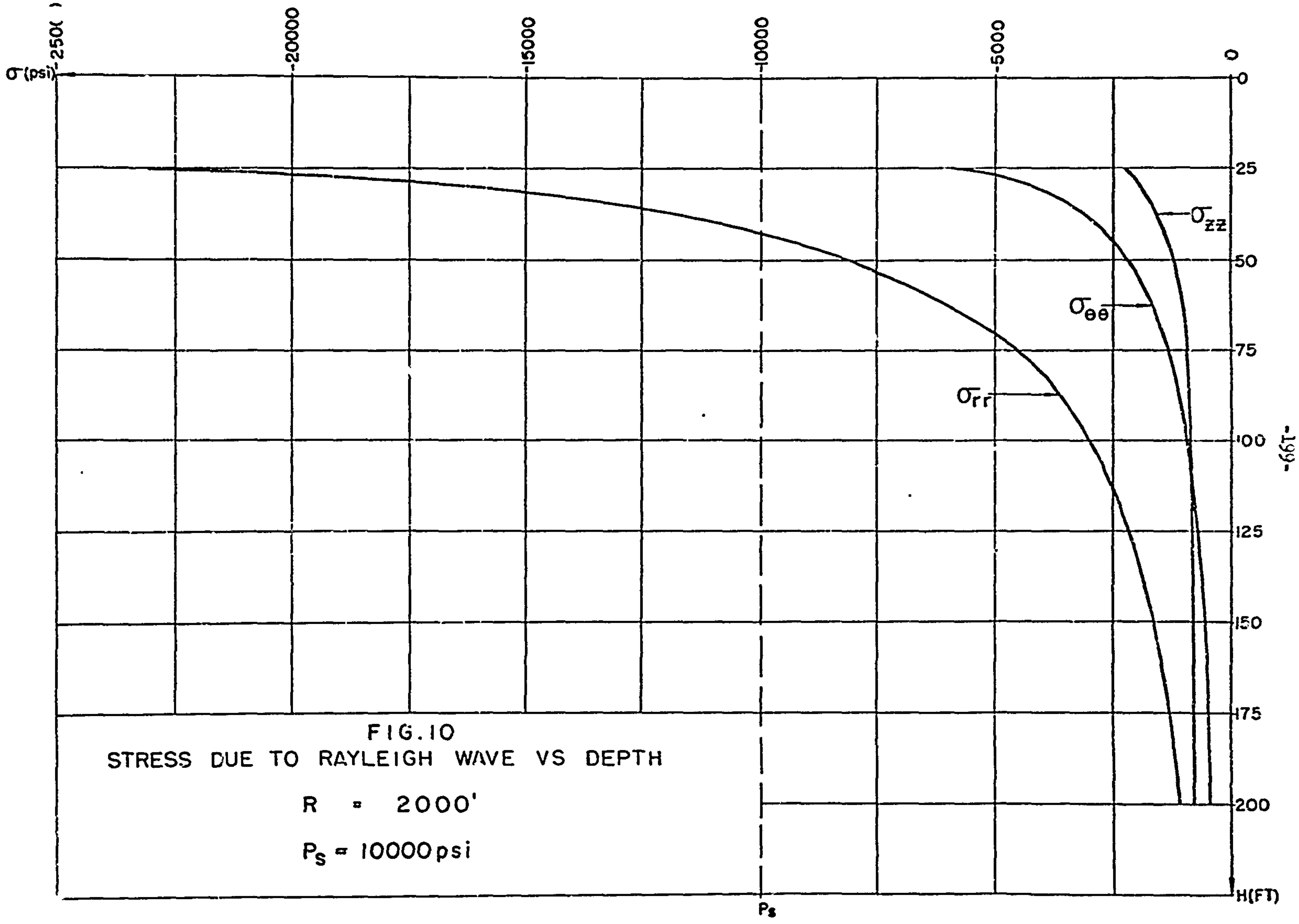

FIG.10
STRESS DUE TO RAYLEIGH WAVE VS DEPTH

R = 2000'

P_S = 10000 psi

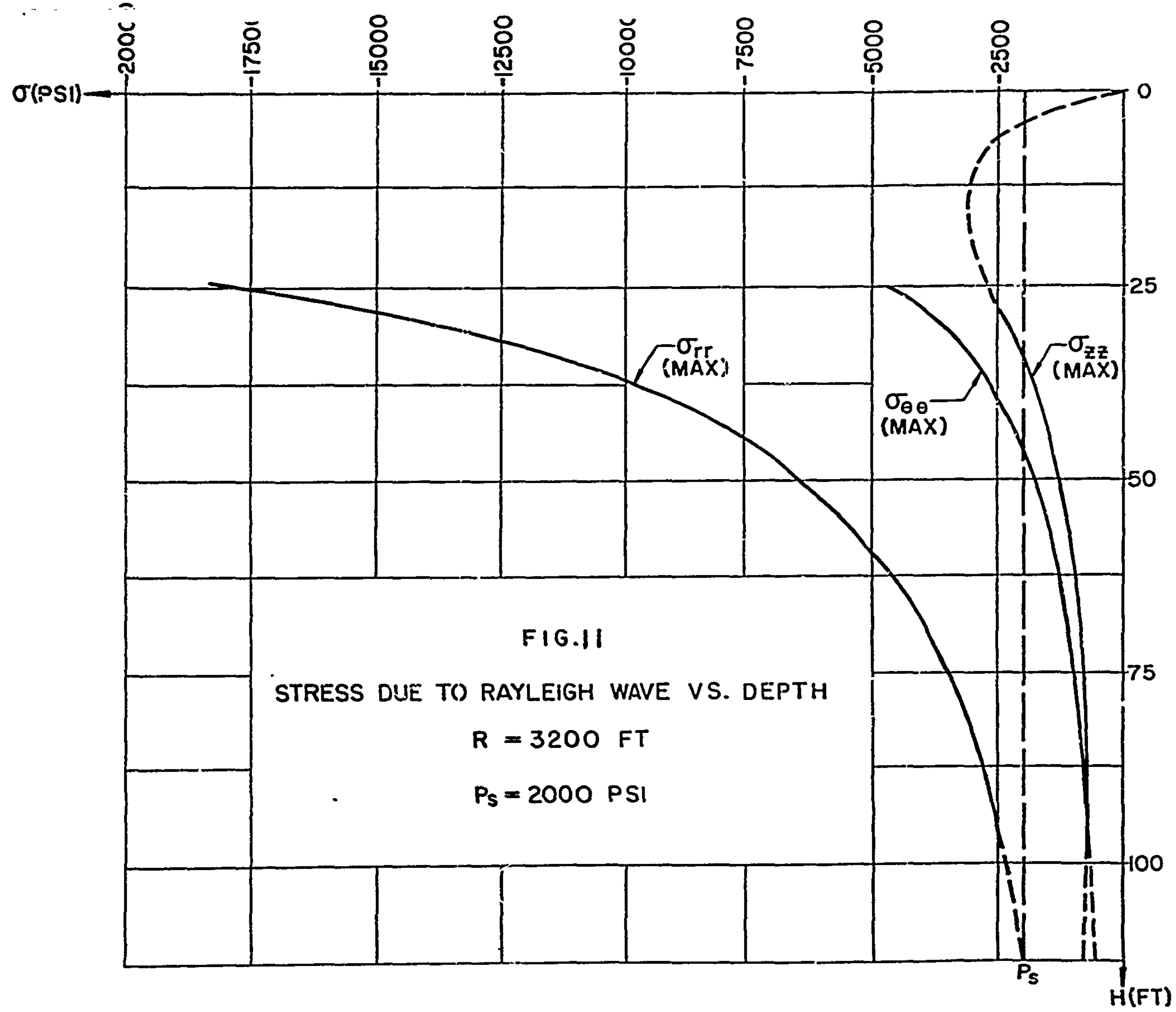

FIG. 11

STRESS DUE TO RAYLEIGH WAVE VS. DEPTH

R = 3200 FT

P_s = 2000 PSI

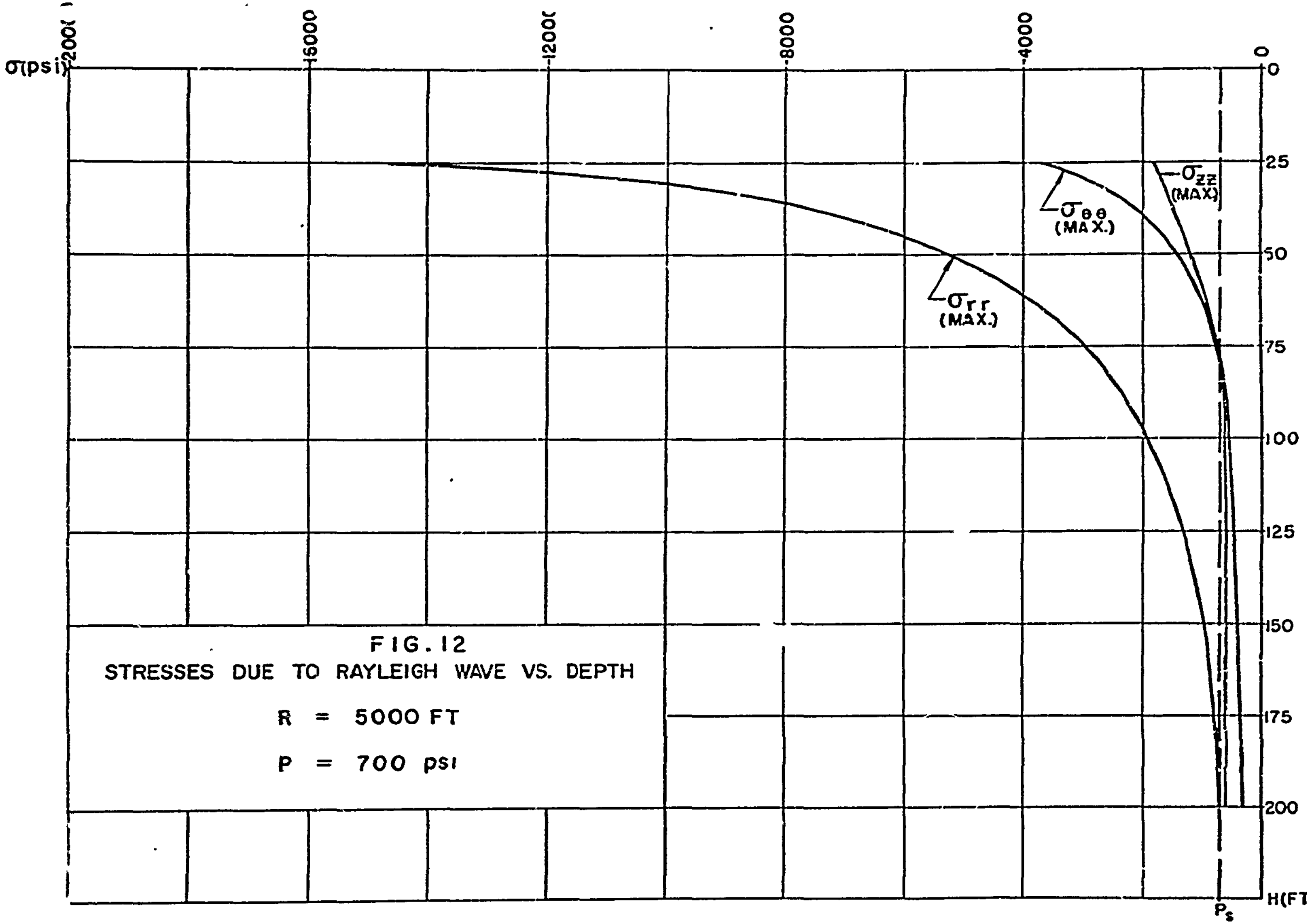

FIG. 12
STRESSES DUE TO RAYLEIGH WAVE VS. DEPTH

R = 5000 FT

P = 700 psi

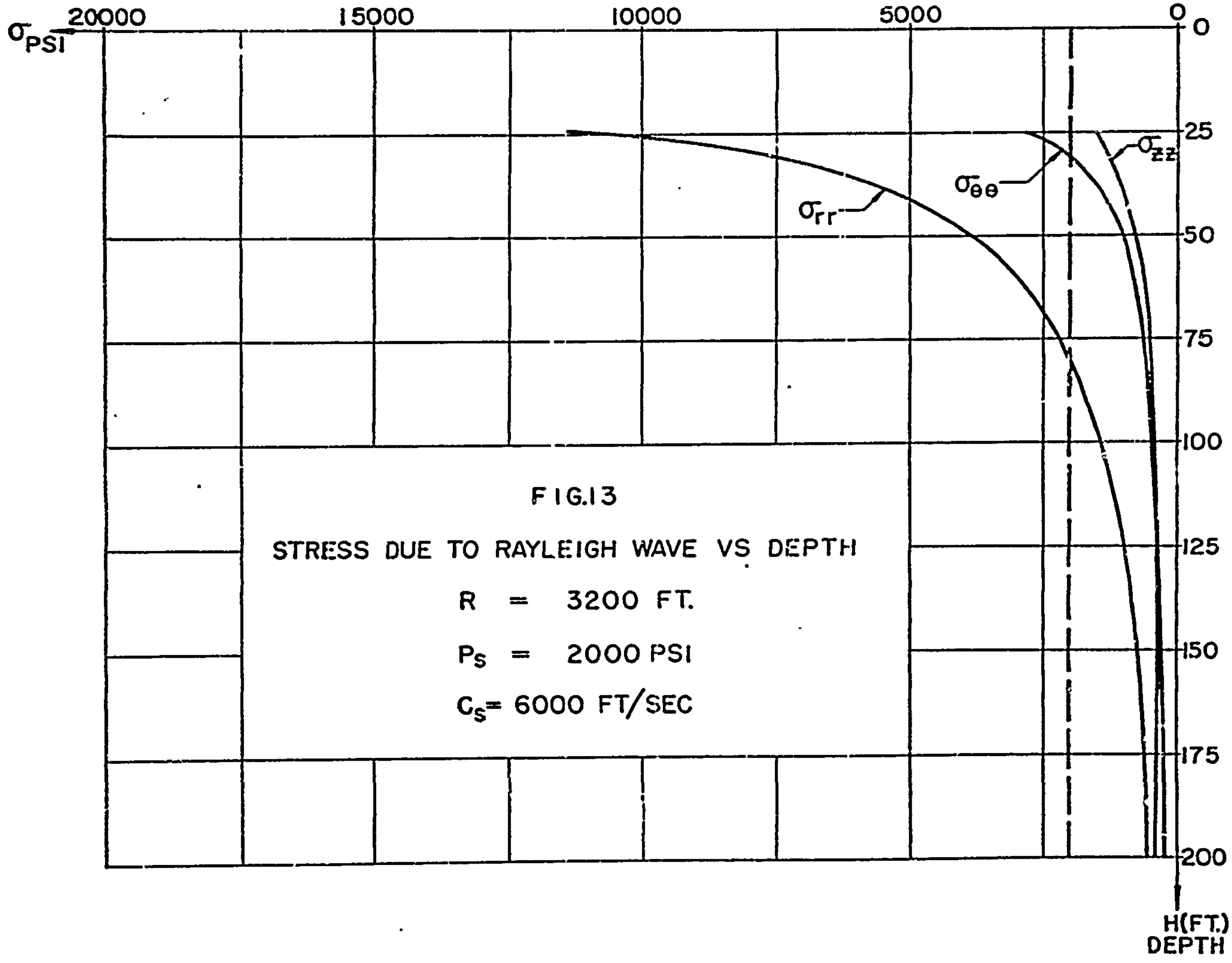

FIG.13

STRESS DUE TO RAYLEIGH WAVE VS DEPTH

$R = 3200$ FT.

$P_s = 2000$ PSI

$C_s = 6000$ FT/SEC

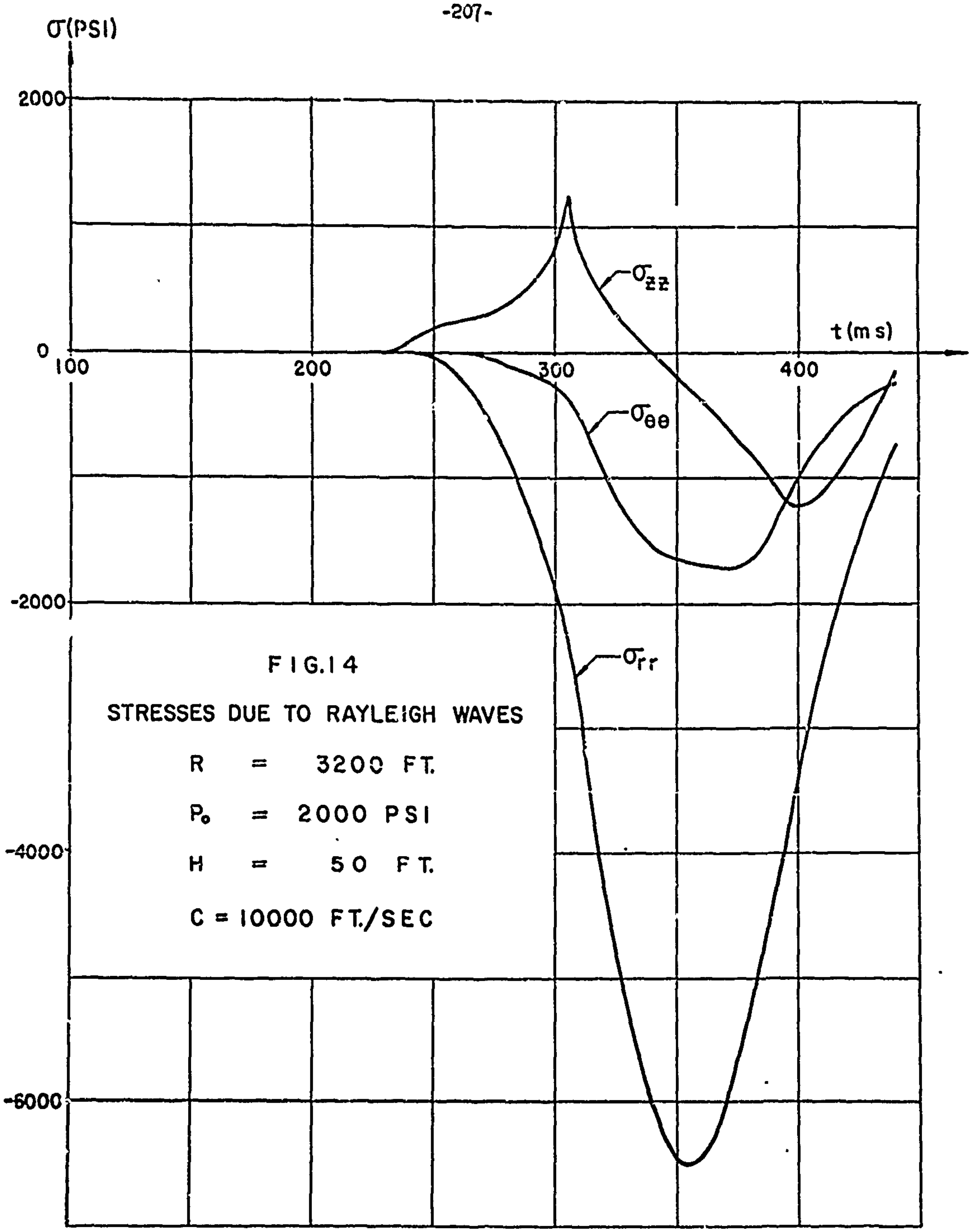

FIG.14

STRESSES DUE TO RAYLEIGH WAVES

R = 3200 FT.

P_o = 2000 PSI

H = 50 FT.

C = 10000 FT./SEC

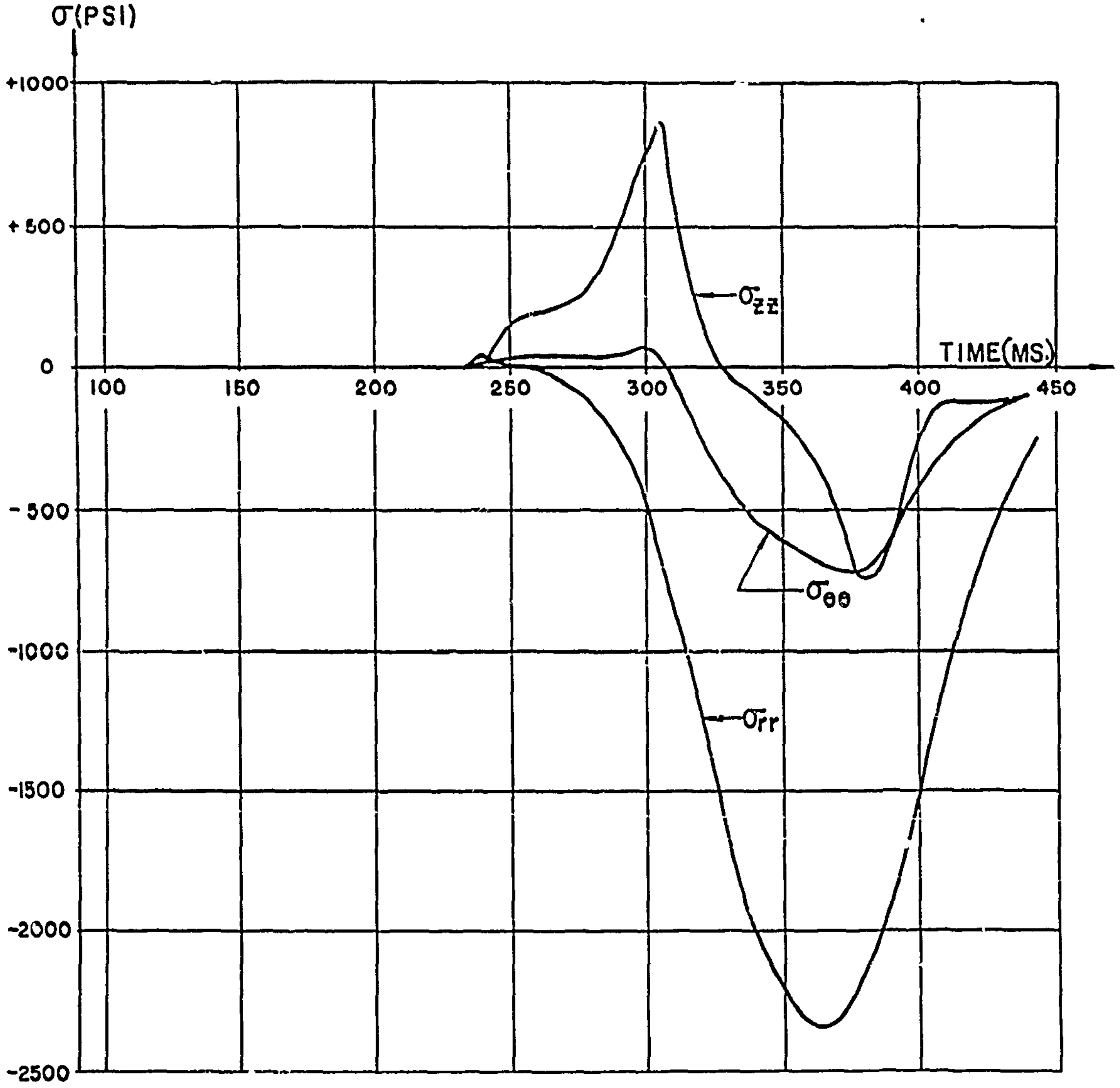

FIG.15 STRESSES DUE TO RAYLEGH WAVES

R = 3200 FT.
H = 100 FT.
P_s = 2000 PSI.
C = 10,000 FT/SEC.

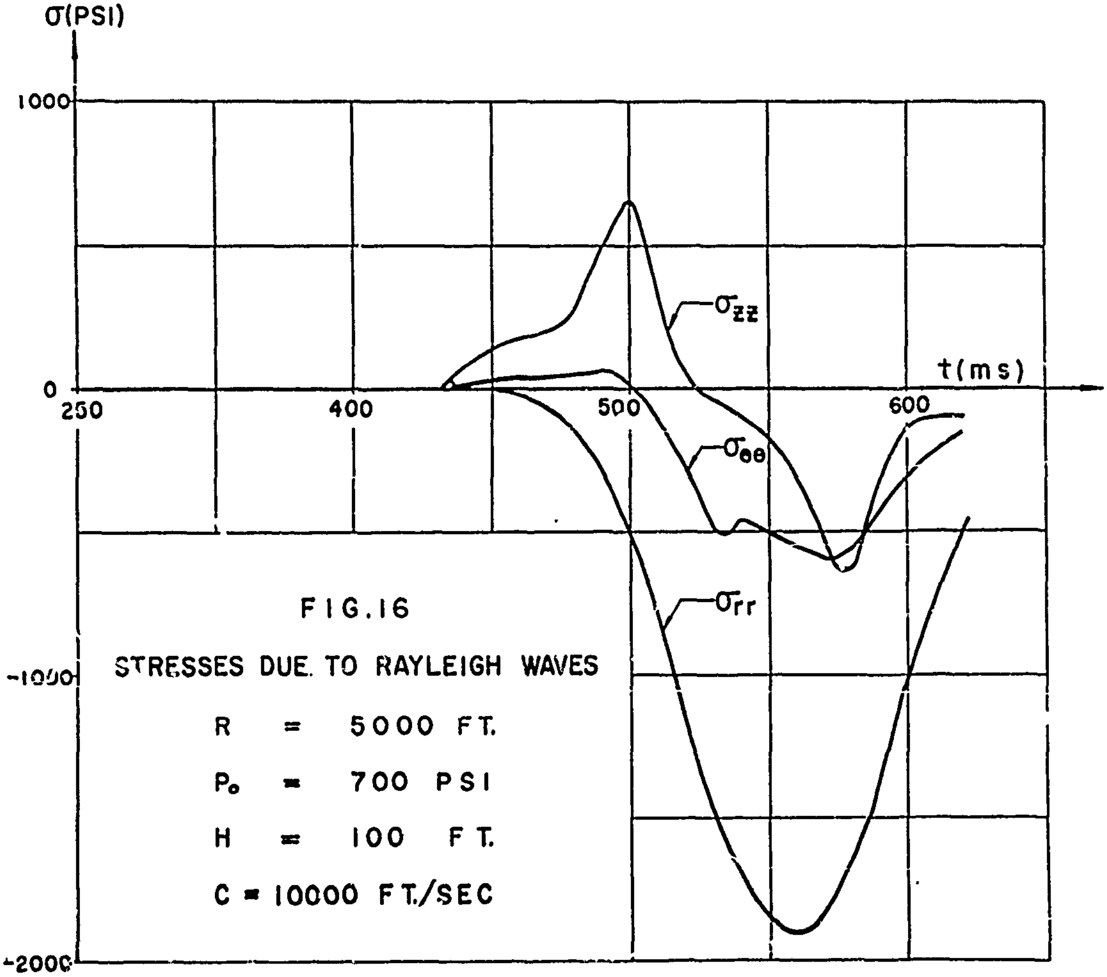

FIG.16

STRESSES DUE TO RAYLEIGH WAVES

R = 5000 FT.

P_o = 700 PSI

H = 100 FT.

C = 10000 FT./SEC

APPENDIX C

DIFFRACTION OF A SHEAR WAVE (S WAVE) BY A CYLINDRICAL CAVITY IN AN ELASTIC MEDIUM

I INTRODUCTION

An infinitely long cylindrical cavity in an infinite elastic homogeneous and isotropic medium is acted on by a plane shear wave whose front is parallel to the axis of the cavity. The shock wave propagates through the medium with a constant velocity c_s and carries the shear stresses $\tau U(t)$ [see Fig.(1)].

By means of a suitable transformation of coordinates, the problem can be solved by a procedure which utilizes the results obtained in the solution of the problem of the diffraction of a P wave by a cylindrical cavity in an elastic medium. An integral transform technique is used to determine the stress field produced in the medium by the diffraction of the incoming shock wave by the cavity. Expressions for the hoop stress $\sigma_{\theta\theta}$, the radial stress σ_{rr} and the shear stress $\sigma_{r\theta}$ are derived and numerical results are presented for the hoop stress $\sigma_{\theta\theta}$ at the cavity boundary. Although the problem is considered for S waves with a step distribution in time, the results obtained for this case may be used as influence coefficients to determine, by means of Duhamel integrals, the stress field produced by waves with time varying pressures.

II GENERAL PROCEDURE

Consider an infinite elastic medium which does not contain a cavity. The stresses σ_{rr} , $\sigma_{r\theta}$ and $\sigma_{\theta\theta}$ produced by the incoming shock wave at points lying on a circle of radius "a" [Fig.(2)] are given by the expressions

$$\sigma_{rr} = \tau \sin 2\bar{\theta} \tag{1}$$

$$\sigma_{r\theta} = \tau \cos 2\bar{\theta} \tag{2}$$

$$\sigma_{\theta\theta} = -\tau \sin 2\bar{\theta} \tag{3}$$

The superposition of the tractions

$$\sigma_{rr} = -\tau \sin 2\bar{\theta} \tag{4}$$

$$\sigma_{r\theta} = -\tau \cos 2\bar{\theta} \tag{5}$$

which are equal and opposite to those given by Eq. (1) and (2) on the surface $r = a$, produces a traction free surface which can be considered to be the boundary of a cavity of radius "a" in the medium. The total stress field produced by the incoming S wave is obtained by superimposing the free field stresses [Eq. (1)-(3)] and the stresses produced by the application of the surface tractions σ_{rr} and $\sigma_{r\theta}$ [Eq. (4)-(5)] to the boundary of the cavity.

A transformation of the coordinate $\bar{\theta}$ can now be made. This transformation brings the applied tractions of Eq. (4)-(5) into coincidence with those of Eq. (4)-(5) of [20]. Consequently, certain of the formulæ and influence coefficients developed in [20] for the case of an incoming P wave, may be used to obtain similar results for the case of the S wave. Letting, [Fig. (3a)],

$$\bar{\theta} = \theta - \pi/4 \tag{6}$$

and substituting Eq. (6) in Eq. (4)-(5), the tractions become

$$\sigma_{rr} = -\tau \sin 2(\theta - \pi/4) = \tau \cos 2\theta \tag{7}$$

$$\sigma_{r\theta} = -\tau \cos 2(\theta - \pi/4) = -\tau \sin 2\theta \tag{8}$$

The boundary tractions σ_{rr} and $\sigma_{r\theta}$ [Eq. (7)-(8)] are expanded into a Fourier Series in θ [Fig.(3b)]:

$$\sigma_{rr} = \sum_{n=1}^{\infty} a_{ns}(t) \cos n\theta \tag{9}$$

$$\sigma_{r\theta} = \sum_{n=1}^{\infty} b_{ns}(t) \sin n\theta \tag{10}$$

where

$$a_{ns}(t) = \frac{1}{\pi} \int_{\pi/4 - \bar{\alpha}(t)}^{\pi/4 + \bar{\alpha}(t)} \sigma_{rr}(\theta) \cos n\theta \, d\theta \tag{11}$$

$$b_{ns}(t) = \frac{1}{\pi} \int_{\pi/4 - \bar{\alpha}(t)}^{\pi/4 + \bar{\alpha}(t)} \sigma_{r\theta}(\theta) \sin n\theta \, d\theta \tag{12}$$

and

$$\bar{\alpha}(t) = \cos^{-1}\left(1 - \frac{c_s t}{a}\right) \tag{13}$$

Substituting Eq. (7), (8) into Eq. (11), (12), the expansion coefficients become

<u>During envelopment $t \leq \frac{2a}{c_s}$</u>

$$a_{ns}(t) = \frac{\tau}{\pi}\left[\frac{\sin (2-n)\,\bar{\alpha}}{2-n} - \frac{\sin (2+n)\,\bar{\alpha}}{2+n}\right] \sin \frac{n\pi}{4} \tag{14}$$

$$b_{ns}(t) = -\frac{\tau}{\pi}\left[\frac{\sin (2-n)\,\bar{\alpha}}{2-n} + \frac{\sin (2+n)\,\bar{\alpha}}{2+n}\right] \sin \frac{n\pi}{4} \tag{15}$$

<u>After envelopment $t > \frac{2a}{c_s}$</u>

$$a_{ns}(t) = b_{ns}(t) = 0 \qquad n \neq 2 \tag{16}$$

$$a_{2s}(t) = -b_{2s}(t) = \tau \tag{17}$$

It should be noted that there is no contribution from a series term for $n = 0$, and that since only the series term for $n = 2$ has a non zero coefficient after envelopment, only the $n = 2$ mode will contribute to the long time (static) solution for the stress field in the medium.

The plane strain problem for the stress field around a cavity of radius "a" which has the surface tractions σ_{rr_n} and $\sigma_{r\theta_n}$ applied to the boundary $r = a$, is now considered. The surface tractions σ_{rr_n} and $\sigma_{r\theta_n}$ are given by

$$\sigma_{rr_n} = a_{ns}(t) \cos n\theta \tag{18}$$

$$\sigma_{r\theta_n} = b_{ns}(t) \sin n\theta \tag{19}$$

As in [20], to make the problem more tractable, the tractions σ_{rr_n} and $\sigma_{r\theta_n}$ are first applied to the cavity boundary as step functions in time:

$$\sigma_{rr_n} = \tau U(t) \cos n\theta \tag{20}$$

$$\sigma_{r\theta_n} = k\tau U(t) \sin n\theta \tag{21}$$

The stress field components produced by the pressure inputs Eq. (20)-(21) are evaluated in Section III of Reference [20] and are used as influence coefficients in Duhamel integrals for the determination of the corresponding components produced by the true boundary tractions of Eq. (18)-(19). For convenience, the auxiliary problem is solved for the following two sets of applied boundary tractions,

$$\left.\begin{aligned} \sigma_{rr_n} &= U(t) \cos n\theta \\ \sigma_{r\theta_n} &= 0 \end{aligned}\right\} \tag{22}$$

$$\left.\begin{aligned} \sigma_{rr_n} &= 0 \\ \sigma_{r\theta_n} &= U(t) \sin n\theta \end{aligned}\right\} \tag{23}$$

As an illustration of this procedure, consider the hoop stress $\sigma_{\theta\theta}$ at the cavity boundary. Let the quantities $\sigma_{\theta\theta_n}^{*}$ and $\sigma_{\theta\theta_n}^{**}$ be the time dependent portions of the hoop stress $\sigma_{\theta\theta}$ at $r = a$ produced by the applied tractions given by Eq. (22) and (23) respectively. The corresponding stress components due to the boundary tractions of Eq. (18)-(19) are given by the Duhamel integrals:

$$\tilde{\sigma}_{\theta\theta_n} = \int_0^t \left[\dot{a}_{ns}(\eta)\, \sigma_{\theta\theta_n}^{*}\,(t-\eta)\right] d\eta \tag{24}$$

$$\tilde{\tilde{\sigma}}_{\theta\theta_n} = \int_0^t \left[\dot{b}_{ns}(\eta)\, \sigma_{\theta\theta_n}^{**}\,(t-\eta)\right] d\eta \tag{25}$$

The total hoop stress $\sigma_{\theta\theta}$ produced at the boundary of the cavity by the incoming S wave is given by the superposition of the free field stress, Eq. (3), and the stresses from Eq. (24)-(25):

$$\sigma_{\theta\theta}(t) = -\tau \cos 2\theta + \sum_{n=1}^{\infty} \left[\tilde{\sigma}_{\theta\theta_n}(t) + \tilde{\tilde{\sigma}}_{\theta\theta_n}(t)\right] \cos n\theta \tag{26}$$

The method of superposition can also be used in a similar manner to evaluate the stress field, σ_{rr}, $\sigma_{\theta\theta}$, $\sigma_{r\theta}$ at points in the medium beyond the boundary of the cavity, i.e., $r > a$.

III AUXILIARY PROBLEM - STRESS FIELD PRODUCED BY THE BOUNDARY TRACTIONS $\sigma_{rr_n} = U(t) \cos n\theta$ and $\sigma_{r\theta_n} = kU(t) \sin n\theta$ [Fig. (4)].

The stress field produced by the boundary tractions $\sigma_{rr_n} = U(t) \cos n\theta$ and $\sigma_{r\theta_n} = kU(t) \sin n\theta$ has been determined in [20], Section III, and the analytical results are given in detail in that reference. The hoop stress component, $\sigma_{\theta\theta_n}$, can be evaluated from an inversion integral of the type

$$\frac{\sigma_{\theta\theta_n}(r,\theta,t)}{\cos n\theta} = \frac{1}{2\pi i}\int_{-\infty-i\gamma}^{\infty-i\gamma} \frac{I(r,\xi)e^{i\xi\frac{c_p t}{a}}}{\xi\,[FB + DE]}\,d\xi \tag{27}$$

where

$$I(r,\xi) = \left\{\begin{array}{l} [B + kE]\ [2\xi\frac{a}{r}\,H^{(2)}_{n-1}(\frac{\xi r}{a}) - \left\{(2n^2 + 2n)\frac{a^2}{r^2} + \xi^2\right\} H^{(2)}_n(\frac{\xi r}{a})] + \\ \\ + [kF - D]\ [2n(n+1)\frac{a^2}{r^2}\,H^{(2)}_n(\frac{c_p\xi r}{c_s a}) - \frac{2c_p na}{cr}\,\xi H^{(2)}_{n-1}\,(\frac{c_p\xi r}{c_s a})] \end{array}\right\} \tag{28}$$

and

$$F = [2n(n+1) - 3\xi^2]\,H^{(2)}_n(\xi) - 2\xi\,H^{(2)}_{n-1}(\xi) \tag{29}$$

$$B = [-2n(n+1) + \frac{c_p^2}{c_s^2}\xi^2]\,H^{(2)}_n(\frac{c_p}{c_s}\xi) + 2\frac{c_p}{c_s}\xi\,H^{(2)}_{n-1}(\frac{c_p}{c_s}\xi) \tag{30}$$

$$D = 2n(n+1)\,H^{(2)}_n(\xi) - 2n\,\xi\,H^{(2)}_{n-1}(\xi) \tag{31}$$

$$E = 2n(n+1)\,H^{(2)}_n(\frac{c_p}{c_s}\xi) - 2n\frac{c_p}{c_s}\xi\,H^{(2)}_{n-1}(\frac{c_p}{c_s}\xi) \tag{32}$$

Similar inversion integrals for $\frac{\sigma_{rr_n}}{\cos n\theta}$ and $\frac{\sigma_{r\theta_n}}{\sin n\theta}$ are presented in [20]. The integral of Eq. (27) has been evaluated in Section (IV) of [20] for the hoop stress $\sigma_{\theta\theta_n}$ at the cavity boundary, $r = a$. The hoop stress $\sigma_{\theta\theta_n}$ is given by the relation

$$\frac{\sigma_{\theta\theta_n}}{\sigma} = [-1 + R + I]\cos n\theta \tag{33}$$

where R and I are given by Eq. (75) and (71) of [19] respectively.

IV NUMERICAL RESULTS AND CONCLUSIONS

Numerical results are presented for the hoop stress at $r = a$, which is produced by an incoming plane shear (S) wave with a step pressure distribution in time. As in the case of the P wave, it was found that the maximum values of the stress are not materially affected by the early-time stress contributions which come from the coefficients $\tilde{\sigma}_{\theta\theta_n}$ and $\tilde{\tilde{\sigma}}_{\theta\theta_n}$, n larger than 2, and consequently, the series in Eq. (26) may be terminated after the $n = 2$ term for computational purposes. Moreover, only the contribution from the $n = 2$ component combines with the free field stress in Eq. (26) to give the asymptotic long-time value of $\sigma_{\theta\theta}$.

Fig. (9-8) shows the hoop stress $\sigma_{\theta\theta}$ at the cavity boundary for the locations $\bar{\theta} = 0^{\circ}$ and $\bar{\theta} = 45^{\circ}$.

The hoop stress produced by the step shear wave may be used as an influence function to determine the hoop stress produced by a wave with varying pressure-time history by means of the Duhamel integral of Eq. (9-1). [See Fig. (9-5).]

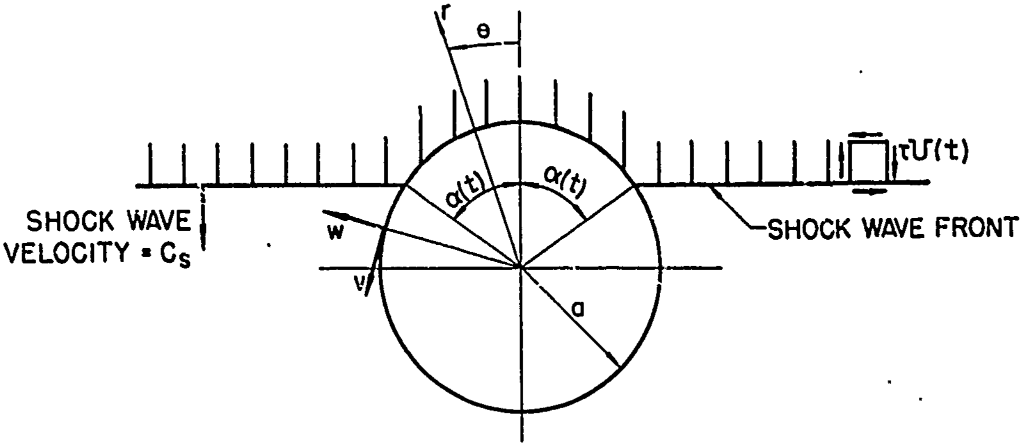

FIG. 1 GEOMETRY OF PROBLEM

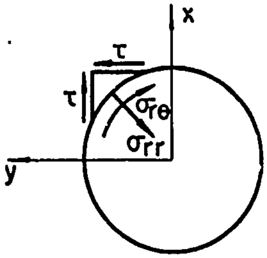

FIG. 2

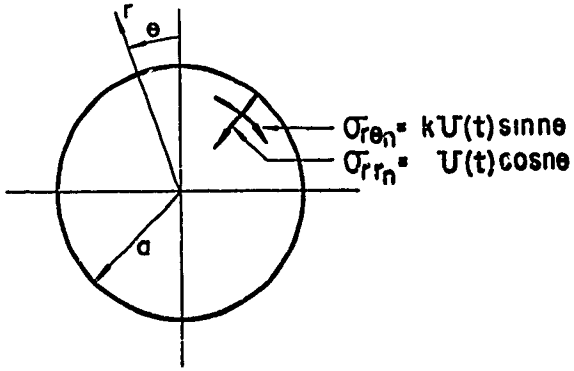

FIG. 4

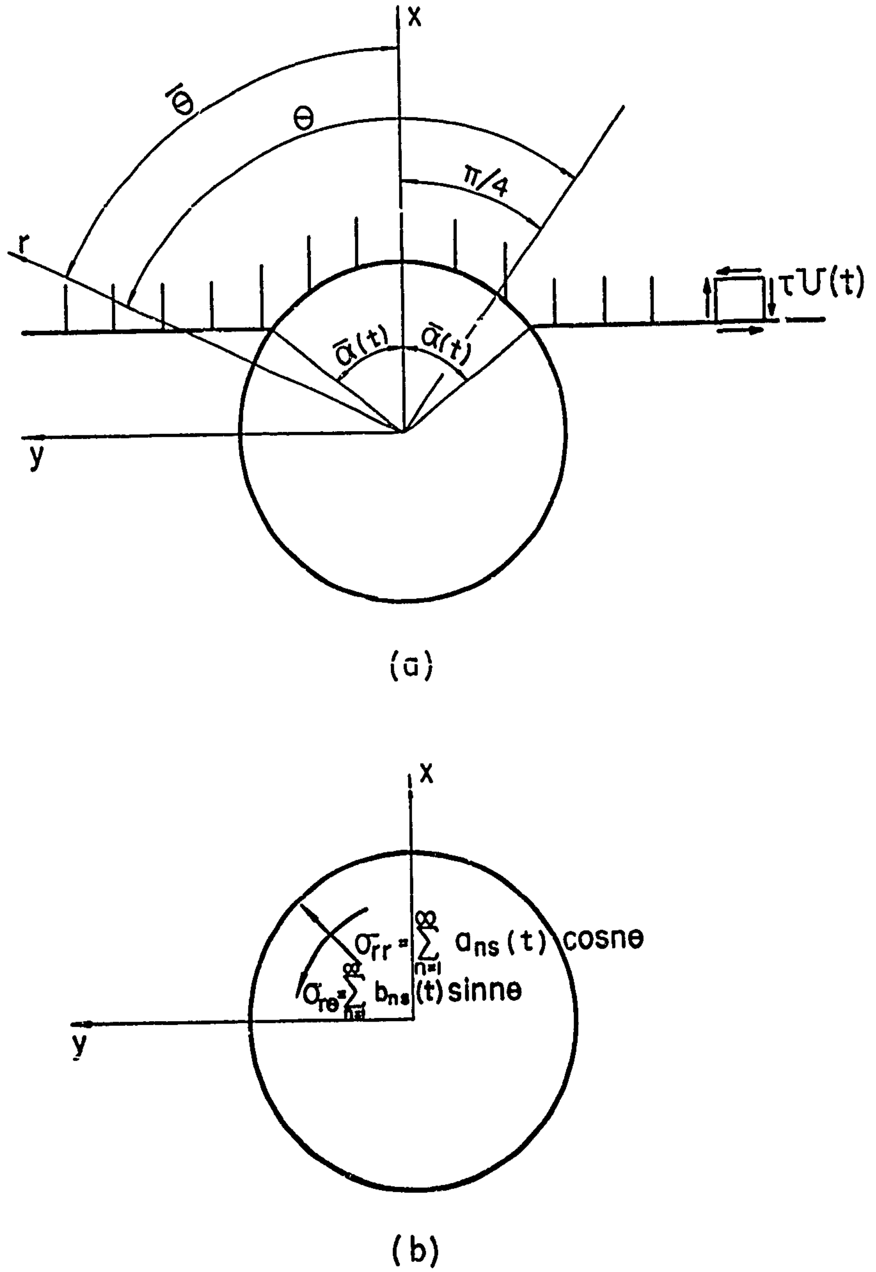
x
$\bar{\theta}$
θ
$\pi/4$
r
$\tau U(t)$
$\bar{\alpha}(t)$
$\bar{\alpha}(t)$
y
(a)
x
$\sigma_{rr} = \sum_{n=1}^{\infty} a_{ns}(t) \cos n\theta$
$\sigma_{r\theta} = \sum_{n=1}^{\infty} b_{ns}(t) \sin n\theta$
y
(b)

FIG. 3

Appendix D

DISPLACEMENTS AND VELOCITIES PRODUCED BY THE DIFFRACTION OF A PRESSURE WAVE BY A CYLINDRICAL CAVITY IN AN ELASTIC MEDIUM

NOMENCLATURE

The following nomenclature is used in this paper.

θ, r = polar coordinates, see Figure (1).

$\underline{u}(r, \theta, t)$ = displacement vector of a point in the medium.

$\left.\begin{matrix} w(r, \theta, t) \\ v(r, \theta, t) \end{matrix}\right\}$ = radial and tangential displacements of a point in the medium. (Note that a positive displacement w is outward).

a = radius of cylindrical cavity.

$a_n(t), b_n(t)$ = Fourier series coefficients for expansion of stresses σ_{rr} and $\sigma_{r\theta}$

c_p, c_s = Propagation velocity of dilatational and shear waves respectively in medium.

$d_n^f, d_n^c, h_n^f, a_n^c$ = Fourier series coefficients, See Equations(102)and (103)

$d(t)$ = Time dependent coefficients for rigid body motions.

$\left.\begin{matrix} \underline{f}(r, \theta, t) \\ \bar{f}(r, \theta, \Omega) \end{matrix}\right\}$ = function of r, θ, t and corresponding transformed function with respect to time.

F, B, D, E = functions [See Equation (59)-(62)]

$H_n^{(1)}, H_n^{(2)}$ = Hankel functions of first and second kind of order n.

$P(\xi, r), Q(\xi, r)$ = Functions appearing in transformed displacements and velocities.

$I_n(y), K_n(y)$ = modified Bessel functions of the first and second kind respectively, of order n.

$\underline{k_r}, \underline{k_\theta}$ = unit vectors in r and θ directions respectively.

k = coefficient.

t = time

t^* = delay time [Equation (8)].

$P(t)$ = variable pressure-time history of incoming pressure wave, see Section (VII).

$U(t)$ = unit step function.

$\alpha(t)$ = angle of envelopment.

n = number of circumferential waves, integer.

ϵ = ratio of stress components in incoming wave, see Figure(1).

λ = Lamé constant.

μ = shear modulus of medium.

ν = Poisson's Ratio

ξ = $\frac{\Omega a}{c_p}$

ρ = mass density of medium.

σ_{rr}, $\sigma_{r\theta}$ = radial and shear stresses respectively at a point in the medium.

σ = stress intensity of incoming wave.

$\left.\begin{matrix}\phi(r, \theta, t)\\ \psi(r, \theta, t)\end{matrix}\right\}$ = potential functions of reflected and radiated waves in the medium.

Ω = transform variable.

Additional symbols are defined as they occur in the text. Subscripts and dots used with displacement and potential functions indicate differentiation; e.g. $u_{rr} = \frac{\partial^2 u}{\partial r^2}$, $\ddot{u} = \frac{\partial^2 u}{\partial t^2}$, etc.

I. INTRODUCTION

An infinitely long cylindrical cavity in an infinite elastic homogeneous and isotropic medium is acted upon by a plane shock wave whose front is parallel to the axis of the cavity. The shock wave propagates through the medium with a constant velocity c_p and envelops the cavity [Fig. (1)]. The direct stress components $\sigma U(t)$ and $\epsilon\sigma U(t)$ which are respectively parallel and perpendicular to the direction of wave propagation, are carried by the shock wave.

An integral transform technique is used to determine the displacements and velocities produced at various points in the medium by the diffraction of the incoming shock wave by the cavity. Expressions for radial and tangential components of the displacement and velocity are derived and numerical results are presented for these quantities at points on the boundary of the cavity. Although the problem is considered for pressure waves with a step distribution in time, the results obtained for this case may be used as influence coefficients to determine, by means of Duhamel integrals, the displacements and velocities produced by waves with time-dependent pressures.

II. GENERAL PROCEDURE

The stress field produced by the diffraction of a plane step shock wave by a cylindrical cavity in an elastic medium was evaluated in Ref. [20]. The present paper utilizes a similar approach in determining the displacements and velocities of mass points in the elastic medium. Essentially, the displacement and velocity components at any point in the medium are obtained by superimposing the free-field velocity and displacement components, i.e those produced by the pressure wave in the medium with no cavity, and the velocity and displacement components produced by the application of corrective tractions at the boundary of the cavity in order to make the boundary surface traction free.

a) Free-Field Velocities and Displacements.

Consider an infinite elastic medium which does not contain a cavity. The stresses σ_{rr} and $\sigma_{r\theta}$ produced by the incoming shock wave at points lying on a circle of radius "a", [Figure (2a)] are given by the expressions

$$\sigma_{rr} = -\sigma \left[\cos^2\theta - \epsilon \sin^2\theta\right] \tag{1}$$

$$\sigma_{r\theta} = \sigma \left[\frac{1+\epsilon}{2}\right] \sin 2\theta \tag{2}$$

The radial and tangential components of the particle velocity of points in the medium behind the step wave front are given by the relations

$$\dot{w}_f = -\frac{\sigma}{\rho c_p} \cos\theta \tag{3}$$

$$\dot{v}_f = \frac{\sigma}{\rho c_p} \sin\theta \tag{4}$$

The displacement $\underline{u}_f$ of a point in the medium contains two components

$$\underline{u}_f = w_f(r,\theta,t)\underline{k_r} + v_f(r,\theta,t)\underline{k_\theta}, \tag{5}$$

where, by integrating Eq. (3)-(4), the radial and tangential components of the displacement are given by

$$w_f(r,\theta,t) = -\frac{\sigma}{\rho c_p}[\cos\theta](t-t^*) \tag{6}$$

$$v_r(r,\theta,t) = \frac{\sigma}{\rho c_p}[\sin\theta]\,(t-t^*) \tag{7}$$

where the time t is measured from the arrival of the shock wave at the point $r = a$, $\theta = 0^0$ [Fig. (3)] and the delay time t^* is given by

$$t^* = \frac{a - r\cos\theta}{c_p} \tag{8}$$

b) Velocities and Displacements produced by corrective boundary tractions applied to the surface of the cavity, $r = a$.

The stresses produced in an infinite elastic medium with no cavity, at points lying on a circle of radius "a", are given by Eq. (1) - (2). The superposition of the tractions

$$\sigma_{rr} = \sigma\left[\cos^2\theta - \epsilon\sin^2\theta\right] \tag{9}$$

$$\sigma_{r\theta} = -\sigma\left[\frac{1+\epsilon}{2}\right]\sin 2\theta \tag{10}$$

which are equal and opposite to those given by Eq. (1) and (2) on the surface $r = a$, produces a traction-free surface which can then be considered to be the boundary of a cavity of radius "a" in the medium. The total displacement and velocity field produced by the incoming pressure wave is obtained by superimposing the free field quantities [Eq. (3)-(4), (6)-(7)] and the velocities and displacements produced by the application of the surface tractions of Eq. (9)-(10) to the boundary of the cavity.

Proceeding as in Ref. [1], the boundary tractions σ_{rr} and $\sigma_{r\theta}$ [Eq. (9) - (10)] are expanded into a Fourier Series [Fig. (2b)]:

$$\sigma_{rr} = \frac{a_o(t)}{2} + \sum_{n=1}^{\infty} a_n(t) \cos n\theta \tag{11}$$

$$\sigma_{r\theta} = \sum_{n=1}^{\infty} b_n(t) \sin n\theta \tag{12}$$

where

$$a_n(t) = \frac{2}{\pi}\int_0^{\alpha(t)} \sigma_{rr}(\theta) \cos n\theta \; d\theta \tag{13}$$

$$b_n(t) = \frac{2}{\pi}\int_0^{\alpha(t)} \sigma_{r\theta}(\theta) \sin n\theta \; d\theta \tag{14}$$

For times which are less than one full envelopment, i.e., $t \leq \frac{2a}{c_p}$, the angle $\alpha(t)$ is given by the expression

$$\alpha(t) = \cos^{-1} \left(1 - \frac{c_p t}{a}\right) \tag{15}$$

For $t > \frac{2a}{c_p}$, the angle $\alpha(t) = \pi$. Substituting Eq. (9) - (10) into Eq. (13) - (14), the expansion coefficients become:

<u>During envelopment $t \leq \frac{2a}{c_p}$</u>

$$\frac{a_o}{2}(t) = \frac{\sigma}{\pi}\left[\frac{\alpha(1-\epsilon)}{2} + \left(\frac{1+\epsilon}{4}\right) \sin 2\alpha\right] \tag{16}$$

$$a_n(t) = \frac{2\sigma}{\pi(n+2)}\left[\sin n\alpha(\cos^2\alpha - \epsilon \sin^2\alpha) + \left(\frac{1-\epsilon}{2-n}\right) \sin (2-n)\alpha + \left(\frac{1-\epsilon}{n}\right) \sin n\alpha\right] \tag{17}$$

$$b_n(t) = -\frac{\sigma}{2\pi}(1+\epsilon)\left[\frac{\sin(2-n)\alpha}{2-n} - \frac{\sin(2+n)\alpha}{2+n}\right] \tag{18}$$

After envelopment $t > \frac{2a}{c}$

$$\frac{a_o(t)}{2} = \sigma\left(\frac{1+\epsilon}{2}\right) \qquad (19)$$

$$a_n(t) = b_n(t) = 0 \qquad n \neq 0 \text{ and } 2 \qquad (20)$$

$$a_2(t) = - b_2(t) = \sigma\left(\frac{1+\epsilon}{2}\right) \qquad (21)$$

For a wave with a plane wave front, the parameter ϵ becomes

$$\epsilon = - \frac{\nu}{1-\nu} \qquad (22)$$

The plane strain problem for the displacement and velocity fields around a cavity of radius "a" which has the surface tractions σ_{rr_n} and $\sigma_{r\theta_n}$ applied to the boundary $r = a$, is now considered. The tractions σ_{rr_n} and $\sigma_{r\theta_n}$ are given by

$$\left.\begin{aligned} \sigma_{rr_n} &= a_n(t) \cos n\theta \\ \sigma_{r\theta_n} &= b_n(t) \sin n\theta \end{aligned}\right\} \qquad (23)$$

$$2\,\sigma_{rr_o} = a_o(t) \quad ; \quad \sigma_{r\theta_o} = 0 \qquad (24)$$

To make the problem more tractable, the tractions σ_{rr_n} and $\sigma_{r\theta_n}$ are first applied to the cavity boundary as step functions in time:

$$\sigma_{rr_n} = \sigma\, U(t) \cos n\theta \qquad (25)$$

$$\sigma_{r\theta_n} = k\, \sigma\, U(t) \sin n\theta \qquad (26)$$

$$\sigma_{rr_o} = \sigma\, U(t) \qquad (27)$$

where k is an arbitrary number which is used to identify that part of the solution that comes from the $\sigma_{r\theta_n}$ traction.

The displacement and velocity components produced by the traction inputs of Eq. (25) - (27) are evaluated in Section (III) and are used as influence coefficients in Duhamel integrals for the determination of the corresponding components produced by the boundary tractions of Eq. (23) - (24). For convenience, the auxiliary problem is solved for the following three sets of applied boundary tractions

$$\left.\begin{aligned} \sigma_{rr_n} &= U(t)\cos n\theta \\ \sigma_{r\theta_n} &= 0 \end{aligned}\right\} \qquad (28)$$

$$\left.\begin{aligned} \sigma_{rr_n} &= 0 \\ \sigma_{r\theta_n} &= U(t)\sin n\theta \end{aligned}\right\} \qquad (29)$$

$$\sigma_{rr_o} = U(t) \quad ; \quad \sigma_{r\theta_o} = 0 \qquad (30)$$

To illustrate the procedure, let the quantities w_n^*, w_n^{**} and w_o^* represent the r and t dependent portions of the radial displacement at any point r,θ, produced by the applied tractions of Eq. (25) - (27) repectively. The corresponding displacement components due to the boundary tractions of Eq. (23) - (24) are given by the Duhamel integrals

$$\hat{w}_n(r,t) = \int_o^t \left[\dot{a}_n(\tau)\, w_n^*(r,t-\tau)\right] d\tau \qquad n \geq 1 \qquad (31)$$

$$\hat{w}_n(r,t) = \int_o^t \left[\dot{b}_n(\tau)\, w_n^{**}(r,t-\tau)\right] d\tau \qquad n \geq 1 \qquad (32)$$

$$\hat{w}_o(r,t) = \int_o^t \frac{1}{2}\left[\dot{a}_o(\tau)\, w_o^*(r,t-\tau)\right] d\tau \qquad n = 0 \qquad (33)$$

The total radial displacement $w(r,\theta,t)$ of a point in the medium, which is behind the incoming shock wave front is obtained by superimposing the components given by Eq. (6) and Eq. (31) - (33):

$$w(r,\theta,t) = -\frac{\sigma}{\rho c_p}[\cos\theta](t-t^*) + \hat{w}_o(r,t) + \sum_{n=1}^{\infty}\left[\hat{w}_n(r,t) + \hat{\hat{w}}_n(r,t)\right]\cos n\theta \qquad (34)$$

In a similar manner, expressions for $v(r,\theta,t)$, $\dot{w}(r,\theta,t)$ and $\dot{v}(r,\theta,t)$ can be obtained by superposition of the free field quantities and those produced by the application of the corrective boundary tractions to the surface of the cavity, $r = a$:

$$v(r,\theta,t) = \frac{\sigma}{\rho c_p}[\sin\theta](t-t^*) + \sum_{n=1}^{\infty}\left[\hat{v}_n(r,t) + \hat{\hat{v}}_n(r,t)\right]\sin n\theta \qquad (35)$$

$$\dot{w}(r,\theta,t) = -\frac{\sigma}{\rho c_p}\cos\theta + \dot{\hat{w}}_o(r,t) + \sum_{n=1}^{\infty}\left[\dot{\hat{w}}_n(r,t) + \dot{\hat{\hat{w}}}_n(r,t)\right]\cos n\theta \qquad (36)$$

$$\dot{v}(r,\theta,t) = \frac{\sigma}{\rho c_p}\sin\theta + \sum_{n=1}^{\infty}\left[\dot{\hat{v}}_n(r,t) + \dot{\hat{\hat{v}}}_n(r,t)\right]\sin n\theta \qquad (37)$$

Eq. (34) - (37) are given in a form suitable for those points in the medium over which the shock wave has already passed and which have already received signals from the reflected and the radiated waves originating at the cavity boundary. For other situations, the free field and corrective traction components must be superimposed with appropriate delay times, relating to the arrival of the various waves at the point under consideration.

III. AUXILIARY PROBLEM - Displacements and Velocities Produced by the Boundary Tractions $\sigma_{rr_n} = \sigma U(t)\cos n\theta$ and $\sigma_{r\theta_n} = k\sigma U(t)\sin n\theta$ [Figure (4)].

The equation of motion for the linearly elastic medium is given by:

$$\mu\nabla^2\underline{u} + (\lambda + \mu)\nabla\nabla\cdot\underline{u} = \rho\ddot{\underline{u}} \tag{38}$$

where for the plane strain problem, the displacement $\underline{u}$ contains two components

$$\underline{u} = w(r,\theta,t)\underline{k_r} + v(r,\theta,t)\underline{k_\theta} \tag{39}$$

Defining two potential functions, $\phi(r,\theta,t)$ and $\psi(r,\theta,t)$ such that

$$w(r,\theta,t) = \phi_r + \frac{1}{r}\psi_\theta \tag{40}$$

$$v(r,\theta,t) = \frac{1}{r}\phi_\theta - \psi_r \tag{41}$$

and substituting Equations (40) - (41) into Equation (38), the functions ϕ and ψ satisfy the following wave equations:

$$c_p^2\nabla^2\phi = \ddot{\phi} \tag{42}$$

$$c_s^2\nabla^2\psi = \ddot{\psi} \tag{43}$$

where

$$c_p = \sqrt{\frac{\lambda + 2\mu}{\rho}} \quad ; \quad c_s = \sqrt{\frac{\mu}{\rho}} \tag{44}$$

are the velocities of propagation of dilatational and shear waves respectively in the infinite elastic medium.

A transform with respect to time is applied.

$$\overline{f}(r,\theta,\Omega) = \frac{1}{2\pi}\int_0^\infty f(r,\theta,t)e^{-i\Omega t}\,dt \tag{45}$$

$$f(r,\theta,t) = \int_{-\infty-i\gamma}^{\infty-i\gamma} \overline{f}(r,\theta,\Omega)e^{i\Omega t}\,d\Omega \tag{46}$$

Writing the transformed potentials $\bar{\phi}$ and $\bar{\psi}$ as:

$$\bar{\phi}(r, \theta, \Omega) = \bar{\bar{\phi}}(r, \Omega)\cos n\theta \qquad (47)$$

$$\bar{\psi}(r, \theta, \Omega) = \bar{\bar{\psi}}(r, \Omega)\sin n\theta \qquad (48)$$

the transformed wave equations become

$$\bar{\bar{\phi}}_{rr} + \frac{1}{r}\bar{\bar{\phi}}_r + \left(\frac{\Omega^2}{c_p^2} - \frac{n^2}{r^2}\right)\bar{\bar{\phi}} = 0 \qquad (49)$$

$$\bar{\bar{\psi}}_{rr} + \frac{1}{r}\bar{\bar{\psi}}_r + \left(\frac{\Omega^2}{c_s^2} - \frac{n^2}{r^2}\right)\bar{\bar{\psi}} = 0 \qquad (50)$$

and the solutions for divergent waves are given by the expressions

$$\bar{\phi}_n(r, \theta, \Omega) = A_n H_n^{(2)}\left(\frac{\Omega r}{c_p}\right)\cos n\theta \qquad (51)$$

$$\bar{\psi}_n(r, \theta, \Omega) = B_n H_n^{(2)}\left(\frac{\Omega r}{c_s}\right)\sin n\theta \qquad (52)$$

The coefficients A_n and B_n are obtained from the boundary conditions at the cavity boundary $r = a$:

$$\sigma_{rr}\Big]_{r=a} = \sigma U(t)\cos n\theta \qquad (53)$$

$$\sigma_{r\theta}\Big]_{r=a} = k\sigma U(t)\sin n\theta \qquad (54)$$

The stresses σ_{rr} and $\sigma_{r\theta}$ are first expressed in terms of the potential functions ϕ and ψ

$$\sigma_{rr} = \lambda\nabla^2\phi + 2\mu\left[\phi_{rr} - \frac{1}{r^2}\psi_\theta + \frac{1}{r}\psi_{r\theta}\right] \qquad (55)$$

$$\sigma_{r\theta} = \mu\left[\frac{2}{r}\phi_{r\theta} - \frac{2}{r^2}\phi_\theta + \frac{1}{r}\psi_r - \psi_{rr} + \frac{1}{r^2}\psi_{\theta\theta}\right] \qquad (56)$$

Transforming Equations (55)-(56) and substituting Equations (51)-(52) into the transformed equations, the constants A_n and B_n may be computed. The transformed potential functions become(*)

$$\bar{\phi}_n = \frac{\sigma a^2 (B + kE)}{2\pi i \Omega\, \mu [FB + DE]} \quad H_n^{(2)} \left(\frac{\Omega r}{c_p}\right) \cos n\theta \tag{57}$$

$$\bar{\psi}_n = \frac{\sigma a^2 (-D + kF)}{2\pi i \Omega\, \mu [FB + DE]} \quad H_n^{(2)} \left(\frac{\Omega r}{c_s}\right) \sin n\theta \tag{58}$$

where

$$F = [2n(n + 1) - 3\xi^2]\, H_n^{(2)}(\xi) - 2\xi H_{n-1}^{(2)}\ (\xi) \tag{59}$$

$$B = [-2n(n + 1) + \frac{c_p^2}{c_s^2}\ \xi^2]\, H_n^{(2)}\ (\frac{c_p}{c_s}\,\xi) + 2\frac{c_p}{c_s}\xi\, H_{n-1}^{(2)}\ (\frac{c_p}{c_s}\,\xi) \tag{60}$$

$$D = 2n(n + 1)\, H_n^{(2)}(\xi) - 2n\xi\, H_{n-1}^{(2)}\ (\xi) \tag{61}$$

$$E = 2n(n + 1)\, H_n^{(2)}\ (\frac{c_p}{c_s}\,\xi) - 2n\frac{c_p}{c_s}\,\xi\ \ H_{n-1}^{(2)}\ \ (\frac{c_p}{c_s}\,\xi) \tag{62}$$

and

$$\xi = \frac{\Omega a}{c_p}$$

The transformed displacements are obtained by substituting Equations (57)-(58) into the transformed Equations (40)-(41).

$$\bar{w}_n(r,\ \theta,\ \Omega) = \frac{\sigma a}{2\pi i \Omega \mu}\ \frac{P_n(\xi,\ r) \cos n\theta}{(FB + DE)} \tag{63}$$

$$\bar{v}_n(r,\ \theta,\ \Omega) = \frac{\sigma a}{2\pi i \Omega \mu}\ \frac{Q_n(\xi,\ r)\ \sin n\theta}{(FB + DE)} \tag{64}$$

where

$$P_n(\xi,\ r) = \quad [B + kE][-\frac{na}{r}\, H_n^{(2)}(\frac{r}{a}\xi) + \ \xi H_{n-1}^{(2)}(\frac{r\xi}{a})] - [D - kF][\frac{na}{r} H_n^{(2)}(\frac{c_p r\xi}{c_s a})] \tag{65}$$

(*) The following results are given for the specific case of $\lambda = \mu$, i.e. for a value of Poisson's ratio $\nu = 1/4$.

and

$$Q_n(\xi,r) = [B + kE][-\frac{na}{r} H_n^{(2)}(\frac{r\xi}{a})] + [D - kF][-\frac{na}{r} H_n^{(2)}(\frac{c_p r\xi}{c_s a}) + \frac{c_p}{c_s} \xi H_{n-1}^{(2)}(\frac{c_p r\xi}{c_s a})] \tag{66}$$

Similarly, using the transform for the derivative with respect to time of the displacement components w and v, the transforms of the velocity components become

$$\bar{\dot{w}}_n(r, \theta, \Omega) = \frac{\sigma a}{2\pi\mu} \frac{P_n(\xi, r) \cos n\theta}{(FB + DE)} \tag{67}$$

$$\bar{\dot{v}}_n(r, \theta, \Omega) = \frac{\sigma a}{2\pi\mu} \frac{Q_n(\xi, r) \sin n\theta}{(FB + DE)} \tag{68}$$

The radial displacement and velocity components, w_n and $\dot{w}_n$, may be evaluated from the inversion integral, Equation (46), i.e.

$$w_n(r, \theta, t) = \frac{\sigma a}{2\pi i\mu} \int_{-\infty-i\gamma}^{\infty-i\gamma} \frac{P_n(\xi, r)e^{i\xi c_p t/a}}{\xi(FB + DE)} \, d\xi \cos n\theta \tag{69}$$

and

$$\dot{w}_n(r, \theta, t) = \frac{\sigma c_p}{2\pi\mu} \int_{-\infty-i\gamma}^{\infty-i\gamma} \frac{P_n(\xi, r)e^{i\xi c_p t/a}}{(FB + DE)} \, d\xi \cos n\theta \tag{70}$$

The corresponding inversion integrals for v_n and $\dot{v}_n$ may be derived by replacing the quantity $P_n(\xi, r) \cos n\theta$ with $Q_n(\xi, r) \sin n\theta$ in Equations (69)-(70) respectively.

The inversion integrals for the velocity components $\dot{w}_n$ and $\dot{v}_n$ at the boundary of the cavity, r = a, will be evaluated in Section (IV).

IV. INVERSION OF EQUATIONS FOR THE RADIAL AND TANGENTIAL VELOCITY COMPONENTS, $\dot{w}_n$ AND $\dot{v}_n$ AT THE CAVITY BOUNDARY, $r = a$.

The radial velocity $\dot{w}_n$ at $r = a$ is evaluated by inverting the integral

$$\frac{\dot{w}_n(a,\theta,t)\mu}{\sigma c_p \cos n\theta} = \frac{1}{2\pi i} \int_{-\infty-i\gamma}^{\infty-i\gamma} \frac{iP_n(a,\xi)e^{i\xi\frac{c_p t}{a}}}{[FB + DE]} \, d\xi \qquad (71)$$

where

$$P_n(a,\xi) = \left\{ [B + kE] \, [-nH_n^{(2)}(\xi) + \xi H_{n-1}^{(2)}(\xi)] - [D - kF] \, [nH_n^{(2)}(\frac{c_p \xi}{c_s})] \right\} \qquad (72)$$

All computations were made using a value of Poisson's Ratio $\nu = 1/4$; this corresponds physically to a granite rock medium. For $\nu = 1/4$, the relation

$$c_p = \sqrt{3}\, c_s \qquad (73)$$

exists between the dilatational and shear wave velocities and this will be introduced into Equation (72) in the following transform inversion.

The singularities of the integrand of Equation (71) are a branch point at the origin $\xi = 0$, and simple poles defined by the roots of the equation $FB + DE = 0$:

$$\left\{ \begin{aligned} & 4\sqrt{3}\,\xi^2(n^2 - 1)H_{n-1}^{(2)}(\xi)H_{n-1}^{(2)}(\sqrt{3}\,\xi) + 3\xi^2[4n(n+1) - 3\xi^2]H_n^{(2)}(\xi)\,H_n^{(2)}(\sqrt{3}\,\xi) + \\ & + [-6\xi^3 + 4n\xi(1 - n^2)]H_{n-1}^{(2)}(\xi)H_n^{(2)}(\sqrt{3}\,\xi) + [-6\sqrt{3}\,\xi^3 + 4\sqrt{3}\,\xi\, n(1-n^2)]H_n^{(2)}(\xi)H_{n-1}^{(2)}(\sqrt{3}\xi) \end{aligned} \right\} = 0 \qquad (74)$$

Consider the contour ABCDEF shown in Figure (5) where the arcs AB and EF are of infinite radius and the lines BC and DE are branch cuts. By the residue theorem and Jordan's lemma, the integral of Equation (71) may be evaluated as

$$\int_A^F \frac{1}{2\pi} \frac{P_n(\xi, a)e^{i\xi c_p t/a}}{(FB + DE)} d\xi = \int_{BCDE} \frac{1}{2\pi} \frac{P_n(\xi, a)e^{i\xi c_p t/a}}{(FB + DE)} d\xi + 2\pi i \sum_j R_j \qquad (75)$$

where $\sum_j R_j$ is the sum of the residues of the poles defined by Equation (74) of the pertinent branch of the integrand.

The contribution to the velocity component $\dot{v}_n$ of the integration over the path CD is equal to zero. This value represents the asymptotic value of $\dot{v}_n$ for very long times.

The contribution of the integration over the branch cuts BC and DE leads to a branch integral which must be evaluated numerically. Letting

$$\xi_{DE} = ye^{i\pi/2} \quad ; \quad \xi_{BC} = ye^{-i3\pi/2} \qquad (76)$$

and using the recurrence relations,(*)

$$\left.\begin{aligned} H_n^{(2)}(\xi) &= 2J_n(\xi) - H_n^{(1)}(\xi) \\ H_n^{(2)}(\xi e^{-2\pi i}) &= -2J_n(\xi) - H_n^{(1)}(\xi) \end{aligned}\right\} \qquad (77)$$

the branch integral becomes:

$$I = (-1)^n \int_0^\infty \frac{[N_1 - kN_2]}{y^2 D_n} e^{-c_p ty/a} dy \qquad (78)$$

where

$$N_1 = \left\{ \begin{aligned} & 12n^2(n+1)^2y^2 [\pi^2 I_n^2(y) + K_n^2(y)] + \\ & + 3y^2[4n^2(n+1)^2 + 12n(n+1)y^2 + 9y^4][\pi^2 I_n^2(\sqrt{3}\,y) + K_n^2(\sqrt{3}\,y)] + \\ & + 12n^2y^4[\pi^2 I_{n-1}^2(y) + K_{n-1}^2(y)] + 36y^4[\pi^2 I_{n-1}^2(\sqrt{3}\,y) + K_{n-1}^2(\sqrt{3}\,y)] + \\ & - 24n^2(n+1)y^3[\pi^2 I_{n-1}(y)I_n(y) - K_{n-1}(y)K_n(y)] - \\ & - 12\sqrt{3}\,y^3[2n(n+1) + 3y^2][\pi^2 I_{n-1}(\sqrt{3}\,y)I_n(\sqrt{3}\,y) - K_{n-1}(\sqrt{3}\,y)K_n(\sqrt{3}\,y)] \end{aligned} \right\} \qquad (79)$$

(*) "A Treatise on the Theory of Bessel Functions", by G.N. Watson, Cambridge University Press, 1952, Pg. 75.

$$N_2 = \left\{ \begin{aligned} & 6n(n+1)y^2[2n(n+1)+3y^2][\pi^2 I_n^2(y) + K_n^2(y)] \\ & + 6n(n+1)y^2\,[2n(n+1)+3y^2][\pi^2 I_n^2(\sqrt{3}\,y) + K_n^2(\sqrt{3}\,y)] \\ & + 12ny^4\,[\pi^2 I_{n-1}^2(y) + K_{n-1}^2(y)] \\ & + 36ny^4\,[\pi^2 I_{n-1}^2(\sqrt{3}\,y) + K_{n-1}^2(\sqrt{3}\,y)] \\ & - 6ny^3[3y^2 + 2(n+1)^2][\pi^2 I_{n-1}(y) I_n(y) - K_{n-1}(y) K_n(y)] \\ & - 6\sqrt{3}\,ny^3[3y^2 + 2(n+1)^2][\pi^2 I_{n-1}(\sqrt{3}\,y) I_n(\sqrt{3}\,y) - K_{n-1}(\sqrt{3}\,y) K_n(\sqrt{3}\,y)] \end{aligned} \right\} \tag{80}$$

and where D_n is given by eq. (81), Pg. 242.

Equation (78) can be evaluated numerically for values of the time parameter $\frac{c_p t}{a}$.

The contributions from the poles ξ_j which are roots of Equation (74) may be evaluated by the Residue Theorem:

$$R = 2\pi i \sum_j R_j$$

where

$$2\pi i R_j = \frac{\left\{ \begin{aligned} & 2\sqrt{3}\,(1 - nk)\xi_j^2\; H_{n-1}^{(2)}(\xi_j)\, H_{n-1}^{(2)}(\sqrt{3}\,\xi_j) \\ & + 2\sqrt{3}\,n(nk-1)\xi_j\, H_n^{(2)}(\xi_j)\, H_{n-1}^{(2)}(\sqrt{3}\,\xi_j) \\ & + [2n(nk-1) + 3\xi_j^2]\xi_j\, H_{n-1}^{(2)}(\xi_j)\, H_n^{(2)}(\sqrt{3}\,\xi_j) \\ & - 3n(1+k)\xi_j^2\, H_n^{(2)}(\xi_j) H_n^{(2)}(\sqrt{3}\,\xi_j) \end{aligned} \right\} i e^{\frac{i c_p t}{a}\xi_j}}{\left\{ \begin{aligned} & -12\sqrt{3}\,\xi_j^3\, H_{n-1}^{(2)}(\xi_j) H_{n-1}^{(2)}(\sqrt{3}\,\xi_j) \\ & + 2[3\xi_j^3(3n-2) + 4n(1-n^2)\xi_j] H_n^{(2)}(\xi_j) H_n^{(2)}(\sqrt{3}\,\xi_j) \\ & + 3\xi_j^2(4n - 3\xi_j^2)\, H_{n-1}^{(2)}(\xi_j) H_n^{(2)}(\sqrt{3}\,\xi_j) \\ & + \sqrt{3}\,[8\xi_j^2(n^2-1) + 3\xi_j^2(4n - 3\xi_j^2)]\, H_n^{(2)}(\xi_j) H_{n-1}^{(2)}(\sqrt{3}\,\xi_j) \end{aligned} \right\}} \tag{82}$$

$$D_n = \left\{ \begin{aligned} & 9y^2[3y^2 + 4n(n+1)]^2 [\pi^2 I_n^2(y) + K_n^2(y)] [\pi^2 I_n^2(\sqrt{3}\,y) + K_n^2(\sqrt{3}\,y)] \; + \\ & + 48y^2(n^2-1)^2 [\pi^2 I_{n-1}^2(y) + K_{n-1}^2(y)] [\pi^2 I_{n-1}^2(\sqrt{3}\,y) + K_{n-1}^2(\sqrt{3}\,y)] \; + \\ & + 12[3y^2 - 2n(n^2-1)]^2 [\pi^2 I_n^2(y) + K_n^2(y)] [\pi^2 I_{n-1}^2(\sqrt{3}\,y) + K_{n-1}^2(\sqrt{3}\,y)] \; + \\ & + 4[3y^2 - 2n(n^2-1)]^2 [\pi^2 I_{n-1}^2(y) + K_{n-1}^2(y)] [\pi^2 I_n^2(\sqrt{3}\,y) + K_n^2(\sqrt{3}\,y)] \; + \\ & + 8\sqrt{3}[-9(n^2-2)y^4 - 12n(n^2-1)(n+2)y^2 + 4n^2(n^2-1)^2][\pi^2 I_n(y) I_{n-1}(y) - K_n(y) K_{n-1}(y)][\pi^2 I_n(\sqrt{3}\,y) I_{n-1}(\sqrt{3}\,y) \; - \\ & \qquad\qquad\qquad\qquad\qquad\qquad\qquad\qquad\qquad\qquad\qquad\qquad\qquad\qquad - K_n(\sqrt{3}\,y) K_{n-1}(\sqrt{3}\,y)] \; + \\ & + 12\sqrt{3}\,y[-9y^4 + 6n(n-3)(n+1)y^2 + 8n^2(n+1)(n^2-1)][\pi^2 I_n^2(y) + K_n^2(y)][\pi^2 I_n(\sqrt{3}\,y) I_{n-1}(\sqrt{3}\,y) - K_n(\sqrt{3}\,y) K_{n-1}(\sqrt{3}\,y)] \; + \\ & + 12y[-9y^4 + 6n(n-3)(n+1)y^2 + 8n^2(n+1)(n^2-1)][\pi^2 I_n(y) I_{n-1}(y) - K_n(y) K_{n-1}(y)][\pi^2 I_n^2(\sqrt{3}\,y) + K_n^2(\sqrt{3}\,y)] \; + \\ & + 48y(n^2-1)[3y^2 - 2n(n^2-1)][\pi^2 I_n(y) I_{n-1}(y) - K_n(y) K_{n-1}(y)][\pi^2 I_{n-1}^2(\sqrt{3}\,y) + K_{n-1}^2(\sqrt{3}\,y)] \; + \\ & + 16\sqrt{3}\,y(n^2-1)\,[3y^2 - 2n(n^2-1)]\,[\pi^2 I_{n-1}^2(y) + K_{n-1}^2(y)]\,[\pi^2 I_n(\sqrt{3}\,y) I_{n-1}(\sqrt{3}\,y) - K_n(\sqrt{3}\,y) K_{n-1}(\sqrt{3}\,y)] \\ & + 8\pi^2\,[9n^2y^2 + 12n^2(n^2-1) + \frac{4n^2}{y^2}(n^2-1)^2\,] \end{aligned} \right\} \tag{81}$$

The velocity component $\dot{v}_n$ then becomes:

$$\frac{\dot{v}_n \mu}{\sigma c_p} = [I + R] \cos n\theta \tag{83}$$

In a similar manner, the tangential velocity $\dot{v}_n$ at $r = a$ is evaluated by inverting the integral

$$\frac{\dot{v}_n(a,\ \theta,\ t)\mu}{\sigma c_p \sin n\theta} = \frac{1}{2\pi i} \int_{-\infty-i\gamma}^{\infty-i\gamma} \frac{iQ_n(a,\ \xi) e^{i\xi \frac{c_p t}{a}}}{[FB + DE]} d\xi \tag{84}$$

where

$$Q_n(a,\ \xi) = \left\{[B + kE][-nH_n^{(2)}(\xi)] + [D - kF][-nH_n^{(2)}(\frac{c_p}{c_s}\xi) + \frac{c_p}{c_s}\xi\ H_{n-1}^{(2)}(\frac{c_p}{c_s}\ \xi)]\right\} \tag{85}$$

Again, using the relation $\nu = 1/4$, i.e., $c_p = \sqrt{3}\ c_s$, the singularities of the integrand of Equation (84) are a branch point at the origin $\xi = 0$, and simple poles defined by the roots of the equation $FB + DE = 0$, Equation (74). The integral is inverted over the contour shown in Figure (5). Proceeding as in the inversion for $\dot{v}_n$, the tangential velocity component $\dot{v}_n(a,\ \theta,\ t)$ can be evaluated from the relation

$$\frac{\dot{v}_n(a,\ \theta,\ t)\mu}{\sigma c_p} = [\bar{I} + \bar{R}] \sin n\theta \tag{86}$$

The branch integral $\bar{I}$ is given by

$$\bar{I} = (-1)^n \int_0^\infty \frac{[N_3 - kN_4]}{y^2 D_n} e^{-\frac{c_p t y}{a}} dy \tag{87}$$

where

$$N_3 = \left\{ \begin{array}{l} -6n(n + 1)y^2[2n(n + 1) + 3y^2][\pi^2 I_n^2(y) + K_n^2(y)] - \\ -6n(n + 1)y^2[2n(n + 1) + 3y^2][\pi^2 I_n^2(\sqrt{3}\ y) + K_n^2(\sqrt{3}\ y)] - 12ny^4[\pi^2 I_{n-1}^2(y) + K_{n-1}^2(y)] \\ -36ny^4[\pi^2 I_{n-1}^2(\sqrt{3}\ y) + K_{n-1}^2(\sqrt{3}\ y)] \\ + 6ny^3[2(n + 1)^2 + 3y^2][\pi^2 I_{n-1}(y) I_n(y) - K_{n-1}(y) K_n(y)] \\ + 6\sqrt{3}\ ny^3[2(n + 1)^2 + 3y^2][\pi^2 I_{n-1}(\sqrt{3}\ y) I_n(\sqrt{3}\ y) - K_{n-1}(\sqrt{3}\ y) K_n(\sqrt{3}\ y)] \end{array} \right. \tag{88}$$

$$N_4 = \left\{\begin{array}{l} -3y^2[4n^2(n+1)^2 + 12n(n+1)y^2 + 9y^4][\pi^2 I_n^2(y) + K_n^2(y)] \\ -12n^2(n+1)^2 y^2\,[\pi^2 I_n^2(\sqrt{3}\,y) + K_n^2(\sqrt{3}\,y)] \\ -12y^4[\pi^2 I_{n-1}^2(y) + K_{n-1}^2(y)] \\ -36n^2y^4[\pi^2 I_{n-1}^2(\sqrt{3}\,y) + K_{n-1}^2(\sqrt{3}\,y)] \\ +12y^3[2n(n+1) + 3y^2][\pi^2 I_{n-1}(y) I_n(y) - K_{n-1}(y) K_n(y)] \\ +24\sqrt{3}\,n^2(n+1)y^3[\pi^2 I_{n-1}(\sqrt{3}\,y)\, I_n(\sqrt{3}\,y) - K_{n-1}(\sqrt{3}\,y) K_n(\sqrt{3}\,y)] \end{array}\right\} \qquad (89)$$

and D_n is given by Equation (81). Equation (87) may be evaluated numerically for values of the time parameter $\frac{c_p t}{a}$.

The contributions from the poles ξ_j which are roots of Equation (74) may be evaluated by the Residue theorem:

$$\overline{R} = 2\pi i \sum_j R_j$$

where

$$2\pi i P_j = \frac{\left\{\begin{array}{l} 2\sqrt{3}\,(-n+k)\xi_j^2\; H_{n-1}^{(2)}(\xi_j) H_{n-1}^{(2)}(\sqrt{3}\,\xi_j) \\ +\sqrt{3}\,[2n(n-k) + 3k\xi_j^2]\xi_j\; H_n^{(2)}(\xi_j) H_{n-1}^{(2)}(\sqrt{3}\,\xi_j) \\ +2n(n-k)\xi_j\; H_{n-1}^{(2)}(\xi_j)\, H_n^{(2)}(\sqrt{3}\,\xi_j) \\ -3n(1+k)\xi_j^2\; H_n^{(2)}(\xi_j) H_n^{(2)}(\sqrt{3}\,\xi_j) \end{array}\right\} ie^{\frac{ic_p t}{a}\xi_j}}{\left\{\begin{array}{l} -12\sqrt{3}\,\xi_j^3\; H_{n-1}^{(2)}(\xi_j)\, H_{n-1}^{(2)}(\sqrt{3}\,\xi_j) \\ +2[3\xi_j^3(3n-2) + 4n(1-n^2)\xi_j]\, H_n^{(2)}(\xi_j) H_n^{(2)}(\sqrt{3}\,\xi_j) \\ +3\xi_j^2\,(4n - 3\xi_j^2)\, H_{n-1}^{(2)}(\xi_j) H_n^{(2)}(\sqrt{3}\,\xi_j) \\ +\sqrt{3}\,[8\xi_j^2(n^2-1) + 3\xi_j^2(4n - 3\xi_j^2)]\, H_n^{(2)}(\xi_j)\, H_{n-1}^{(2)}(\sqrt{3}\,\xi_j) \end{array}\right\}} \qquad (90)$$

V. DISPLACEMENTS AND VELOCITIES PRODUCED BY THE BOUNDARY TRACTIONS $\sigma_{rr_o} = U(t)$ AND $\sigma_{r\theta_o} = 0$.

The displacement $\underline{u}$ for the case $n = 0$ has a radial component only

$$\underline{u} = w_o(r,t)\ \underline{k_r} \tag{91a}$$

The coefficient $w_o(r,t)$ is expressed in terms of a single potential function $\phi(r,t)$:

$$w_o(r,t) = \phi_r(r,t) \tag{91b}$$

Proceeding as in Section (IV), the radial displacement w_o and the radial velocity $\dot{w}_o$ can be obtained from an inversion of the following integrals:

$$w_o(r,t) = \frac{\sigma a}{2\pi i\mu} \int_{-\infty-i\gamma}^{\infty-i\gamma} \frac{H_1^{(2)}(\xi\frac{r}{a})\, e^{i\xi\frac{c_p t}{a}}\, d\xi}{\xi[-2H_1^{(2)}(\xi) + 3\xi H_0^{(2)}(\xi)]} \tag{92}$$

and

$$\dot{w}_o(r,t) = \frac{\sigma c_p}{2\pi\mu} \int_{-\infty-i\gamma}^{\infty-i\gamma} \frac{H_1^{(2)}(\xi\frac{r}{a})\, e^{i\xi\frac{c_p t}{a}}\, d\xi}{[3\xi H_0^{(2)}(\xi) - 2H_1^{(2)}(\xi)]} \tag{93}$$

The quantities w_o and $\dot{w}_o$ at the cavity boundary are evaluated by integrating Eq. (92) - (93) with $r = a$ over the contour ABCDEF, Figure (5). Proceeding as in Section (IV), the velocity $\dot{w}_o$ is computed from the relation

$$\frac{\dot{w}_o(a,t)\mu}{\sigma c_p} = [I + R] \tag{94}$$

where the branch integral I and the sum of the residues R are given below:

$$I = \int_0^\infty \frac{3e^{-y\frac{c_p t}{a}}\,dy}{[2K_1(y) + 3yK_0(y)]^2 + \pi^2[2I_1(y) - 3yI_0(y)]^2} \tag{95}$$

$$R = -\sum_j \left[\frac{iH_1^{(2)}(\xi_j)e^{i\xi_j\frac{c_p t}{a}}}{[3\xi_j - \frac{2}{\xi_j}]\,H_1^{(2)}(\xi_j) - H_0^{(2)}(\xi_j)} \right] \tag{96}$$

The summation over j in Eq. (96) is carried out for all values of ξ_j which lie [illegible] the first and fourth quadrants and are roots of the equation

$$3\xi H_0^{(2)}(\xi) - 2H_1^{(2)}(\xi) = 0. \tag{97}$$

VI. DETERMINATION OF THE RIGID BODY MOTION OF THE CAVITY BOUNDARY [Fig. 6].

A portion of the total motion of the boundary of the cavity consists of a rigid body translation in which the cavity maintains its shape and translates in the direction of propagation of the incoming wave. This rigid body motion can be extracted from the total motion of points on the cavity boundary. Essentially, one must superimpose a portion of both the $n = 1$ component of a Fourier expansion of the free field motion and the $n = 1$ component of the motion produced by the corrective boundary tractions, $\sigma_{rr} = a_1(t) \cos \theta$, $\sigma_{r\theta} = b_1(t) \sin \theta$ [Eq.(23)].

Consider, for example, the determination of the velocity components, $\dot{w}$ and $\dot{v}$, for the rigid body translation of the cavity. The free field velocity components, $\dot{w}_f$ and $\dot{v}_f$, Eq. (3)-(4) respectively, which are produced at points on the cavity boundary, $r = a$, by the incoming plane step shock wave are expanded into a Fourier series in θ:

$$\dot{w}_f(a,\theta,t) = \frac{d_o^f(t)}{2} + \sum_{n=1}^{\infty} d_n^f(t) \cos n\theta \tag{98}$$

$$\dot{v}_f(a,\theta,t) = \sum_{n=1}^{\infty} h_n^f(t) \sin n\theta \tag{99}$$

where

$$d_n^f(t) = \frac{2}{\pi} \int_0^{\alpha(t)} \dot{w}_f(a,\theta) \cos n\theta \, d\theta \tag{100}$$

$$h_n^f(t) = \frac{2}{\pi} \int_0^{\alpha(t)} \dot{v}_f(a,\theta) \sin n\theta \tag{101}$$

and $\dot{w}_f$ and $\dot{v}_f$ are given by Eq. (3)-(4).

The velocity components $\dot{w}_{f_1}$ and $\dot{v}_{f_1}$, corresponding to $n = 1$, can be written in the following manner:

$$\dot{w}_{f_1} = \left[\frac{d_1^f(t) + h_1^f(t)}{2}\right] \cos\theta + \left[\frac{d_1^f(t) - h_1^f(t)}{2}\right] \cos\theta \qquad (102)$$

$$\dot{v}_{f_1} = \left[\frac{d_1^f(t) + h_1^f(t)}{2}\right] \sin\theta - \left[\frac{d_1^f(t) - h_1^f(t)}{2}\right] \sin\theta \qquad (103)$$

The coefficient, $\left[\frac{d_1^f + h_1^f}{2}\right]$ represents a deformational component of the velocities while the coefficient $\left[\frac{d_1^f - h_1^f}{2}\right]$ represents the rigid body velocity components. For the step shock wave under consideration

$$d_1^f(t) = \begin{cases} -\frac{\sigma}{\rho c}\,\frac{1}{\pi}\,[\alpha + \sin\alpha\cos\alpha] & t \leq \frac{2a}{c} \\ -\frac{\sigma}{\rho c} & t > \frac{2a}{c} \end{cases} \qquad (104)$$

$$h_1^f(t) = \begin{cases} \frac{\sigma}{\rho c}\,[\alpha - \sin\alpha\cos\alpha] & t \leq \frac{2a}{c} \\ \frac{\sigma}{\rho c} & t > \frac{2a}{c} \end{cases} \qquad (105)$$

In a similar manner, the velocities, $\dot{w}_{c_1}$ and $\dot{v}_{c_1}$, (*) produced by the corrective boundary tractions $\sigma_{rr} = a_1(t)\cos\theta$ and $\sigma_{r\theta} = b_1(t)\sin\theta$ can be written in the form:

(*) The quantities $\dot{w}_{c_1}(\theta,t)$ and $\dot{v}_{c_1}(\theta,t)$ can be evaluated from the formulas in Section (IV).

$$\dot{w}_{c_1}(\theta,t) = d_1^c(t)\cos\theta = \left[\frac{d_1^c(t) + h_1^c(t)}{2}\right]\cos\theta + \left[\frac{d_1^c(t) - h_1^c(t)}{2}\right]\cos\theta \tag{106}$$

$$\dot{v}_{c_1}(\theta,t) = h_1^c(t)\sin\theta = \left[\frac{d_1^c(t) + h_1^c(t)}{2}\right]\sin\theta - \left[\frac{d_1^c(t) - h_1^c(t)}{2}\right]\sin\theta \tag{107}$$

where the terms containing the quantities $\left[\frac{d_1^c(t) - h_1^c(t)}{2}\right]$ are the rigid body components of the velocities.

The total rigid body velocity of points on the cavity boundary is obtained by superposition of the rigid body components in Eq. (102)-(103) and Eq. (106)-(107):

$$\dot{w}(\theta,t) = d(t)\cos\theta \tag{108}$$

$$\dot{v}(\theta,t) = -\,d(t)\sin\theta \tag{109}$$

where

$$d(t) = \left[\frac{d_1^f(t) + d_1^c(t) - h_1^f(t) - h_1^c(t)}{2}\right] \tag{110}$$

In a similar manner, results for the rigid body displacements and accelerations can also be determined. The corresponding free field expansion coefficients, d_1^f and h_1^f for the displacements and accelerations are given below:

Displacement coefficients

$$w_1^f(t) = d_1^f(t)\cos\theta \quad ; \quad v_1^f(t) = -\,h_1^f(t)\sin\theta$$

where

$$d_1^f(t) = \begin{cases} \dfrac{\sigma a}{\rho c_p^2} \, \dfrac{1}{\pi} \left[\alpha \cos \alpha - \sin \alpha - \dfrac{\sin^3 \alpha}{3} \right] & t \leq \dfrac{2a}{c} \\[2ex] -\dfrac{\sigma a}{\rho c_p^2} \left[\dfrac{c_p t}{a} - 1 \right] & t > \dfrac{2a}{c} \end{cases} \tag{111}$$

$$h_1^f(t) = \begin{cases} \dfrac{\sigma a}{\rho c_p^2} \, \dfrac{1}{\pi} \left[-\alpha \cos \alpha + \sin \alpha - \dfrac{\sin^3 \alpha}{3} \right] & t \leq \dfrac{2a}{c} \\[2ex] \dfrac{\sigma a}{\rho c_p^2} \left[\dfrac{c_p t}{a} - 1 \right] & t > \dfrac{2a}{c} \end{cases} \tag{112}$$

Acceleration coefficients:

$$\ddot{v}_1^f(t) = d_1^f(t) \cos \theta \quad ; \quad \ddot{v}_1^f(t) = h_1^f(t) \sin \theta$$

where

$$d_1^f(t) = \begin{cases} -\dfrac{\sigma}{\rho a} \, \dfrac{2}{\pi} \cot \alpha \cos \alpha & t \leq \dfrac{2a}{c} \\[2ex] 0 & t > \dfrac{2a}{c} \end{cases} \tag{113}$$

$$h_1^f(t) = \begin{cases} \dfrac{\sigma}{\rho a} \, \dfrac{2}{\pi} \sin \alpha & t \leq \dfrac{2a}{c} \\[2ex] 0 & t > \dfrac{2a}{c} \end{cases} \tag{114}$$

VII. NUMERICAL RESULTS AND CONCLUSIONS.

Numerical results are presented for the displacement and velocity components at various points on the cavity boundary $r = a$; these quantities are produced by a plane step shock wave.

As in the case of the stress [19], it was found that the maximum values of the displacement and velocity are not materially affected by the early-time contributions which come from the terms for which n is larger than 2, and consequently, the series in Equations (34)-(37) may generally be terminated after the $n = 2$ term for computational purposes.

Figures [(9-13)-(9-14)] show the displacement and velocity components, w and $\dot{w}$ for the locations $\theta = 0^{\circ}$ and $\theta = 90^{\circ}$ on the boundary of the cavity. Figures [(7)-(8)] of the Appendix show the radial and tangential velocity components $\dot{w}$ and $\dot{v}$ at the locations $\theta = 0^{\circ}$, 22.5°, 45°, 67.5°, 90°, 135° and 180° on the cavity boundary.

The rigid body motions of the cavity under a step wave loading are computed from Section (VI) and the components from the free field and corrective traction ($n = 1$) effects are shown in Figures [(9)-(10)] respectively. The total rigid body displacements, velocities and accelerations are shown in Figure (9-15) of Section (9).

The motions of points in the media which are produced by the step shock wave may be used as influence coefficients to determine the corresponding motions produced by a wave with a varying pressure-time history. For example, denoting the radial component of the velocity produced at the boundary by a step wave as $\dot{w}_s(\theta, t)$, the radial velocity due to a wave with the pressure-time history $P(t)$ is easily computed from the Duhamel integral

$$\dot{w} = P_o \dot{w}_s(\theta, t) + \int_0^t \frac{dP(\tau)}{d\tau} \dot{w}_s(t - \tau) d\tau$$

by numerical integration [See Figure (9-5)].

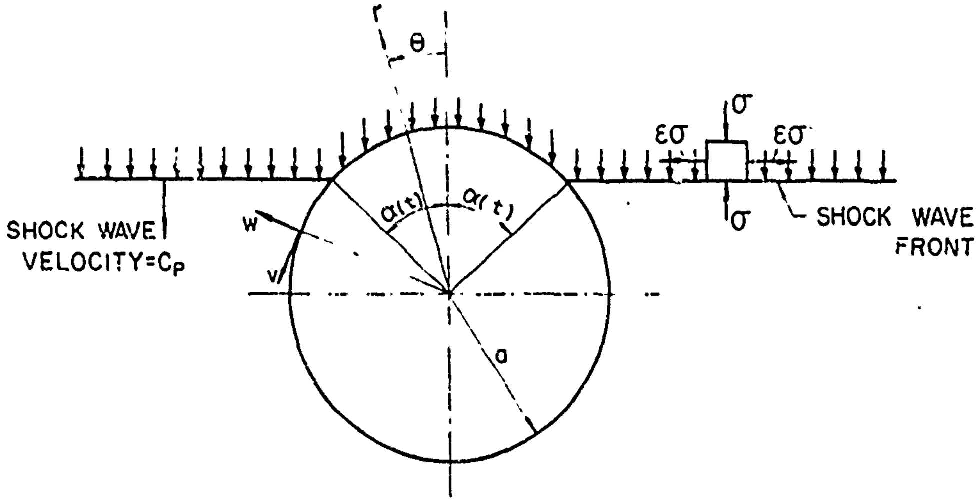

FIG. 1 GEOMETRY OF PROBLEM

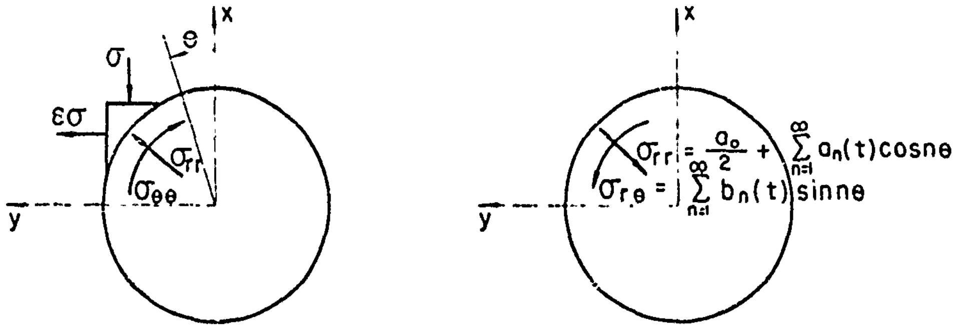

(a) (b)

FIG. 2 BOUNDARY TRACTIONS

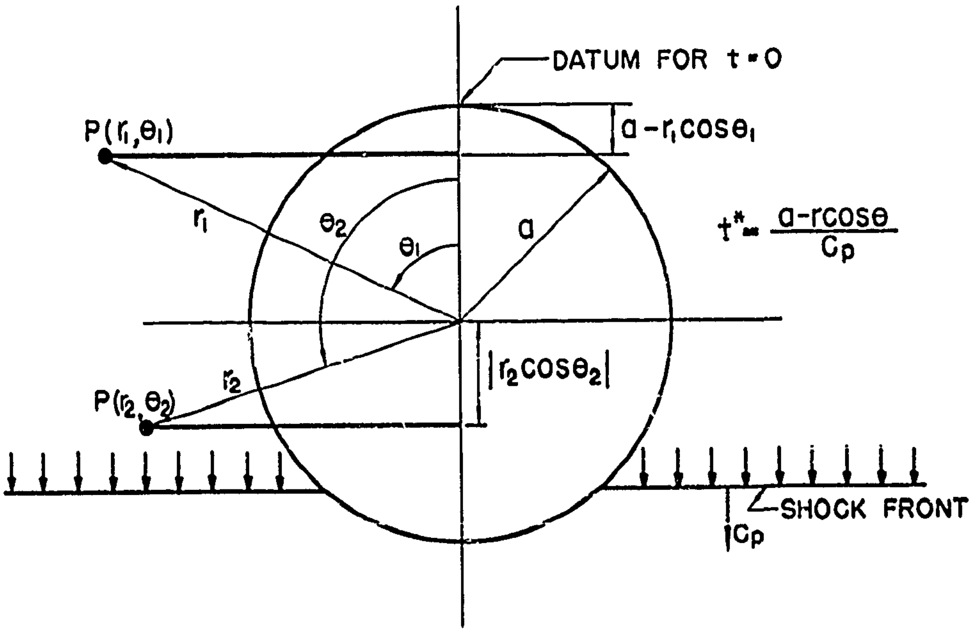

FIG.3 DELAY TIME t^*

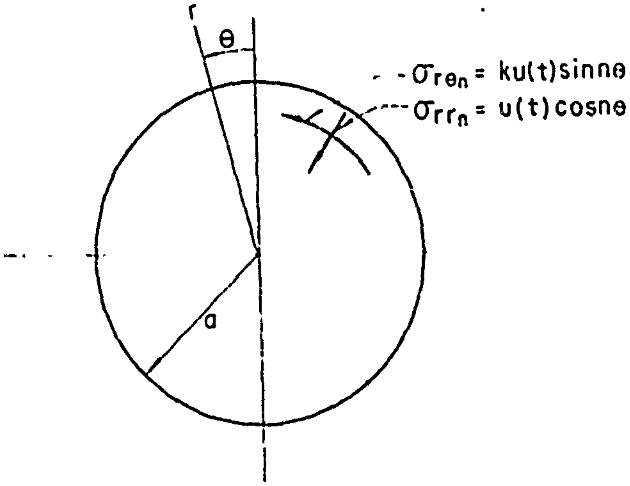

FIG.4 AUXILIARY PROBLEM

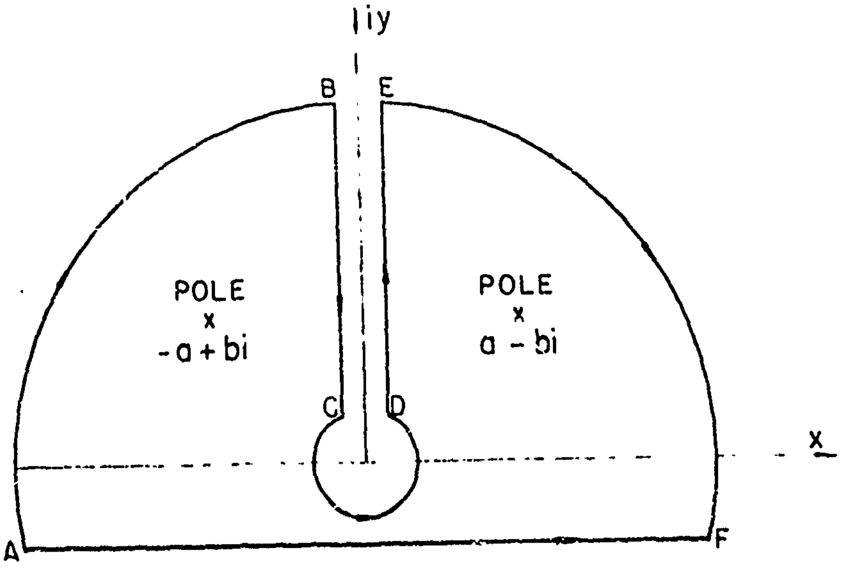

FIG.5 - INTEGRATION CONTOUR

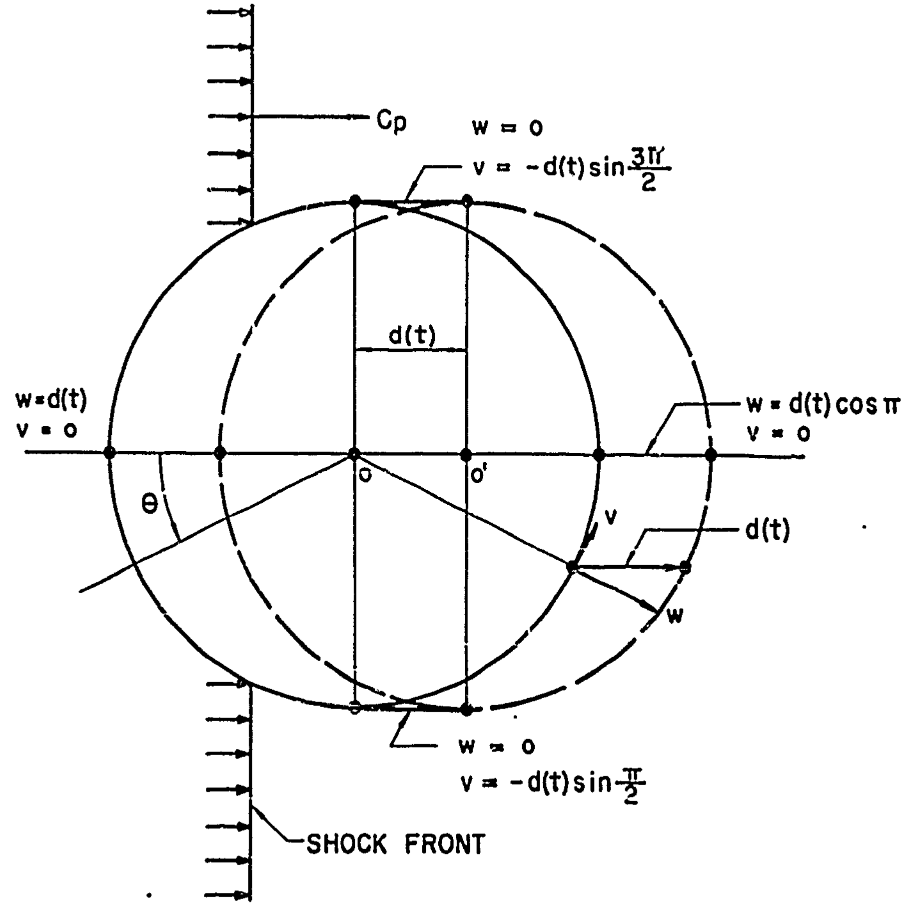

FIG. 6 RIGID BODY MOTION OF CAVITY

NOTE: THE QUANTITY d(t) IS INHERENTLY NEGATIVE.

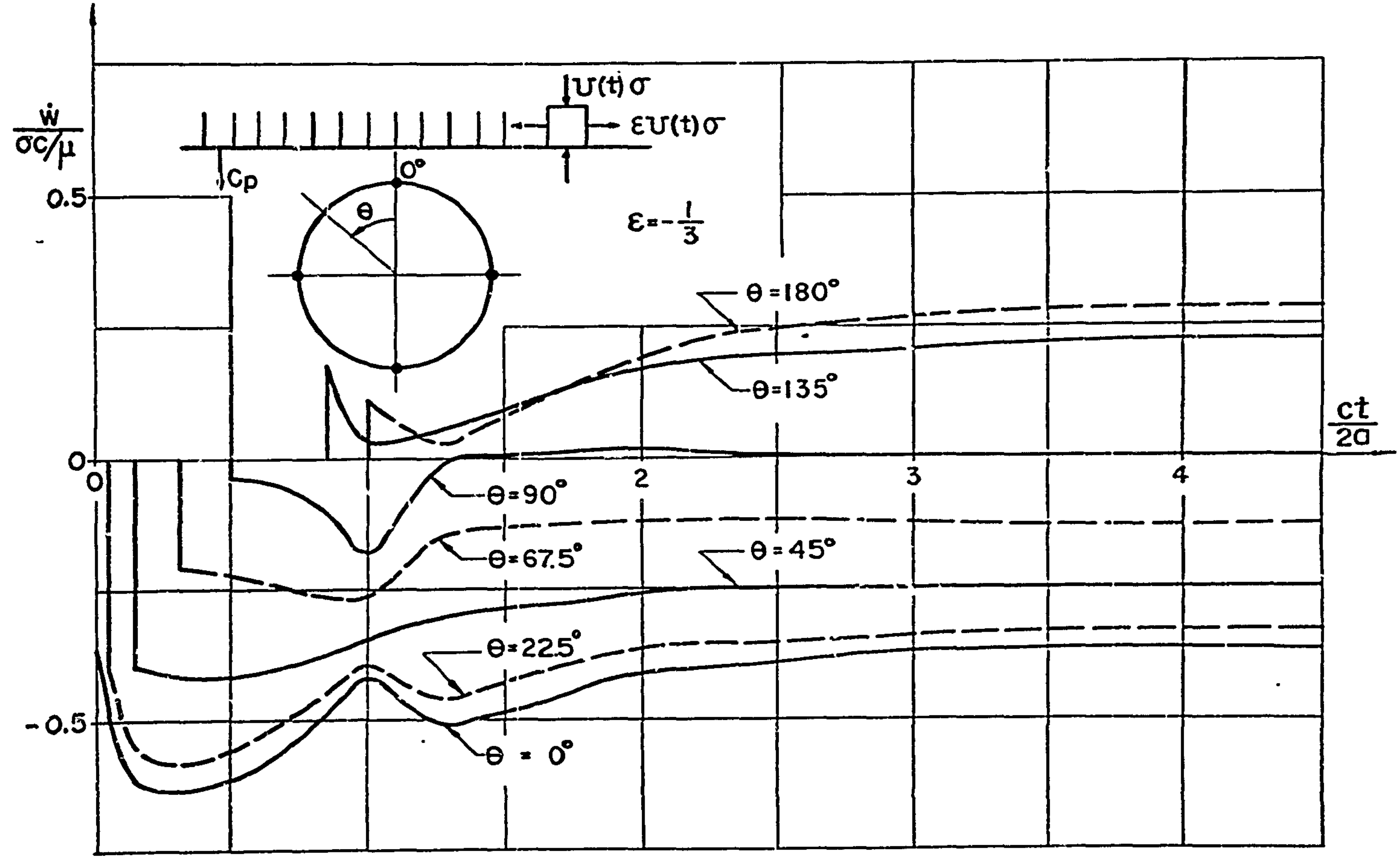

FIG.7 RADIAL VELOCITY $\dot{w}(\theta,t)$

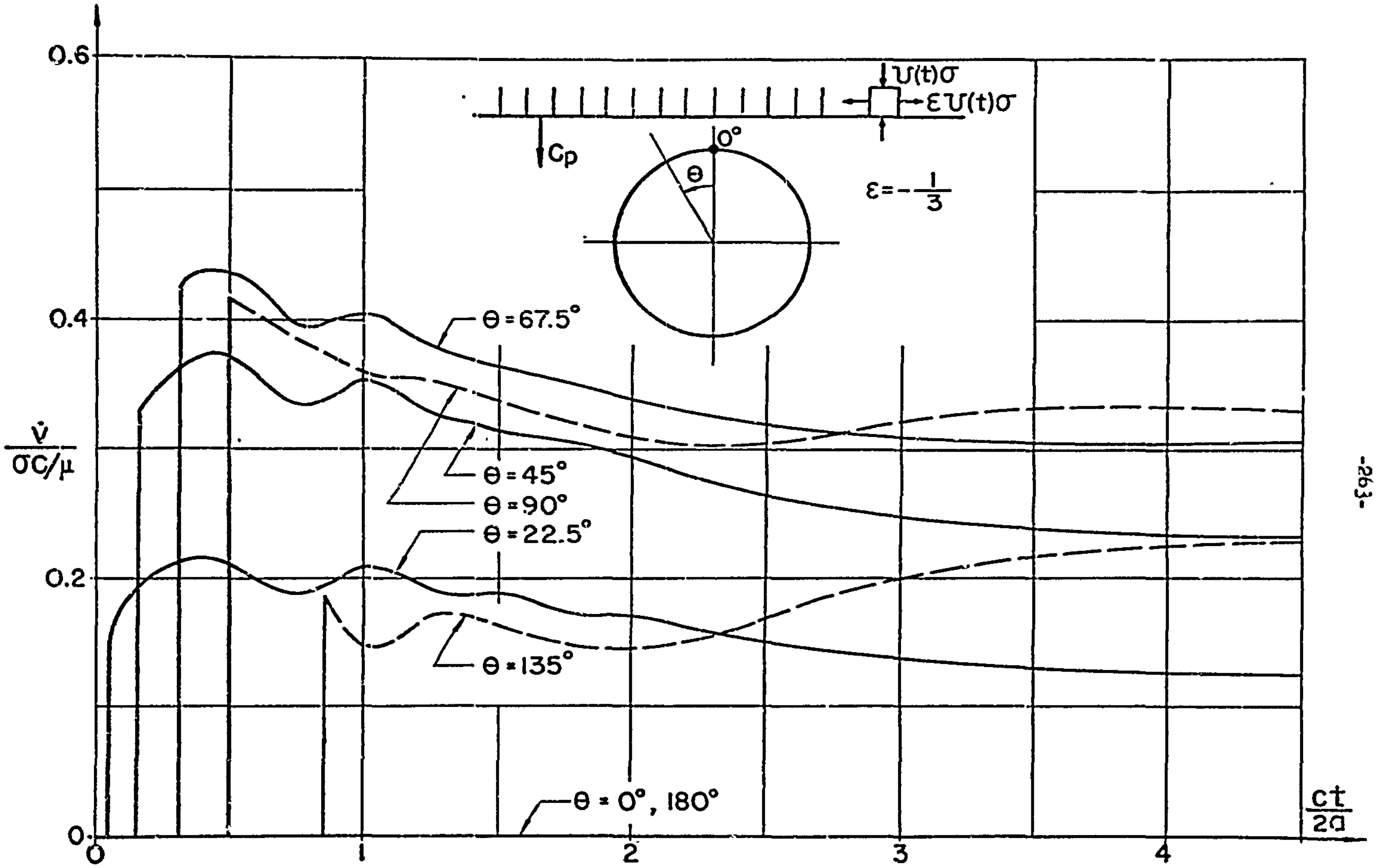

FIG.8 TANGENTIAL VELOCITY $\dot{V}(\theta, t)$

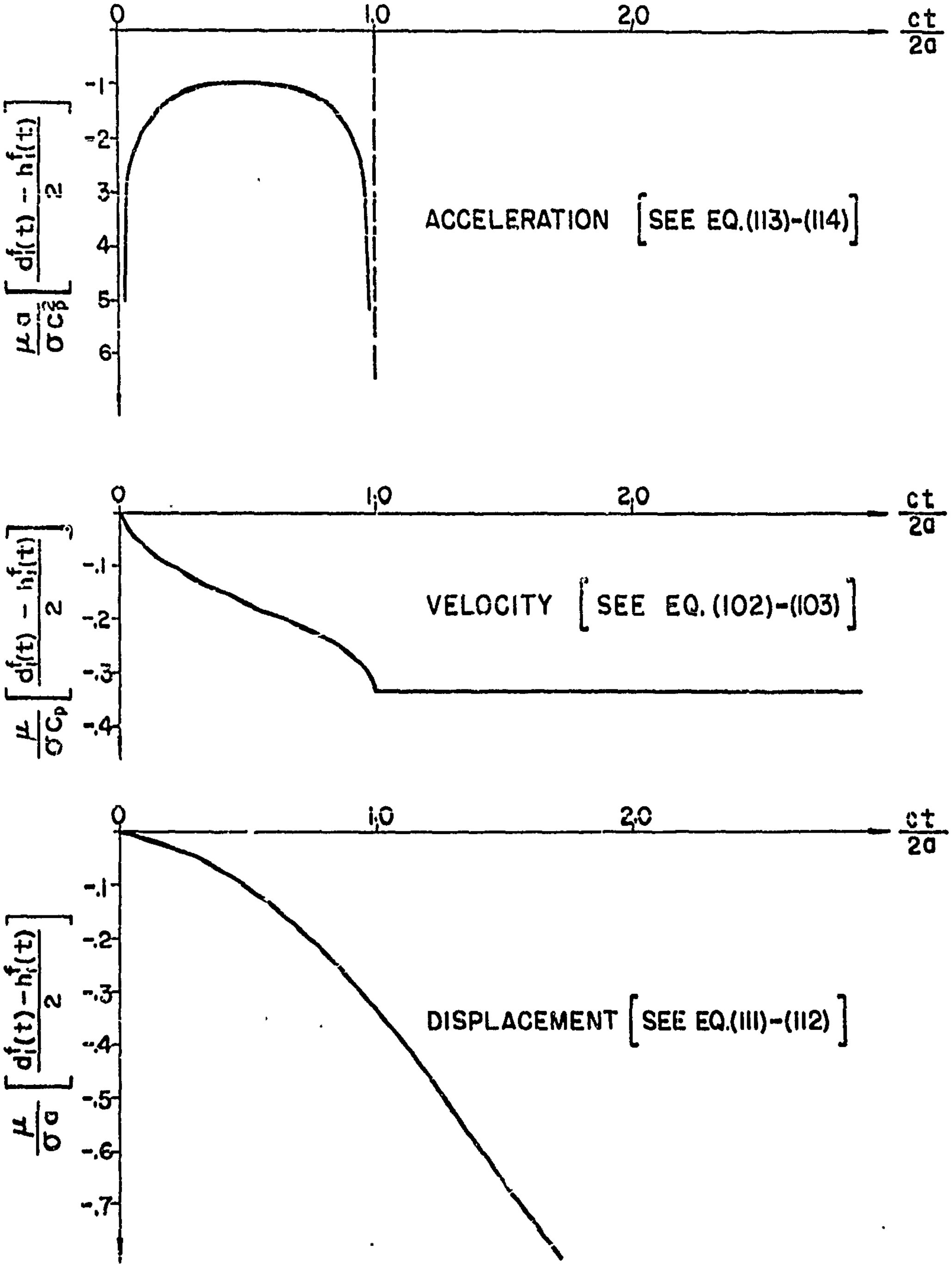

FIG. 9 MEAN MOTION OF CAVITY··FREE FIELD CONTRIBUTION

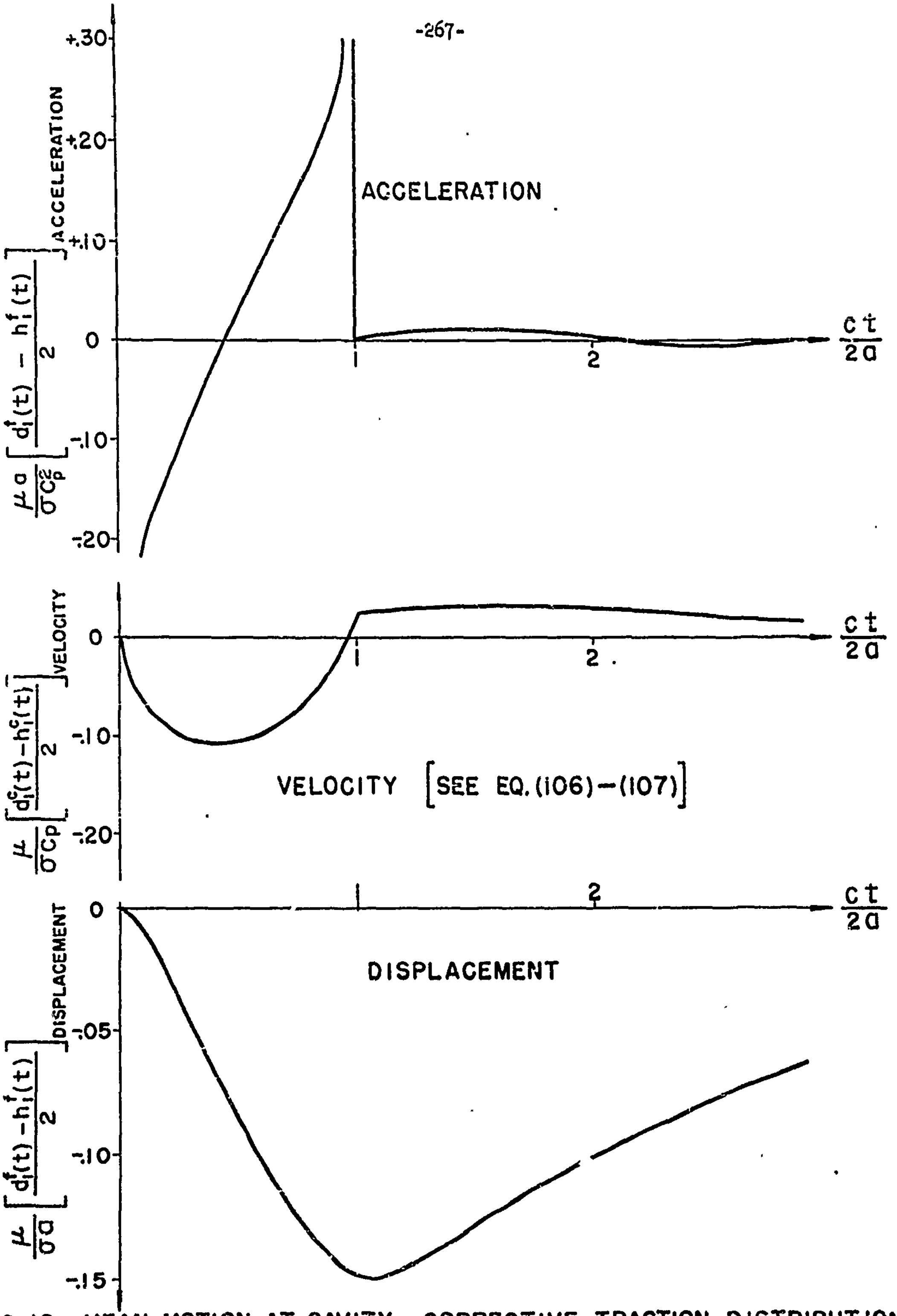

FIG. 10—MEAN MOTION AT CAVITY—CORRECTIVE TRACTION DISTRIBUTION

APPENDIX E

DETERMINATION OF SHOCK SPECTRA FOR INSTALLATIONS IN CYLINDRICAL CAVITIES IN ELASTIC MEDIA.

I. Introduction.

The motion of points on the boundary of a cavity subjected to shock waves, impart accelerations to installations which are located within the tunnel and are attached to these points. In many cases, these installations will be quite shock sensitive and consequently, they may require special mountings to absorb the shock effects produced by the pressure waves.

In order to optimalize the design of shock mounted equipment, shock spectra are frequently utilized. Two types of spectra are particularly useful in the present problem: 1) Spectra for the peak relative displacement of the installation in the cavity, with respect to the motion of the points on the cavity boundary to which it is attached; 2) Spectra for the peak absolute acceleration which is imparted to the shock mounted installation in the cavity. The latter spectra give data which is required for the actual design of the installation to be shock mounted, namely the peak accelerations to which it will be subjected; the former spectra give clearance requirements for the mounting of the installation within the cavity.

The theoretical formulation of the problem of the determination of shock spectra of the type described will be presented in this Appendix for waves which carry decaying pressure-time histories as given by Brode [35]:

$$P(t) = p_o\left(1 - \frac{t}{D_p}\right)\left[\bar{A}e^{-\frac{\bar{\alpha}t}{D_p}} + \bar{B}e^{-\frac{\bar{\beta}t}{D_p}}\right] + 14.7\ (\text{lb./in}^2) \quad (1)$$

The quantity P_o is the peak overpressure in the shock wave, and the constants D_p, $\bar{A}$, $\bar{\alpha}$, $\bar{B}$ and $\bar{\beta}$ are defined in [35]. The displacements of points on the cavity boundary for waves with the decaying pressure-time history are obtained from the corresponding displacements due to waves with step pressures by Duhamel integrals [Section (9)]. The spectra curves for typical cases are shown in Section (10) of the main report.

It is of interest to note that heretofore, shock spectra which were used in the design of underground installations were computed from free field input pressures, and the effects of the diffraction of the shock wave by the cavity were neglected. The spectra developed in this Appendix include the diffraction effects; consequently they are more appropriate and should supersede the free field spectra. It will be noted that for shock mounted equipment with high frequency components, the free field spectra are quite erroneous and the more accurate spectra presented in Section (10) should be used.

II. General Procedure.

Consider an installation which is shock mounted to the walls of a cylindrical cavity in an elastic medium. The problem can be idealized by considering a linear oscillator consisting of a concentrated mass M on a linear spring of constant K. The oscillator is attached to a support which is subjected to a motion equal in magnitude to the displacement of the point or points on the cavity boundary at which the mass is attached [Figure (1)]. Let the displacement of the support and of the mass, both relative to a fixed datum, be $\bar{U}(t)$ and $Y(t)$ respectively; the relative motion of the mass M with respect to the support is $Y(t) - \bar{U}(t)$. The equation of motion of the oscillator is:

$$M\ddot{Y} + K\,[Y - \bar{U}] = 0 \tag{2}$$

Defining the frequency ω of the oscillator,

$$\omega = \sqrt{\frac{K}{M}} \tag{3}$$

Equation (1) is written as

$$\ddot{Y} + \omega^2 Y = \omega^2 \bar{U} \tag{4}$$

For initial rest conditions, i.e. $Y(0) = 0$ and $\dot{Y}(0) = 0$, the solution of Equation (4) is given by the integral.

$$Y(t) = \int_0^t \omega\bar{U}(\tau)\,\sin\omega(t - \tau)\,d\tau \tag{5}$$

Shock spectra showing the peak absolute acceleration and the peak relative displacement (relative to the moving support) as a function of the frequency ω of the oscillator are required. For a given value of ω, the peak acceleration of the mass

$$\left|\omega^2(Y - \bar{U})\right|_{\text{maximum}} \tag{6}$$

and the peak relative displacement

$$\left|Y - \bar{U}\right|_{\text{maximum}} \tag{7}$$

are evaluated.

For this study, Brode pressure curves produced at different locations by a hypothetical 20 M.T. surface burst were considered, and the resulting displacements, $\bar{U}(t)$ at various points, $\theta = \theta_1$, on the cavity boundary were determined. These were introduced as forcing functions into the right hand side of Equation (4), and for various values of ω, the acceleration and displacement responses, given by Equation (6) and (7) were computed and plotted as a function of ω. These shock spectra are presented in

Figure (10-2)-(10-5).

The computations were made using an IBM 704 computer. The analytical formulation of the problem in detail is given in Section III of this Appendix.

III. Analytical Formulation of the Problem.

The determination of acceleration and displacement shock spectra may be formulated analytically in two steps. First, the displacement $\overline{U}(t)$ produced at a point $\theta = \theta_1$ on the cavity boundary by a shock wave with a Brode pressure decay must be evaluated. Secondly, the values of $\overline{U}(t)$ are substituted as input functions into the right hand side of Equation (4); the equation is then integrated and the expressions for the maximum acceleration, Equation (6), and relative displacement, Equation (7) are evaluated for each value of ω. The analytical formulation of the problem follows:

a) Evaluation of $\overline{U}(t)$, produced at a point, $\theta = \theta_1$, of the boundary of the cavity by a shock wave with a Brode pressure decay.

Expressions for the displacement, $U(t)$ produced at a point, $\theta = \theta_1$, on the cavity boundary by a step shock wave (P wave) are given in Appendix D.(*). The corresponding displacement curve, $\overline{U}(t)$, produced by a wave carrying a pressure with a Brode decay, may be evaluated by means of the Duhamel integral

$$\overline{U}(t) = \int_0^t P(\tau) \frac{\partial U(t-\tau)}{\partial \tau} d\tau \qquad (8)$$

---

* See Appendix (D), Eq. (34)-(35).

where $P(\tau)$ is given by Equation (1). To perform this integration, ninth order polynomial curves are fitted to the function $U(t)$. Due to the nature of the $U(t)$ curve, a single polynomial fit is only valid over a certain region of the curve, and hence several polynomials are used, each being valid in a certain region. Using the notation below, the displacement

$$U^{(r_i)}(T) = \sum_{n=0}^{9} a_n^{(r_i)} T^n \qquad (9)$$

where

$$T = \frac{c_p t}{a} \qquad (10)$$

is valid in the region R which is bounded by r_i and r_{i+1},

$$\text{Region R:} \quad r_i \leq T < r_{i+1} \quad , \quad U^{(r_i)}(T). \qquad (11)$$

$$i = 0, 1, 2, \ldots .$$

Substituting Equation (9) into Equation (8), the displacement $\bar{U}^{(r_i)}(T)$ which is valid in the region R, $r_i \leq T < r_{i+1}$, is obtained by integration. This quantity is written in the form

$$\bar{U}^{(r_i)}(T) = \bar{U}^{(A,\ r_i)}(T) + \bar{U}^{(B,\ r_i)}(T) + \bar{Z}^{(r_i)}(T). \qquad (12)$$

The expression $\bar{U}^{(A,\ r_i)}(T)$ is given by the expression

$$\bar{U}^{(A,\ r_i)}(T) = \frac{a}{G} \sum_{n=0}^{9} U^{(A,\ r_i)}(T) \qquad (13)$$

where

$$U^{(A,\ r_i)}(T) = A\left\{ \sum_{j=1}^{i} \left[\left(a_n^{(r_j-1)} - a_n^{(r_j)}\right) E_n^{(A,\ r_j)}(T) \right] + a_n^{(r_i)} F_n^{(A)}(T) \right\} \qquad (14)$$

$$E_n^{(A,\ r_j)}(T) = \left\{ (-1)^{n-1} [n - \alpha(\mu - T)] V_n^{(A)}(r_j) + \frac{n r_j^n}{\alpha} \right\} e^{-\alpha(T - r_j)} \qquad (15)$$

$$F_n^{(A)}(T) = (-1)^{n-1} [n - \alpha(\mu - T)] V_n^{(A)}(T) + \frac{n T^n}{\alpha} \qquad (16)$$

$$V_n^{(A)}(T) = \frac{1}{\alpha} \sum_{m=n}^{\infty} (-1)^m \frac{n!}{m!} T^m \alpha^{m-n} \tag{17}$$

and the constants A, α, and μ are given in terms of the parameters of the Brode curves [See Equation (1)],

$$A = \frac{\bar{A}a}{c_p D_p} P_o; \quad \alpha = \frac{\bar{\alpha}a}{c_p D_p}; \quad \mu = \frac{c_p D_p}{a} \tag{18}$$

The expression for $\bar{U}^{(B,\ r_1)}(T)$ is obtained by substituting B for A and β for α in Equation (13)-(18), where

$$B = \frac{\bar{B}a}{c_p D_p}; \quad \beta = \frac{\bar{\beta}a}{c_p D_p} \tag{19}$$

The term $\bar{Z}^{(r_1)}(T)$ represents the displacement due to the atmospheric pressure term in Equation (1) and is given by the relation

$$\bar{Z}^{(r_1)}(T) = 14.7 \frac{a}{G} \sum_{n=0}^{9} a_n^{(r_1)} T^n \tag{20}$$

b) Integration of Equation (4) and the evaluation of the maximum acceleration [Equation (6)] and the maximum relative displacement [Equation (7)].

Once the displacement $\bar{U}(T)$ is evaluated, the displacement Y(T) is obtained by integrating Equation (4) for a particular value of the frequency ω. In terms of the non-dimensional variable T, Equation (4) becomes

$$\frac{d^2Y}{dT^2} + \bar{\omega}^2 Y = \bar{\omega}^2 \bar{U}(T) \tag{21}$$

where

$$\bar{\omega} = \frac{\omega a}{c} \tag{22}$$

The computed values of Y(T) are then used to determine the maximum acceleration, Equation (6) and the maximum relative displacement, Equation (7).

Generally, Equation (21) can easily be integrated numerically by a forward step integration in time. Letting "k" be the interval of the non-dimensional time steps, and using the Noumerov procedure(*) for second order differential equations, a recurrence formula for $Y(T + k)$ is obtained:

$$Y(T + k) = \frac{k^2\bar{\omega}^2}{12+k^2\bar{\omega}^2} [\bar{U}(T - k) + 10\bar{U}(T) + \bar{U}(T + k)] + [\frac{24 - 10k^2\bar{\omega}^2}{12 + k^2\bar{\omega}^2}]Y(T) - Y(T-k) \tag{23}$$

Equation (23) allows the determination of the displacement $Y(T + k)$ in terms of the previously computed values of Y at the two previous time steps, T and $T - k$. When the integration is started from the initial time, $T = 0$, the starting formula

$$Y(0) = 0 \tag{24}$$

$$Y(k) = \frac{k^2\bar{\omega}^2}{12+k^2\bar{\omega}^2} [\bar{U}(k) + 5\bar{U}(0)] \tag{25}$$

must be used.

Stability considerations(*) for the numerical solution of Equation (21) by the Noumerov recurrence formula, Equation (23), requires that the time step k satisfy the condition

$$k < \frac{1.55}{\bar{\omega}} \tag{26}$$

A further requirement for accuracy of the solution results in the use of a substantially reduced value of "k" from that of Equation (26). In the numerical computations reported in Section (10), a value of $k = \frac{0.155}{\bar{\omega}}$ was used in each case.

(*) See, Numerical Methods in Engineering, by M. G. Salvadori and M. L. Baron, Prentice-Hall, Second Printing, 1955, Page 118 ff.

For high frequency oscillators in which the value of $\bar{\omega}$ is large, it becomes impractical to use a numerical procedure because of the small values of the spacing "k" that are required. Consequently, for use with high frequency oscillators, an analytical expression for Y(T), valid in the range, $0 < T < 2$, has been developed from the integral in Equation (5).

Consider the displacement $\bar{U}(T)$ in the region $r_1 = 0$, corresponding to the bounds $0 \leq T \leq 2$. From the Equation (12),

$$\bar{U}^{(0)}(T) = \bar{U}^{(A,\,0)}(T) + \bar{U}^{(B,\,0)}(T) + \bar{Z}^{(0)}(T) \qquad (27)$$

Substituting Equation (27) into Equation (5) and performing the integration, the displacement $Y^{(0)}(T)$ valid in the region $0 \leq T \leq 2$, is obtained:

$$Y^{(0)}(T) = Y^{(A,\,0)}(T) + Y^{(B,\,0)}(T) + Y^{(Z,\,0)}(T) \qquad (28)$$

where

$$Y^{(A,\,0)}(T) = \sum_{n=1}^{9} Y_n^{(A,\,0)}(T) \qquad (29)$$

$$Y^{(B,\,0)}(T) = \sum_{n=1}^{9} Y_n^{(B,\,0)}(T) \qquad (30)$$

$$Y^{(Z,\,0)}(T) = 14.7\,\frac{\bar{\omega}}{C} \sum_{n=0}^{9} Y_n^{(Z,\,0)}(T) \qquad (31)$$

The function $Y_n^{(A,\,0)}(T)$ is given by

$$Y_n^{(A,\,0)}(T) = a_n^{(0)}(-1)^{n-1} A\frac{a}{G}\, n! \Bigg\{ (n - \alpha\mu) \sum_{j=n}^{\infty} (-1)^j \frac{\alpha^{j-n-1}}{\bar{\omega}^j} \Bigg[-(-1)^{\frac{j}{2}} \sum_{\substack{k=j+2\\ k\ \text{even}}}^{\infty} (-1)^{\frac{k}{2}} \frac{(\bar{\omega}T)^k}{k!} + (-1)^{\frac{j+1}{2}} \sum_{\substack{k=j+2\\ k\ \text{odd}}}^{\infty} (-1)^{\frac{k-1}{2}} \frac{(\bar{\omega}T)^k}{k!} \Bigg] +$$

$$+ \sum_{j=n}^{\infty} (-1)^j (j+1) \frac{\alpha^{j-n}}{\bar{\omega}^{j+1}} \Bigg[-(-1)^{\frac{j+1}{2}} \sum_{\substack{k=j+3\\ k\ \text{even}\\ j\ \text{odd}}}^{\infty} (-1)^{\frac{k}{2}} \frac{(\bar{\omega}T)^k}{k!} + (-1)^{\frac{j+2}{2}} \sum_{\substack{k=j+3\\ k\ \text{odd}\\ j\ \text{even}}}^{\infty} (-1)^{\frac{k-1}{2}} \frac{(\bar{\omega}T)^k}{k!} \Bigg]$$

$$- \frac{(-1)^n n}{\alpha\bar{\omega}^n} \Bigg[-(-1)^{\frac{n}{2}} \sum_{\substack{k=n+2\\ k,n\ \text{even}}}^{\infty} (-1)^{\frac{k}{2}} \frac{(\bar{\omega}T)^k}{k!} + (-1)^{\frac{n+1}{2}} \sum_{\substack{k=n+2\\ k,n\ \text{odd}}}^{\infty} (-1)^{\frac{n-1}{2}} \frac{(\bar{\omega}T)^k}{k!} \Bigg] \Bigg\} \qquad (32)$$

The expression for $Y_n^{(B,\,0)}(T)$ is obtained by substituting B for A and β for α in Equation (32). The coefficients B and β in terms of the Brode parameters are given by Equations (19)-(20).

The expression for $Y_n^{(Z,\,0)}(T)$ is given by the following expressions:

$$Y_n^{(Z,\,0)}(T) = \frac{a_n^{(0)} n!}{\bar{\omega}^n} \Bigg[(-1)^{\frac{n}{2}} \sum_{\substack{k=n+2\\ k,n\ \text{even}}}^{\infty} (-1)^{\frac{k}{2}} \frac{(\bar{\omega}T)^k}{k!} + (-1)^{\frac{n+1}{2}} \sum_{\substack{k=n+2\\ k,n\ \text{odd}}}^{\infty} (-1)^{\frac{k-1}{2}} \frac{(\bar{\omega}T)^k}{k!} \Bigg] \qquad (33)$$

In performing the computations for determining the shock spectra for acceleration and relative displacement shown in Section (10) of the main report, it was found advantageous to use the analytical expression for $Y(T)$ [Equation (3)] to determine $Y(T)$ in the range $0 \leq T \leq 2$, even for the intermediate range of the frequency $\bar{\omega}$. The recurrence formula, Equation (23), was then used to prolong the solution numerically beyond the range $T = 2$. In such cases, the numerical integration was started with the formulas

$$Y(2) = Y_2; \quad Y(2 - k) = Y_{2-k} \qquad (34)$$

where Y_2 and Y_{2-k} were computed from Equation (28).

The displacements $\bar{U}(T)$ and $Y(T)$ were computed using an IBM 704 computer. Once these displacements are known, the acceleration and relative displacement time histories can be determined from Equations (6) and (7) respectively. In each case, the maximum value of the quantity is evaluated. This procedure is repeated over the entire range of the oscillator frequency ω. The curves of maximum acceleration and maximum relative displacement versus the frequency ω are the required shock spectra.

IV. Determination of the "Free Field" Shock Spectra for Comparison Purposes.

The shock spectra developed in Parts (I-III) of Appendix (E) include the effects due to the diffraction of the shock wave by the cavity. It is of interest to compare these spectra with the "free field" shock spectra which heretofore have been used in the design of underground installations. These "free field" spectra are computed from the effects of the free field input pressures only; all diffraction effects due to the cylindrical cavity are neglected. Hence, essentially the "free field" spectra are developed from the pressures that a gage placed at a point in the medium with no tunnel, would read. Analytical expressions for the determination of the "free field" acceleration and relative displacement spectra are developed in this Section.

Let U(t) be the displacement of a point in the medium produced by a plane step shock wave with a constant pressure P and a velocity of propagation c_p. The displacement U(t) is measured in the direction of propagation of the step wave.

The particle velocity at the point, produced by the step wave becomes:

$$\dot{U}(t) = \frac{P}{\rho c_p} \qquad (35)$$

The displacement curve $\overline{U}(t)$ produced by a wave carrying a pressure with a Brode decay, [Equation (1)] may be evaluated by means of the Duhamel integral of Equation (8). Substituting Equations (35) and Equation (1) into Equation (8) and integrating the displacement $\overline{U}(T)$ is obtained:

$$\overline{U}(T) = \frac{Aa}{\rho c_p^2 \alpha} \left[(\mu - 1/\alpha)(1 - e^{-\alpha T}) + Te^{-\alpha T} \right] + $$
$$+ \frac{Ba}{\rho c_p^2 \beta} \left[(\mu - 1/\beta)(1 - e^{-\beta T}) + Te^{-\beta T} \right] \qquad (36)$$

where the non-dimensional time T is given by

$$T = \frac{c_p t}{a} .$$

The coefficients A, B, α, β and μ are given by Equations (18)-(19).

The displacement of the oscillator, Y(T) is obtained by substituting Equation (36) into Equation (5) and integrating:

$$Y(T) = \frac{Aa}{\rho c_p^2 \alpha} \left\{ [\mu - \frac{1}{\alpha}][1 - \cos\bar{\omega}T - \frac{\bar{\omega}^2 e^{-\alpha T}}{\alpha^2 + \bar{\omega}^2} - \frac{\alpha\bar{\omega}}{\alpha^2 + \bar{\omega}^2} \sin\bar{\omega}T + \frac{\bar{\omega}^2}{\alpha^2 + \bar{\omega}^2} \cos\bar{\omega}T] + \right.$$

$$\left. + \frac{e^{-\alpha T}}{\alpha^2 + \bar{\omega}^2} [\bar{\omega}^2 T + \frac{2\alpha\bar{\omega}^2}{\alpha^2 + \bar{\omega}^2}] + \bar{\omega}[\frac{\alpha^2 - \bar{\omega}^2}{(\alpha^2 + \bar{\omega}^2)^2}]\sin\bar{\omega}T - \frac{2\bar{\omega}^2\alpha}{(\alpha^2 + \bar{\omega}^2)^2} \cos\bar{\omega}T \right\} +$$

$$+ \frac{Ba}{\rho c_p^2 \beta} \left\{ [\mu - \frac{1}{\beta}][1 - \cos\bar{\omega}T - \frac{\bar{\omega}^2 e^{-\beta t}}{\beta^2 + \bar{\omega}^2} - \frac{\beta\bar{\omega}}{\beta^2 + \bar{\omega}^2} \sin\bar{\omega}T + \frac{\bar{\omega}^2}{\beta^2 + \bar{\omega}^2} \cos\bar{\omega}T] + \right.$$

$$\left. + \frac{e^{-\beta T}}{\beta^2 + \bar{\omega}^2} [\bar{\omega}^2 T + \frac{2\beta\bar{\omega}^2}{\beta^2 + \bar{\omega}^2}] + \bar{\omega}[\frac{\beta^2 - \bar{\omega}^2}{(\beta^2 + \bar{\omega}^2)^2}] \sin\bar{\omega}T - \frac{2\bar{\omega}^2\beta}{(\beta^2 + \bar{\omega}^2)^2} \cos\bar{\omega}T \right\} \tag{37}$$

where $\bar{\omega} = \frac{\omega a}{c}$.

Using the values of $\bar{U}(T)$ and Y(T), the acceleration and relative displacement time histories can be determined from Equations (6) and (7) respectively. Frequency spectra for the acceleration and the relative displacement of the oscillator mass may then be constructed following the procedure in Section (III) of this Appendix.

V. Numerical Results.

Acceleration and relative displacement shock spectra have been obtained for cavities which are subjected to P waves with Brode pressure decays, from a 20 MT surface burst. Spectra for the rigid body motion (average motion) of the cavity are presented in Section (10) for waves with $P_o = 6500$ psi [Figure (10-2)] and $P_o = 2000$ psi [Figure (10-3)]. In addition, spectra based on the motion of the cavity boundary at the points $\theta = 0^\circ$ and $\theta = 180^\circ$

are presented in Figure (10-4) and (10-5) respectively, for P_o = 6500 psi.

For comparison purposes, the "free field" acceleration spectrum is also given in each case. The reader is referred to Section (10) for a discussion of the results and a comparison of the spectra developed in the Appendix (which include diffraction effects) with the free field spectra.

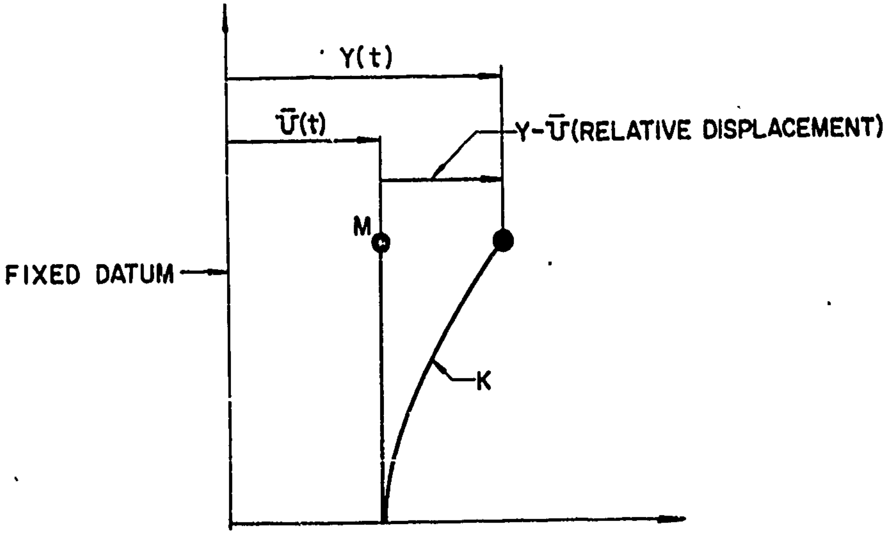

FIG. 1

Appendix F

ELASTIC PROPERTIES OF GRANITES UNDER STATIC LOADING(*)

I. PROCEDURE.

Compression tests were performed on two different domestic granites of structural and architectural quality to determine typical stress-strain diagrams and elastic constants for these materials.

Specimens having the shape of parallelepipeds of approximately three inches height and one square inch cross-sectional area were cut using a diamond rock saw. Electrical resistance strain gages, [SR-4 AX-5], which measure both longitudinal and transverse strains were affixed to the specimens. The specimens were loaded statically on a Baldwin Universal testing machine.

Table (1) presents the description, composition and elastic properties of the materials used as listed by the U. S. Bureau of Standards.(**) Table (2) shows the dimensions, conditions of loading and test results for the specimens tested. Figure (1)-(3) show the stress-strain diagrams which were obtained from the tests.

II. Discussion of Test Results.

It appears from Tables 1 and 2 that the tested specimens failed at lower loads than expected. However, the Bureau of Standards does not list

---

(*) The tests were performed by Dr. Robert Heller, Assistant Professor of Civil Engineering, Columbia University.

(**) See, D. W. Kessler, H. Insley, W. H. Sligh, "National Bureau of Standards", Paper No. R. P. 1320, J. of Research, V. 25, 1940, Page 161-206.

more than one of two test results for each material and consequently a statistical distribution of properties for a particular type of granite cannot be deduced from the tabulation. The test results for each material are remarkably well duplicated since the specimens were all cut from one large block and consequently have nearly uniform properties. The ordinary grey granite has a higher compressive strength, but somewhat lower average modulus of elasticity than the pink one. Grain structure, in evidence in the grey granite, had no apparent effect though on one specimen the load was applied perpendicular and on two others parallel to the grain. The pink granite which does not exhibit any particular grain structure had a high elastic modulus because of a greater quartz content.

All specimens failed in transverse tension forming columnar fibers. The shape of the stress-strain diagrams is similar to those obtained by other investigators.(*)

Poisson's ratio and a shear modulus may be computed, and Poisson's ratio is found to be variable for all specimens. A typical curve of Poisson's ratio is shown in Figure (1). Some data indicating the loading rate sensitivity for these materials is presented by Wuerker.(*) The loading rate in the present tests was held to approximately 5000 lb/min. For higher rates of loading, the modulus of elasticity increases considerably, but no appreciable increase in compressive strength is shown. Hydrostatic pressure combined with axial loading has also been used by some investigators where work could be surveyed in the future to determine the necessity and feasibility of future tests.

(*) See, R. G. Wuerker, Petroleum Branch, AIME, Dec. 1956 (D552W95).

TABLE 1 DESCRIPTION OF MATERIALS(*)

Source	Classification	Color	Major Mineral Constituents	Compressive Strength psi Perpendicular (A) and Parallel (B) to Rift.			
				Specimens Dry		Specimens Wet	
				A	B	A	B
West Chelmsford, Massachusetts	Muscovite, biotite Granite, gneiss	Light Grey	Microline and orthoclase Quartz, rutile, muscovites, biotite	24,000	27,000	20,000	19,000
Salisbury, N.C.	Biotite, Granite	Pink	Orthoclase, Quartz, Microline, Plagioclase, Biotite	29,700	32,200	30,000	34,000

TABLE 2 TEST RESULTS

Spec. No.	Source	Dimensions (inches)	Direction of load	Compressive Strength(psi)	Modulus of Elasticity(psi)
1	West Chelmsford, Mass.	3 1/8 x 1.203 x 1.188	Perpendicular to grain	22,110	6.9×10^6
2	West Chelmsford, Mass.	3 1/32 x .972 x .956	Parallel to grain	16,411	6.9×10^6
3	West Chelmsford, Mass.	3 1/32 x .992 x .968	Parallel to grain	20,045	6.9×10^6
4	Salisbury, N. C.	2 31/32 x .965 x 1.002	No grain	16,030	9.2×10^6
5	Salisbury, N.C.	3 1/16 x .970 x .955	No grain	14,840	9.2×10^6

(*) D. W. Kassler, H. Insley, W. E. Sligh, "National Bureau of Standards," Paper No. R. P. 1320, J. of Research, V. 25, 1940, Pgs. 161-206.

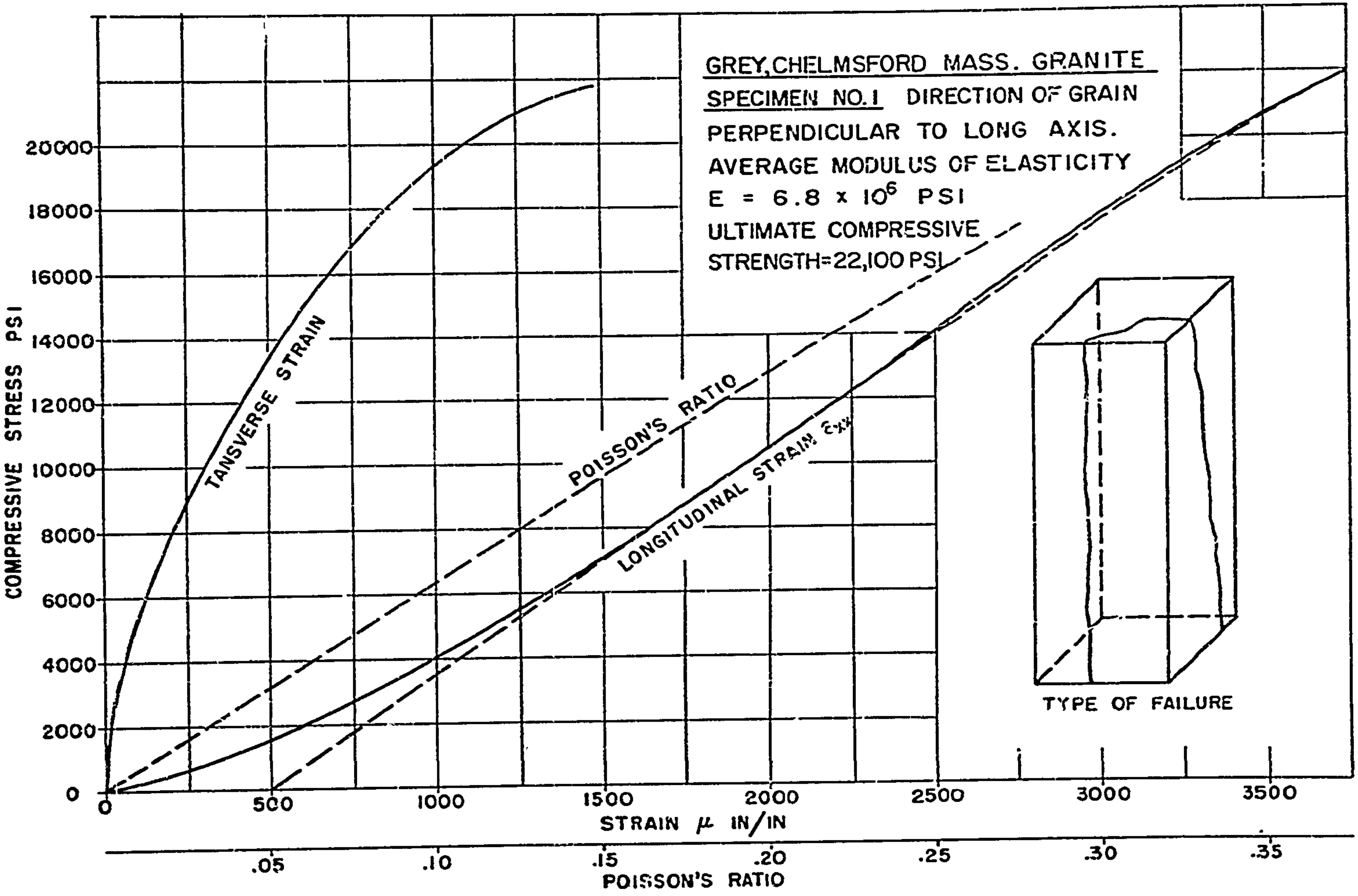
GREY, CHELMSFORD MASS. GRANITE
SPECIMEN NO. 1 DIRECTION OF GRAIN
PERPENDICULAR TO LONG AXIS.
AVERAGE MODULUS OF ELASTICITY
E = 6.8 x 10^6 PSI
ULTIMATE COMPRESSIVE
STRENGTH=22,100 PSI
TANSVERSE STRAIN
POISSON'S RATIO
LONGITUDINAL STRAIN ε-xx
TYPE OF FAILURE
COMPRESSIVE STRESS PSI
0
2000
4000
6000
8000
10000
12000
14000
16000
18000
20000
STRAIN μ IN/IN
0
500
1000
1500
2000
2500
3000
3500
POISSON'S RATIO
.05
.10
.15
.20
.25
.30
.35

FIG. 1

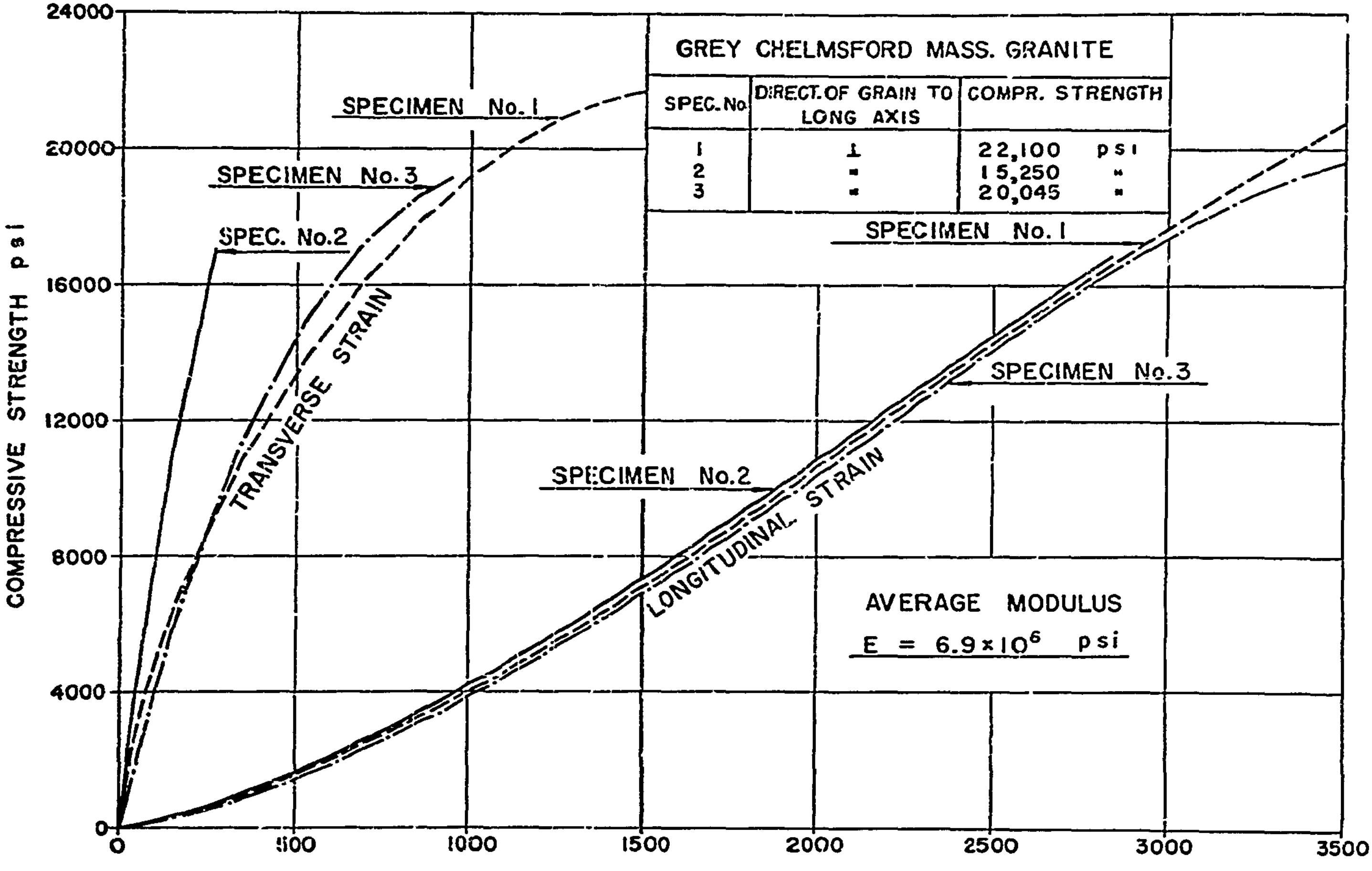
GREY CHELMSFORD MASS. GRANITE
SPEC. No
DIRECT. OF GRAIN TO LONG AXIS
COMPR. STRENGTH
1 ⊥ 22,100 psi
2 " 15,250 "
3 " 20,045 "
SPECIMEN No. 1
SPECIMEN No. 3
SPEC. No. 2
TRANSVERSE STRAIN
SPECIMEN No. 1
SPECIMEN No. 3
SPECIMEN No. 2
LONGITUDINAL STRAIN
AVERAGE MODULUS
E = 6.9×10⁶ psi
COMPRESSIVE STRENGTH psi
24000
20000
16000
12000
8000
4000
0
0
500
1000
1500
2000
2500
3000
3500
STRAIN μ IN/IN

FIG. 2

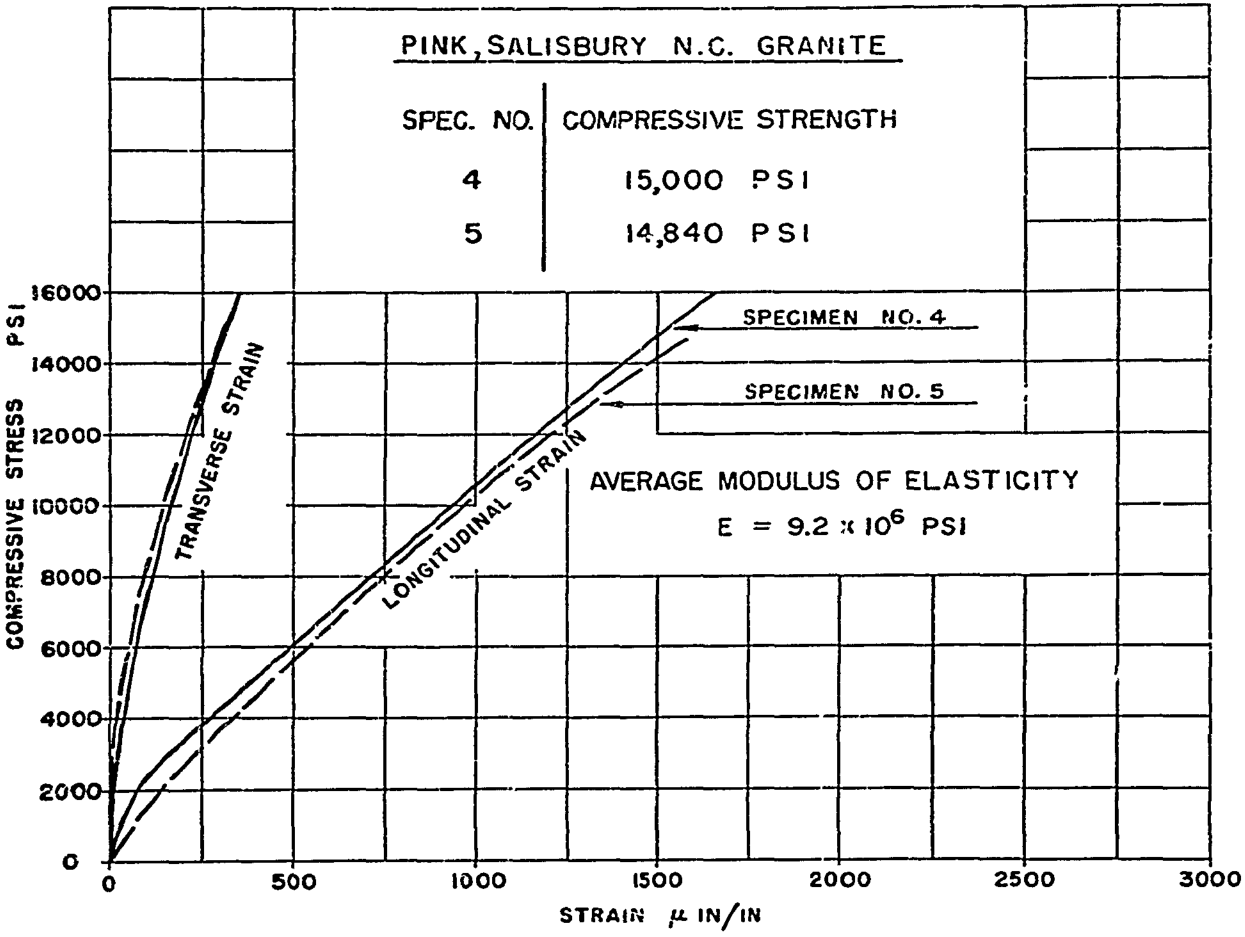
PINK, SALISBURY N.C. GRANITE
SPEC. NO.
COMPRESSIVE STRENGTH
4
15,000 PSI
5
14,840 PSI
SPECIMEN NO. 4
SPECIMEN NO. 5
AVERAGE MODULUS OF ELASTICITY
E = 9.2 x 10^6 PSI
TRANSVERSE STRAIN
LONGITUDINAL STRAIN
COMPRESSIVE STRESS PSI
0
2000
4000
6000
8000
10000
12000
14000
16000
STRAIN μ IN/IN
0
500
1000
1500
2000
2500
3000

FIG.3